Roinn Cumarsáide, Gníomhaithe ar son na hAeráide & Comhshaoil
Department of Communications, Climate Action & Environment

epa

NIEA Northern Ireland Environment Agency
www.daera-ni.gov.uk

Unconventional Gas Exploration and Extraction (UGEE) Joint Research Programme

Final Report 2: Baseline Characterisation of Seismicity

Authors: Brian Baptie, Colm Jordan, Ilaria Mosca, Francesca Cigna, Sean Burke, John McCloskey, Mairéad Nic Bhloscaidh, Chris Bean and Martin Möllhoff

Broadband seismometer deployed in a field pit

CDM Smith
British Geological Survey NATURAL ENVIRONMENT RESEARCH COUNCIL
PHILIP LEE SOLICITORS DUBLIN • BRUSSELS • SAN FRANCISCO
amec
UCD DUBLIN
University of ULSTER

www.ugeeresearch.ie

Funding Organisations

The Environmental Protection Agency (EPA) is an independent statutory body, established under the Environmental Protection Agency Act with a wide range of responsibilities including regulation of large scale industrial and waste facilities, monitoring and reporting on the state of the environment, overseeing local authorities' environmental responsibilities, coordinating environmental research in Ireland, promoting resource efficiency and regulating Ireland's greenhouse gas emissions. Through the Department of Communications, Climate Action and Environment (DCCAE) (and formerly through the Department of Environment, Community and Local Government - DECLG), the EPA has provided funding for environmental research since 1994. The current EPA Research Programme 2014-2020 is designed to identify pressures, inform policy and develop solutions to environmental challenges through the provision of strong evidence-based scientific knowledge.

On the 23rd of July 2016, the Department of Communications, Energy and Natural Resources (DCENR) became the DCCAE. Along with a name change, the new Department incorporates functions that were formerly held within the Environment Division of the DECLG. The Department retains responsibility for the Telecommunications, Broadcasting and Energy sectors. It regulates, protects, develops and advises on the Natural Resources of Ireland. Of particular relevance is the role of the Petroleum Affairs Division (PAD) to maximise the benefits to the State from exploration for and production of indigenous oil and gas resources, while ensuring that activities are conducted safely and with due regard to their impact on the environment and other land/sea users. The Geological Survey of Ireland (GSI) is also within DCCAE and provides advice and guidance in all areas of geology including geohazards and groundwater and maintains strong connections to geoscience expertise in Ireland.

The Department of Agriculture, Environment and Rural Affairs (DAERA) in Northern Ireland has responsibility for food, farming, environmental, fisheries, forestry and sustainability policy and the development of the rural sector in Northern Ireland. As an executive agency of DAERA, the Northern Ireland Environment Agency (NIEA) seeks to safeguard the quality of the environment as a whole through effective regulation of activities that have the potential to impact on the environment.

Administration of the Research Programme and Steering Committee

This Research Programme is being administered by the EPA and steered by a committee with representatives from DCCAE (formerly DCENR and the Environment Division of the DECLG), the Commission for Energy Regulation (CER), An Bord Pleanála (ABP), the GSI, NIEA, the Geological Survey of Northern Ireland (GSNI), as well as a Health representative nominated by the Health Service Executive (HSE).

UGEE Joint Research Programme

Environmental Impacts of Unconventional Gas Exploration and Extraction (UGEE)

(2014-W-UGEE-1)

Final Report 2:

Baseline Characterisation of Seismicity

by

British Geological Survey, University of Ulster and University College Dublin

Authors:

Brian Baptie, Colm Jordan, Ilaria Mosca, Francesca Cigna, Sean Burke, John McCloskey, Mairéad Nic Bhloscaidh, Chris Bean and Martin Möllhoff

ENVIRONMENTAL PROTECTION AGENCY
An Ghníomhaireacht um Chaomhnú Comhshaoil
PO Box 3000, Johnstown Castle, Co. Wexford, Ireland

Telephone: +353 53 916 0600 Fax: +353 53 916 0699
Email: info@epa.ie Website: www.epa.ie

ACKNOWLEDGEMENTS

This report is published as part of the Joint Research Programme on the Environmental Impacts of Unconventional Gas Exploration and Extraction. This Research Programme is being administered by the EPA and steered by a committee with representatives from the Department of Communications, Climate Action and Environment [DCCAE, formerly the Department of Communications, Energy and Natural Resources (DCENR) and the Environment Division of the Department of the Environment, Community and Local Government (DECLG)], the Commission for Energy Regulation (CER), An Bord Pleanála (ABP), the Geological Survey of Ireland (GSI), the Northern Ireland Environment Agency (NIEA), the Geological Survey of Northern Ireland (GSNI) and the Health Service Executive (HSE) of Ireland.

DISCLAIMER

References to government departments (DCENR and DCELG) throughout the report use the names of these departments prior to July 2016. References to the Department for the Economy (DfE) throughout the report use the name of its predecessor, the Department of Enterprise Trade and Investment (DETI), the department responsible for petroleum licensing in Northern Ireland until May 2016.

UGEE Joint Research Programme
Published by the Environmental Protection Agency, Ireland

ISBN: 978-1-84095-688-7 November 2016

Price: Free Online version

Project Authors

Dr Brian Baptie
British Geological Survey
Environmental Science Centre
Nicker Hill
Keyworth
Nottingham
NG12 5GG
UK
Tel.: +44 115 936 3100
Email: bbap@bgs.ac.uk

Dr Colm Jordan
British Geological Survey
Environmental Science Centre
Nicker Hill
Keyworth
Nottingham
NG12 5GG
UK
Tel.: +44 115 936 3100

Dr Ilaria Mosca
British Geological Survey
Environmental Science Centre
Nicker Hill
Keyworth
Nottingham
NG12 5GG
UK
Tel.: +44 115 936 3100

Dr Francesca Cigna
British Geological Survey
Environmental Science Centre
Nicker Hill
Keyworth
Nottingham
NG12 5GG
UK
Tel.: +44 115 936 3100

Dr Sean Burke
British Geological Survey
Environmental Science Centre
Nicker Hill
Keyworth
Nottingham
NG12 5GG
UK
Tel.: +44 115 936 3100
Email: seanb@bgs.ac.uk

Professor John McCloskey
School of Environmental Sciences
University of Ulster
Coleraine Campus
Cromore Road
Coleraine
Co. Londonderry
BT52 1SA
UK
Tel.: +44 28 7167 5610
Email: j.mccloskey@ulster.ac.uk

Mairéad Nic Bhloscaidh
School of Environmental Sciences
University of Ulster
Coleraine Campus
Cromore Road
Coleraine
Co. Londonderry
BT52 1SA
UK

Dr Chris Bean
Geophysics Group
Room G16A, Science West
University College Dublin
Belfield
Dublin 4
Ireland
Tel.: +353 1 716 2079
Email: geophysics@ucd.ie

Dr Martin Möllhoff
Geophysics Group
Room G16A, Science West
University College Dublin
Belfield
Dublin 4
Ireland
Tel.: +353 1 716 2079
Email: geophysics@ucd.ie

Project A2 Partners

CDM Smith Ireland
Alan Hooper
15 Wentworth
Eblana Villas
Dublin 2
D02 WK10
Ireland
Tel.: +353 1 232 1044
Email: hooperag@cdmsmith.com

University of Ulster
Professor John McCloskey
School of Environmental Sciences
University of Ulster
Coleraine Campus
Cromore Road
Coleraine
Co. Londonderry
BT52 1SA
UK
Tel.: +44 28 7167 5610
Email: j.mccloskey@ulster.ac.uk

University College Dublin
Dr Martin Möllhoff
Geophysics Group
Room G16A, Science West
University College Dublin
Belfield
Dublin 4
Ireland
Tel.: +353 1 716 2079
Email: geophysics@ucd.ie

British Geological Survey
Dr Sean Burke
British Geological Survey
Environmental Science Centre
Nicker Hill
Keyworth
Nottingham
NG12 5GG
UK
Tel.: +44 115 936 3100
Email: seanb@bgs.ac.uk

Project A2 Internal Review Panel[1]

University College Dublin, British Geological Survey, University of Ulster

1 More details available at: http://www.epa.ie/pubs/reports/research/ugeejointresearchprogramme/ugeejrptasksorganisations.html

Contents

List of Figures

List of Tables

Executive Summary

Unconventional Gas Exploration & Extraction (UGEE) involves hydraulic fracturing (fracking) of low permeability rock to permit the extraction of natural gas on a commercial scale from unconventional sources, such as shale gas deposits, coal seams and tight sandstone. The Environmental Protection Agency (EPA), the Department of Communications, Energy and Natural Resources (DCENR) and the Northern Ireland Environment Agency (NIEA) awarded a contract in August 2014 to a consortium led by CDM Smith Ireland Limited to carry out a 24-month research programme looking at the potential impacts on the environment and human health from UGEE projects and operations (including construction, operation and after-care).

The UGEE Joint Research Programme (JRP)[2] is composed of five interlinked projects and involves field studies (baseline monitoring of water and seismicity), as well as an extensive desk-based literature review of UGEE practices and regulations worldwide. The UGEE JRP has been designed to produce the scientific basis, which will assist regulators – both North and South – in making an informed decision about whether it is environmentally safe to allow fracking. As well as research in the island of Ireland, the UGEE JRP is looking at and collating evidence from other countries.

Project A2: Seismicity addressed the baseline characterisation of seismicity, which is required to enable potential impacts to be assessed and involved several tasks:

- Task 1: Assessment of existing baseline monitoring operated worldwide for UGEE projects/operations;
- Task 2: Evaluation of methodologies for the monitoring of ground deformation that may be associated with UGEE projects/operations;
- Task 3: Assessment of existing data on natural seismicity in the island of Ireland; and
- Task 4: Assessment of the magnitude and physical effects of induced seismicity that may be associated with UGEE projects/operations in the island of Ireland.
- Task 5: Technical Specification for Sub-Regional Seismic Baseline Monitoring.
- Task 8: Examination of global experience of seismic events stimulated by UGEE operations.
- Task 9: Assessment of pre-fracturing modelling techniques.

Task 1: Assessment of Existing Baseline Monitoring Operated Worldwide for UGEE Projects/Operations

Recent experience in UGEE suggests that baseline monitoring should be an essential requirement of future exploration and extraction, so that background levels of seismicity can be reliably characterised and any active faults that could potentially be affected by exploration and extraction operations can be identified. Baseline monitoring is also essential for discriminating any induced earthquakes from natural background earthquake activity, allowing seismicity rates before, during and after operations to be reliably compared and any differences to be identified.

Baseline monitoring must be established prior to the commencement of any activity that is known to induce earthquakes. However, the duration of the monitoring required before operations start will depend on both the state of existing monitoring and the activity rate of the natural seismicity. In general, areas with higher activity rates will require shorter periods of monitoring. In areas where activity rates are low, the number of earthquakes in a given period of time may be very low, so longer durations of baseline monitoring are

2 www.ugeeresearch.ie

required to reliably determine seismicity rates. This is in keeping with experience in the geothermal industry, where monitoring periods of 6–12 months are common.

Current best estimates of the seismicity rate across Ireland and the surrounding offshore area are low, in keeping with the low numbers of observed earthquakes. Scaling these rates to the two study areas (the Northern Carboniferous Basin and the Clare Basin), suggests that there would be an earthquake with a magnitude of 2 or greater roughly every 60 years in the larger of the two study areas, and even fewer earthquakes in the smaller study area. It may require many decades of baseline monitoring to fully characterise the rates in each of the two study areas, if the levels of natural seismicity are as low as expected from the available historical and instrumentally recorded data. However, it is important to test the assumption that seismicity rates are uniform across Ireland. Therefore, detailed monitoring will be required in each study area to detect any unusual seismicity that may suggest that seismicity rates are higher in the study areas, or that there is seismicity associated with any specific fault structure. One to two years may be an appropriate monitoring period for this purpose.

Reliable and uniform detection of seismic events across a given area of interest requires a uniform distribution of monitoring stations. The density of the stations along with the noise levels at each station control the lowest magnitudes that can be reliably detected. Higher station densities will be required to detect and locate lower magnitudes. Noise levels at individual stations also affect detection capability, and these should be low in order to maximise detection potential. A monitoring network must also extend beyond the limits of the area of interest in order to be able to reliably detect earthquakes that occur close to these limits. Detection capability for different station distributions and densities can be readily modelled using a number of relationships that determine the amplitude of seismic waves as a function of magnitude and distance.

Extensive experience of seismic monitoring developed by the geothermal industry may be considered as “best practice” for UGEE. This would allow many of the methods used for the monitoring of earthquake activity, along with appropriate control measures for the mitigation of risks associated with induced earthquakes, to be readily adopted. A design for the proposed baseline monitoring system is presented in Section 7. However, it should be noted that while seismic monitoring is used before, during and after geothermal operations, the aim of this study is solely to characterise the background natural seismicity in the study areas.

The case studies discussed in this report highlight the importance of an appropriate monitoring network for reliable detection and location of any seismic events before, during and after any operations that may induce seismic activity. In particular, the example of the seismicity induced by hydraulic fracturing at Preese Hall, near Blackpool, shows how local monitoring stations are essential to reduce uncertainty and also allay public concern.

Task 2: Evaluation of the Methodologies for the Monitoring of Ground Deformation That May Be Associated with UGEE Projects/Operations

Authoritative ground surface monitoring is vital in relation to UGEE projects to accurately understand the degree of any surface motion during operations. Seismic events have been linked to hydraulic fracturing operations in the UK at Preese Hall and in the USA. Quantitative measurements of ground motion, both historic and current, are required to confirm any surface displacement and enable the assessment of the impacts to the surface environment and the structures built upon or within it and therefore investment in ground surface monitoring equipment essential.

Interferometric Synthetic Aperture Radar (InSAR) can provide millimetric measurements of surface ground motion from satellite platforms and has been validated by the British Geological Survey (BGS) in several projects. It has also been successfully used in CO_2 sequestration monitoring projects in locations such as In Salah.

InSAR interrogates the differences in phase from a series of radar images (generally acquired from a satellite) to generate maps of surface motion either in the satellite Line of Sight or in absolute vertical/horizontal motion. InSAR is an ideal technology for monitoring surface motion because archive radar data (acquired since 1992) can be utilised (where available) to analyse regions where *in situ* Global Navigation Satellite System (GNSS)/Electronic Distance Meter (EDM)/tiltmeter data are not available historically. InSAR studies can also provide a more regional picture than the interpolated point coverage derived from traditional techniques such as GNSS stations. Ideally, the remote and *in situ* methods should be integrated because they provide complementary information at a range of scales.

GNSS/EDM/tiltmeter technology is applied routinely to monitoring surface motion related to volcanic activity and CO_2 storage. However, a review has yielded little published evidence of the application of these technologies for monitoring surface motion related to UGEE projects/operations, or of the magnitude and geographical distribution of ground deformation associated with UGEE operations worldwide. It is suspected that InSAR has not yet been applied to UGEE operations primarily due to the challenge of gaining results in non-urban vegetated areas; however newly-developed methods such as Intermittent Small Baseline Subset (ISBAS) are addressing this limitation.

This study evaluated the potential for InSAR to monitor the landmass of the island of Ireland (with high resolution results presented for the two study areas in Co. Clare and the Northwest Carboniferous Basin) by modelling the three primary environmental factors that affect the efficacy of InSAR monitoring over an area. It was found that none of these preclude the use of InSAR in Ireland; there is a suitable archive of radar imagery (and new radar imagery is currently being acquired by satellites such as Sentinel 1A), topographic distortions would only affect 0.1% of the landmass, and land cover modelling indicates that techniques such as ISBAS could provide suitable coverage of scatterers across the island.

In conclusion, this method is suitable for monitoring ground motion, which is required to confirm any surface displacement and enable the assessment of impacts to the surface environment and structures that may be associated with UGEE operations in Ireland.

Task 3: Assessment of Existing Data on Natural Seismicity in the Island of Ireland

It is well known that Ireland is a region of low seismic activity. The historical seismicity of Ireland has been studied by a number of researchers and a review of published data confirms that earthquake activity is very low. Historical accounts of seismic events felt in Ireland amount to only 26 events in the time period 1500 to 1970, which can be deemed credible. Given the good standard of historical records in Ireland in this period, it seems quite unlikely that any significant earthquakes are yet to be discovered. Half of these accounts can be attributed to earthquakes that occurred outside Ireland in England, Scotland or Wales, where there is substantial evidence of widely felt and occasionally damaging earthquakes stretching back many hundreds of years. These were nearly all events of around magnitude 5 ML or above that occurred in the western part of Britain and were widely felt across Britain and Ireland. The other thirteen events occurred in Ireland and the immediate offshore area.

Earthquake intensity is a qualitative measure of an earthquake determined from the observed effects on people, objects and buildings. For a given earthquake, intensity is normally greatest at the epicentre and decreases with distance from the epicentre. Intensity can be determined from historical accounts of earthquakes and used to estimate an earthquake location and magnitude. Historical earthquakes in Ireland have low intensities and were generally only felt over small areas suggesting that these were of small magnitude. Locations have been assigned to these earthquakes directly from the area of maximum felt intensity, however, magnitudes have not been determined, except for the magnitude 4.4 ML earthquake in the Irish Sea in 1951, for which instrumental data from the seismograph at Rathfarnham Castle was available. Historical earthquakes in Ireland are observed in three localities: Wicklow, Wexford and the Irish Sea on the east coast; Donegal, in the north; and the south coast of Ireland around Cork.

Instrumental data from the Dublin Institute of Advanced Studies (DIAS) and the British Geological Survey (BGS) catalogues also confirm these low rates of seismic activity. Almost all the instrumental seismicity lies in areas where historical earthquakes have occurred, i.e. Wicklow and the Irish Sea; Wexford, Waterford and Cork on the south coast of Ireland; and, Donegal in the north. The exception to this is the magnitude 4.0 ML earthquake off the coast of Mayo in 2012, which is the largest Irish event in the catalogue. Nearly all the seismic activity in Ireland, both instrumental and historical, is concentrated around the coast and there is an almost complete absence of seismicity inland, with only two instrumentally recorded earthquakes in County Leitrim.

Comparison of the DIAS and BGS instrumental earthquake catalogue clearly shows that the locations and magnitudes for the common events in each are very similar, although small differences arise for those earthquakes which are a considerable distance offshore to the west of Ireland.

The combined historical and instrumental catalogue was used to determine earthquake activity rates for Ireland, i.e. the number of earthquakes above a given magnitude in a given period of time. However, the calculated rates were found to vary depending on the assumed level of completeness of the earthquake catalogue. Using the same catalogue completeness thresholds as for Britain suggests that there should be an earthquake, with a magnitude of 4 MW or greater, somewhere in Ireland and the surrounding offshore area, approximately every 476 years. This is in reasonable agreement with the observed data. However, using a more conservative estimate of catalogue completeness leads to a higher activity rate, which would lead to significantly more earthquakes than observed. This highlights the problem of estimating reliable rates in low seismicity regions that allow seismic hazard to be reliably quantified.

The average activity rate for Britain suggests that there should be an earthquake with a magnitude of 4 MW or greater approximately every six years. The reasons for this dramatic difference between Ireland and Britain remain poorly understood, given the geological and tectonic similarities of the two landmasses.

Modelled ground motions for earthquakes with moderate magnitudes that may occasionally occur in or around Ireland suggest that ground velocities are unlikely to exceed typical levels at which cosmetic damage might occur, except close to the earthquake source.

Task 4: Assessment of the Magnitude and Physical Effects of Induced Seismicity That May Be Associated with UGEE Projects/Operations in the Island of Ireland

The expected magnitude of seismicity induced by hydraulic fracturing cannot be gleaned from past experience, and a forecast modelling approach is proposed that will be able to take into account detailed baseline data and real time observed seismicity. Also that physical effects and consequences of small events are addressed in Task 3. A forecasting protocol for seismicity induced from a generic fluid injection (as is used in fracking operations) was developed and tested. The results were used:

(a) to illustrate the large uncertainties inherent in forecasting seismicity where underlying activity is low; and

(b) to inform decisions about the specification of baseline monitoring schemes.

The essential scientific background was reviewed and a detailed description given of the theoretical and statistical elements of the algorithm, particularly including the quantification of the associated uncertainties. The chosen input parameters of the simulation are necessarily arbitrary and hypothetical at this stage because of the absence of suitable data sets; the software was designed as a generic tool that could be applied to any injection scenario (i.e. not limited to hydraulic fracturing).

Several key observations were made from a series of three scenarios, including different background seismicity models and magnitude detection thresholds:

1. The choice of model for the active faults has a first order effect on the success of forecasts. Important information on the active faults might be obtained from detailed structural studies and high quality earthquake catalogues in the area of the project;

2. Forecasts will rely on a high-quality baseline monitoring network and current best practice in data analysis;

3. Significant errors are introduced into forecasts by ignoring spatial heterogeneity in background seismicity rates. Monitoring networks should ideally be designed to resolve heterogeneous rates in detail. However statistical models for fault distributions in the region would potentially allow these uncertainties to be estimated, using an extension of the methodology employed here; and

4. Current catalogues are completely inadequate for forecast modelling on these spatial scales and to the standard required for this application (see Task 3). The use of synthetic catalogues to represent hypothetical baseline scenarios allows illustration of the nature of the uncertainties that might be expected, but does not enable specific forecast from an injection at a particular site at present.

Task 5: Technical Specification for Sub-regional Seismic Baseline Monitoring

The main goal of seismic baseline monitoring is to establish the rate of naturally occurring seismicity in an area. Any seismicity induced in the future can then be quantified by comparing the seismicity recorded during the operational phase with the baseline seismicity. In addition, a baseline study is useful to locate active faults and to map seismic noise levels in detail.

The aim of this task was to answer two questions:

1. Is the detection threshold of existing seismic networks in Ireland sufficient to detect and to determine the location and magnitude of all local earthquakes with magnitudes ML ≥ 0.5 in the two study areas?

2. What kind of local seismic network is required if existing seismic networks in Ireland are insufficient for baseline monitoring of all local earthquakes with ML ≥ 0.5?

Experience shows that up to 20% of stations in a temporary network experience technical problems at any one time. Because six station recordings are required to provide reliable location parameters it is suggested that temporary networks should consist out of at least eight seismic stations. The detection threshold value of ML = 0.5 was chosen because events with ML < 0.5 are unlikely to be felt by humans or to cause any structural damage. Considering a detection threshold value of ML = 0.5 is consistent with the limit recommended for cessation of injection in the UK traffic light scheme proposed by Green *et al*. (2012). Dependent on hypocentral depth and local ground properties in general only events with magnitudes ML ≥ 2 are perceptible to humans (Musson, 2007) and only events with magnitudes ML ≥ 2.7 are thought to potentially cause minor damage (Baisch and Voros, 2011).

It is important to identify the seismic frequency range of interest when considering instrumentation specifications. The frequency content of an earthquake signal is band-limited and depends in addition to path (in particular distance) and site effects on the source dimensions and hence the event magnitude. In order to obtain good quality data, the seismic system should be able to provide an undistorted recording of ground motion in the main frequency range of local earthquakes.

The seismometers should be installed directly on bedrock to minimise the effect of seismic noise. Sites in stiff overburden should be chosen if bedrock sites cannot be realised. Installation methods should follow international best practice to ensure good data quality. This includes a pit with solid concrete base, water proofing, thermal insulation and low sensitivity to wind.

It was recommended that data from the proposed baseline network should be integrated with the National Data Centre and operated as part of the Irish National Seismic Network (INSN). The UCD Waveobs project is of temporary nature and ends in 2016 and so Waveobs data will not be available long term. For logistical reasons the baseline network should be site selected, permissioned, deployed and operated by a commercial entity. The network operation includes data management and should provide for adequate documentation of network operation parameters (station calibrations, station downtimes, technical problems, details of maintenance and service work etc.) and archiving of continuous seismic data, response files and other relevant metadata in standard seismological community formats. The data analysis should follow international best practice in routine seismological observatory operation. The resulting earthquake catalogue together with the seismic raw data should be made publicly available via the NDC to ensure transparency.

Task 8: Examination of Global Experience of Seismic Events Stimulated by UGEE Operations

This task provided an extensive review of induced seismicity in UGEE operations, discussing examples of recent seismicity related to waste water disposal in the eastern United States. Where possible, available UGEE data from recent examples, such as the induced seismicity in Blackpool, UK, as well as data from other analogues were used to investigate the controlling factors on induced seismicity during fluid injection and examine the relationships between injection volume and pressure and induced seismicity. Finally, a number of measures were suggested for mitigating the risk of induced earthquakes, specifically for UGEE operations and for energy technologies in general.

The process of hydraulic fracturing in order to increase the permeability of reservoir formations and stimulate the recovery of hydrocarbons is generally accompanied by microseismicity, usually defined as earthquakes with magnitudes of 2 or less, that are too small to be felt. Two types of induced events can be defined: “fracked” events, whose size is constrained by the energy of the injection process; and “triggered” events, whose size depends largely on the amount of stored up elastic strain energy already in the rocks. The “fracked” events are caused by the formation and growth of new cracks and fractures in a previously intact rock mass as a result of the injection of high pressure fluids. The “triggered” events are a result of both presence of high pressure fluid and the stress perturbation caused by the fluid, which changes the effective stress on pre-existing faults, causing them to fail. These earthquakes can be “triggered” by very small stress perturbations, however, the potential for such events depends very much on the geological context and, given the low levels of background seismicity, the probability of large triggered in Ireland can be considered as small.

The general consensus among most authors is that the process of hydraulic fracturing a well, as presently implemented for shale gas recovery, does not pose a high risk for inducing either felt, damaging or destructive earthquakes. Experience in the USA, where many thousands of stimulations have been carried out suggest that the magnitudes of the induced earthquakes in reservoirs such as the Barnett and Marcellus Shales are typically less than 1 Mw. However, it should be pointed out that most sites of UGEE operations lack independent instrumentation for monitoring induced seismicity and that earthquakes with magnitudes of 2.5 or less will fall below the detection thresholds of regional seismic monitoring networks. Earthquakes of this size are unlikely to be felt or even detected unless local seismic monitoring networks are in place.

There are at least five documented examples of earthquakes with magnitudes greater than two that have been conclusively linked to hydraulic fracturing for shale gas exploration/recovery:

- A magnitude 2.3 ML earthquake in Blackpool, UK in 2011;
- Garvin County, South-Central Oklahoma in 2011 where the largest earthquake had a magnitude 2.9 ML;
- Horn River, Canada, in 2011 with a largest magnitude of 3.8 ML;

- Montney Trend, Canada from May 2013 to October 2014 where 15 earthquakes had magnitudes of 3.0 ML or greater (the largest being Mw). To date, this is the largest known earthquake triggered by hydraulic fracture operations in a hydrocarbon field anywhere in the world; and

- Crooked Lake, Alberta, Canada in 2013 – 2104 where the largest event in the sequence had a magnitude of 3.8 Mw. Earthquake activity has continued in this region and a magnitude 4.4 earthquake on 12 January 2016, 15 km west-northwest of Fox Creek is also suspected to be due to hydraulic fracturing.

It is likely that an earthquake similar in magnitude to the largest that occurred in Horn River, Canada, events (4.4 MW) would be strongly felt and could even cause some superficial damage. In addition, if an earthquake of such a magnitude were to occur in Ireland where felt seismicity is very rare, it would be likely to cause rather more concern among the local population than it would in other parts of the world where earthquakes of this magnitude are more frequent. However, the maximum magnitudes observed in Blackpool and Garvin County would be unlikely to cause any damage, although they could be felt by people close to the epicentre and may cause some concern.

Tasks 3 and 4 of this Project discussed the large uncertainties in forecasting seismicity in areas such as Ireland where the background activity rates are low. However, although it is difficult to quantify, the probability of significant triggered seismicity depends strongly on the prior activity of the area. As a result, significant events are very unlikely in areas such as Ireland where the background seismicity rate is extremely low, and there is no evidence to suggest that the process of hydraulic fracturing for shale gas recovery poses a higher risk for inducing earthquakes than in other parts of the world. This risk may be further reduced by effective mitigation.

By contrast, the growing body of evidence of changes in observed seismicity rates and significant earthquakes linked to long term disposal of wastewater by deep well injection from the hydrocarbon and other industries, suggests that this activity may pose a rather greater seismic risk. Earthquakes with magnitudes comparable to the magnitude 5.7 earthquake in Prague, central Oklahoma have a non-negligible contribution to the seismic hazard in such regions and should be considered in any long term assessments of seismic hazard.

Experience of induced seismicity in Enhanced Geothermal Systems has led to a series of measures to address induced seismicity that may be considered as “industry best practice”, and, as such, may be considered appropriate for mitigating the risk of induced seismicity in UGEE operations. For example, an operational traffic light system linked to real-time monitoring of seismic activity is an essential mitigation strategy that will also need to accompany any UGEE operations in Ireland. Existing regulatory guidelines for ground vibrations caused by blasting could also provide a useful framework for this purpose. The direct use of ground motion thresholds rather than derived magnitudes may, in some case, be preferable. Other means of mitigating earthquake risk may require improved understanding of the Earth’s sub-surface in areas of unconventional hydrocarbon potential, such as better characterisation of existing fault zones, which may be difficult to achieve without detailed geophysical surveying.

Controlling factors on seismicity induced by hydraulic fracturing include: the strength of rocks in the geological formations of interest; the size and state of stress of any faults in the area likely to be affected by fluid injection; and, the pressure change induced by the hydraulic fracture process. The pre-existing state of stress on a fault determines how close it is to failure, so faults that are critically stressed may require only a small stress perturbation to cause them to fail. The pressure change induced by the hydraulic fracture process is mainly controlled by the volume of injected fluid and the rate of injection, where larger volumes and higher injection rates generate higher pressures. Recent work suggests that maximum magnitude is related to the total volume of injected fluid.

There remain a number of gaps in our existing knowledge of induced seismicity. For example, pre-existing state of stress and pore pressure acting on a fault are usually unknown as are the hydrological properties

of the sub-surface. Measuring the initial stress state and pore pressure, tracking the injection history, and careful seismic monitoring may help improve understanding.

Finally, it should be noted that seismological methods alone cannot discriminate between man-made and natural tectonic earthquakes. This strengthens the case for site specific seismic monitoring and detailed recording of injection parameters, to reduce uncertainties in earthquake locations and to compare the temporal evolution of seismic activity with any hydraulic fracture operations.

Overall recommendations from this task were to follow the seven steps for mitigating seismic risk identified in the US Department of Energy "Protocol for Addressing Induced Seismicity Associated with Enhanced Geothermal Systems" (Majer *et al*., 2012) and listed in Table 8.1; a traffic light system linked to real-time monitoring of seismic activity is an essential mitigation strategy that will also need to accompany any UGEE operations in Ireland; direct use of a ground motion threshold, such as peak ground velocity, may be a suitable alternative to earthquake magnitude; and characterisation of any possibly active faults in the area of interest using all available geological and geophysical data.

Task 9: Assessment of Pre-fracturing Modelling Techniques

Fracturing generates microearthquakes. Tracking the location of these, using techniques from crustal seismology, therefore allows the identification of the volume surrounding a perforation which is experiencing fracturing. Each seismic event is extended in space so fractures generated by microearthquakes extend beyond the fractured volume by an amount which is related to the location of the event and the fracture length producing it. The length is related to the magnitude, so knowledge of the location and magnitude of seismicity allows us to estimate the likely maximum extent of fracturing from the perforation.

This task surveyed published data on microseismicity surrounding UGEE perforations and described a stochastic approach which, assuming the distribution of event sizes from other wells, allows modelling of the formation of fractures from widely accepted empirical scaling relations. Results were presented for a synthetic scenario and added to the statistics of seismicity data from North America. However, the modelling parameters leading to these results should be updated in near-real-time during any fracking operation.

The literature on the fractures associated with unconventional hydrocarbon recovery by fracking was reviewed and showed that microseismic observations are likely to provide a reasonable guide to the distribution of fracturing activity surrounding any particular well. It was then argued that estimates of likely fracture heights are given by the addition of the likely length of fractures associated with these microseismic events. A protocol was then developed to forecast the distribution of hydraulic fracture dimensions from a known magnitude distribution using empirically determined scaling relations between earthquake magnitude and rupture length. The parameters used for the stochastic model here are for illustration; they should be replaced by values determined firstly from the baseline survey and then further updated in near-real-time during any fracking operation.

Data from tiltmeters provides clear evidence that vertical fractures can propagate into shallow depths where they might interact with aquifers. Inspection of the vertical extent of microseismic activation shows that the vertical extent of fracturing is likely to be insensitive to frack depth. Data show that the distribution of distance of microseismic events from the perforation is skewed to shallow depths but support the conclusion that 95% of North American projects had worst case events less than 300m above the perforation.

Variability in microseismic magnitude appears to be controlled by sub-horizontal layering and is largely insensitive to frack depth. The top of a lithological unit, such as the top of the shale, would expect to provide a significant, though not impenetrable, barrier to upward fracture propagation particularly at shallow depths. This definitely moderates the threat of extreme fractures propagating to an aquifer far above the

shale top. Given the unpredictability both of the location and magnitude of the worst microseismic event (in the sense that it produces the shallowest fracture) and the associated uncertainty in the length of the fracture it generates, the expected worst case vertical extent of fracturing is very uncertain;

Finally, it should be noted that seismological methods alone cannot discriminate between man-made and natural tectonic earthquakes. This strengthens the case for site specific seismic monitoring and detailed recording of injection parameters, to reduce uncertainties in earthquake locations and to compare the temporal evolution of seismic activity with any hydraulic fracture operations. It was also noted that, while forecasts are likely to be uncertain in the Irish context, given the very low seismic activity recorded on national networks, this implies that the probability of significant induced seismicity in an Irish hydraulic fracturing project is likely to be very low.

Tasks 6 and 7: Installation of Additional Monitoring Points and Baseline Monitoring

Following a comprehensive assessment of the two study areas and the existing provisions for monitoring, the JRP made proposals for baseline monitoring for the assessment of water and naturally-occurring seismicity, with a window of up to two which would result in the overall findings of the research being delivered after the project deadline of 2016.

The original timeline for the research envisaged that the entire programme, including water and seismicity baseline data acquisition, would conclude by 2016. The Steering Committee considered that were the baseline acquisition to commence, the revised timeline for the overall research programme would now be to report in 2018 at the earliest. The decision was therefore taken to prepare an integrated synthesis report now, drawing together the conclusions of the research to date in order that these findings could be reviewed and policy decisions formulated with regard to the use of this technology in Ireland.

It is noted that the baseline monitoring programme proposed by the JRP remains valid and the report includes a recommendation that such a programme should be implemented in advance of the consideration of any application for a Petroleum Exploration Licence (Ireland) or application to carry out High Volume Hydraulic Fracturing (Northern Ireland). It should be noted that such a baseline monitoring programme should provide independent information and is therefore different from any baseline characterisation and monitoring that would be required of UGEE operators as part of a licensing process, which would be project- and site-specific, and would be designed to monitor specific receptors.

Conclusions

This assessment of the potential risk of seismic activity induced by UGEE operations has examined international experience of such induced activity, natural seismic activity in the island of Ireland, methodologies for monitoring distortion of the surface and of background and induced seismic activity, and developed techniques for predicting induced seismicity.

There is general consensus that UGEE operations can result in low magnitude seismic activity from the hydraulic fracturing process but that these events are unlikely to cause damage or even be felt. Larger events could occur if slip on existing faults is initiated, but again this is considered to be high unlikely in Ireland where the available data indicates the rate of natural seismicity to be extremely low. A greater risk is perceived through injection of high volumes of wastewater that might result from UGEE operations and so any such proposals should be examined in detail in the context of the local site geology.

Modelling techniques developed by this project offer potential to predict earthquake activity, including fracture lengths, but better baseline data on the geological structure of the study areas and background seismicity is required to provide input parameters for the models. Using conservative assumptions, the modelling demonstrated that fracture lengths from hydraulic fracturing are relatively short and extremely unlikely to exceed 500m; as a consequence, pollution of aquifers would not occur by movement of

pollutants along fracture paths as long as the separation between the fracture zone and the aquifer exceeds this distance.

Detailed seismic monitoring would be required during any UGEE operations and linked to a traffic light system implemented to control operations should seismic activity occur.

1 Introduction

Unconventional Gas Exploration & Extraction (UGEE) involves hydraulic fracturing (fracking) of low permeability rock to permit the extraction of natural gas on a commercial scale from unconventional sources, such as shale gas deposits, coal seams and tight sandstone. The Environmental Protection Agency (EPA), the Department of Communications, Energy and Natural Resources (DCENR) and the Northern Ireland Environment Agency (NIEA) awarded a contract in August 2014 to a consortium led by CDM Smith Ireland Limited, to carry out a 24-month research programme looking at the potential impacts on the environment and human health from UGEE projects and operations (including construction, operation and after-care).

The UGEE Joint Research Programme (JRP) is composed of five interlinked projects and involves field studies (baseline monitoring of water and seismicity), as well as an extensive desk-based literature review of UGEE practices and regulations worldwide. The UGEE JRP has been designed to produce the scientific basis, which will assist regulators – both North and South – in making an informed decision about whether it is environmentally safe to permit UGEE projects/operations involving fracking. As well as research in Ireland, the UGEE JRP is looking at and collating evidence from other countries.

The environmental impacts of UGEE projects/operations to be considered are those arising from UGEE projects/operations in their totality, not just from fracking activities. All stages of UGEE projects/operations must be considered (i.e. including construction, commissioning, operation, decommissioning and aftercare, as well as off-site and other developments).

1.1 Context

In Ireland, Onshore petroleum Licensing Options were awarded in March 2011, as preliminary authorisations, to three exploration companies seeking to assess the shale gas potential within the Northwest Carboniferous Basin (NCB) and the Clare Basin (CB). In Northern Ireland, one exploration company secured a Petroleum Licence from the Department of Enterprise, Trade and Investment (DETI) to explore the potential for shale gas reserves in Co. Fermanagh, within the NCB. The specific UGEE exploration areas are shown in Figure 1.1, based on the licences that were held until recently.

In Ireland, exploration drilling, including drilling that would involve hydraulic fracturing, is not allowed under current Licensing Options. Nonetheless, two of the three companies have submitted applications for follow-on licences, which would include exploration drilling. The DCENR is not considering these applications further until the findings of this UGEE Joint Research Programme have been published. Also, the DCENR will not consider any applications for exploration authorisations in other onshore areas until the UGEE Research Programme has concluded. In Northern Ireland, the referenced DETI licence was terminated as the licence conditions (a "drill or drop" work programme requiring specified exploration, including drilling a stratigraphic borehole, in the first three years and, before the end of Year Three, a commitment to drilling an exploration well within the following two years) were not met.

In May 2012, the Environmental Protection Agency (EPA) released the report from a preliminary study “Hydraulic Fracturing or ‘Fracking’: A Short Summary of Current Knowledge and Potential Environmental Impacts”. This short desk study was conducted for the EPA by the University of Aberdeen and provided an introduction to the environmental aspects of UGEE projects/operations including a review of regulatory approaches used in other countries and areas for further investigation and research.

In brief, some of the key findings of the study were:

- The importance of adequate knowledge of local geology in order to assess potential impacts on groundwater quality and the possibility of induced seismic activity;
- The importance of well integrity for preventing groundwater contamination;

- The uncertainty regarding the "carbon footprint" of shale gas in comparison to conventional natural gas. This is an important climate change issue;
- Baseline studies are needed before drilling begins (surface water; groundwater; seismic); and
- UGEE is a relatively new area of research (i.e. only a limited number of published, peer-reviewed, scientific studies are available in this area).

The information provided by the preliminary research project was used along with other sources, such as European Commission reports, to develop the Terms of Reference for a more comprehensive Research Programme. Between the 11th January and 8th March 2013, the EPA administered a Public Consultation in relation to the draft Terms of Reference for this Research Programme. Submissions were assessed and relevant comments taken into account, when finalising the document.

In order to assist government bodies in making informed decisions about any potential future licensing and management of UGEE projects/operations on the island of Ireland, comprehensive knowledge of the potential impacts of this process on the environment and human health is required. This knowledge will be generated from a number of sources including EU and international research and through this programme of research.

The key questions to be addressed by the UGEE JRP are:

1. Can UGEE projects/operations be carried out in the island of Ireland whilst also protecting the environment and human health?
2. What is "best environmental practice" in relation to UGEE projects/operations?

The Joint Research Programme is funded by the EPA, DCENR and NIEA. It is managed by a steering committee comprising the EPA, the Department of Environment, Community & Local Government; DCENR; the Geological Survey of Ireland; Commission for Energy Regulation; An Bord Pleanála; NIEA, the Geological Survey of Northern Ireland and the Health Services Executive.

1.2 Overview of the UGEE Joint Research Programme

The main aim of the UGEE Joint Research Programme is to further the understanding of potential impacts on the environment and human health from UGEE projects/operations. It comprises five separate but interlinked projects as follows:

- **Baseline Characterisation:**
    - Project-A1 (Groundwater, Surface Water and Associated Ecosystems)
    - Project-A2 (Seismicity)
    - Project-A3 (Air Quality)
- **Impacts and Mitigation Measures:**
    - Project-B: UGEE Projects/Operations: Impacts & Mitigation Measures
- **Regulatory Framework:**
    - Project-C: Regulatory Framework for Environmental Protection**.**

Figure 1.1. Overview of the case study areas of the UGEE Joint Research Project.

Baseline characterisation of seismicity is required to enable potential impacts to be assessed. The research covered by Project A2 (Seismicity) includes:

- A review of records of natural seismicity in the island of Ireland;
- An assessment of the nature and magnitude of induced seismicity and other activities associated with hydraulic fracturing operations worldwide;
- Review of seismic risk control regimes operated worldwide for UGEE projects/operations and make recommendations for systems applicable to the island of Ireland, with particular reference to the case study areas;
- Assessment of the capability of existing seismic monitoring network(s) to allow detection and location of seismic events down to low thresholds. Recommendations for future development of the seismic monitoring network;
- Assessment of micro-seismic monitoring methodologies enabling real time assessment of seismicity associated with hydraulic fracturing; and
- Linking with Project B - Assessment of the success of pre-fracturing modelling techniques to predict the propagation of fractures and the risk of fractures creating preferential pathways for pollutants.

This report, *Final Report 2: Baseline Characterisation of Seismicity*, covers Tasks 1, 2, 3, 4, 5 7 and 8 of Project A2. The structure of the entire Project A2 is shown in Figure 1.2.

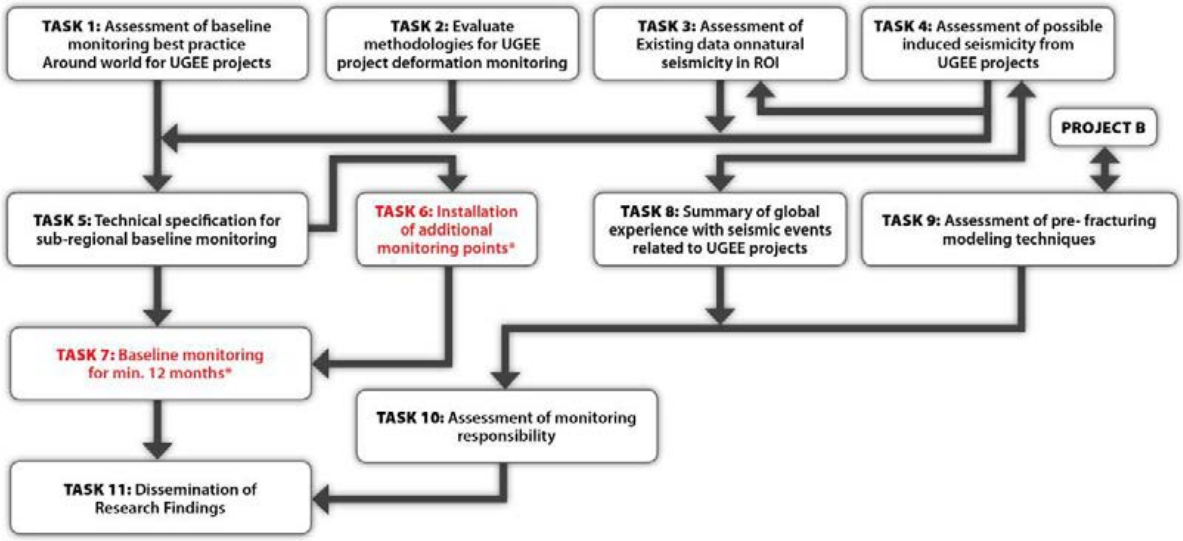

Figure 1.2 .Project A2 tasks and goals.

1.3 Task 1: Assessment of Existing Baseline Monitoring Operated Worldwide for UGEE Projects/Operations

This task examines some of the fundamental principles of earthquakes and seismology that are important for seismic monitoring. These include frequency-magnitude distributions for earthquakes and how activity rates are likely to affect required durations of monitoring both before commencement and after cessation of any UGEE operations. It also considers requirements for reliable detection and location of earthquakes, particularly how station density needs to increase in order to detect and locate smaller earthquakes in any given region. Finally, some examples of how baseline monitoring has been used in the geothermal industry are described as well as a how microseismic monitoring can be used to monitor a fractured volume.

1.4 Task 2: Evaluation of Methodologies for the Monitoring of Ground Deformation That May Be Associated with UGEE Projects/Operations

This task outlines the radar data availability and presents the results of a study on the feasibility of InSAR for the island of Ireland using elevation and land cover data. The potential for this technique is highlighted by selected services across Europe e.g. PanGeo (http://www.pangeoproject.eu/) and results from ground monitoring studies such as at In Salah, with Mathieson (2010) stating that “perhaps the most valuable, and initially surprising, monitoring method so far has been the use of satellite based Interferometric synthetic aperture radar (InSAR) to detect subtle ground deformation”. As well as the regional coverage afforded by InSAR, the technique also benefits from an archive of data (from 1992) which can be used to gain a baseline of surface motion over a site where tiltmeters or GNSS were not already installed prior to operations. Since InSAR monitoring is generally applied to urban areas (due to the presence of abundant reflectors) this task also examines the application of this technique for monitoring potential ground deformation in non-urban areas of Ireland.

1.5 Task 3: Assessment of existing data on natural seismicity in the island of Ireland

This task provides an updated review of earthquakes in Ireland. Historical data from a number of available sources (e.g. Davison, 1924; Richardson, 1975) have been combined with modern instrumental data to construct a single coherent catalogue with a uniform moment magnitude scale. This catalogue was then

used to estimate the background rate of natural seismicity that represents a numerical expression of the expected likely future seismicity of the region and that is consistent with the expected low strain rates. However, given that Ireland is a low seismicity region and that data are sparse, the calculated activity rates significantly overestimate the observed seismicity. Finally, a stochastic modelling approach was used to explore possible ground motions for realistic examples of small to moderate earthquakes that might occur in Ireland, and compare these with some existing limits above which cosmetic damage may occur.

1.6 Task 4: Assessment of the Magnitude and Physical Effects of Induced Seismicity That May Be Associated with UGEE Projects/Operations in the Island of Ireland

There are few deterministic models that can accurately model fluid induced seismic events. Therefore, a new modelling approach was developed for both monitoring and short term forecasting of fluid induced seismic sequences. Uncertainty in forecasting was then highlighted in such non-linear process extremely complex environments to help develop a baseline for continuous monitoring.

State of the art developments in Coulomb Rate State (CRS) theory, together with Bayesian Monte Carlo (BMC) statistical methods was applied to model and forecast the triggered seismicity surrounding a hydraulic fracturing operation.

The theoretical background of the forecast model is described and a CRS based forecast implemented, given non-ideal baseline estimates. Forecasts are derived for a series of scenarios given different reference activity levels and baseline network qualities.

The implications for the nature of the uncertainties in the forecasts of increased activity or decreased M_c are illustrated.

1.7 Task 5: Technical Specification for Sub-regional Seismic Baseline Monitoring

The main goal of seismic baseline monitoring is to establish the rate of naturally occurring seismicity in an area. Any seismicity induced in the future can then be quantified by comparing the seismicity recorded during the operational phase with the baseline seismicity. In addition, a baseline study is useful to locate active faults and to map seismic noise levels in detail. The aim of this task is to answer two questions:

1. Is the detection threshold of existing seismic networks in Ireland sufficient to detect and to determine the location and magnitude of all local earthquakes with magnitudes ML ≥ 0.5 in the two study areas?

2. What kind of local seismic network is required if existing seismic networks in Ireland are insufficient for baseline monitoring of all local earthquakes with ML ≥ 0.5?

1.8 Tasks 6 and 7: Installation of Additional Monitoring Points and Baseline Monitoring

Baseline monitoring is frequently cited as a pre-condition for licensing of unconventional gas exploration and extraction (UGEE) activity. Therefore, the Terms of Reference and scope of work for the Joint Research Project (JRP) on the environmental impacts of UGEE identified a requirement to identify, evaluate and undertake appropriate potential baseline monitoring requirements for water, air and seismicity (earthquake activity). Requirements for baseline monitoring are embodied in the (2014/70/EU) EC Recommendation on minimum principles for the exploration and production of hydrocarbons (such as shale gas) using high-volume hydraulic fracturing, but a review of international literature provides relatively little on the specifics of baseline monitoring.

Following a comprehensive assessment of the two study areas and the existing provisions for monitoring, the JRP made proposals for baseline monitoring for the assessment of water and naturally occurring

seismicity, with a window of up to 2 years proposed to complete the aforementioned baseline monitoring programme. Consequently, such a baseline monitoring programme would result in the overall findings of the research being delivered after the project deadline of 2016.

The original timeline for the research envisaged that the entire programme, including water and seismicity baseline data acquisition, would conclude by 2016. The steering committee considered that, were the baseline acquisition to commence, the revised timeline for the overall research programme would now be to report in 2018 at the earliest. The decision was therefore taken to prepare an integrated synthesis report now, drawing together the conclusions of the research to date in order that these findings could be reviewed and policy decisions formulated with regard to the use of this technology in Ireland.

It is noted that the baseline monitoring programme proposed by the JRP remains valid and the report includes a recommendation that such a programme should be implemented in advance of the consideration of any application for a Petroleum Exploration Licence (Ireland) or an application to carry out high-volume hydraulic fracturing (Northern Ireland). It should be noted that such a baseline monitoring programme should provide independent information and is therefore different from any baseline characterisation and monitoring that would be required of UGEE operators as part of a licensing process, which would be project and site specific, and would be designed to monitor specific receptors.

1.9 Task 8: Examination of Global Experience of Seismic Events Stimulated by UGEE Operations

This task provides an extensive review of induced seismicity in UGEE operations, discussing examples of recent seismicity related to waste water disposal in the eastern United States. Where possible, available UGEE data from recent examples, such as the induced seismicity in Blackpool, UK, as well as data from other analogues is used to investigate the controlling factors on induced seismicity during fluid injection and examine the relationships between injection volume and pressure and induced seismicity. Finally, a number of measures are suggested for mitigating the risk of induced earthquakes, specifically for UGEE operations and for energy technologies in general.

1.10 Task 9: Assessment of Pre-fracturing Modelling Techniques

Fracturing generates microearthquakes. Tracking the location of these, using techniques from crustal seismology, therefore allows us to identify the volume surrounding a perforation which is experiencing fracturing. Each seismic event is extended in space so fractures generated by microearthquakes extend beyond the fractured volume by an amount which is related to the location of the event and the fracture length producing it. The length is related to the magnitude, so knowledge of the location and magnitude of seismicity allows us to estimate the likely maximum extent of fracturing from the perforation. This task surveys published data on microseismicity surrounding UGEE perforations and describes a stochastic approach which, assuming the distribution of event sizes from other wells, allows modelling of the formation of fractures from widely accepted empirical scaling relations. Results are presented for a synthetic scenario and added to the statistics of seismicity data from North America. However, the modelling parameters leading to these results should be updated in near-real-time during any fracking operation.

2 Definitions and Concepts

2.1 What and Where

Earthquakes are the result of sudden movement along faults within the Earth that releases stored up elastic strain energy in the form of seismic waves that propagate through the Earth and cause the ground surface to shake. Such movement on the faults is generally a response to long term deformation and build-up of stress, caused by processes such as plate tectonics. When this stress exceeds the static frictional stress that resists the motion of the rocks on either side of the fault, they slide or slip past each other.

The size of any earthquake depends on both the area of the fault that ruptures and also the amount of slip or displacement on the rupture plane. The larger the rupture area and the larger the displacement, the larger the earthquake. The largest earthquakes occur on ruptures that are many hundreds of kilometres long, with areas of several thousand square kilometres, and that have displacements of many metres.

Earthquake activity is greatest at the boundaries between the Earth's tectonic plates, where the differential movement of the plates results in repeated accumulation and release of strain. These include the margins of the Pacific and the collision zones between both India and Eurasia, and Africa and Eurasia. These are commonly referred to as *interplate* earthquakes. However, earthquakes can also occur within the plates far from the plate boundaries, and where strain rates are low. These are often referred to as *intraplate* earthquakes. Large areas of Asia, Australia, Europe and North America all experience intraplate earthquakes, although these events are relatively rare in comparison to seismicity rates at plate boundaries.

2.2 Measuring the Size of an Earthquake

Earthquake magnitude is a measure of the amount of energy released during an earthquake. A number of different magnitude scales have been developed generally based on the amplitude of different parts of the observed record of ground motion, often in a particular frequency range, and with specific corrections for distance. However, the most standard and reliable measure of earthquake size is moment magnitude, M_W, which is based on seismic moment, defined as

$$M_0 = \mu A D \qquad \text{Equation 2.1}$$

where μ is the modulus of rigidity of the faulted rock, A is the area of the rupture and D is the amount of slip on the rupture. Typical values for μ are 32 GPa in the crust and 75 GPa in mantle. Moment is therefore related to both the area of the rupture and the displacement on the rupture. Following Hanks and Kanamori (1979) seismic moment is related to the moment magnitude, M_w, by

$$M_W = \frac{2}{3}\log_{10} M_0 - 6.06 \qquad \text{Equation 2.2}$$

The scale is logarithmic so that each whole number increase in magnitude represents a tenfold increase in measured amplitude and about 32 times the energy released. Seismic moment is usually estimated directly from recordings of earthquake ground motions.

The first magnitude scale was developed by Richter (1935) using observations of earthquakes in Southern California and although the scale is only strictly applicable there, it has been used all around the world and is commonly referred to as Local Magnitude, M_L. Richter (1935) defined this as

$$M_L = \log_{10}\left(\frac{A}{A_0}\right) \qquad \text{Equation 2.3}$$

where A is the maximum deflection, zero to peak in millimetres registered by the earthquake on a Wood-Anderson seismograph, and A_0 is the deflection produced by a "standard" magnitude zero earthquake at the same distance. The A_0 factor allows observed amplitudes to account for decay between the seismograph and the epicentre of the earthquake.

Throughout this report we refer to both local and moment magnitude. Where we do so, we use the units M_L and M_W, respectively. M_L and M_W may be considered roughly equivalent for small earthquakes, although there may be small differences. These differences usually increase as magnitude increases. We also discuss earthquake magnitudes more generally and in these cases we may not always append a specific unit.

2.3 Behaviour in Space and Time

The relationship between the magnitude and number of earthquakes in a given region and time period generally takes an exponential form that is referred to as the Gutenberg-Richter (GR) law (Gutenberg and Richter, 1954), and is commonly expressed as

$$\log_{10} N = a - bM \qquad \text{Equation 2.4}$$

where, N is the number of earthquakes above a given magnitude M. The constant a, is a function of the total number of earthquakes in the sample and is known as the earthquake rate. This is commonly normalised over a period of time, such as a year. The constant b gives the proportion of large events to small ones, and is commonly referred to as the b-value. In general, b-values are close to unity. This means that for each unit increase in magnitude, the number of earthquakes reduces tenfold.

Although earthquakes occurrence can be modelled as a Poisson process, i.e. the probability of an earthquake at any given time is constant and independent of the time of the last event, they often occur in sequences that are clustered in space and time. The largest earthquake in such a sequence is known as the mainshock. The mainshock is followed by aftershocks, which occur due to readjustment to a new state of stress along the portion of a fault that slipped at the time of the mainshock. The pattern of the aftershock sequence depends on the size of the event and the local tectonic setting. Aftershock behaviour follows two well-known empirical laws: Omori's Law and its further modification by Utsu (1961) which states that the rate of aftershocks is inversely proportional to the time after the mainshock. The number of aftershocks is also observed to increase exponentially with the magnitude of the mainshock (Utsu scaling). Båth's Law (Båth, 1965) states that the difference in magnitude between the mainshock and the largest aftershock is approximately constant and independent of the mainshock magnitude, typically 1.1–1.2

Additionally, slip on one fault imparts stress into the surrounding rocks and on to other nearby faults. These stress changes can move faults closer to failure, leading to further triggered earthquakes which may be the same size or even larger. Both aftershocks and triggered earthquakes lead to earthquake activity that is clustered in space and time.

2.4 Types of Earthquakes Generated by Fracking

This section concentrates on earthquakes which result from the injection of high pressure fluid into the earth. This process can potentially generate two distinct populations of earthquakes which have different origins and present different hazard profiles. Firstly, as an essential part of the fracking process, cracks are generated in intact rock. These cracks increase the permeability of the rock, allowing trapped hydrocarbons to escape into a borehole and thence to the surface. Every new crack is essentially a brittle failure of the rock and, while the exact mechanism of the failure is different to a tectonic earthquake, the effect is similar; seismic waves are generated and travel outwards causing the ground surface to shake where they are incident on it. The energy for these events is almost entirely derived from the fluid injection process. Since this process is strictly limited in energy to the amount of energy contained in the high pressure fluid, then the largest earthquake that can be produced by this method is also strictly energy limited. To date it is

thought that the maximum magnitude for events generated by this process is approximately 3 M_L, though the largest earthquakes experienced in most fracking projects are considerably smaller.

High pressure fluid injected into a rock mass also deforms the mass and produces stress changes within it. If the rock mass contains pre-existing faults, which most rock does, these stress changes may make such faults fail. There are two processes which contribute to this. 1. Increasing the pore-fluid pressure on a fault plane effectively reduces the stress that stops it from sliding. This decrease in so-called normal stress can therefore induce earthquakes. 2. The deformation of the rock around the injection site changes the stress field for many hundreds of metres around the injection. This perturbed stress field, where it interacts with pre-existing faults can cause them to fail, generating an earthquake.

Since the energy for these events comes largely from forces stored in the rock mass prior to injection they do not have a well-defined maximum magnitude. Two important points must be made. Firstly, while increase in fluid pressure along the fault always makes it more likely to fail, stress perturbation can bring an existing fault closer to or farther from failure. Thus it is not certain even if a potentially active fault experiences a stress change as a result of fracking, that this fault will generate triggered earthquake. Secondly, the probability that such an event is triggered depends strongly on the prior activity of the area. Thus these events are very unlikely in areas such as Ireland where the background seismicity is extremely low.

We adopt, and will adhere to, a constant nomenclature for these events throughout this report. Events of the first type which are an essential part of rock fracturing which releases the sought after hydrocarbons we will call “Fracked” events. Those which are generated on pre-existing faults either by increased pore fluid pressure or by stress interaction we will call “triggered” events. We will refer to all earthquakes generated by the fracking operation as “induced” earthquakes. Thus fracked events are deliberately generated to increase permeability, they are an essential part of the fracking project, they have very high rates, but maximum magnitudes are probably limited to 3 ML. Triggered events on the other hand, are an unintended consequence of the fracking process, they are relatively infrequent but have no well-defined maximum magnitude.

2.5 Geographic and Tectonic Context

In the context of Plate Tectonics, earthquake activity is greatest at the boundaries between the Earth’s tectonic plates, where the differential movement of the plates results in repeated accumulation and release of strain. Plate boundary zones include the margins of the Pacific and the collision zones between both India and Eurasia, and Africa and Eurasia. However, earthquakes can also occur within the plates far from the plate boundaries, and where strain rates are low. Such earthquakes are often referred to as intraplate earthquakes. Large areas of Asia, Australia, Europe and North America all experience intraplate earthquakes, although these events are relatively rare in comparison to seismicity rates at plate boundaries.

Ireland lies on the northwest part of the Eurasian plate and at the northeast margin of the North Atlantic Ocean. The nearest plate boundary lies approximately 1,500 km to the northwest where the formation of new oceanic crust at the Mid-Atlantic ridge has resulted in a divergent plate boundary and significant earthquake activity. Around 2,000 km south, the collision between Africa and Eurasia has resulted in a diffuse plate boundary with intense earthquake activity throughout Greece, Italy and, to a lesser extent, North Africa. This activity extends North through Italy and Greece and into the Alps. The deformation arising from the collision between the African and European plates results in compression, commonly referred to as “Alpine compression”, that is generally directed in a north–south direction. The northeast margin of the North Atlantic Ocean is passive and is characterised by unusually low levels of seismic activity in comparison to other passive margins around the world.

As a result of this geographic position, Ireland is characterised by low levels of earthquake activity and low seismic hazard. Evidence for this comes from observations of earthquake activity dating back to the 14th century, which suggests that earthquakes felt by people are very rare.

Figure 2.1. Distribution of earthquakes with a magnitude of greater than 5 across Europe. The red line shows the margins of the Eurasian plate. The great majority of earthquake activity (black dots) is located at the southern margin in Greece and Italy along the collision zone between Africa and Eurasia.

3 Task 1: Assessment of Existing Baseline Monitoring Operated Worldwide for UGEE Projects/Operations

3.1 Introduction

It is well known that anthropogenic activity can result in man-made or "induced" earthquakes. Although such events are generally small in comparison to natural earthquakes, they are often perceptible at the surface and a small number have been quite large with magnitudes greater than 5 M_W. Underground mining, deep artificial water reservoirs, oil and gas extraction, geothermal power generation and waste disposal have all resulted in cases of induced seismicity. There are numerous examples of induced earthquakes in hydrocarbon fields related to oil and gas production (Suckale, 2010). These are often a response to long-term production, where the extraction-related subsidence is compensated by, for example, normal faulting on existing faults near or inside the reservoir (Van Eijs *et al*., 2006). Induced earthquakes with magnitudes as large as 3.5–4.0 are well documented in Enhanced Geothermal Systems (EGS) (Majer *et al*., 2007), where the injected volumes are relatively large and the reservoir rocks may be rather stronger than those of oil reservoirs. For example, McGarr (2014) uses a number of examples of earthquakes induced by hydraulic fracturing, disposal of waste water in wells and enhanced geothermal systems to suggest that the maximum magnitude of earthquakes related to fluid injection is related to both the total volume of injected fluid and the modulus of rigidity (a measure of strength) of the rockmass.

With this in mind, it is important to be able to discriminate between the naturally occurring, background levels of seismicity that are a response to long-term deformation from tectonic processes such as plate motions or secondary processes such as glacio-isostatic adjustment, and man-made seismicity resulting from industrial processes. However, this is not always a straightforward task, given that induced earthquakes often exhibit many of the characteristics of tectonic earthquakes. An essential part of the discrimination process in any region, is the establishment of accurate baselines for background earthquake activity, prior to the commencement of any activity that may induce earthquakes. This allows seismicity rates before, during and after to be reliably compared and any differences to be identified. Since background earthquake rates are controlled by tectonic processes such as first order plate motions, these should remain relatively stable over long periods of time (although they may occur in clusters), whereas rates of induced earthquakes are likely to vary more strongly with time. In addition, networks in place for regional monitoring are usually only reliable above a certain magnitude threshold, depending on the number and distribution of sensors in the network. In many cases this threshold is around magnitude 2.0. Reliable detection and location of earthquakes with lower magnitudes is only possible using a local monitoring network designed to detect and locate these events. This can help identify any seismogenic features, such as active faults, allowing them to be avoided during subsequent operations. Figure 3.1 shows the change in seismicity rate that has been observed in Eastern North America (Ellsworth, 2013). After decades of a steady earthquake rate (average of 21 events/year), the number of observed earthquakes began to increase around 2001, and peaked at 188 earthquakes in 2011. Induced seismicity caused by long term disposal of large volumes of waste fluid in deep boreholes is suspected to be partially responsible for the increase. A number of these earthquakes had magnitudes in excess of 4.0 and were widely felt. For example, the magnitude 4.0 M_W earthquake on 31 December 2011 in Youngstown, Ohio, appears to have been induced by injection of wastewater (Kim, 2013).

While microseismic monitoring for imaging stimulated volumes and fracture networks is now standard practice in unconventional gas exploration and extraction (e.g. Rutledge and Phillips, 2003), baseline monitoring prior to operations is not. However, this seems likely to change. Induced earthquakes during hydraulic fracturing operations in the Etsho and Kiwigana fields in Horn River, Canada, resulted in over 200 detected earthquakes during 2009–2011 (BC Oil and Gas Commission, 2012). The largest event had a magnitude of 3.8 M_L and, to date, this is the largest known earthquake induced by hydraulic fracture

operations in a hydrocarbon field anywhere in the world. In Lancashire, UK, 58 earthquakes were linked to fluid injection during hydraulic fracturing of a shale gas reservoir in the Bowland basin at the Preese Hall well in 2011 (de Pater and Baisch, 2011). The largest had a magnitude of 2.3 M_L and was felt locally. The earthquake activity resulted in a UK-wide suspension of fracking activity and considerable public concern about the impacts of fracking. The BC Oil and Gas Commission (2012) recommended that the accuracy of the Canadian National Seismograph Network in northeast B.C. needed to be improved and that additional ground motion sensors should be installed in affected communities to quantify risk from ground motion. In the UK a series of recommendations by Green *et al*. (2012) led to a number of non-legislative regulatory measures, requiring operators to review the available information on faults in the area of proposed wells to minimise the risk of activating any fault by fracking, and also to monitor background seismicity before operations commence. A review by the Royal Society and the Royal Academy of Engineering (2012) into the risks associated with hydraulic fracturing suggested that monitoring should be carried out before, during and after shale gas operations to inform risk assessments.

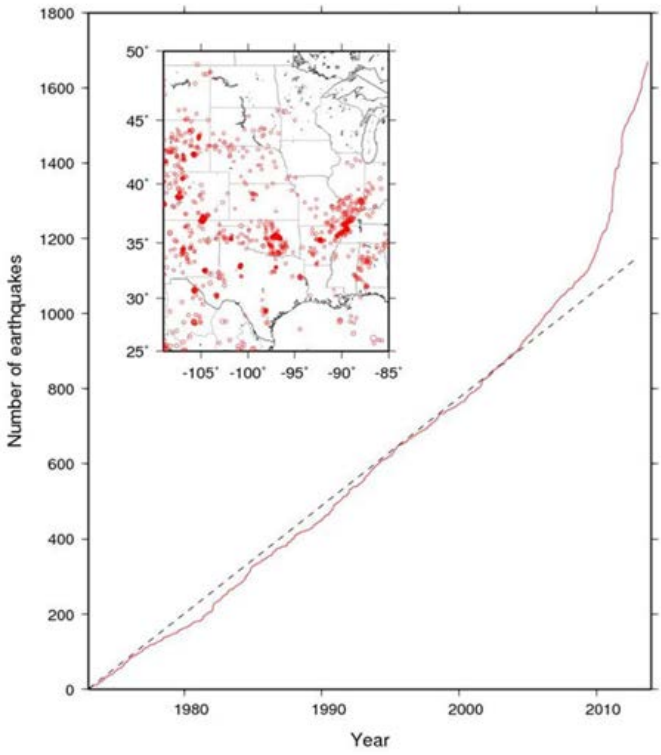

Figure 3.1. Cumulative count of earthquakes with M ≥ 3 in the central and eastern United States, 1967–2012 (from Ellsworth, 2013). Reproduced with permission from the American Association for the Advancement of Science.

3.2 Earthquake Frequency Magnitude Relationship

The relationship between the magnitude and number of earthquakes in a given region and time period generally takes an exponential form that is referred to as the Gutenberg-Richter law (Gutenberg and Richter, 1954), and is commonly expressed as

$$\log_{10} N = a - bM \qquad \text{Equation 3.1}$$

Where, *N* is the number of earthquakes above a given magnitude *M*. The constant *a,* is a function of the total number of earthquakes in the sample and is known as the earthquake rate. This is commonly normalised over a period of time, such as a year. The constant *b* gives the proportion of large events to small ones, and is commonly referred to as the *b*-value. In general, *b*-values are close to unity. This means that for each unit increase in magnitude, the number of earthquakes reduces tenfold. Plotting earthquake

magnitudes against the logarithm of frequency gives a straight line (Figure 3.2a) where the slope of the line is the *b*-value (and determines the relative number of earthquakes of different magnitudes) and the rate, *a*, is the value where the line intersects with the Y-axis at magnitude zero.

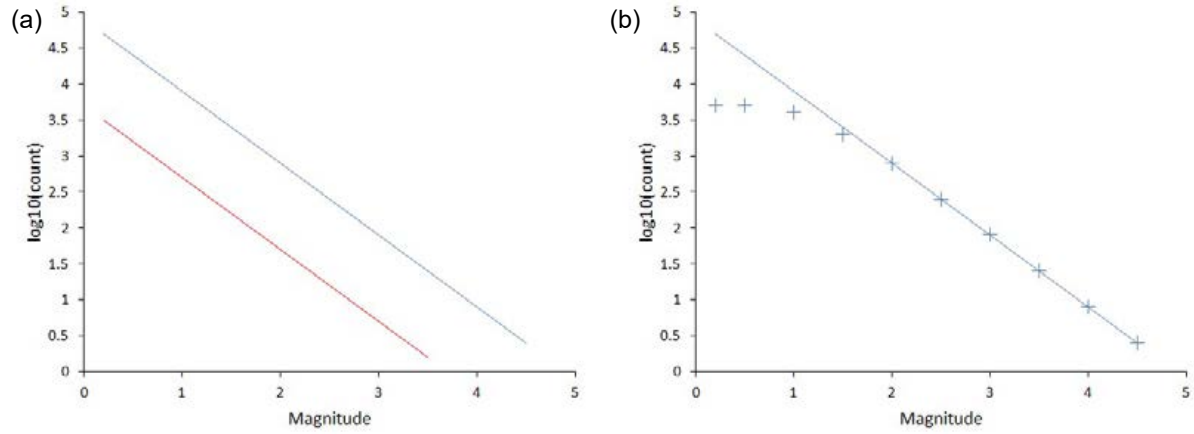

Figure 3.2. The cumulative number of earthquakes above a given magnitude plotted against magnitude. (a) shows an exponential distribution leading to the Gutenberg-Richter law. Two different activity rates are shown by the blue and red lines. An observed roll-off in the number of earthquakes at low magnitudes shown by the blue crosses in (b) is typically seen due to inability of regional seismic networks to detect small earthquakes.

The rate parameter varies from place to place, such that an active region will have a higher value of than a less active region. Two different rates are shown by the red and blue lines in Figure 3.2a, with the red line corresponding to a lower rate of activity. Also, in a region of homogeneous seismicity, the value of the rate parameter in any sub-region scales with relative size of the two regions. For example, a region where seismicity is homogeneous and $a = 3$, will have 1000 earthquakes above a magnitude of zero each year. A sub-region, whose area is ten times smaller will have $a = 2$, i.e. 100 earthquakes above a magnitude of zero each year. This has important implications for baseline monitoring in small regions, particularly where activity rates are low, since the number of earthquakes in a given period of time may be very low, so longer durations of baseline monitoring are required to reliably determine seismicity rates. It is sometimes assumed that baseline monitoring for a few months may be sufficient to characterise seismicity, however, this will depend on activity rate and also the detection capability of the monitoring network. The recent SHARE project (Giardini *et al*., 2013) determined a rate parameter for the source zone containing Ireland of $a = 2.1756$, i.e. approximately 150 earthquakes with a magnitude above zero each year and three earthquakes with a magnitude of 2 or above every two years. Note that a magnitude of 2 is around the threshold above which an earthquake might commonly be felt by people. Figure 3.3 shows the extent of this source zone, with an approximate area of 300,000 km^2, since it extends offshore. The two study areas for this project are also shown in Figure 3.3. The larger of the two study areas has an area of approximately 2,200 km^2, at least 100 times smaller than the entire source zone. Therefore, assuming that seismicity is homogeneous and given an appropriate detection capability, we might only expect to record three earthquakes with a magnitude of 0 or above every two years and an earthquake with a magnitude of 2 or greater roughly every 60 years. There will be even fewer earthquakes in the smaller study area. Such low expected seismicity rates presents a significant challenge for this project, since it may require many decades of baseline monitoring to reliably determine the rates for each area, if the levels of natural seismicity are as low as expected from the available historical and instrumentally recorded data. However, seismicity may not necessarily be homogenous across Ireland, therefore detailed monitoring will be required in each study area to detect any earthquake activity that might suggest that seismicity rates are higher than expected, or to determine if there is seismicity associated with any specific fault structure.

The detection capability of any seismic network is a complex function of many factors including the distribution, density and characteristics of individual stations, their local site and noise conditions, as well as

processing software and processing strategies. The amplitude of the ground motions caused by any earthquake is a function of both the magnitude of the earthquake and the distance of the earthquake from the recording position. An event may be undetected because it is too small or too distant, so its signal is indistinguishable from the background noise on the seismograph. Also, many detection algorithms require the signal from an event to exceed the background noise level by a certain ratio on a number of stations for an event to be detected. If the station density is low, this will only happen for larger events. The detection of small earthquakes thus requires relatively high station densities.

Seismic moment, M_0, is a physical measure of the size of an earthquake and, following Hanks and Kanamori (1979) is related to the moment magnitude, M_w, by

$$M_W = \frac{2}{3} \log M_0 - 6 \qquad \text{Equation 3.2}$$

The low frequency level, Ω_0 of the far-field displacement amplitude spectrum of a P- or S-wave is related to the seismic moment by (Keilis-Borok, 1960)

$$M_0 = \frac{4\,\pi\,\rho_0\,v_0^3\,r\,\Omega_0}{R_c\,F_c} \qquad \text{Equation 3.3}$$

Where ρ_0 is the density of the rocks at the source, v_0 is the seismic velocity of the rocks at the source, r is the distance from the source and R_c is a correction factor for the *P*- or *S*-wave radiation factor and F_c is a correction factor for free surface amplification. In addition, the Brune (1970) source model for the amplitude spectrum gives

$$\Omega\,(f) = \frac{\Omega_0\,e^{-(\pi f \frac{t}{Q})}\,e^{-\pi f \kappa}}{1 + \left(\frac{f}{f_c}\right)^2} \qquad \text{Equation 3.4}$$

Where Q is the quality factor to account for anelastic attenuation, κ is the site attenuation and f_c is the corner frequency in the source spectrum.

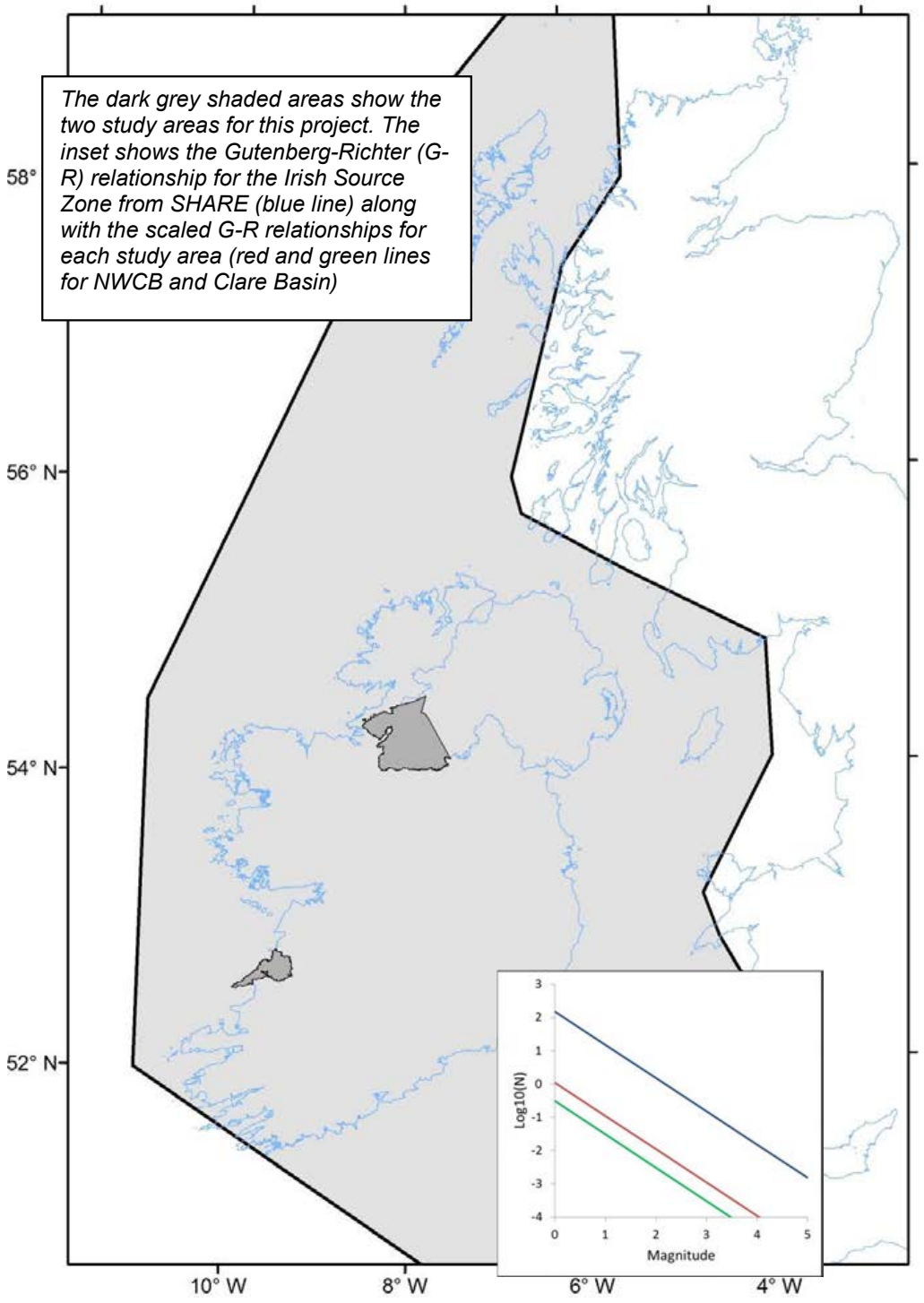

Figure 3.3. The source zone for Ireland (light grey areas) used in the recent SHARE seismic hazard project (from Giardini *et al.*, 2013).

These three equations give us a relatively simple means to model the amplitude of seismic waves as a function of magnitude and distance. Combining this with a given station density and estimates of seismic noise at each station, we can calculate a theoretical detection capability for a given network of stations. Figure 3.4 shows the variation in the magnitude of earthquakes that would be detected by a network of eight sensors in a 100 km by 100 km region, where a signal in excess of three times the noise level needs to be recorded on at least three sensors for an earthquake to be detected. Noise levels at each station vary in this example, but are similar to the Peterson (1993) high noise model. A more uniform distribution of stations may be preferred, but this may not always be possible for logistical reasons, so a rather more

irregular distribution is used in this model. The amplitude of the signal was based on an octave bandwidth centred on the earthquake corner frequency. In this case, the L_g wave quality factor determined for the UK by Sargeant and Ottemöller (2009) is used, along with a site attenuation factor of κ = 0.01 to model frequency dependent attenuation.

At the centre of the network, where the station spacing is 10–20 km, it is possible to detect earthquakes with magnitudes as low as 0.5 M_W. Further from the centre, only larger magnitudes can be detected. This demonstrates that station density must be reasonably uniform in order to achieve a uniform detection capability, and that higher station densities will allow detection of smaller earthquakes. Noise levels at each station should also be similar. A monitoring network must also extend beyond the limits of the area of interest in order to be able to reliably detect earthquakes that occur close to these limits.

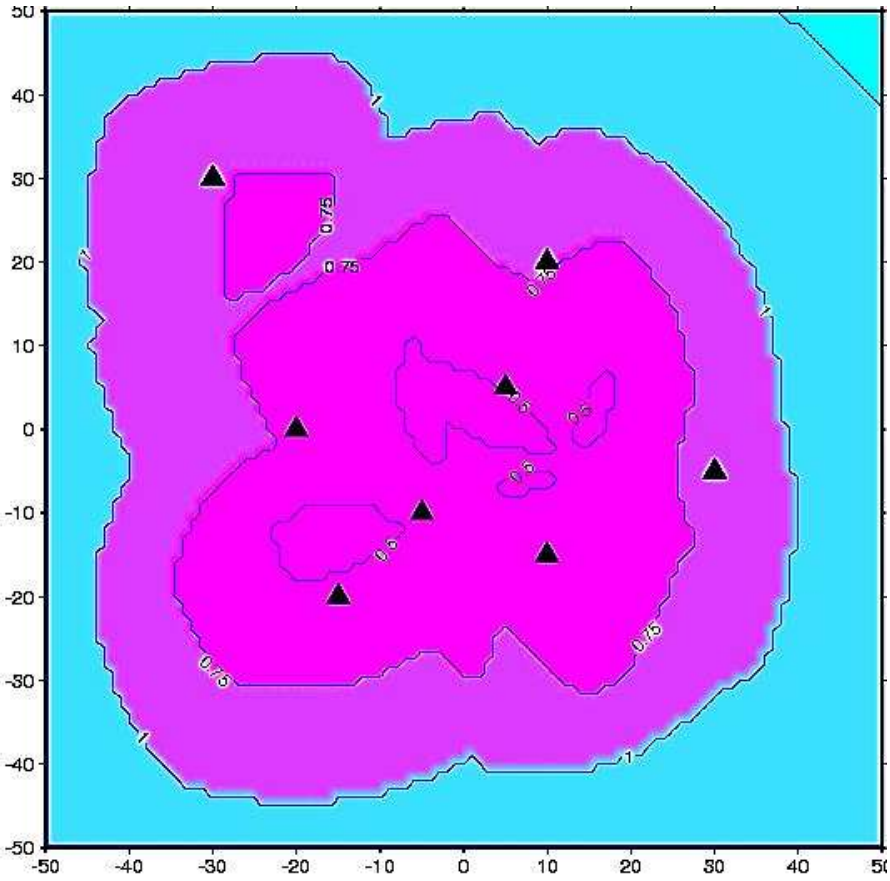

Figure 3.4. Modelled detection capability for a network of sensors (black triangles) within a 100 km by 100 km area.

While signal levels in excess of three times the noise level recorded at three stations may be enough to detect an earthquake, it is generally not sufficient to reliable determine the location or magnitude of the earthquake. For this, we need signals in excess of three times the noise level at five or more stations. The effect of this on the magnitude of detection is shown in Figure 3.5. Whereas in Figure 3.4 earthquakes with magnitudes as low as 0.5 M_W could be detected, earthquakes of this size can no longer be detected when the required number of stations increases to five. The minimum magnitude that can be detected is now 0.75. M_W. This suggests higher station densities are required for reliable earthquake location than for detection alone.

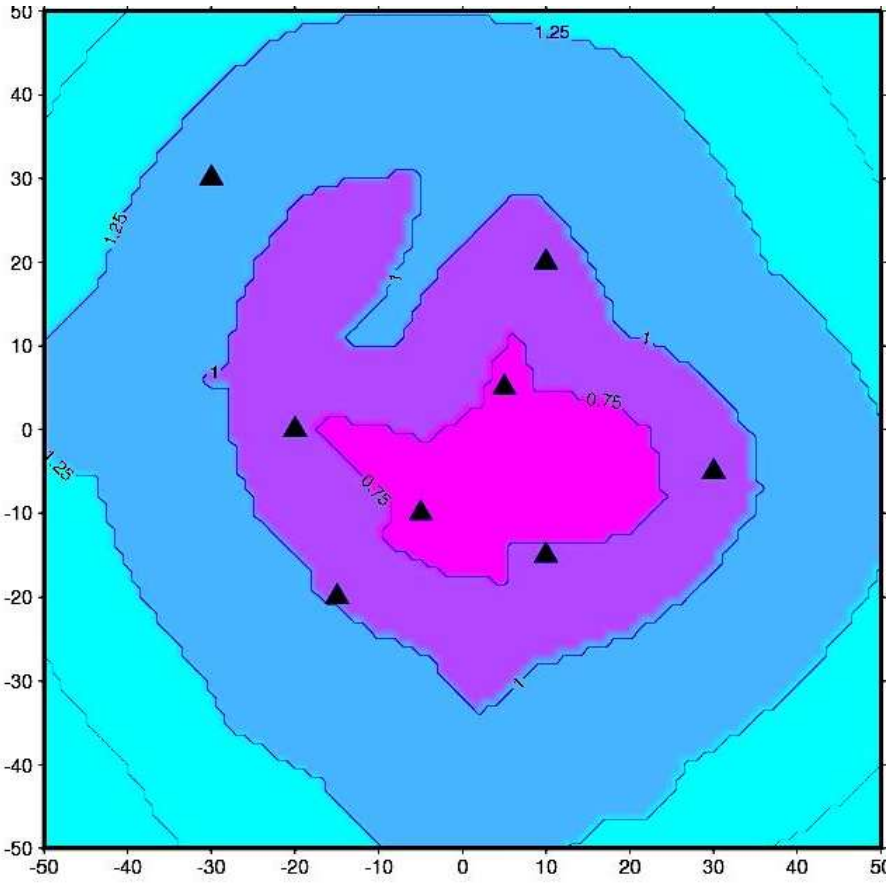

Figure 3.5. Modelled detection capability for a network of sensors (black triangles) within a 100 km by 100 km area, showing the spatial variation in magnitudes that can be detected.

3.3 Earthquake Location

An impulsive source of seismic energy can be thought of as a point source in time and space, defined by an origin time (t_0) and hypocentre (x_0, y_0, z_0), respectively. The travel time of a seismic wave propagating away from such a source will depend on the distance from the source and the velocity of the medium, and, in general, will increase with distance from the source. Measured arrival times at different points can be used to estimate the location of the seismic event. The problem of estimating source location from travel time data has been extensively studied in earthquake seismology and numerous algorithms of this type have been developed and are in widespread use. Given observations of arrival times at a number of points we can compute predicted travel times to the same points by assuming a reference velocity model. We can then try to minimise the difference between the observed and modelled travel times and estimate the best fitting location for the event. Although the travel-times are not linearly dependent on the earthquake location, the problem can be linearized by considering only small perturbations from an initial target location. Iterative, linearized methods are largely based on the method of Geiger (1912) and solve the problem using partial derivatives and matrix inversion. These usually converge rapidly unless the data are badly configured or the initial guess is very far away from the mathematically best solution. Nonlinear methods (e.g. Lomax *et al.*, 2000) solve the earthquake location problem by sampling the full solution space. They have the advantage of obtaining a more complete solution with uncertainties as compared to the linearized methods and do not rely on the quality of an initial guess.

Uncertainties in earthquake locations are dominated by three factors (Pavlis, 1986): (1) measurement errors of seismic arrival times; (2) modelling errors of calculated travel times; and (3), nonlinearity of the earthquake location problem. Measurement errors may arise because it is difficult to clearly identify the arrival time of the seismic phase because the signal is small and cannot clearly be discriminated from the

noise. Assuming that the measurement errors are normally distributed, confidence regions may be computed. The size of the confidence regions depends on the variance and is commonly computed using either the F-statistic (e.g. Flinn, 1965) or the χ^2 statistic (Evernden, 1969). The orientation of the error ellipsoid depends on both the number and geometry of the recording stations. For example, a single line of recording stations will result in significantly larger errors in the direction perpendicular to the line than along the line. When designing an experiment, it is important to position recording stations around the expected source location to get good azimuthal coverage. It is also important to have sufficient stations close to the expected location to constrain the depth of the events.

There are a number of "rules of thumb" that are commonly required to obtain well constrained earthquake locations. For example, at least eight travel time arrivals should be used, including at least one S-wave arrival, and at least one arrival from a station within a focal depth's distance from the epicentre. Also, the largest azimuthal gap between two stations should not exceed 180°. S-wave arrivals within 1.4 focal depth's distance from the epicentre provide significant constraint on the focal depth.

To further examine location capability, theoretical travel times were calculated for a source at a depth of 10 km in the centre of a 100 km by 100 km region recorded by the same eight stations shown in Figure 3.4. The travel times were calculated using a 1-D velocity model in which velocity was a function of depth only, and consisted of three layers representing the upper, mid and lower Crust. These data were used to calculate arrival time data that was used to locate the event with NonLinLoc, a probabilistic, non-linear, global-search earthquake location algorithm (Lomax *et al*., 2009). Gaussian noise, with a mean error of 0.1 seconds was added to the theoretical arrival times.

Figure 3.6 shows the location calculated using only the predicted P-wave arrival times from all eight stations. The red dots show density-scatter representing the geometrical properties of the location probability distribution function, where regions with a higher probability of containing the earthquake have a higher number of samples. The blue star gives the maximum likelihood location. The calculated location is less than 100 m from the true location. The location is also well constrained with an epicentre error range of only 1–2 km. The depth error is slightly larger, approximately 5 km, but remains well constrained.

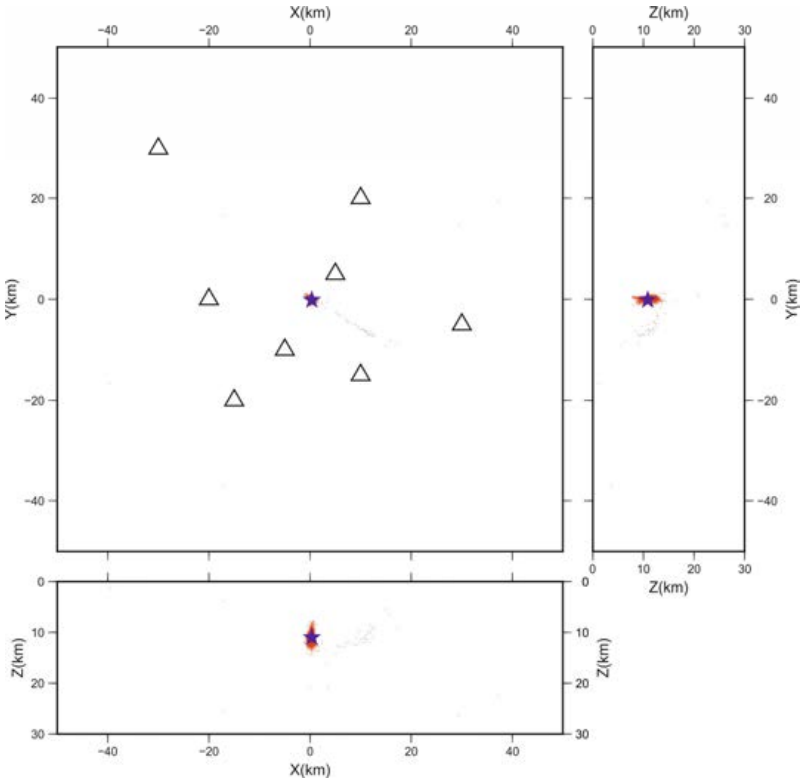

Figure 3.6. Location calculated at a depth of 10 km in the centre of a 100 km by 100 km grid.

The effect of reducing the number of P-wave arrivals used to locate the earthquake is shown in Figure 3.7. In this case, P-wave travel times for five stations were used. The calculated epicentre is only slightly further (less than 2 km) from the true epicentre. However, the fact that most of the stations are a similar distance from the source and that there are no stations within a focal depth of the source, has a dramatic effect on the calculation of depth. The calculated depth is 26 km and the scatter in the probable solutions extends to the surface, demonstrating that the depth is very poorly resolved. A real example of this problem can be found in the case of the earthquake activity induced by hydraulic fracturing near Blackpool, UK in April 2011. The closest station that recorded the largest event was at a distance of around 80 km from the epicentre, with a number of other stations at a similar distance but different azimuths. Although the epicentre was relatively well constrained, the depth was very poorly constrained, which meant that the events could not be conclusively linked to the hydraulic fracture operations at the time.

Finally, the location capability for an event outside the network is shown in Figure 3.8. The modelled earthquake is at a depth of 10 km and offset from the centre of the grid by a distance of 40 km in the X direction and 30 km in the Y direction. P-wave travel-times calculated for all eight stations shown by the triangles were used to determine the location. The calculated epicentre is approximately 1 km from the true location, however, the calculated depth of 2 km is significantly different from the true depth. In addition, there is a large scatter in both epicentre and depth. The uncertainty in the epicentre is stretched out in the northeast-southwest direction, as a result of the geometry of the recording stations and the fact that the largest azimuthal gap is greater than 270°.

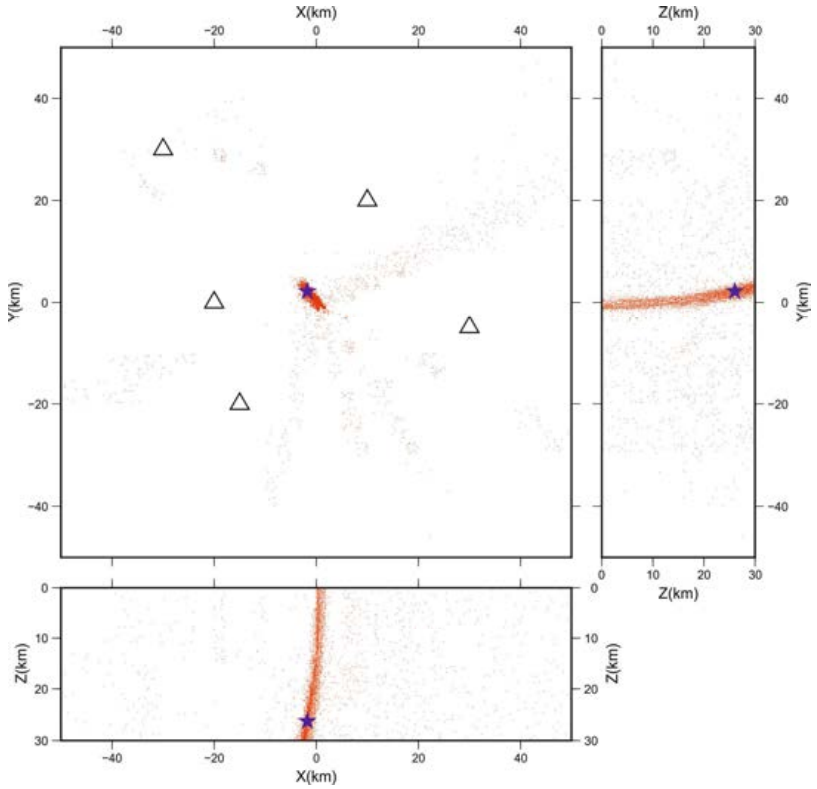

Figure 3.7. Location calculated at a depth of 10 km in the centre of a 100 km by 100 km grid.

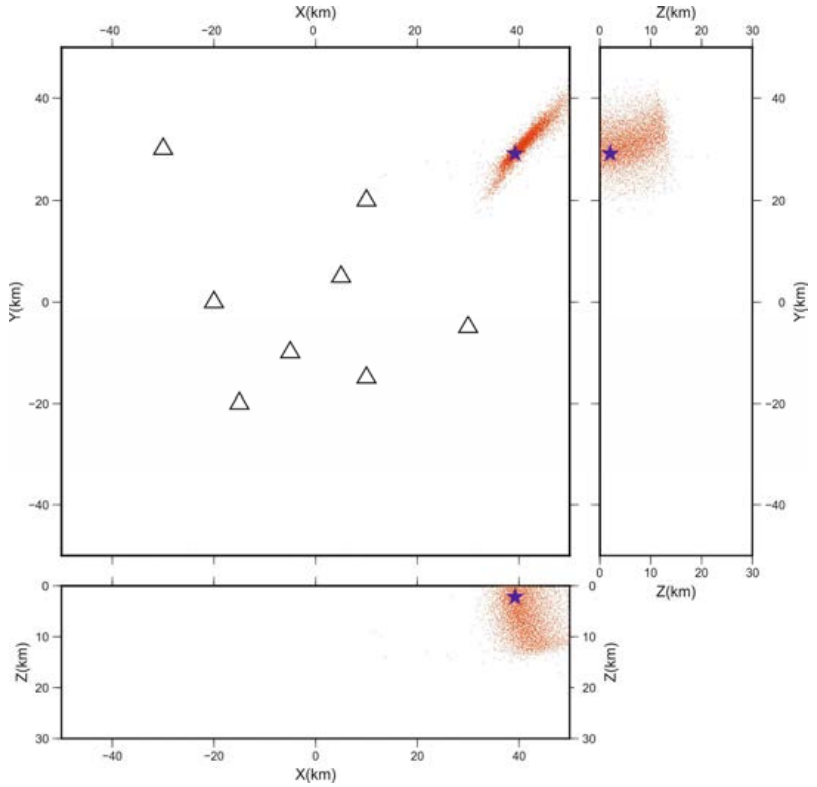

Figure 3.8. Location calculated at a depth of 10km offset from the centre of a 100 km by 100 km grid, by a distance of 40 km in the X direction and 30 km in the Y direction.

These simple examples demonstrate how location capability is a complex function of station distribution and density. In order to reliably locate earthquakes and reduce the uncertainty in location estimates it is necessary to be able to measure arrival times on a relatively large number of stations, some of which need

to be close to the epicentre in order to constrain focal depth. In addition, to provide a uniform location capability within a given region, a network of stations must extend beyond the region itself, otherwise, the capability to locate earthquakes at the edges of the monitored region will be compromised.

3.4 Borehole Sensors

Ambient seismic noise from both natural and cultural sources propagates mainly as high-frequency surface waves (>1–10 Hz, 1–0.1 sec) that attenuate rapidly as a function of depth. In addition, the effects of the free-surface, near-surface velocity gradients, and low impedance surface layers all have a significant influence on seismic waves recorded at the surface of the Earth. Research has shown that installing sensors in boreholes significantly improves signal-to-noise ratios, which is critical for both recording of high quality data and the detection and measurement of small earthquakes. For example, Shearer and Orcutt (1987) compared borehole and surface recordings of both seismic refraction shots and earthquakes in the southwest Pacific, finding that the borehole seismometer had significantly better signal-to-noise advantage over the surface instruments. Borehole arrays are likely to offer significantly better performance than surface instruments and such arrays have become standard practice for the operational phase of many geothermal projects (Majer *et al*., 2007) and also for microseismic monitoring in the UGEE operations (Rutledge *et al*., 2004). Note, however that the aim of this study is to characterise semi regional baseline monitoring rather than project specific operational monitoring.

3.5 Baseline Monitoring in the Geothermal Industry

Seismic monitoring is used widely in the geothermal industry before, during and after EGS operations, although it should be noted that the aim of this study is solely to characterise the background natural seismicity in the study areas. For example, during EGS operations, it can be used to image the stimulated volume and effectively manage geothermal reservoirs (Majer *et al*., 2007). Moreover, the risk of felt earthquakes means that seismic data is also essential for forecasting induced seismicity and mitigating the risk of potentially damaging events. Experience suggests that a reliable measurement of seismicity at low magnitudes (M 0 to 1) is needed for many geothermal projects to enable active seismic zones to be properly identified. Also, since most geothermal induced seismicity is below magnitudes of about 2.0, it is important to know the baseline level of seismicity at the lower magnitudes. Majer *et al*. (2012) make the following four recommendations for baseline monitoring in the geothermal industry.

1. Monitoring needs to fully characterise background seismic activity and identify any faults with the potential to be affected by operations, and should not be biased in time or space in the vicinity of the potential geothermal project The duration of the background monitoring may be relatively short (one month) if there is already existing monitoring that can detect small earthquakes with magnitude around 1. If there is no existing monitoring, the duration may need to be extended for as long as six months;

2. High resolution instrumentation will allow induced activity to be modelled and forecast more accurately. As the induced earthquakes may span several orders of magnitude, say from –2 to 4, the monitoring system requires a high dynamic range to ensure that data of sufficient quality is recorded. Also, borehole installations are better than surface sensors as the signal-to-noise ratio is better, and this allows smaller events to be recorded, increasing resolution and location capability. The monitoring network should be able to provide comprehensive background monitoring over an area at least twice as large as the area of geothermal potential;

3. Data processing must provide locations, magnitudes and source mechanisms. A typical geothermal project, consisting of one or two injection wells and several production wells in an area with a diameter of 5 km, will require at least eight monitoring stations distributed over the area of interest; and

4. Monitoring should be maintained throughout the injection activity to validate the engineering design of the injection in terms of fluid movement directions, and to guide the operators on optimal injection volumes and rates. This will also allow induced events to be discriminated from natural seismicity and ensure that local vibration guidelines are being followed.

Site specific monitoring systems in the geothermal industry often consist of several three-component sensors (geophones or accelerometers) installed in boreholes surrounding the volume of rock to be stimulated, at distances of 100 m to 10 km from the injection well. The sensors are generally placed at a range of depths (~100 - 2000m) and sensors at greater depths designed to withstand high temperatures and pressures. These are linked to a near real-time data acquisition and processing system that automatically detects events and determines locations and magnitudes. The monitoring array used for a project in the Cooper Basin, Australia in 2003 consisted of eight, three component geophones installed in boreholes around the central injection well, at depths of 88 to 1793 m. The recording system recorded over 11,000 located events during stimulation between 30 November and 9 December 2003. The largest event had a magnitude of 3.7 M_W and saturated the recording system (Majer *et al*., 2007).

3.6 Monitoring Case Studies

3.6.1 The Hot Dry Rock Project, Cornwall, UK

The Hot Dry Rock (HDR) project was a geothermal research project designed to test the feasibility of extracting geothermal energy from the Carnmenellis granite in Cornwall by circulating water between deep boreholes (Parker, 1989). The experiments were conducted at Rosemanowes quarry between 1982 and 1991. A historical earthquake study of Cornwall and Devon by Musson (1989) identified some 41 felt seismic disturbances within a 25 km radius of the HDR site in the period 1750 to 1988. The British Geological Survey carried out background seismic monitoring around the site starting in 1981, one year before the start of injection (Walker, 1987), and this continued until the end of the project in 1991.The monitoring network, Figure 3.9, consisted of three seismometers up to 30 km from the site, a further six seismometers within a 9 km range, and a seismometer at the site itself. The network was capable of detecting any earthquake with a magnitude of 0.0 M_L or above within approximately 20 km of the HDR site.

Several hundreds of natural background earthquakes were detected using this network before, during and after the project, many of which could have otherwise been attributed to the project itself. On 25 February 1981, only a few days after the installation of the network, a series of almost 200 earthquakes was detected immediately to the south of the HDR site, around the village of Constantine. The largest had a magnitude of 3.5 M_L and was widely felt by people in the area. This activity continued over the following years, with a further magnitude 2.9 M_L earthquake on 2 September 1986.

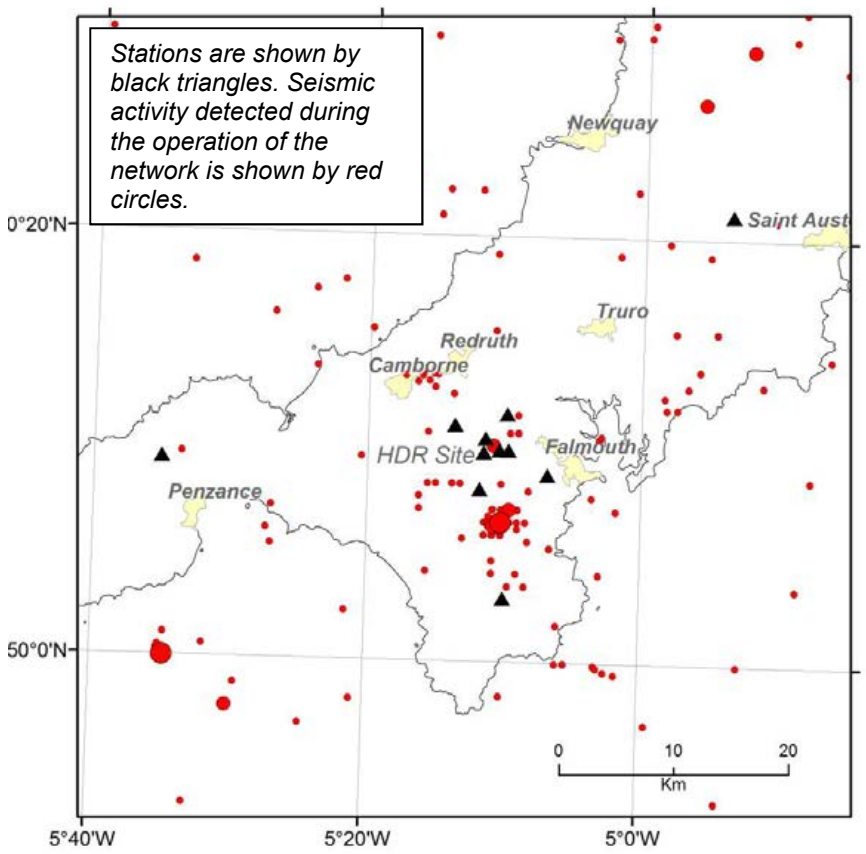

Figure 3.9. The seismic monitoring network around the HDR site at Rosemanowes.

Fluid injection at the site started in 1982, and went on to generate over 11,000 induced events between 1982 and 1987 (Baria and Green, 1990). Most of these were very small and could only be detected by a separate network of borehole geophones installed at the site. However, a number of these were also detected by the background monitoring network. The largest induced event occurred on 12 July, 1987, had a magnitude of 2.0 M_L, and was felt locally.

3.6.2 Basel, Switzerland

Background seismic monitoring for the Basel Deep Heat Mining EGS project began in early 2006, many months before stimulation of the reservoir began in December that year. The monitoring system consisted of six borehole seismometers installed near the injection well and up to 30 seismic surface stations in the Basel area (Häring *et al*., 2008). There was also a contingency shutdown plan in case of felt earthquakes.

Stimulation of the reservoir was accompanied by significant increase in the number of seismic events and injection was stopped on December 8 after earthquakes with magnitudes of 2.6 and 2.7 were recorded. During this injection period, approximately 11,500 m^3 of water were injected (Deichmann and Giardini, 2009) and more than 10,500 seismic events were recorded (Häring *et al*., 2008). While the well was shut-in (operations terminated), seismic activity continued, so it was decided to “bleed off” the pressure (reduce pressure through controlled release). On December 8, an earthquake of M 3.4 occurred in Basel and was clearly felt by the local population. This was followed by three more events greater than M 3.0. The project was immediately suspended and then ultimately abandoned almost 3 years later following further study and risk evaluation after these seismic events (Giardini, 2009).

3.6.3 Earthquakes induced by hydraulic fracturing operations near Blackpool, UK

On 1 April an earthquake with a magnitude of 2.3 M_L was detected in the Blackpool area of the UK. The earthquake was felt by a number of people in the area with a maximum intensity of 4 EMS. Since this

earthquake was subsequently directly linked to hydraulic fracturing operations, this example highlights a number of important considerations for seismic monitoring both before and during future operations elsewhere. The earthquake occurred in an area of low seismicity even for the UK, with few recorded earthquakes in the immediate vicinity of Blackpool. Figure 3.10 shows both instrumentally recorded (red circles) and historical earthquakes (yellow circles) from the British Geological Survey catalogue in a 100 km square centred on the epicentre of the 2011 earthquake. The largest recorded earthquake in the region was a magnitude 4.4 earthquake near Lancaster in 1835 with a maximum intensity of 6 EMS. However, there are roughly 20 earthquakes of this size or greater somewhere in the UK each year, and small earthquakes in areas where there has been little other earthquake activity are not completely unprecedented.

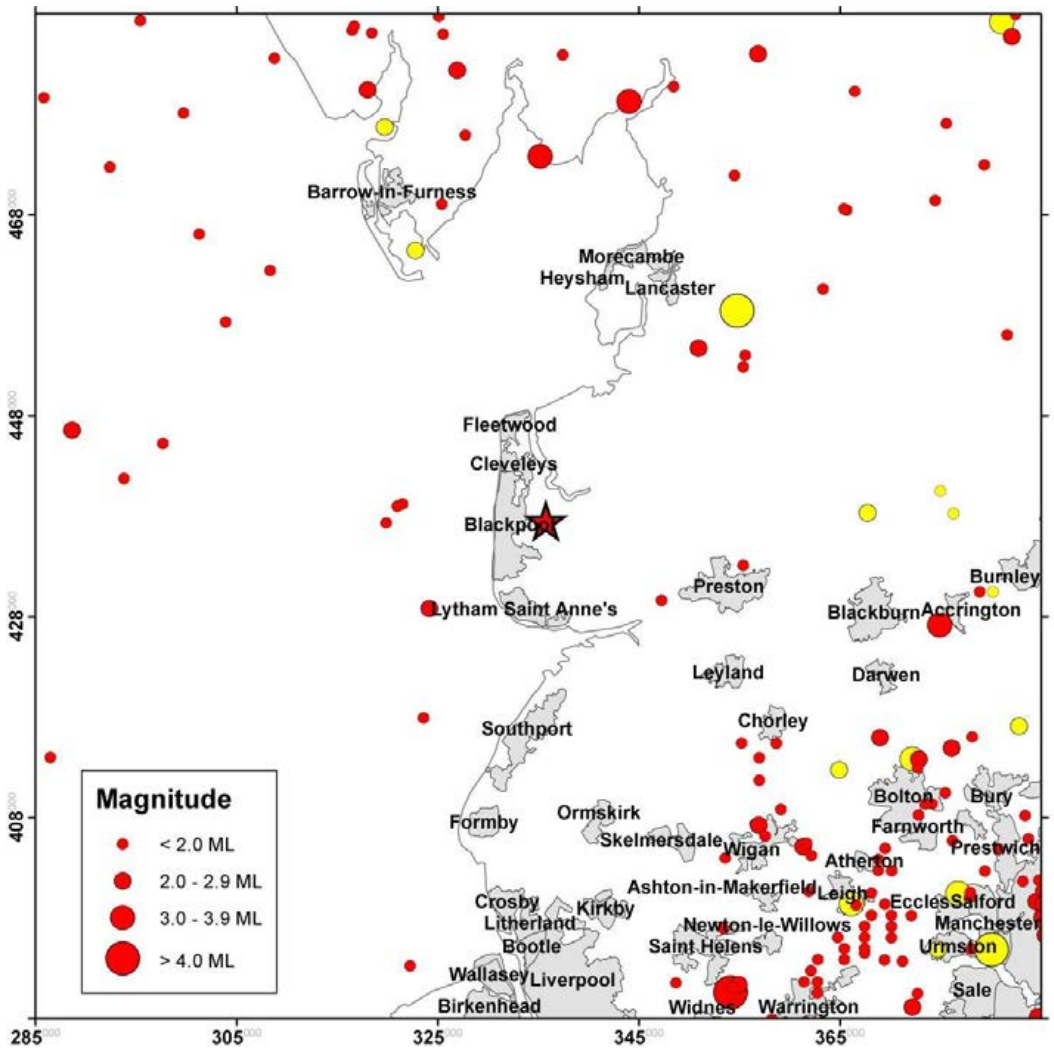

Figure 3.10. Instrumentally recorded earthquakes (red circles) from 1970 to present and historical earthquakes (yellow circles) prior to 1970.

Nevertheless, the proximity of the epicentre to the site of ongoing hydraulic fracturing operations during exploration of a shale gas reservoir in the Bowland basin by Cuadrilla Resources Ltd. led to immediate speculation that the earthquake was linked to this. However, the closest seismometer to the site was approximately 75 km away, and although the calculated epicentre was less than 2 km northwest of the drill site, uncertainties in the location, particularly the depth were large, making it difficult to conclusively link the earthquake with operations at the Preese Hall drill site. Figure 3.11 shows the earthquake location calculated using the NonLinLoc non-linear earthquake location algorithm (Lomax *et al*., 2009) with 36 phase arrivals from 25 stations. The scatter in the location probability distribution function (red dots), extends approximately 4 km in the horizontal plane and 5 km in the vertical plane. It should be noted

retrospectively, that the earthquake still met a number of the criteria set out by Davis and Frohlich (1993) for earthquakes induced by fluid injection. For example, the earthquake occurred only a few hours after fracking operations stopped, with an epicentre within 5 km of the injection well and at a depth near the injection depth.

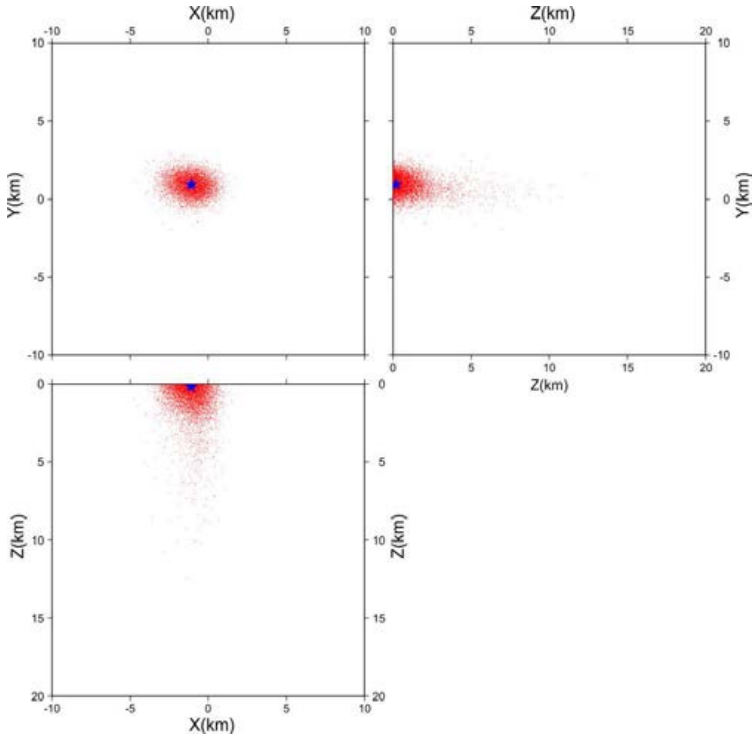

Figure 3.11. Location calculated using NonLinLoc for the earthquake on 1 April 2011.

In May 2011, the British Geological Survey installed two seismometers close to the Preese Hall site. A further earthquake with a magnitude of 1.5 M_L occurred on 27 May 2011, and again this was felt locally. Data from the nearby stations helped to reduce the uncertainty in location estimates (Figure 3.12) providing more conclusive evidence that the earthquakes were linked to the hydraulic fracturing. In addition, a number of other smaller earthquakes were also detected on 26 and 27 May while hydraulic fracturing was ongoing, and, as a result, operations were suspended at Preese Hall pending further investigation.

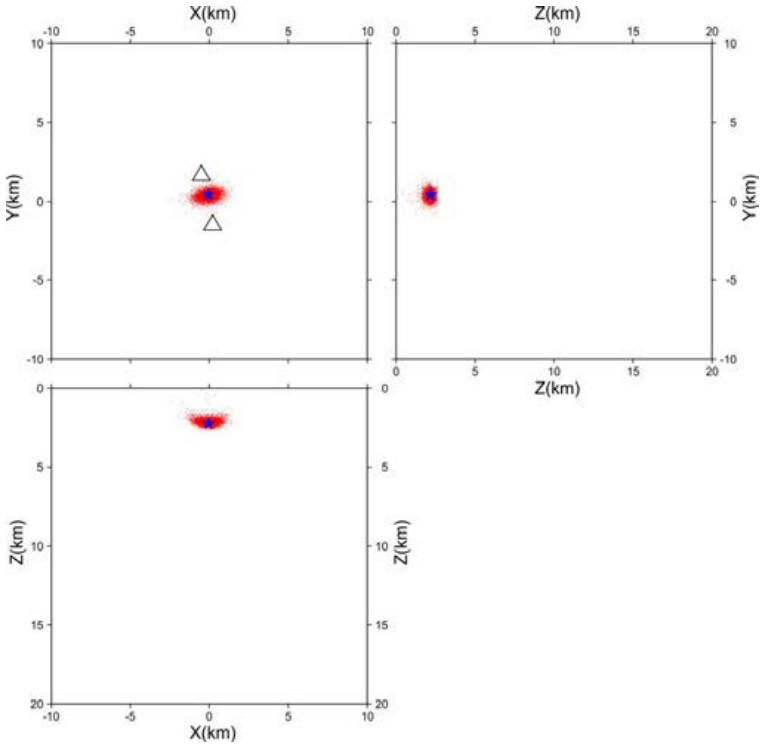

Figure 3.12. Location calculated using NonLinLoc for the earthquake on 27 May 2011.

This led to a number of detailed studies of the relationship between the earthquakes and hydraulic fracturing operations (for example, de Pater and Baisch, 2011; Eisner *et al*., 2011). In total, 58 earthquakes were detected in the time period between 31st March and 30th August 2011, nearly all of these either during or within a few hours of fracturing operations at Preese Hall (Figure 3.13). De Pater and Baisch (2011) concluded that the earthquake activity was caused by fluid injection directly into a nearby fault zone, which reduced the effective normal stress on the previously unmapped fault and caused it to fail repeatedly in a series of small earthquakes. The previously unmapped fault was later identified following a detailed 3-D seismic reflection study (Clarke *et al*., 2014). This demonstrates the need for detailed seismic mapping in any area of UGEE operations, particularly where the geological structure is complex.

Figure 3.13 also clearly shows the improvement in detection capability following the installation of additional stations close to the Preese Hall site in May 2011, with the detection of a number of earthquakes with lower magnitudes that could only be observed on these stations. Magnitude is shown as a function of time and the circles are also scaled by magnitude.

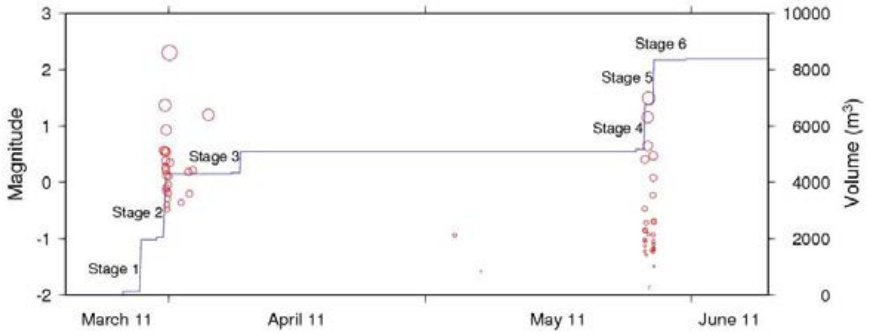

Figure 3.13. Events detected (red circles) near Preese Hall between 1 March and 30 June 2011.

3.6.4 Mining induced earthquakes at New Ollerton

The coalfields of Britain are frequently the source areas of small to moderate earthquakes and tremors in these areas have been reported for at least the last hundred years, for example the Stafford earthquake of 1916 (Davison, 1919). With the growth of instrumental seismic monitoring in the UK in the 1970s many more tremors were recorded in mining areas across the UK (Redmayne *et al*., 1988) and a number of temporary networks of sensors have been deployed to study these events in more detail. This led to the conclusion that these events were related to ongoing mining activity and that these were quite distinct from the natural background seismic activity of the UK.

A temporary network of seven seismometers was deployed north of the New Ollerton, Nottinghamshire, UK, to study a sequence of mining related earthquakes that started in December 2013. The mining induced earthquake activity is shown in Figure 3.14. The red circles show event locations determined using only data from the permanent regional monitoring network operated by BGS (red circles). The yellow circles show the locations for the same events determined using only data from a temporary seismometer network (green triangles). The black rectangles show the mined panels and the relocated events all closely corresponded to the locus of ongoing mining.

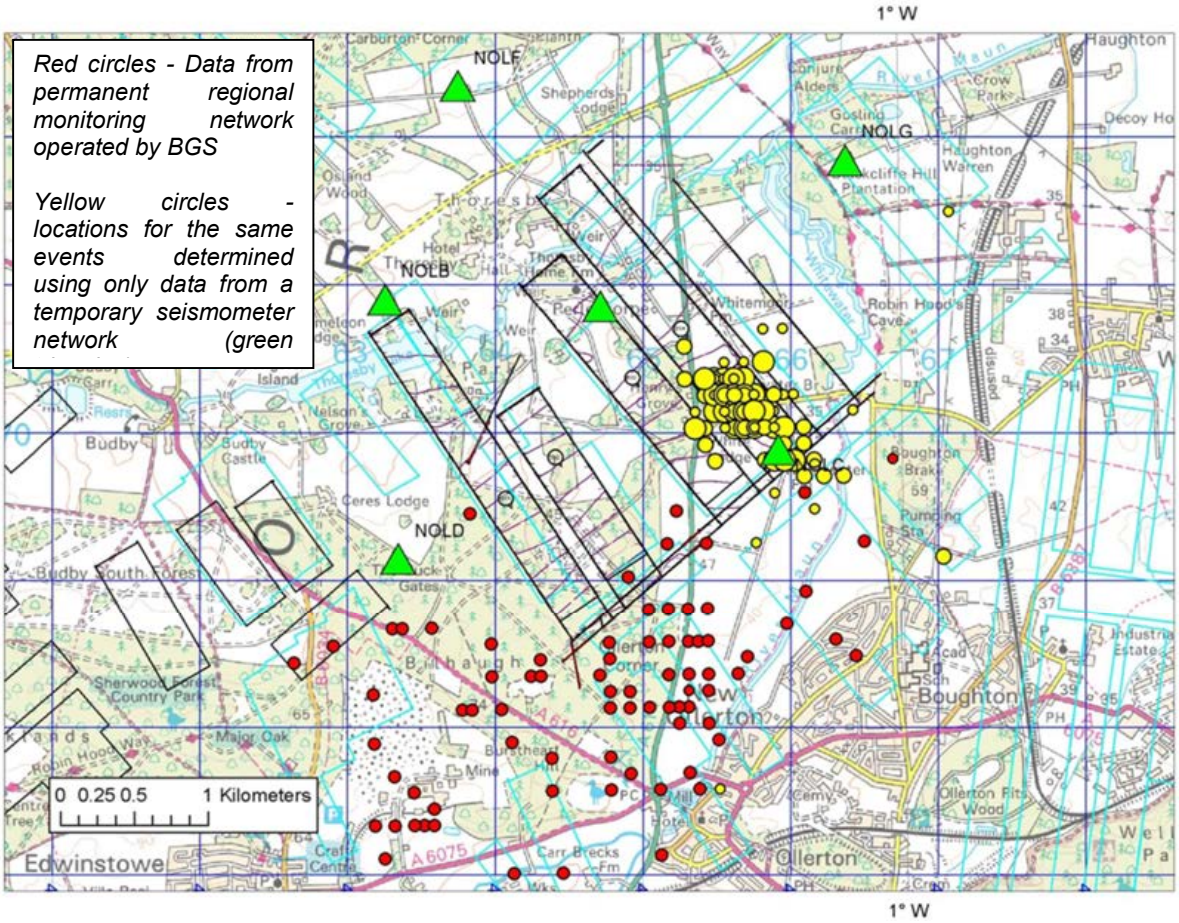

Figure 3.14. Mining induced earthquake activity at New Ollerton, Nottinghamshire, UK, located using only data from permanent regional monitoring network operated by BGS (red circles).

3.7 Monitoring Hydraulic Fracturing Growth in UGEE

Microseismic mapping of hydraulic fractures is widely acknowledged as the best means of characterising stimulated fracture networks in unconventional reservoirs (Maxwell, 2010). Large quantities of microseismic data collected over the past decades, mainly in North America, has transformed understanding of how these fracture systems grow in the sub-surface. Initially, the method was primarily based on arrays of geophones deployed in vertical boreholes close to the stimulated part of the well. Figure 3.15 shows the

microseismicity associated with hydraulic fracture treatments of the Upper Cotton Valley formation in the Carthage gas field, Texas, located using a downhole array of geophones by Rutledge *et al*. (2004).

As with site specific monitoring in geothermal projects, the use of the downhole geophones results in higher signal-to-noise ratios, which means that more seismic events can be detected (Maxwell *et al.*, 2010) and events can be located using fewer geophones. Vertical borehole arrays generally result in event locations that are generally well constrained in depth, but slightly less so in the horizontal plane. For example, Rutledge *et al*. (2004) find average horizontal errors of around 4m for events in the Cotton Valley formation, while the average depth error is less than 1 m.

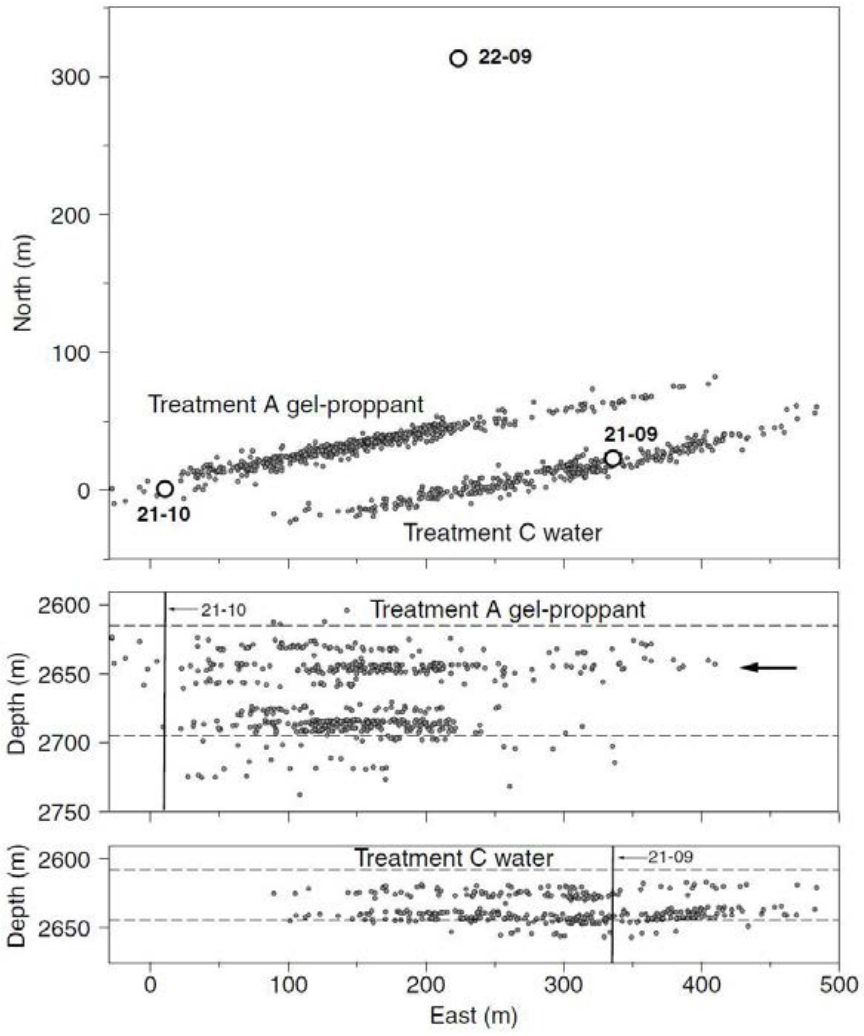

Figure 3.15. Locations of microseismic events during hydraulic fracture treatments A and C within the top of the upper Cotton Valley formation (from Rutledge *et al*., 2004).

More recently, horizontal arrays deployed at the surface or in shallow boreholes have been used as an alternative to vertical borehole arrays (Duncan and Eisner, 2014). Although signal to noise ratios are generally lower, the lateral location accuracy of the events is increased without any measurement bias. In addition, costs can be radically reduced. Typically, these consist of lines of geophones radiating from the treatment well. This pattern allows for effective reduction of surface noise generated by the frack pumps at the wellhead by frequency-wavenumber filtering. Typically, this star pattern has a diameter twice the target depth and therefore may be 2–10 km across. Neale and Smith (2009) show using geophones in shallow boreholes (70 m) results in significant noise reduction, allowing the number of geophones in the near surface array to be reduced by a factor of ten.

3.8 Conclusions

Recent experience in UGEE suggests that baseline monitoring should be an essential requirement of any future exploration and extraction, so that background levels of seismicity can be reliably characterised and any unusual seismicity or active faults that could potentially be affected by operations can be identified. Baseline monitoring is also essential for discriminating any induced earthquakes from natural background earthquake activity, allowing seismicity rates before, during and after operations to be reliably compared and any differences to be identified.

Baseline monitoring must be established prior to the commencement of any activity that is known to induce earthquakes. However, the duration of the monitoring required before operations start will depend on both the state of existing monitoring and the activity rate of the natural earthquake activity. Areas with higher activity rates will require shorter periods of monitoring, whereas in areas where activity rates are low, the number of earthquakes in a given period of time may be very low, so longer durations of baseline monitoring are required to reliably determine seismicity rates. This is in keeping with experience in the geothermal industry, where monitoring periods of 6–12 months are common. Current best estimates of the seismicity rate across Ireland and the surrounding offshore area are low. Scaling these rates to the study areas, suggests that there would be an earthquake with a magnitude of 2 or greater roughly every 60 years in the larger of the two study areas, and even fewer earthquakes in the smaller study area. The low expected seismicity rate presents a significant challenge for this project, since it may require many decades of baseline monitoring to reliably determine the rates in each of the two study areas, if the levels of natural seismicity are as low as expected from the available historical and instrumentally recorded data. However, it is important to test the assumption that seismicity rates are uniform across Ireland. Therefore, detailed monitoring will be required in each study area to detect any unusual seismicity that may suggest that seismicity rates are higher in the study areas, or that there is seismicity associated with any specific fault structure. One to two years may be an appropriate monitoring period for this purpose. More sensitive site-specific real-time monitoring is usually deployed during the operational phases of EGS and UGEE projects to fully characterise the fracture development and to act as part of "traffic light" mitigation/prevention system.

It is of crucial importance that at least some of the background monitoring stations remain installed through all phases of monitoring to ensure continuity and allow relative re-locations of seismicity and analysis of waveform similarity. Reliable and uniform detection of seismic events across a given area of interest requires a uniform distribution of monitoring stations. The density of the stations along with the noise levels at each station control the lowest magnitudes that can be reliably detected. Higher station densities will be required to detect and locate lower magnitudes. Noise levels at individual stations also affect detection capability, and these should be low in order to maximise detection potential. In addition, a monitoring network must also extend beyond the limits of the area of interest in order to be able to reliably detect earthquakes that occur close to these limits. Detection capability for different station geometries and densities can be modelled using a number of relationships that determine the amplitude of seismic waves as a function of magnitude and distance. However, reliable estimates for the quality factor, Q, which controls anelastic attenuation and also near site attenuation factors are also required.

Reliable location and magnitude measurement places additional constraint on network design, since measurements at more stations are needed than for detection alone. In addition, location errors depend on the distribution and density of the recording stations. These errors may be large if the station density is insufficient, or if the closest stations are far from the earthquake source, which may limit the capability to discriminate between induced and natural earthquakes. Again, a uniform station density is required to ensure comparable location accuracy across the region of interest, with monitoring stations extending beyond the area of interest.

Extensive experience of seismic monitoring in the geothermal industry may be considered as “best practice” for UGEE. This will allow many of the methods used for the monitoring of earthquake activity along with appropriate control measures for the mitigation of risks associated with induced earthquakes to

be readily adopted. However, it should be noted that seismic monitoring is used before, during and after EGS operations, whereas the aim of this study is solely to characterise the background natural seismicity in the study areas.

Finally, the case studies discussed in this report highlight the importance of an appropriate monitoring network for reliable detection and location of any seismic events before, during and after any operations that may induce seismic activity. In particular, the example of the seismicity induced by hydraulic fracturing at Preese Hall, near Blackpool, shows how local monitoring stations are essential to reduce uncertainty and also allay public concern.

4 Task 2: Evaluate Methodologies for the Monitoring of Ground Deformation That May Be Associated with UGEE Projects/Operations

4.1 Introduction

The aim of Task 2 is to evaluate methodologies such as InSAR, EDM, tiltmeters and GPS or their equivalent for monitoring ground deformation that may be associated with UGEE projects/operations. It is important to quantitatively monitor the motion at surface in order to gauge potential damage to structures, and to address potential concerns of the public and policy makers regarding impacts to the environment. This should be regarded in light of the fact that Ireland does not have a building code for house construction to resist earthquakes therefore there may be no estimate of the level of ground motion that may cause damage to structures.

There are mature technologies that can measure ground motion at a point in space; these include geodetic sensors such as GNSS (Global Navigation Satellite Systems), sometimes referred to as GPS and geotechnical sensors such as tiltmeters. Geotechnical sensors, located at the surface or down boreholes are used to measure non-georeferenced displacements or movements. Geodetic measuring devices record georeferenced displacements or movements in 1, 2, or 3 dimensions; this group includes GNSS. GNSS is the generic term for a constellation of satellites that provide geospatial positioning. There are various forms of GNSS including the two operational systems; GPS (the US Global Positioning System) and GLONASS (the Russian Global Navigation Satellite System) along with developmental systems such as the European Union's Galileo system and the Chinese Beidou.

The use of integrated GNSS and tiltmeters (either in isolation or integrated at a site) is common practice for successful ground motion monitoring in many applications including volcanology (e.g. Hawaii – http://hvo.wr.usgs.gov/kilauea/update/deformation.php) and CO_2 storage monitoring (e.g. In Salah – Mathieson *et al*., 2010). However, a review has yielded little published evidence of the application of these technologies for monitoring surface motion related to UGEE projects/operations, or in fact of the magnitude and geographical distribution of ground deformation associated with UGEE operations worldwide. The lack of surface motion data was noted by Dost *et al*. (2013) in relation to the Groningen area following the seismic activity in the gas field. Ground motion was deemed important in Groningen, but the mechanism did not exist to measure/monitor it; InSAR would fulfil this requirement. Furthermore, Fisher and Warpinski (2011) published a summary of US microseismic and tiltmeter data in shales based on the Barnett, Woodford, Marcellus and Eagle Ford shales, noting that a surface array of tiltmeters located on the ground surface can be used to measure the deformation pattern and determine some details of the fracture orientation. Tiltmeters can also be installed downhole, with Fisher and Warpinski (2011) concluding that they can be used to measure the height of the hydraulic fracture when installed near the treatment well with an array sufficiently long enough to span the fractured interval's thickness. Typically, between 15 and 100 tiltmeters will be placed on the ground around the well.

The application of *in situ* point measurement sensors for ground deformation monitoring is reported in the literature, therefore this section focuses on the application of radar interferometry from satellites to the island of Ireland. The potential for this technique is highlighted by selected services across Europe e.g. PanGeo (http://www.pangeoproject.eu/) and results from ground monitoring studies such as at In Salah, with Mathieson (2010) stating that "perhaps the most valuable, and initially surprising, monitoring method so far has been the use of satellite based Interferometric synthetic aperture radar (InSAR) to detect subtle ground deformation". As well as the regional coverage afforded by InSAR, the technique also benefits from an archive of data (from 1992) which can be used to gain a baseline of surface motion over a site where tiltmeters or GNSS were not already installed prior to operations.

InSAR monitoring is generally applied to urban areas (due to the presence of abundant reflectors) therefore the application of this technique for monitoring potential ground deformation in non-urban areas of Ireland is the primary aim of this task. Deliverables from this task include:

- this section, which outlines the radar data availability and presents the results of a study on the feasibility of InSAR for the island of Ireland using elevation and land cover data; and
- digital geospatial datasets of the InSAR feasibility results can be made available for display in a geographic information system (GIS).

4.2 Methodology and Results

The methodology for this InSAR feasibility study follows that undertaken for the landmass of Britain by Cigna *et al*. (2014). The three main factors (listed below) that affect the ability for InSAR to be successfully undertaken are addressed in the following sections to gauge whether the methodology could be used in Ireland to monitor ground motion:

1. Availability of satellite radar data;
2. Visibility of the terrain by the satellite sensor; and
3. Presence of Scatterers.

4.3 Availability of SAR Data

Each time the radar satellite passes overhead it captures an image of the terrain (if it is programmed to do so). Multiple images of the same location over a period of time (called a stack) can be processed to provide a time-series showing the elevation of the terrain at each overpass, and therefore it can be determined if the ground is stationary, subsiding or uplifting. If processed appropriately (with suitable ancillary data), the imagery can also be used to determine lateral motion, if it exists. Sufficiently long and populated stacks of Synthetic Aperture Radar (SAR) imagery are required to generate a complete picture of ground motion over an area of interest. Greater numbers of images in a stack result in higher accuracy of ground motion, atmospheric phase components and height errors when processing with multi-interferogram methods such as PSI (Persistent Scatterer Interferometry) and SBAS (Small Baseline Subset) (e.g. Berardino *et al*., 2002 and Ferretti *et al*., 2001). It has been observed that at least ~15–20 images of the same acquisition geometry (i.e. same mode, orbit and track) are required to undertake a multi-interferogram InSAR analysis (e.g. Crosetto *et al*., 2010).

There are several radar satellites currently in orbit that acquire imagery that can be processed for interferometry, including TerraSAR-X, COSMO-SkyMed and Sentinel-1A. Additionally there are satellites that have acquired large archives of imagery over Ireland, but which are no longer operating, such as ENVISAT and ERS-1/2. These archives are vitally important because they can be used to "go back in time" to 1992 (when they first started operating) and to create a baseline of ground motion from that year. Using archive data, the historic ground motion (or stability) can be quantified therefore it could be ascertained if ground motion following hydraulic fracturing (and subsequent to the placement of *in situ* sensors) in an area had been occurring prior to fracking.

Archives of radar imagery exist, although they do not have global coverage so it is necessary to ascertain if data are available for an area of interest. Therefore, the first step in the assessment was to search the catalogues for archive data covering Ireland. The European Space Agency's (ESA) C-band archive provides the most complete database of radar data for Ireland, providing consistent stacks of historic ERS-1/2 and ENVISAT data. Few archive L-band data are available for Ireland for the period between 2006 and 2010 therefore the feasibility study concentrated on C-band data. The ERS data cover the period 1992–2000 while ENVISAT acquired imagery from 2002 to 2010. Each satellite acquires data during ascending and descending orbits i.e. while the satellite passes overhead from south to north, and from north to south

respectively. Therefore, the results are displayed below onto a shaded relief image of Ireland in terms of the orbit parameters (Figure 4.1, Figure 4.2, Figure 4.3 and Figure 4.4). The archive consists of:

- 1917 scenes across 35 frames for the descending orbit of ERS-1/2 (1992–2000), providing an average of 55 images per stack;
- 1173 scenes across 35 frames for the descending orbit of ENVISAT (2002–2010), providing an average of 36 images per stack;
- 532 scenes across 34 frames for the ascending orbit of ERS-1/2 (1992–2000), providing an average of 15 images per stack;
- 591 scenes across 34 frames for the ascending orbit of ENVISAT (2002–2010), providing an average of 17 images per stack.

This archive, with at least 20 scenes for 100% of the ERS and ENVISAT descending mode imagery suggests that multi-interferogram InSAR analysis with PSI or SBAS methodologies should be possible for the island of Ireland. Nevertheless, further analysis of the normal and temporal baselines of the image stacks is needed to verify whether Interferometric phase correlation can be guaranteed across the available stacks (e.g. for SBAS applications with temporal baselines shorter than 4 years, and normal baselines smaller than 130–200m e.g. Berardino *et al*., 2002).

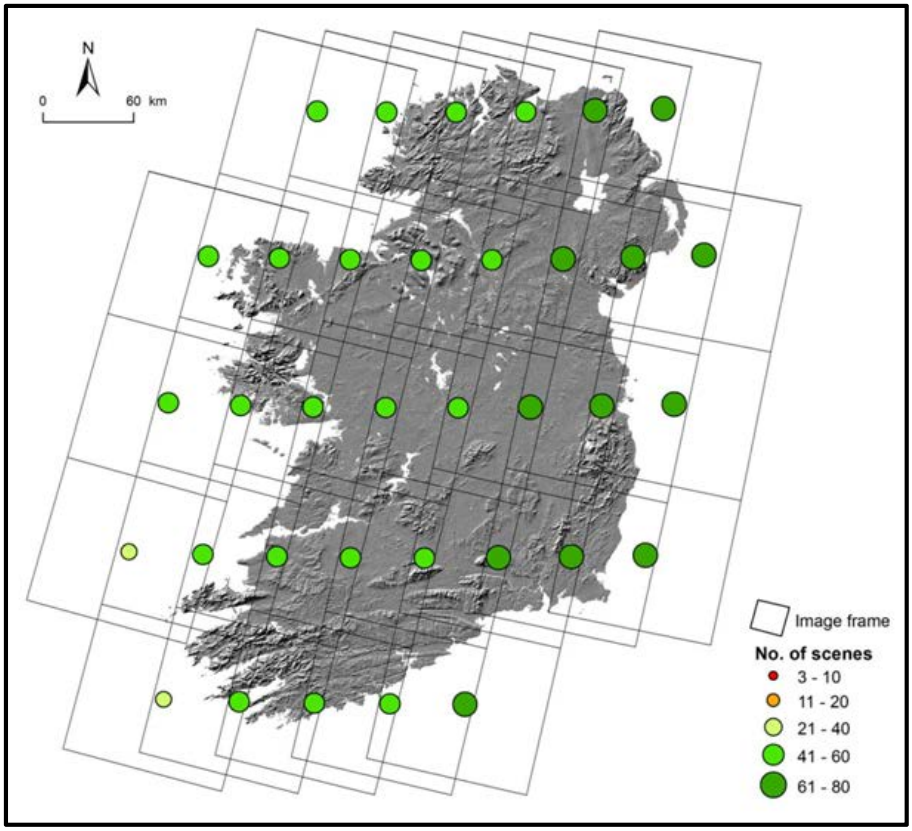

Figure 4.1. ERS-1/2 descending orbit archive radar data for Ireland (1992–2000).

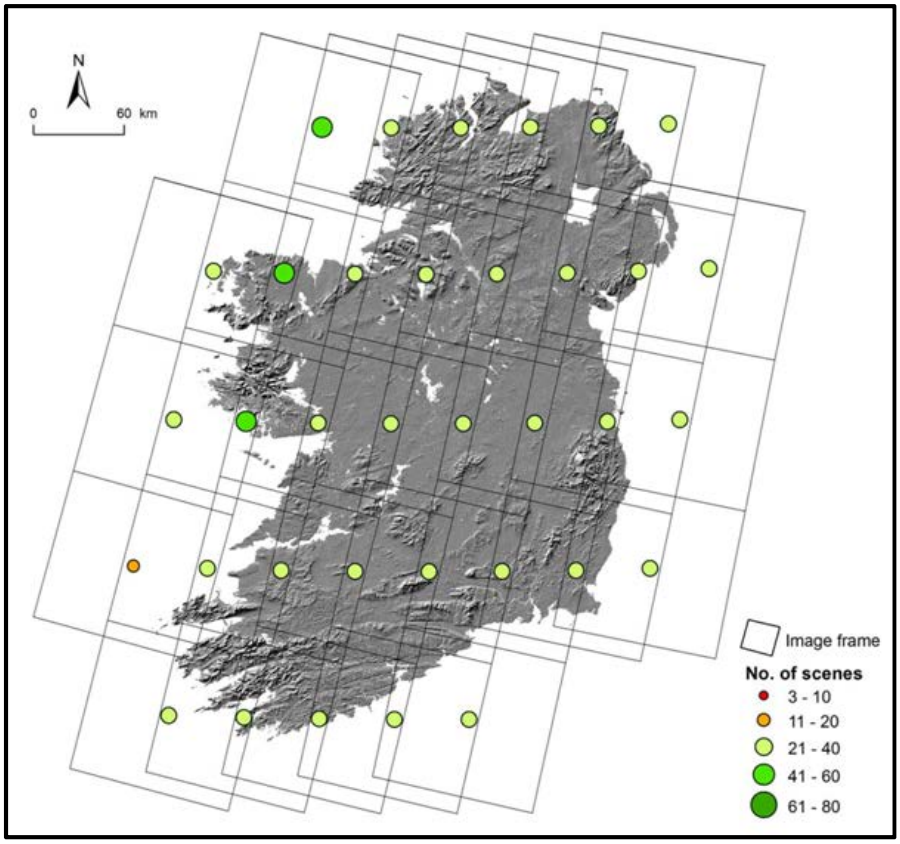

Figure 4.2. ENVISAT descending orbit radar for Ireland (2002–2010).

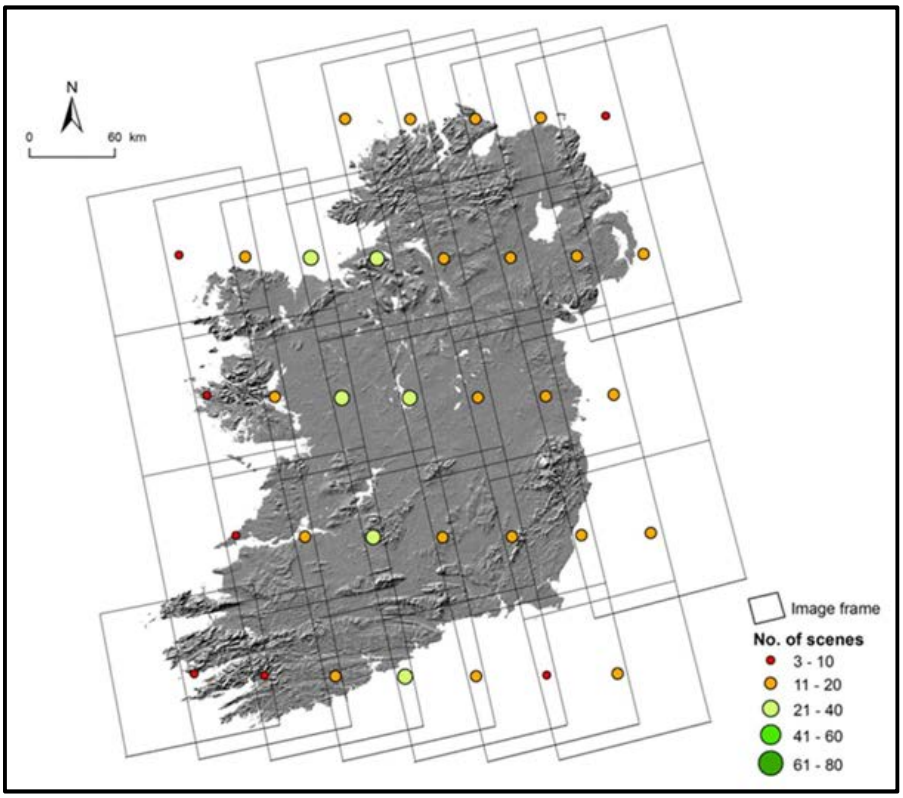

Figure 4.3. ERS-1/2 ascending orbit archive radar data for Ireland (1992–2000).

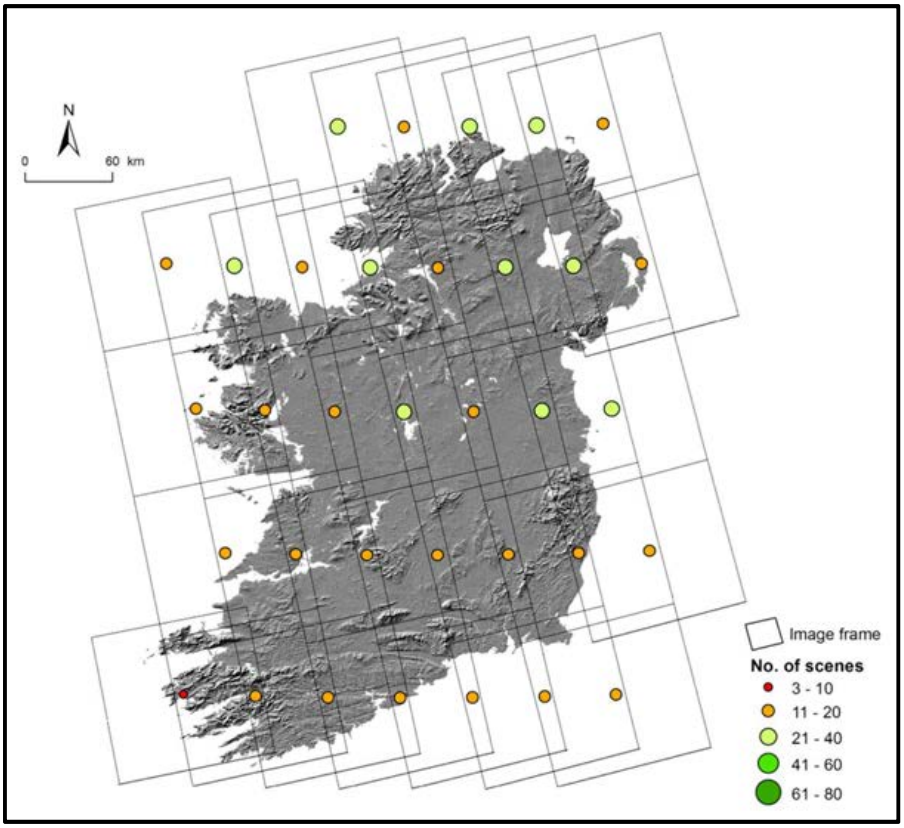

Figure 4.4. ENVISAT ascending orbit radar archive data for Ireland (2002–2010).

ESA launched Sentinel-1A on April 3rd 2014, with a C-band radar sensor on board and as of October 2014 the data were made available to users. These data are provided under a free and open policy therefore there is no cost for data access, even for commercial users. The sister satellite (Sentinel-1B) is due for launch in 2016. Whilst there is not currently a sufficient volume of Sentinel-1A data over Ireland to undertake InSAR analyses, the catalogue is growing and these data will be available for ongoing ground motion projects by the end of 2015.

For commercial applications, it can be assumed that each ERS and ENVISAT scene within the stack would cost approximately €300–500. In the Clare area there are two suitable frames of archive ERS and ENVISAT descending data with 51 and 34 scenes, respectively. In the northwest area there are also two suitable frames of archive ERS and ENVISAT data, with 50 and 35 scenes respectively. In total there are 170 satellite scenes, costing between €51,000 and €85,000. In addition to the cost of the data, there is also an overhead of ordering, processing and interpretation. It is very difficult to provide an estimate of the cost for this component but it is considered to be in the region of €90,000. These costs will vary depending on the level of automation, and it is also worth noting that the quality of processing and interpretation should be taken into account when considering the service supplier.

As mentioned above, the Sentinel-1 data will be free of charge, therefore any costs will be associated with processing and interpretation. The cost for data manipulation and interpretation will depend on the number of frames that have been collected, and this is subject to the start date of any proposed InSAR study using these data.

4.4 Visibility of the Terrain by the Satellite Sensor

Radar satellites are sideways looking and are therefore prone to geometric distortions when viewing the Earth; for example, the presence of radar layover prevents the application of InSAR. Moreover, in areas of high relief there can be radar shadows, making some areas invisible to the sensor. In this study, the EU

Digital Elevation Model (DEM) at 25 m resolution (Figure 4.5) was utilised to model the SAR distortions for foreshortening, layover and shadow with respect to the acquisition parameters of the ERS and ENVISAT satellites in both ascending and descending modes. The terrain visibility analysis was modelled for the entire island of Ireland.

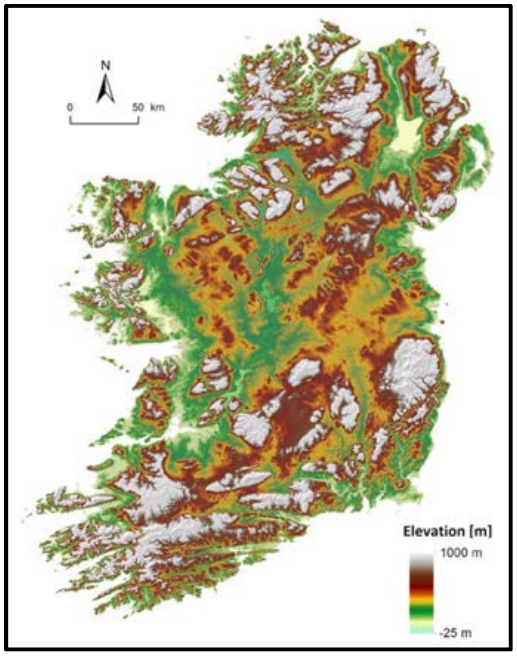

Figure 4.5. EU 25 m resolution DEM (produced using Copernicus data and information funded by the European Union – EU – DEM layers).

The results of the simulation of topographic radar distortions to the ERS and ENVISAT descending mode are illustrated in Figure 4.6, Figure 4.7, Figure 4.8, Figure 4.9, and Figure 4.10. Less than 0.01% of the Irish landmass would be affected by shadow, while layover would affect only ~0.4% in each acquisition mode. Furthermore, most of the landmass (>99.9%) is visible to the radar sensor in at least one acquisition mode; bearing in mind that distortions in hilly areas can be compensated by using either ascending or descending orbits.

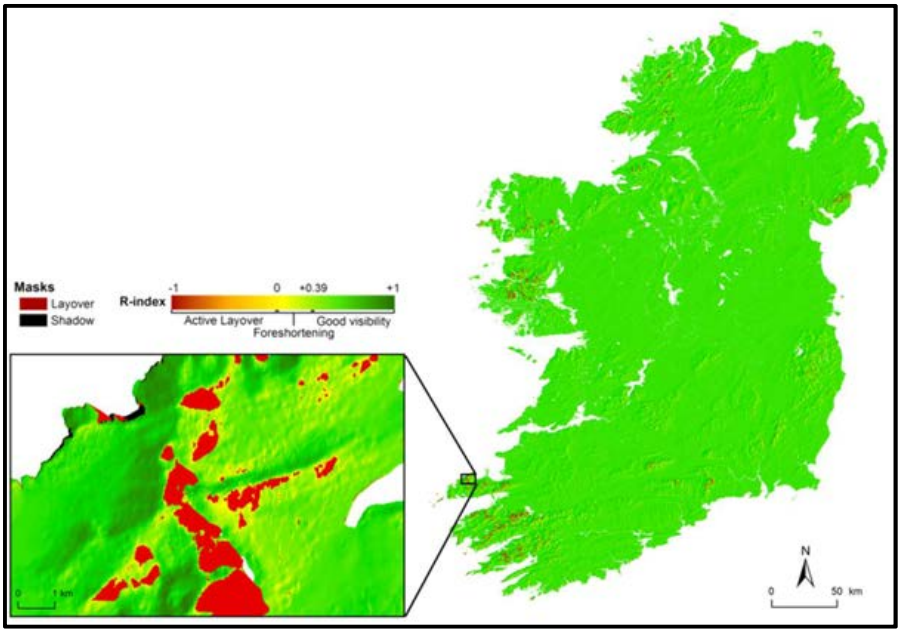

Figure 4.6. Simulation of topographic radar distortions to the ERS – 1/2 and ENVISAT descending mode.

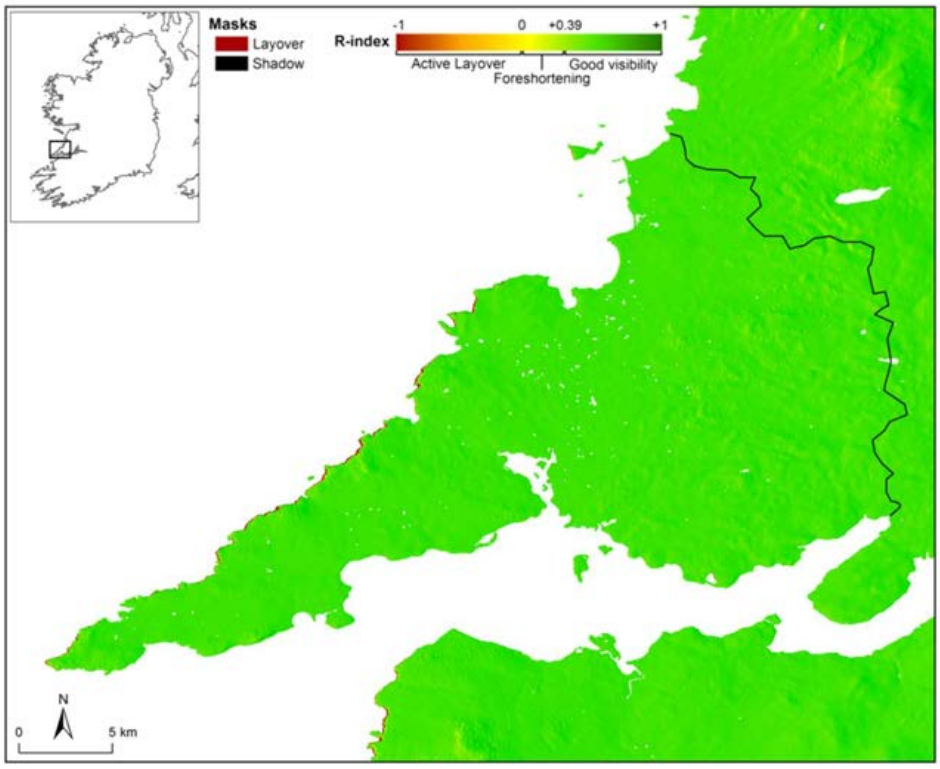

Figure 4.7. Simulation of topographic radar distortions to the ERS – 1/2 ENVISAT ascending mode, County Clare area

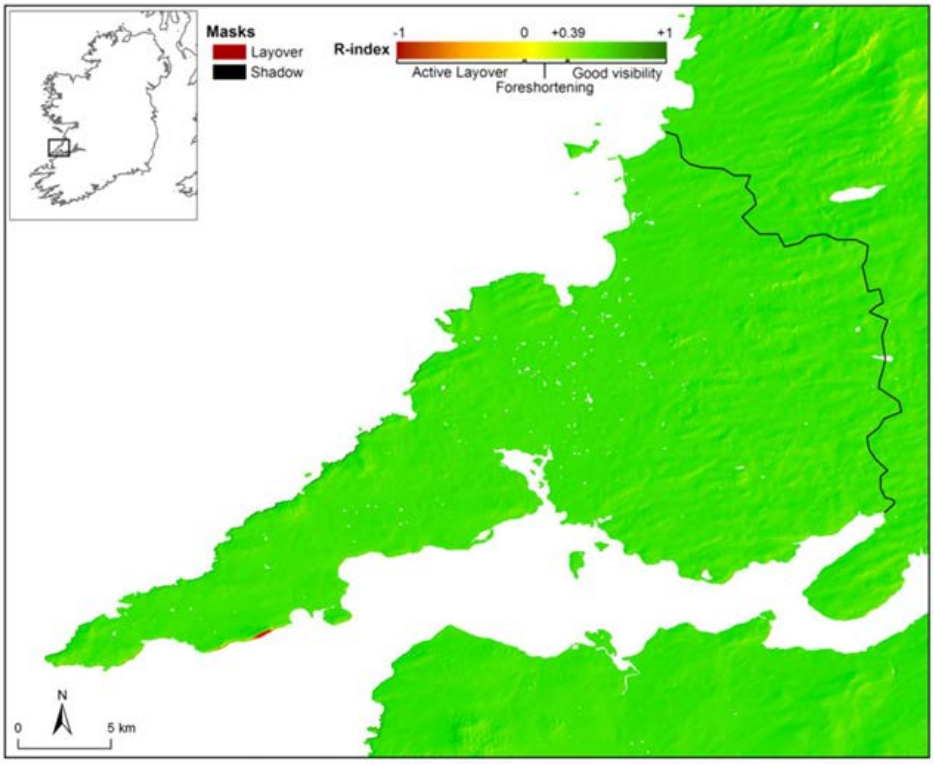

Figure 4.8. Simulation of topographic radar distortions to the ERS – 1/2 and ENVISAT descending mode, County Clare area.

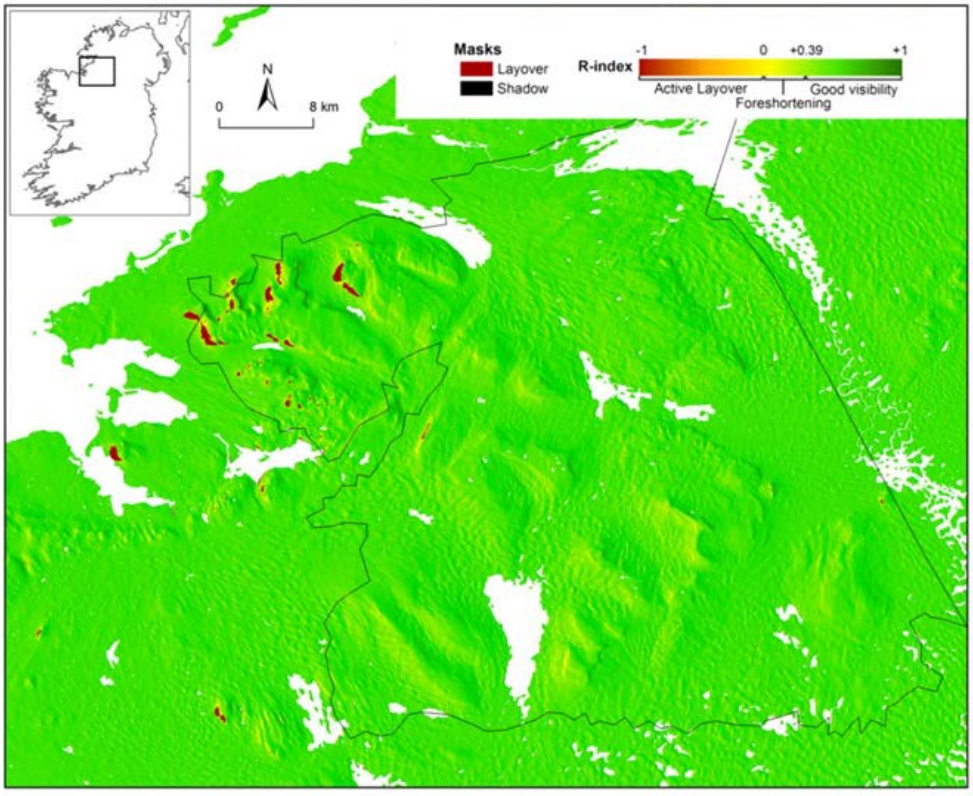

Figure 4.9. Simulation of topographic radar distortions to the ERS – 1/2 and ENVISAT ascending mode, Northwest area.

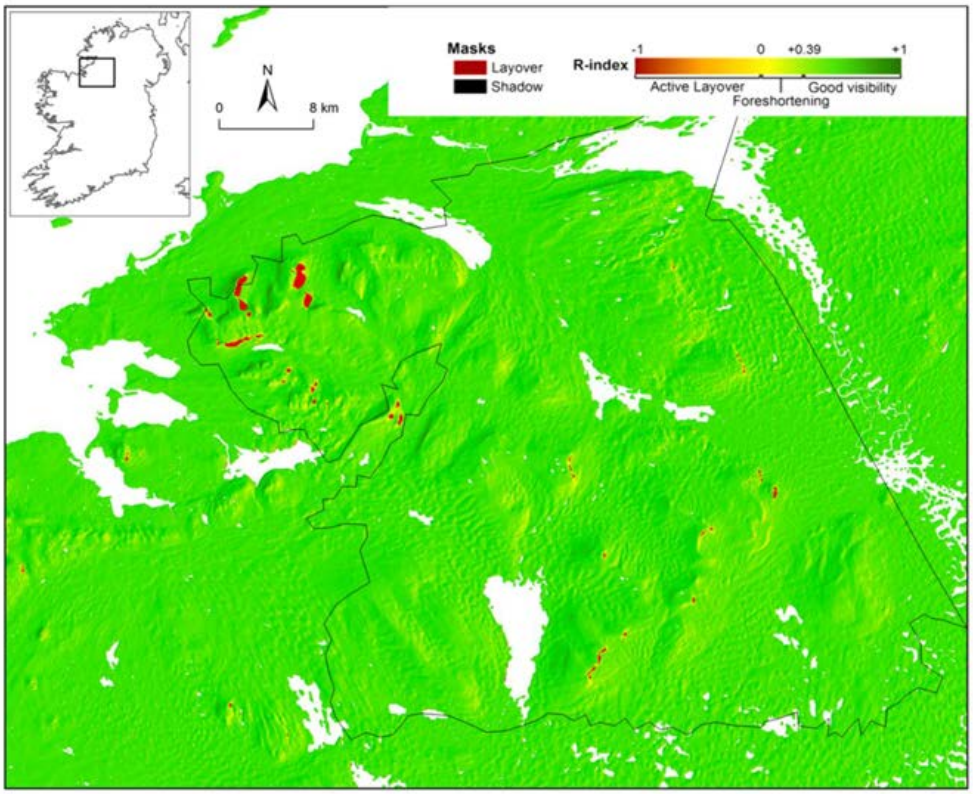

Figure 4.10. Simulation of topographic radar distortions to the ERS – 1/2 and ENVISAT descending mode, Northwest area.

4.5 Presence of Scatterers

A persistent scatterer (PS) is a location on the ground that maintains coherence through several radar images. Persistent scatterers are required for point-based InSAR analyses i.e. they can be compared to the prism/mirror that total stations use for their readings. The ability of surface targets to operate as persistent scatterers is related to ground properties such as geometry and land cover. Therefore, the third component of this feasibility study used the CORINE land cover map of Ireland (Figure 4.11 to Figure 4.13) to model the potential for persistent scatterers across the country.

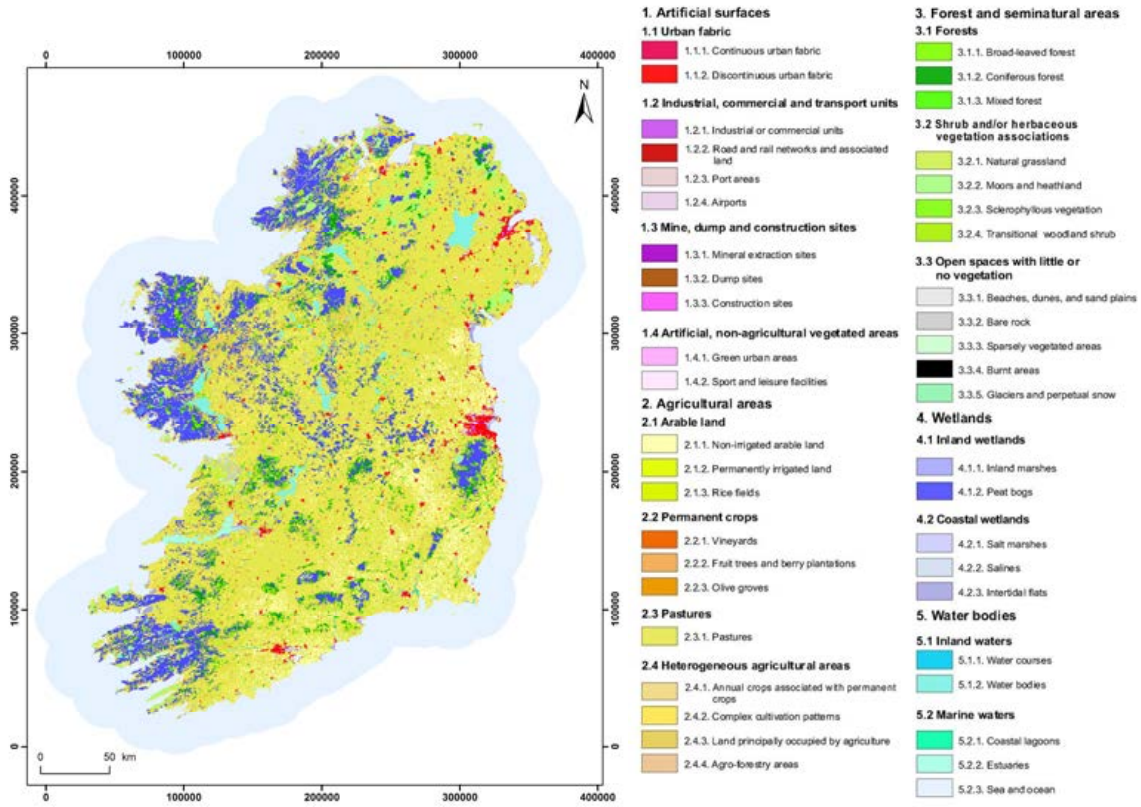

Figure 4.11. Land cover types from the CORINE database for Ireland. CLC2006 @ 2007, European Environment Agency (EEA).

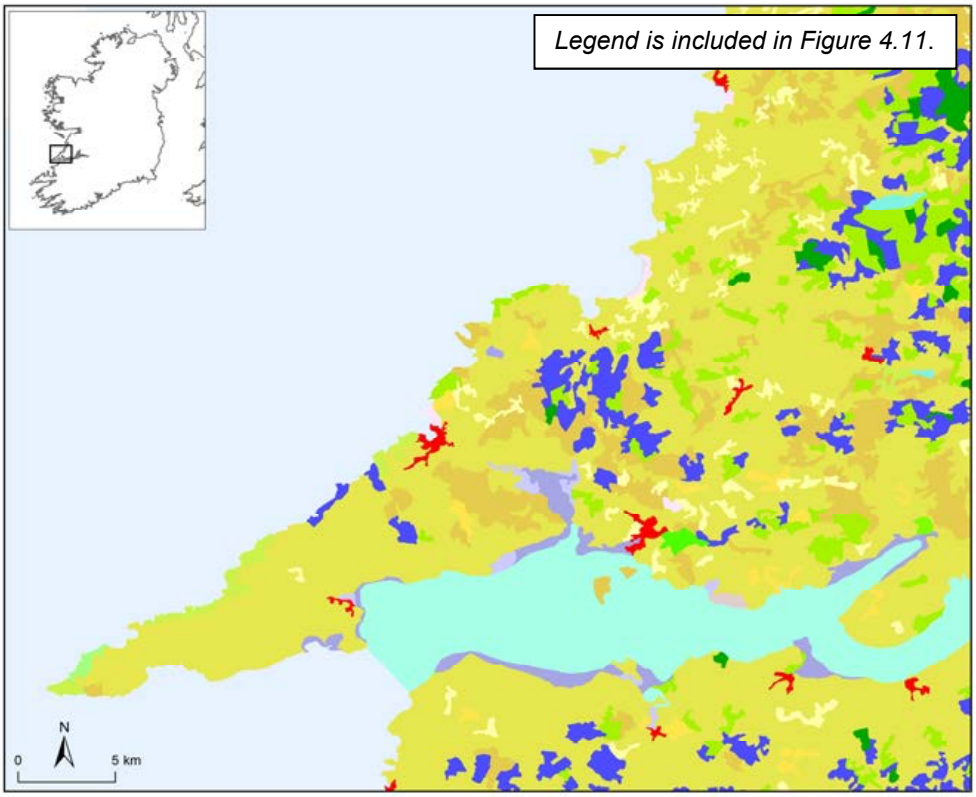

Figure 4.12. Detail of land cover types from the CORINE database for the Clare area. CLC2006 @ 2007, European Environment Agency (EEA).

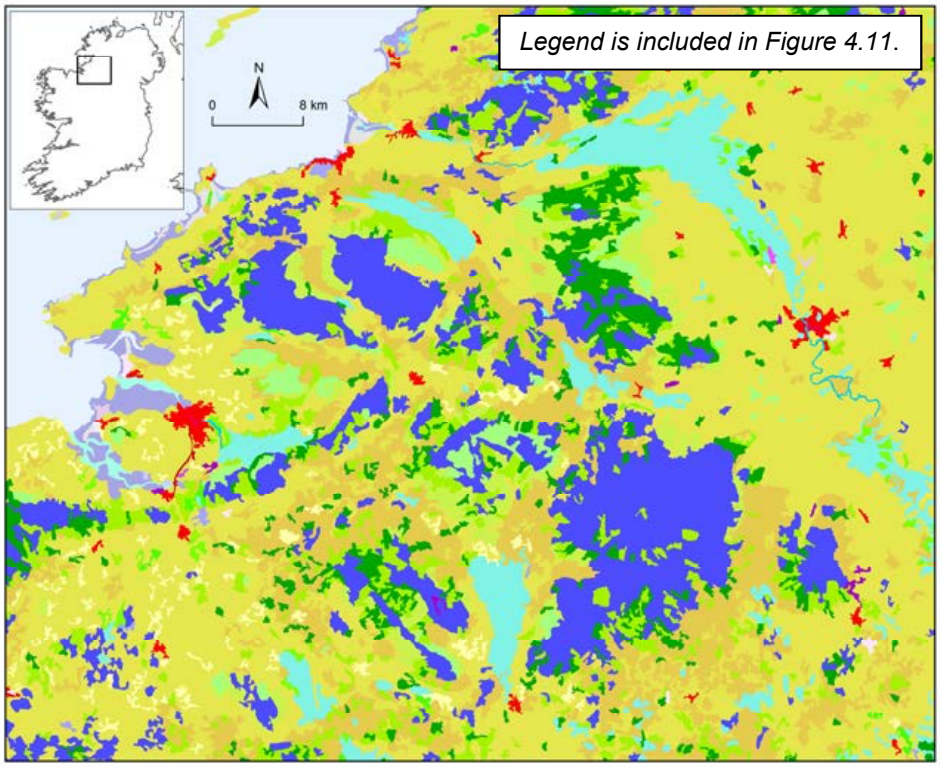

Figure 4.13. Detail of land cover type from CORINE database for the Northwest area. CLC2006 @ 2007, European Environment Agency (EEA).

The BGS feasibility study in Britain utilised PS datasets from Newcastle, Stoke-on-Trent, Greater London and the Bristol & Bath areas for quantitative calibration of the CORINE land cover data (Cigna *et al*., 2014). The datasets were processed using the Interferometric Point Target Analysis (IPTA) and the Permanent Scatterer InSAR (PSInSAR™) techniques. Average PS densities were derived for each CORINE land cover class, thereby deriving the relationship between the cover types and the PS distributions within the six processed InSAR datasets. The same relationship was used to model the occurrence of persistent scatterers in Ireland. The density of persistent scatterers for each land cover class is expected to be the same for Ireland as it is in Britain.

The results of the island-wide PS land cover feasibility are shown in Figure 4.14, with detailed results for the Clare and Northwest Carboniferous Basin areas shown in Figure 4.15 and Figure 4.16. Urban and rocky terrains (classes 1–3) have a higher likelihood of providing reflectors. However, over 90% of Ireland falls into classes 6–8 (predominantly rural land cover types) and would therefore only be partly successful using InSAR, with modelling suggesting that there would be only tens of PS per km^2. Nevertheless, this does not mean that all SAR would be unsuitable in these locations. BGS is currently utilising other techniques such as Intermittent Small Baseline Subset (ISBAS) in British non-urban environments, which is providing very positive results (refer to recommendations and conclusions).

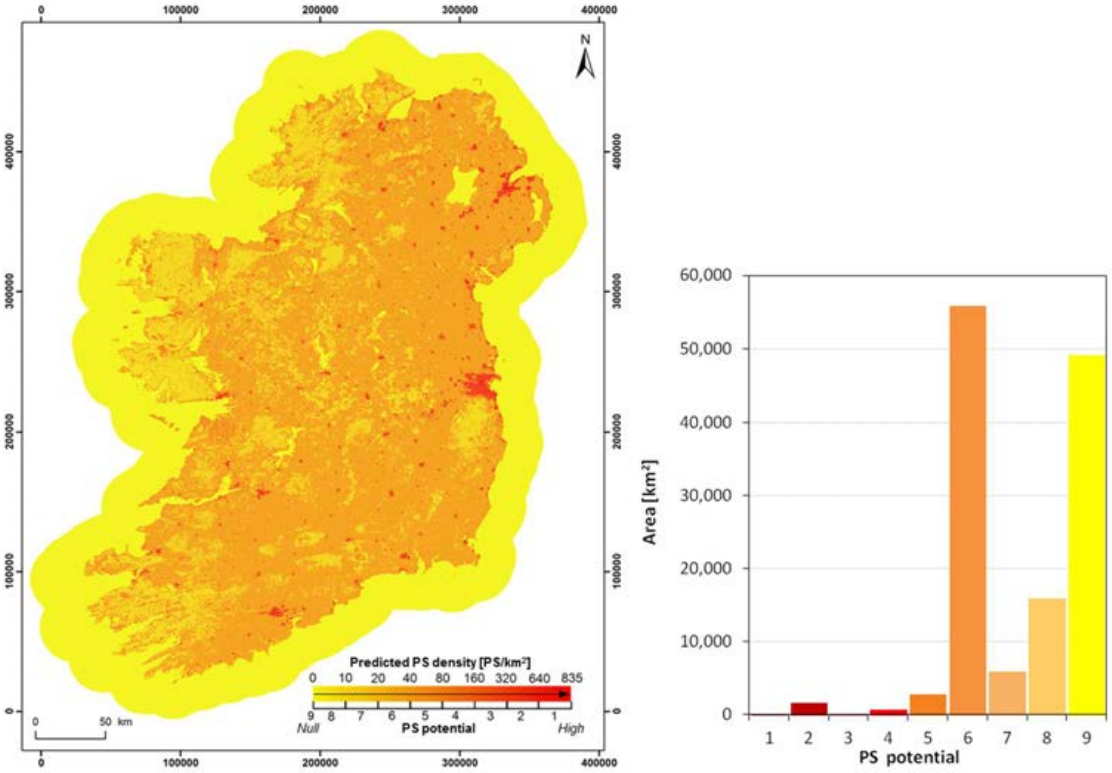

Figure 4.14. Modelled potential for persistent scatterers in Ireland.

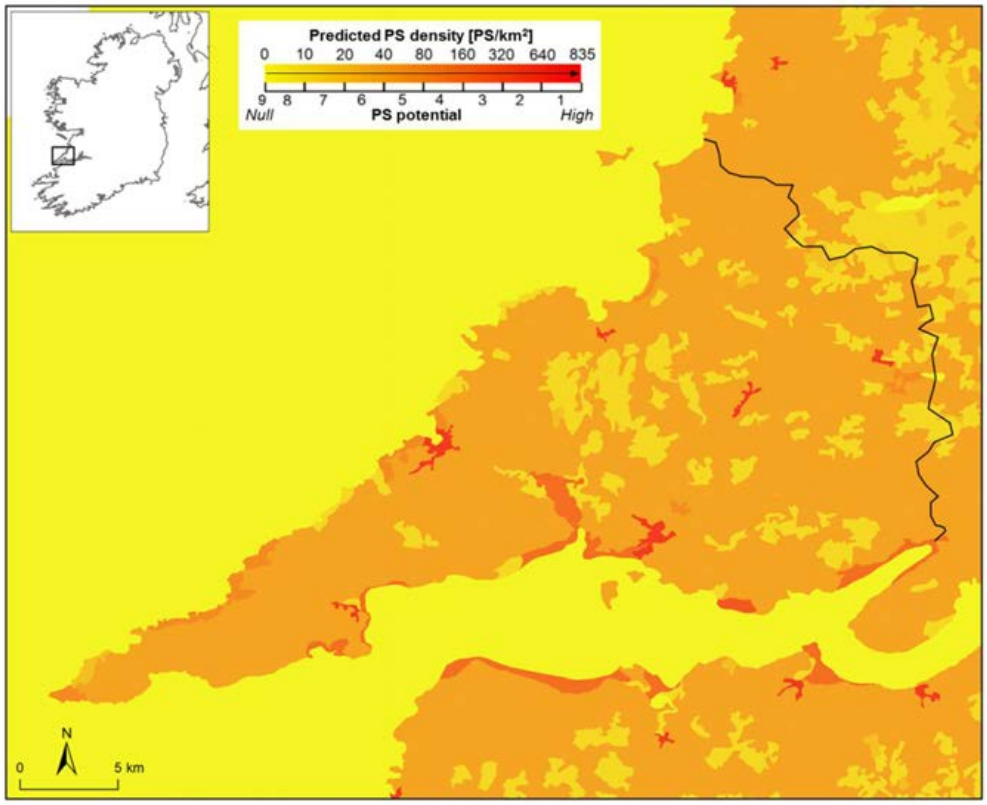

Figure 4.15. Modelled potential for persistent scatterers in the County Clare area.

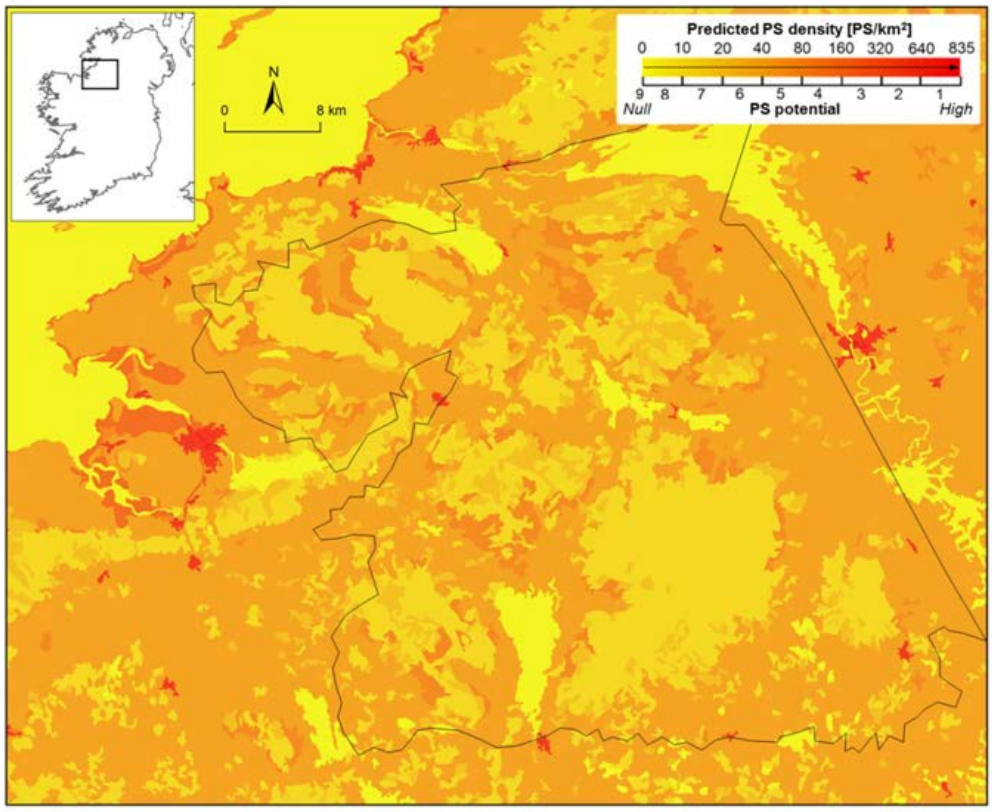

Figure 4.16. Modelled potential for persistent scatterers in the Northwest area.

4.6 Conclusions

The factors affecting InSAR for ground motion monitoring in Ireland were addressed and the assessment has concluded that the technique is valid for the island of Ireland, and the study sites in Co. Clare and the Northwest Carboniferous Basin, in particular.

Availability of SAR data. Approximately 15–20 images of the same acquisition geometry are required for multi-interferogram InSAR analysis. Archive data from ERS and ENVISAT, acquired between 1992 and 2010 were assessed and there are at least 20 scenes for 100% of the descending mode suggesting that PSI or SBAS methodologies should be viable. However, further analysis of the normal and temporal baselines of the image stacks should be done to verify whether interferometric phase correlation can be guaranteed.

For ongoing monitoring using InSAR techniques, the ESA Sentinel-1A was successfully launched on April 3rd 2014 with a C-band radar sensor on board. It is acquiring data, and a sufficient volume will be available for InSAR analysis of Ireland by end 2015.

Visibility of the terrain by the satellite sensor. SAR distortions were modelled using the EU 25 m resolution DEM in relation to the ERS and ENVISAT satellites in both descending and ascending modes. The results indicate that less than 0.01% of the landmass would be affected by shadow, and layover would affect 0.4% in each acquisition mode. Therefore >99.9% of the landmass is visible to the SAR satellites in at least one acquisition mode.

Presence of persistent scatterers. The existence of persistent scatterers was modelled using the CORINE land cover data and PS datasets from Britain where average PS densities were derived for each land cover class. Over 90% of Ireland consists of predominantly rural land cover types and would therefore have approximately 10s of PS per km^2. This would mean that InSAR would only be party successful.

Nevertheless, BGS is currently utilising other techniques such as ISBAS in British non-urban environments, and this technique is providing very positive results (Bateson *et al*., 2014). An example of BGS InSAR processing in South Wales (Figure 4.17) highlights that the number and density of scatterers increased by a factor of ~3.4 using the ISBAS technique compared to conventional SBAS. The increase in spatial coverage provided by the ISBAS approach offers significant advantages for the interpretation of ground motion. The improved density allows the identification of small areas of motion which fall in the gaps of the SBAS result, but it also allows the edges of displacement areas to be more accurately defined (and interpreted). This makes it easier to relate the results to other datasets and hence increases understanding of the ground motion.

Ground deformation from UGEE projects/operations will not necessarily result in damage to structures but it is important to quantitatively monitor the motion at surface in order to gauge potential damage to structures, and to address potential concerns of the public and policy makers regarding impacts to the environment. This technique of ground motion has been used for this purpose in post-mining areas.

It is recommended that UGEE projects operating in Ireland should be monitored using historic and current satellite radar data, processed to provide InSAR results with a technique such as ISBAS, which has been shown to deliver results in non-urban areas. The historic data will provide a baseline of surface millimetric motions back to 1992, confirming stability or otherwise of the surface prior to UGEE operations. Satellites such as Sentinel 1A are currently acquiring radar data that should be used for ongoing monitoring.

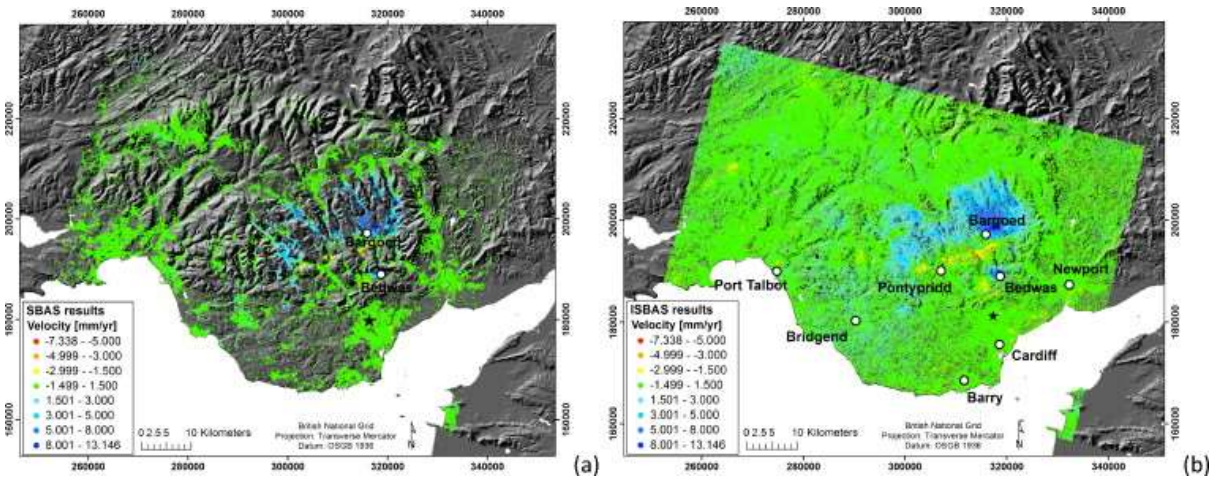

Figure 4.17. ISBAS processing in South Wales (left conventional SBAS; right ISBAS).

In combination with the InSAR technique, complementary *in situ* methods such as GNSS and tiltmeters could be deployed; research has shown that integrating the monitoring techniques provides better and more detailed information on deformation characteristics (Grejner-Brezzinska *et al*., 2005). Each technique has advantages and limitations (Table 4.1). A GNSS station would provide quantitative x,y,z location data, which could be used to identify motion at that point location and also to calibrate the InSAR results. A network of GNSS stations would provide data on regional surface motion, from the time at which the instruments are installed. Tiltmeters would provide complementary data on local micro-deformation and fracture propagation (if installed on the surface and downhole). Task 10 of the project will deal with the "assessment of what baseline monitoring could be undertaken by the state versus by the industry" and this could include requirements for integrated ground deformation monitoring.

Table 4.1 .Comparison of monitoring techniques

Monitoring technique	Advantages	Limitations
InSAR	Measurements are made remotely (non-invasive) Measurements can be made using historic data to gain a baseline prior to UGEE operations Imagery can cover a large area simultaneously Entire deformation field can be imaged, rather than isolated points	Conventional techniques have difficulty in vegetated areas High magnitudes of motion (greater than the satellite phase difference) cannot be measured Temporal and spatial resolution is limited by satellite set up and orbital parameters Affected by steep topography (shown not be an issue in Ireland)
GNSS	High precision Does not require line of sight between benchmarks Continuous site can operate without frequent human interaction	Equipment can be stolen/vandalised/damaged Sampling of deformation field is limited to individual points; several points are required Requires at least 4 satellites in view simultaneously
Tiltmeters	High precision Does not require line of sight between benchmarks Continuous site can operate without frequent human interaction	Equipment can be stolen/vandalised/damaged Sampling of deformation field is limited to individual points Complex installation (e.g. in boreholes) – several tiltmeters are required
EDMs	High precision Continuous site can operate without frequent human interaction	Requires line of sight between benchmarks Generally, they are operated manually, requiring repeat site visits to operate the system

5 Task 3: Assessment of Existing Data on Natural Seismicity in the Island of Ireland

5.1 Introduction

Ireland lies at the northwest margin of Europe, adjacent to the continental shelf and is a region of low seismic activity. The historical seismicity of Ireland has been studied by a number of researchers including Davison (1924) and Richardson (1975). Davison (1924) concluded that few countries were so free from, earthquakes as Ireland, and the absence of earthquakes in Ireland was remarked on by as ancient a source as Ware (1662). Richardson (1975) does find historical evidence of a small number of earthquakes that occurred in Ireland and the immediate offshore area, however, these all appear to be low magnitude events that were only perceptible over small areas. Musson (2007) asserts that the relative absence of earthquakes in Ireland is not a result of poor recording, since documentary sources for Irish seismicity are at least as good as those for Wales, where there is abundant evidence for earthquake activity dating as far back as 1247. This suggests that it is unlikely that there are significant historical earthquakes in Ireland that are yet to be discovered.

Similarly, modern instrumental monitoring also demonstrates the remarkable lack of seismic activity in Ireland. A seismograph was installed at Rathfarnham Castle, County Dublin, in the first decade of the 20th century and operated until the 1960s. This recorded the magnitude 4.4 M_L earthquake on 11 January 1951 off Arklow, in the Irish Sea. A seismograph at the Valencia Observatory, County Kerry, began operation in the 1960s and has continued to present. A network of short period seismometers was installed in Ireland in the 1970s by Dublin Institute of Advanced Studies (DIAS), many of which operated for over two decades. This network was recently upgraded, with the installation of a number of broadband seismometers, beginning in 2011. The largest earthquake recorded by the instrumental network was a magnitude 4.0 M_L earthquake on 6 June 2012, approximately 60 km west of Belmullet, County Mayo. Britain has also had a network of seismometers in operation since the 1970s, which has improved detection capability in Ireland.

Recorded levels of seismic activity in Ireland are significantly lower than in Britain where there is substantial evidence of widely felt and occasionally damaging earthquakes stretching back many hundreds of years (Musson, 1994). Many of these earthquakes have also been felt strongly in Ireland, and, in fact, the most strongly felt earthquake in Ireland was the 1984 Lleyn Peninsula earthquake in North Wales, which had a magnitude of 5.4 M_L. However, the reasons for the dramatic difference remain poorly understood. Geologically, Ireland is very similar to the rest of the British Isles, sharing a common geological history, and many major structures are common to both Ireland and Britain.

This section provides an updated review of earthquakes in Ireland. Historical data from a number of available sources (e.g. Davison, 1924; Richardson, 1975) has been combined with modern instrumental data to construct a single coherent catalogue with a uniform moment magnitude scale. This catalogue is then used to estimate the background rate of natural seismicity that represents a numerical expression of the expected likely future seismicity of the region and that is consistent with the expected low strain rates. Two different catalogue of completeness relationships were used to estimate activity rate, each with different magnitude of completeness thresholds used for different time intervals.

5.2 Data

Data exists from two primary sources:

1. Historical archive containing references to felt earthquakes.
2. Instrumental catalogue data.

Richardson (1975) reviews historical references to seismic events felt in Ireland, providing a descriptive account of each event, along with a summary. This has been the primary source of historical information in

this review. Sources cited by Richardson (1975) include a number of well-known sources of information on historical earthquakes including Mallet and Mallet (1858), O'Reilly (1884), Roper (1889) and Davison (1924), as well as a number of other historical sources. Richardson (1975) assigns creditability ratings to these events based primarily on age: events prior to the 10th Century have a low creditability; events between the 10th and 17th centuries are considered dubious; and, events from the 17th Century on are considered high creditability.

In addition, Richardson (1975) determines the maximum observed earthquake intensity in Ireland from the historical accounts. Earthquake intensity is a qualitative measure of the strength of shaking of an earthquake determined from the observed effects on people, objects and buildings. A number of intensity scales have been developed including the Modified Mercalli (MM) scale and the European Macroseismic Scale (EMS). These consist of increasing degrees of intensity, each designated by Roman numerals or integers. The Modified Mercalli intensity scale ranges from imperceptible shaking (I) to catastrophic destruction (XII). Table 5.1 gives an abbreviated description of the degrees of the Modified Mercalli intensity scale.

Table 5.1: An abbreviated description of the degrees of the Modified Mercalli Intensity scale

Intensity	Shaking	Description/Damage
I	Not felt	Not felt except by a very few under especially favourable conditions.
II	Weak	Felt only by a few persons at rest, especially on upper floors of buildings.
III	Weak	Felt quite noticeably by persons indoors, especially on upper floors of buildings. Many people do not recognise it as an earthquake. Standing motor cars may rock slightly. Vibrations similar to the passing of a truck. Duration estimated.
IV	Light	Felt indoors by many, outdoors by few during the day. At night, some awakened. Dishes, windows, doors disturbed; walls make cracking sound. Sensation like heavy truck striking building. Standing motor cars rocked noticeably.
V	Moderate	Felt by nearly everyone; many awakened. Some dishes, windows broken. Unstable objects overturned. Pendulum clocks may stop.
VI	Strong	Felt by all, many frightened. Some heavy furniture moved; a few instances of fallen plaster. Damage slight.
VII	Very strong	Damage negligible in buildings of good design and construction; slight to moderate in well-built ordinary structures; considerable damage in poorly built or badly designed structures; some chimneys broken.
VIII	Severe	Damage slight in specially designed structures; considerable damage in ordinary substantial buildings with partial collapse. Damage great in poorly built structures. Fall of chimneys, factory stacks, columns, monuments, walls. Heavy furniture overturned.
IX	Violent	Damage considerable in specially designed structures; well-designed frame structures thrown out of plumb. Damage great in substantial buildings, with partial collapse. Buildings shifted off foundations.
X	Extreme	Some well-built wooden structures destroyed; most masonry and frame structures destroyed with foundations. Rails bent.

For a given earthquake, intensity is normally greatest at the epicentre and decreases with distance from this point. Intensity can be determined from historical accounts of earthquakes and used to estimate an earthquake location and magnitude. The spatial variation of intensity determined from historical accounts of earthquakes can be used to estimate an earthquake location and magnitude (e.g. Musson, 1989).

The events listed by Richardson (1975) are summarised in Table 5.2 and shown in Figure 5.1. These have been cross-referenced against Musson (1994) to obtain locations, magnitudes and the intensity at the epicentre (I_0) where possible. Thirteen of the twenty-six events occurred outside Ireland in England, Scotland or Wales. These were nearly all events of around magnitude 5 M_L or above that occurred in the western part of Britain and were widely felt across Britain and Ireland. Earthquakes on the Irish mainland or in the immediate offshore area have low intensities, mainly in the range II to V MM, and were generally only felt over small areas, suggesting that these were small earthquakes.

Locations have been assigned to these earthquakes directly from the area of maximum felt intensity, however, these are uncertain. For example, it is possible that the events felt around Cork could have occurred in the Celtic Sea, rather than in Cork itself. Similarly, the events felt in Wicklow and Wexford could have occurred in the Irish Sea. Magnitudes have not been determined for these events, except for the magnitude 4.4 M_L earthquake in the Irish Sea in 1951, for which instrumental data from the seismograph at Rathfarnham Castle was available

Table 5.2: Earthquakes felt in Ireland from 1500 to 1970 (from Richardson (1975). Locations, magnitudes and I_0 (the intensity at the epicentre) for the British earthquakes from Musson (1994)

Date	Latitude	Longitude	Epicentre	ML	I_0	Imax Ireland	Location of Imax Ireland
11/01/1951	53	–5.5	Irish Sea	4.4		IV	Wicklow Town
27/06/1906	51.62	–3.81	Swansea, Wales	5.2	VII	IV	Carnsore Point
19/06/1903	53.02	–4.49	Caernarvon, Wales	4.9	VI	IV	Wicklow coast
17/12/1896	52.02	–2.55	Hereford, England	5.2	VII	IV	Southeast coast
2/11/1893	51.81	–4.41	Carmarthen, Wales	5	VI	IV	Carnsore Point
18/8/1892	51.7	–5.04	Pembroke, Wales	5.1	VI	V	Carnsore Point
27/08/1881	52.67	–6.29	Gorey, Wexford			III-IV	Gorey, Wexford
28/11/1880	56.19	–5.3	Oban, Scotland	5.2	V	III	Northern Ireland
06/12/1879	54.8	–7.77	Stranorlar, Donegal		VII	V	Stranorlar, Donegal
02/01/1869	52.8	–6.47	Tinahely, Wicklow				Tinahely, Wicklow
24/10/1868	52.14	–8.65	Mallow, Cork		IV-V	IV-V	Mallow, Cork
6/10/1863	52.03	–2.95	Hereford, England	5.4	VI	IV	Southeast coast
9/11/1852	53.05	–4.43	Caernarvon, Wales	5.3	VI	V-VI	Dublin
17/3/1843	54.0	–3.6	Lancashire, England	5.1	VI-VII	II	Belfast
08/01/1840	55.25	–7.26	Inishowen, Donegal		IV-V	IV-V	Inishowen, Donegal
30/12/1832	51.65	–3.95	Swansea, Wales	4.3	VI	II-III	Castlebride, Wexford
25/06/1821	51.9	–8.47	County Cork				County Cork
06/04/1820	51.9	–8.47	Cork Harbour			V-VI	Cork Harbour
11/8/1786	54.53	–3.68	Whitehaven, England	5	VI-VII	II	Dublin
16/6/1786[1]			North Irish Sea				
01/10/1777	51.71	–8.52	Celtic Sea				Kinsale, Cork
15/4/1773	49.8	–2.2	Guernsey	4.4	V		Kerry
16/03/1762	52.34	–6.46	Wexford/Irish Sea			IV-V	Wexford
20/01/1760	52.98	–6.04	Wicklow			III-IV	Wicklow
27/1/1756	53.9815	–7.3018	Cavan/Monaghan		VII	VII	Cavan/Monaghan
7/10/1690	53.1	–4	North Wales	5	VI	III-IV	Dublin
29/7/1534			North Wales			III-IV	Dublin

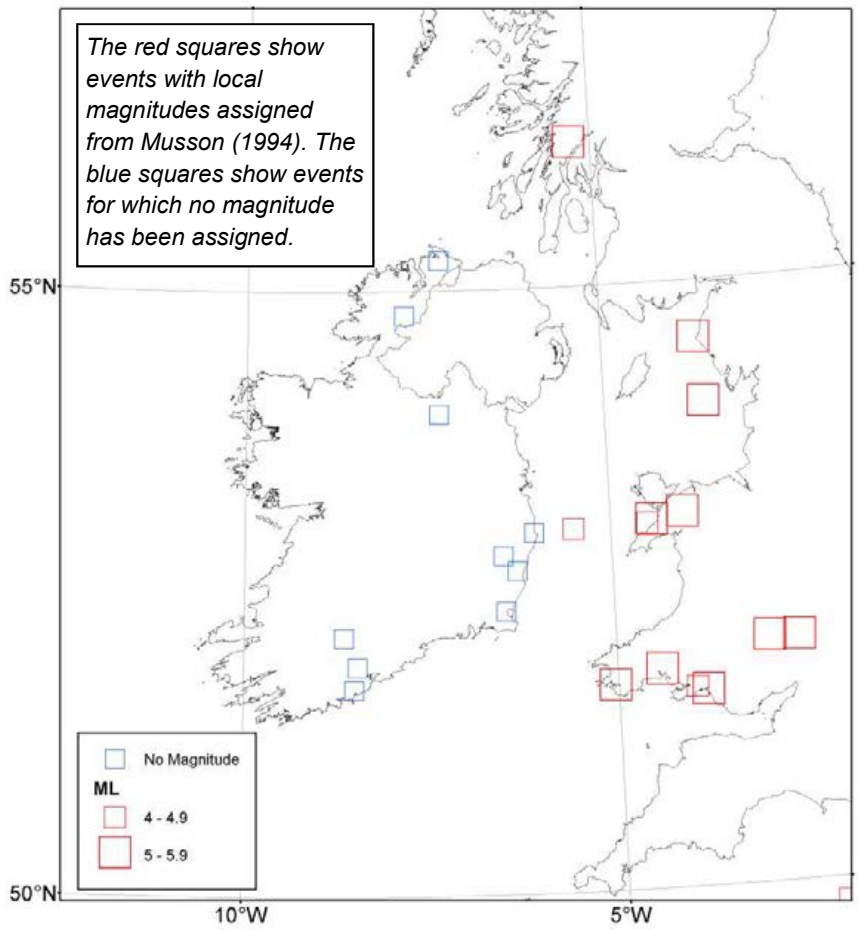

Figure 5.1. Historical earthquakes felt in Ireland (from Richardson, 1975).

Richardson (1975) assigns an intensity of VII MM to the Cavan/Monaghan earthquake of 1756, which corresponds to an earthquake causing superficial damage. However, the historical reports for this earthquake are unusual, and there are no clear reports of damage that are consistent with an earthquake source, suggesting that this may not have been an earthquake.

The historical earthquakes in Ireland occur in three localities: Wicklow, Wexford and the Irish Sea on the east coast; Donegal, in the north; and the south coast of Ireland around Cork. The Irish Sea does not appear to be very seismically active; however, one strong earthquake (5.1 M_L) did occur in 1843 with an epicentre between the Isle of Man and Morecambe Bay (Musson, 1994). Damage was reported from Castletown on the Isle of Man. Otherwise the only event of note is an earthquake on 11th January 1951 just off the coast of County Wicklow. This was felt over a wider area than its instrumental magnitude of 3.7 M_L (Musson, 1994) would suggest, giving it a magnitude determined from the felt intensities of 4.4 M_L.

Instrumental data for the period 1970 to present are available from two main sources: The Dublin Institute of Advanced Studies (DIAS) earthquake catalogue; and the BGS earthquake catalogue. The DIAS catalogue includes 127 instrumentally recorded earthquakes from 17th January 1980 to 19th September 2014. Twenty-eight of these have no magnitude and four have no location or magnitude. The BGS earthquake catalogue is a combination of the historical catalogue of Musson (1994) and later revisions for the period up to 1969, and earthquake parameters determined from instrumental data recorded by the UK National Seismic Monitoring Network thereafter (Musson, 1994; Baptie, 2012). It contains almost 10,000 instrumentally recorded local earthquakes from 1970 to present. Data from both catalogues are shown in Figure 5.2, with blue crosses showing DIAS data and red squares showing BGS data (symbols are scaled by magnitude). It is clear that there is considerable overlap between the two catalogues.

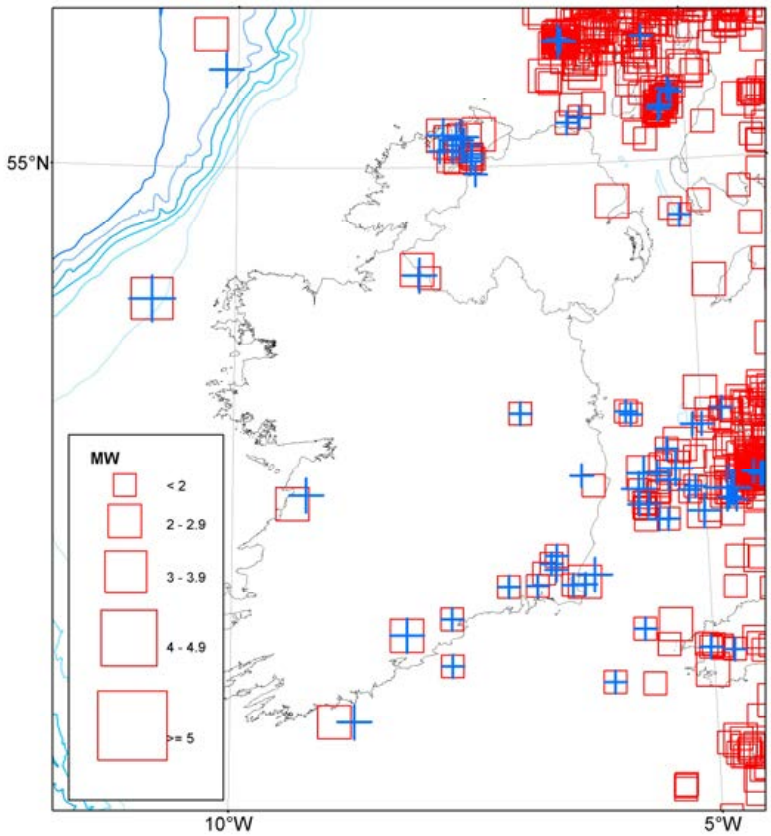

Figure 5.2. Instrumentally recorded seismicity in Ireland and Britain from 1970 to present.

Areas of higher seismic activity are Argyll in the west of Scotland, where earthquakes extend through the Hebrides and into Antrim in the north of Ireland. There is also some seismic activity in Donegal in the northwest of Ireland. Between 1984 and 2012, twelve earthquakes were recorded in this region, with magnitudes ranging from 0.7 M_L to 2.3 M_L. The largest was felt with an intensity of IV. The area of high activity in North Wales around the Lleyn Peninsula extends approximately southwest into the Irish Sea almost as far as the coast of Ireland around Wicklow. There is also some activity around Pembroke and the approaches to the Bristol Channel, as well as activity along the south coast of Ireland in Wexford, Waterford and Cork. A number of the events on the south coast of Ireland were felt, including a magnitude 2.2 M_L earthquake on 18th March 2014 that occurred off Wexford, and a magnitude 2.3 M_L earthquake on 4th December 2012, in the Celtic off County Cork. On 14th December 2005 a 2.8 M_L earthquake in the Irish Sea was felt in Wicklow, close to the magnitude 3.7 ML earthquake on 11th January 1951 event (Galloway, 2006) – the distance between the two epicentres is 27 km, but the 2005 event is much more accurately located.

There is considerably less seismic activity on the west coast of Ireland. However, the magnitude 4.0 M_L that occurred off the west coast of County Mayo on 6th June 2012 is the strongest Irish earthquake on record. This event occurred approximately 60 km west of Belmullet and was felt in Mayo, Sligo and Galway. Further south, a magnitude 2.7 ML earthquake occurred in County Clare on 6th May 2010. The most widely felt earthquake in Ireland remains the 1984 Lleyn Peninsula earthquake in North Wales, which had a magnitude of 5.4 M_L. It was felt with an intensity of IV on east coast of Ireland and III around the Irish Midlands.

It is notable that nearly all the seismic activity in Ireland, both instrumental and historical is concentrated around the coast and there is an almost complete absence of seismicity inland. Two exceptions are earthquakes on 20th August and 30th November 2011 in County Leitrim, with magnitudes of 1.5 M_L and 2.1 M_L, respectively. It is impossible to associate either of these earthquakes with a specific fault or with

anthropogenic activity due to the small magnitudes and uncertainties associated with the locations. The earthquake that occurred near Enfield, Meath, on 11th September 1993, is also an exception, and although the magnitude was only 1.1 M_L, it was felt with intensity III EMS. It is also notable that almost all the instrumental seismicity lies in areas where historical earthquakes have occurred. Mainly, Wicklow and the Irish Sea; Wexford, Waterford and Cork on the south coast of Ireland; and, Donegal in the north. The exception to this is the magnitude 4.0 M_L earthquake off the coast of Mayo in 2012.

To compare the DIAS and BGS catalogues, we excluded the earthquakes with no magnitudes or locations from the DIAS catalogue and find 73 events common to both the DIAS and BGS catalogues. We then compare the latitude, longitude and magnitude of the common events (Figure 5.3). It is clear that the location and magnitudes for the common events are very similar, with only small discrepancies, mainly for those earthquakes which are a considerable distance offshore to the west of Ireland. With this in mind, we opt to use the BGS catalogue in subsequent analysis, since it has a higher degree of completeness for those events closer to Britain.

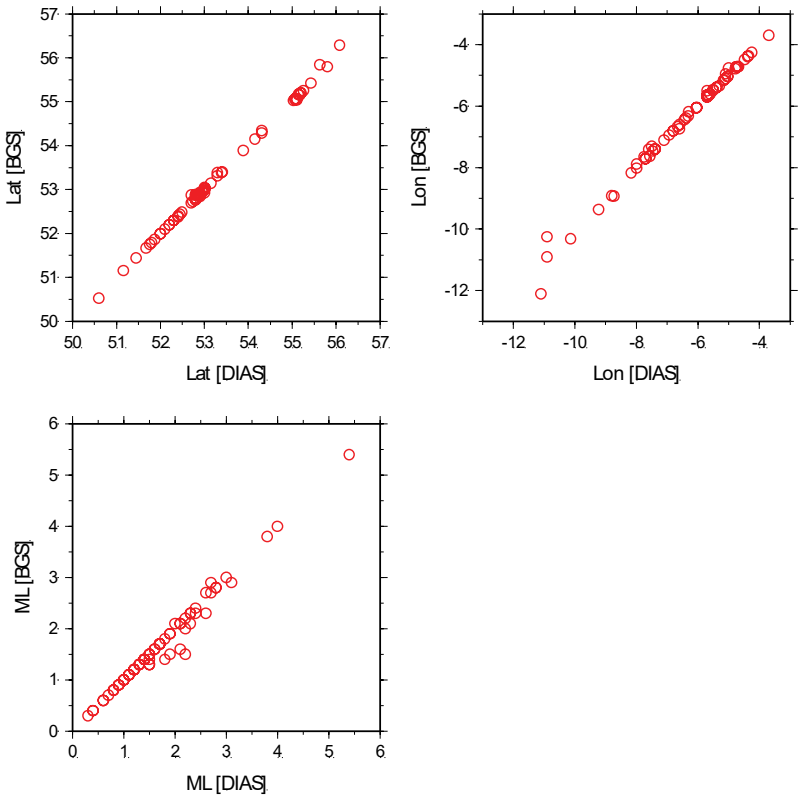

Figure 5.3. Comparison of the location and magnitudes of the 73 events common to both the BGS (y-axis) and the DIAS catalogue (x-axis).

5.3 Tectonic History

During the lower Palaeozoic the northern part of Ireland was located at the accretionary margin of Laurentia, while the southern part was located at the active margin of Avalonia. Between 470 and 380 Ma, the Grampian, Caledonian and Acadian orogenies (Woodcock and Strachan 2000) resulted in the closure of the Iapetus Ocean and the amalgamation of the Avalonian microcontinent (which included South East Ireland, England and Wales) with the edge of the continent of Laurentia (which included North West Ireland and Scotland). The collision zone between these two continents is marked by the Iapetus Suture Zone, which is thought to extend from the Shannon Estuary in the west across the Irish Midlands towards the northeast Highlands and into Britain (Phillips *et al.*, 1976). Figure 5.4 shows the major mapped fault structures in Ireland and Britain from Pharaoh *et al.* (1996), with the structures coloured by age. These Caledonian orogenic events led to intense deformation and much of the present day crustal fabric of

Ireland is dominated by this northeast-southwest Caledonian trend, which is clearly apparent across much of Ireland in Figure 5.4 and includes fault structures through the NCB.

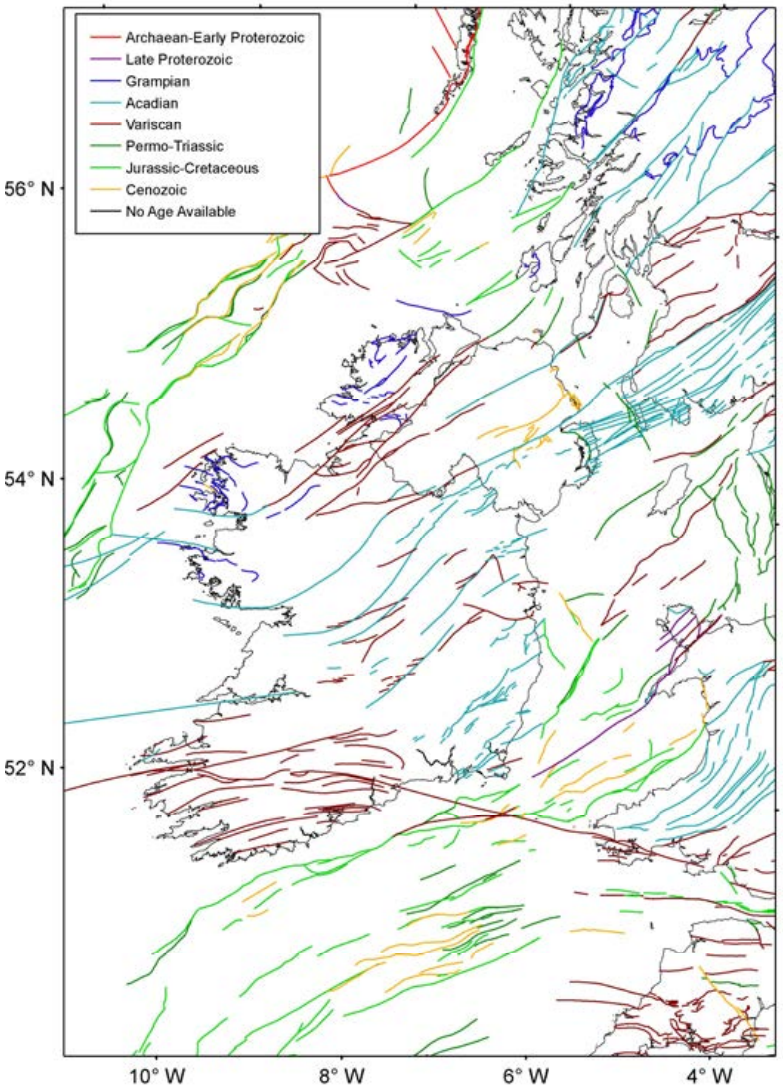

Figure 5.4. Major fault structures in Ireland and Britain (from Pharaoh *et al.*, 1996).

The main collision of Gondwana with Laurentia led to the Variscan orogeny in northwest Europe, forming a mountain belt in North America and Europe. Evidence of this can be found in the Irish Variscides, which are separated from the more weakly deformed rocks to the north by the Variscan Front. The latter is thought to run from Dungarvan Bay in the east to Dingle Bay in the west across the south of Ireland. Variscan deformation in Ireland is characterised by east–west oriented thrusts (e.g. Cooper *et al.*, 1986). These are most apparent in the south of Ireland, as shown by the brown Variscan structures in Figure 5.4, becoming less obvious in central and northern regions (e.g. Gill, 1962; Masson *et al.*, 1999). It remains a source of debate if any of the observed seismicity could be associated with these east-west striking Variscan faults.

During the Jurassic and Cretaceous, Pangea began to split apart. The opening of the Atlantic during the Jurassic and Cretaceous as the Pangea supercontinent began to split apart caused crustal extension in British and Ireland. This led to the formation of large rift basins and fault-bounded troughs offshore western Ireland (e.g. Naylor and Shannon, 2009). Seismicity in the Irish Sea off the Wicklow coast appears to be associated with some of these basin bounding faults (green lines in Figure 5.4). Similarly, seismicity to the south and west of Ireland could also be associated with offshore faults of this nature.

Present day tectonic deformation in Ireland, appears to be dominated by forces generated at the Mid-Atlantic ridge due to gravitational effects acting perpendicular to the spreading ridge, and, to a lesser extent, forces resulting from the collision of Africa with Europe. This is expected to result in a prevailing northwest to north-northwest orientation of the maximum horizontal compressional stress. A number of authors, including Gölke and Coblentz (1996) have modelled tectonic stress in northwest Europe due to ridge push and continental collision, finding a maximum horizontal stress orientation that is consistently northwest southeast. A secondary source of crustal stress in the north of Ireland may be glacio-isostatic adjustment (GIA), resulting from the removal of the British Irish ice sheet. Vertical uplift rates in the north of Ireland modelled by Bradley *et al*. (2009) are around 1mm per annum. In Scotland, a correlation between the spatial extent of seismicity and the expected area of maximum glacio-isostatic uplift has been noted by a number of authors, including Musson (1994).

No Irish or British earthquake recorded either historically or instrumentally has produced a surface rupture and typical fault dimensions for the largest recorded British earthquakes are of the order of 1–2 km (Baptie, 2010), therefore, it is difficult to associate earthquakes with specific faults, particularly at depth, where the fault distributions and orientations are unclear. In addition, the uncertainties in the focal depths determined for earthquakes are generally large. However, focal mechanisms determined for British earthquakes (Baptie, 2010) show mainly strike-slip faulting, with fault planes that are broadly sub-parallel to either a north–south or east–west direction. These appear to be favourably oriented for reactivation under the existing northwest southeast maximum horizontal stress direction.

5.4 Catalogue Analysis

The relationship between the magnitude and number of earthquakes in a given region and time period takes an exponential form that is referred to as the Gutenberg-Richter law (Equation 3.1).

Determining both the activity rate, a, which is a measure of the absolute levels of seismic activity, and the b value, the proportion of large events to small ones, can be problematic when the number of events is small, the uncertainty in the b value is high. Also, the number of earthquakes at lower magnitudes is often underestimated in many earthquake catalogues as a result of the inability to detect smaller events, resulting in a roll-off in the magnitude–frequency relationship at low magnitudes (see section 3.2). This leads to the concept of a completeness magnitude, *Mc*, which can be defined as the lowest magnitude at which 100% of the earthquakes in a space–time volume are detected (Rydelek and Sacks, 1989). It is desirable to be able to specify the different time intervals of the catalogue that have different magnitude of completeness thresholds, in order to maximise the information used. Therefore, a maximum likelihood procedure, originally proposed by Veneziano and Van Dyck (1985) following Weichert (1980), and further elaborated as a penalised maximum likelihood in Johnston *et al*. (1994) is often used. This method computes a 5 x 5 matrix of possible values, expressing the uncertainty in these two parameters while also taking into account the correlation between them. The penalised method allows a weighted prior to be used, which acts as a constraint on the b-value in cases where there are few earthquakes, and prevents unrealistic results from emerging where the data are poor.

A seismic source model describes the occurrence of earthquakes in the region of interest and is generally developed using different types of information including earthquake catalogues (lists of the date, location, and magnitude of all known earthquakes in a region) and tectonic information (including geological and tectonic information like the location of major faults). The probability of an earthquake of a given magnitude in all parts of a source zone is assumed to be equal and a source zone is described by a single a and b value. In this study, the seismic source zone for Ireland developed in the SHARE (Seismic Hazard Harmonization in Europe) project (Giardini *et al*., 2013) is used. The source zone is shown by the black lines in Figure 5.5, along with all historical and instrumental seismicity in and around Ireland from BGS catalogue.

It is common practise is to use moment magnitude, M_W, in seismic catalogues. However, this is not straightforward when values are originally expressed in a mixture of scales, which may not always be

clearly defined. Since the BGS catalogue magnitudes are expressed mainly in terms of local magnitude, M_L, all magnitudes have been converted to moment magnitude, M_W, using the relation of Grünthal *et al*. (2003).

In addition, it has been shown (Tinti and Mulargia, 1985; Rhoades, 1996; Rhoades and Dowrick, 2000; Castellaro *et al*., 2006) that ignoring uncertainty in the magnitude values results in an overestimation of the seismicity (see also the discussion in Musson, 2012). Rhoades and Dowrick (2000) propose a correction factor to be used in the activity rate calculations, based on the standard error of individual earthquake magnitudes, and this is applied here. It is assumed that all magnitude values in the catalogue have an uncertainty of ± 0.3.

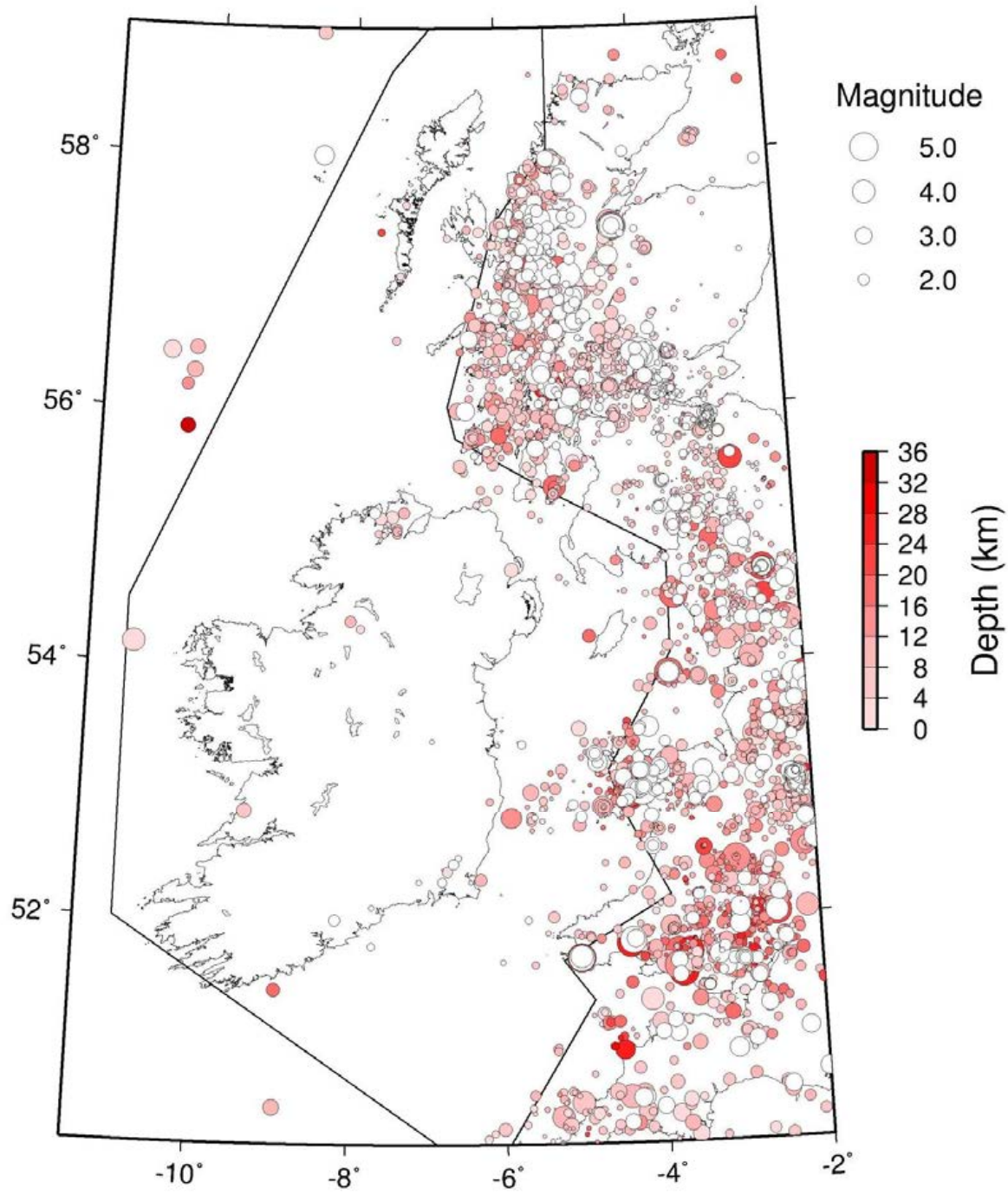

Figure 5.5. All historical and instrumental seismicity in and around Ireland (from BGS catalogue).

Equation 3.1 was applied to all the seismicity contained within the source zone of Ireland, using the penalised maximum likelihood method. Two different catalogue of completeness relationships were considered, each with different magnitude of completeness thresholds used for different time intervals. These are shown in Table 5.3 and Table 5.4. Table 5.3 shows the magnitude of completeness in different time intervals used for offshore areas around Britain**.** Table 5.4 shows the magnitude of completeness in different time intervals used for Britain (Musson and Sargeant, 2007). Using the catalogue completeness for offshore areas, only two earthquakes fall within the source zone. Since two earthquakes are not enough to reliably determine both parameters, a prior b-value of 1.00 is assumed. The results are shown in Figure

5.6, with the red line showing the results using the catalogue completeness for offshore areas around Britain, and the blue line showing the results using the catalogue completeness for Britain. Using the catalogue completeness for offshore areas gives an activity rate of a = 2.1673 for a magnitude of 0. Using the catalogue completeness for Britain gives an activity rate of is a = 1.4142, with b=1.023. The values found in the SHARE project are a = 2.1756 and b=1.00.

Table 5.3. Magnitude of completeness for different periods of time used for offshore areas around Britain

Magnitude	Date
3.0	1980
3.7	1970
4.7	1850
5.7	1700

Table 5.4. Magnitude of completeness for different periods of time used for Britain by Musson and Sargeant (2007)

Magnitude	Date
3.0	1970
3.5	1850
4.0	1750
4.5	1700
5.0	1650
6.5	1000

An activity rate of a = 2.1673 suggests that there should be an earthquake with a magnitude of 4 M_W or greater, somewhere within the Irish source zone approximately every 70 years. However, this would lead to significantly more earthquakes than are observed. An activity rate of a = 1.4142 leads to an earthquake with a magnitude of 4 M_W or greater approximately every 476 years, which agrees with the observed data better. This highlights the problem of estimating reliable rates in low seismicity regions, where data are sparse, that allow seismic hazard to be reliably quantified.

By comparison, the average value for Britain gives a = 3.23 and b = 1, equivalent to a magnitude 4 M_W earthquake every 6 years and 1–2 earthquakes with a magnitude of 3 M_W or above every year. These values are in good agreement with the observed data.

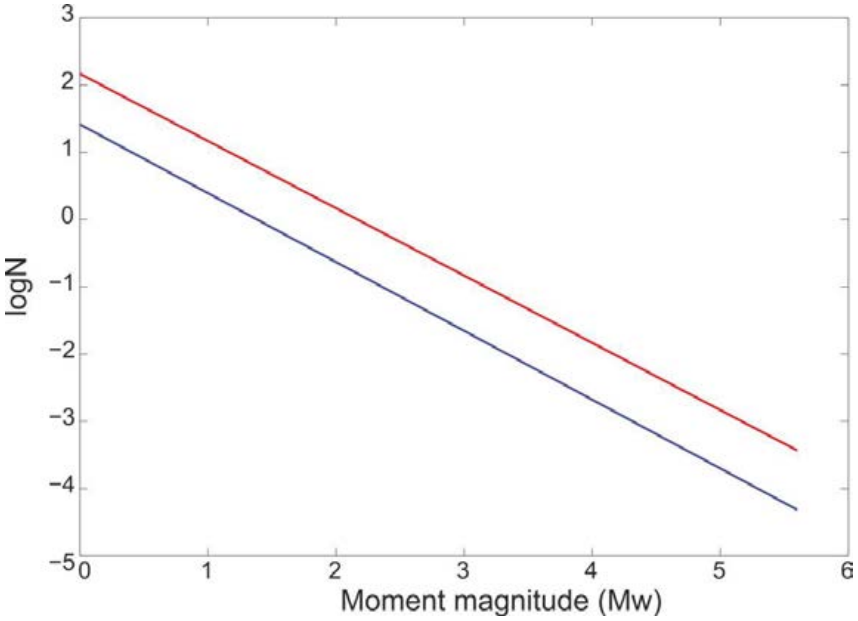

Figure 5.6. Magnitude-frequency data for the source zone of Ireland.

5.5 Possible Ground Motions for Small and Moderate Earthquakes

Seismic hazard is usually defined as the probability of a particular level of ground motion being exceeded within a certain period of time. Accurate assessment of seismic hazard requires knowledge of how ground motion relates to the characteristics of an earthquake, how it attenuates with distance, and how it might be affected by the geological conditions at the site of interest. In the assessment of seismic hazard, strong ground motions are commonly estimated using empirical ground motion prediction equations (GMPEs). Abrahamson *et al*. (2008) provide a comparison of the recent Next Generation Attenuation (NGA) models. However, the choice of an appropriate model is often difficult, since in most parts of the world there are insufficient data to produce well-constrained empirical models. This is certainly the case in Ireland. In such cases it is now becoming generally accepted that it is better to use a robust ground motion model derived from a large international data set with the widest possible sampling of the magnitude-distance domain than a local model that may be less well constrained (Douglas, 2007; Bommer *et al*., 2007). For example, the SHARE project used a number of GMPEs including Chiou and Youngs (2008) and Akkar and Bommer (2010).

An alternative approach is to simulate ground motion using stochastic modelling based on the earthquake source parameters as well as parameters to characterise path and site effects (Boore, 1983, 2003). Here, we use this approach and the SMSIM software (Boore, 2005) to explore possible ground motions for small to moderate earthquakes that might occur in Ireland, and compare these with some existing regulations for vibrations from blasting in the UK.

The earthquake source is parameterised by the seismic moment, source spectrum shape and stress drop. The former can be calculated directly from earthquake magnitude (Hanks and Kanamori, 1979). Here, we assume that for small magnitudes local magnitude, M_L, is approximately equal to moment magnitude, M_W. We use a single corner frequency model for the shape of the source spectrum (Brune, 1970). Stress drop is an important parameter in the dynamics of the rupture process and can have a strong effect on recorded ground motions. However, most earthquakes have stress drops in the range of a few MPa (megapascals) to a few tens of MPa. Here, a fixed stress drop of 3 MPa has been assumed.

Path effects are incorporated using geometrical spreading and anelastic attenuation terms. At short hypocentral distances geometrical spreading is dominated by the body wave term and we use the path attenuation quality factor determined for the UK by Sargeant and Ottemöller (2009). We do not consider

either site specific attenuation or amplification. Note that hypocentral distance is the distance between the earthquakes focus and the observer that includes the effect of the earthquake focal depth. As a result, the greater the focal depth, the greater the hypocentral distance. Historical and instrumental earthquakes from in and around Britain and Ireland from the BGS catalogue are shown in Figure 5.5, with coloured symbols according to earthquake depth. From this, it is clear that earthquakes are confined within the thickness of the crust, with the deepest earthquakes occurring at depths of up to 30 km. However, most earthquakes occur at rather shallower depths of between 5 and 20 km. The available observations of earthquake depths in Ireland show that this is also the case here. By contrast, earthquakes induced by anthropogenic activities often occur at very shallow depth. For example, earthquakes related to coal mining in the UK often have depths of around 1 km, corresponding to the depth of the mining activity. Similarly, the earthquakes induced by hydraulic fracturing operations at Preese Hall, Blackpool, UK, occurred at depths of approximately 3km, close to the point of fluid injection. This means that despite having generally small magnitudes, such induced earthquakes can often be felt as a result of their proximity to the surface.

Figure 5.7 shows curves (coloured lines) of ground velocity as a function of hypocentral distance calculated for earthquakes with magnitudes of 2.0, 3.0, 4.0 and 5.0. The dashed lines show the limits for acceptable levels of ground vibrations caused by blasting from BS 6472-2 and also the limits for vibrations caused by blasting, above which cosmetic damage could take place (BS 7385-2). Blasting occurs on a regular basis throughout the British Isles and maximum magnitudes for quarry blasts recorded in the BGS catalogue are around 2.5 M_L. The limits specified by BS 6472-2 are 6–10 mm/s during the working day, 2mm/s at night time and 4.5mm/s at other times. BS 7385-2 gives limits of 15 mm/s at 4 Hz, increasing to 20 mm/s at 15 Hz and 50 mm/s at 50 Hz. The limits increase with the frequency of the vibration since high frequency vibrations are less likely to cause damage. In simple terms, the observed frequencies for earthquake ground motions are largely controlled by the magnitude of the earthquakes and the stress drop, although anelastic attenuation and site conditions can also play an important role. Figure 5.8 shows corner frequency (equivalent to the peak frequency of ground velocity) as a function of earthquake magnitude for a fixed stress drop of 1 MPa. Corner frequency decreases as magnitude increases, so that earthquakes with magnitudes of 2 or less have corner frequencies of 10 Hz or above, whereas earthquakes with magnitudes of 4 or above have corner frequencies of 1 Hz or less. This means that the 15 mm/s limit at 4 Hz is probably the most relevant for earthquakes in the magnitude range 3–4.

Earthquakes with magnitudes of 4.0 or above may approach the limits for cosmetic damage set out in BS 7385-2 but generally only at hypocentral distances of less than 10 km. Smaller earthquakes, with magnitudes of 3.0 may also exceed the limits for vibration set out in BS 6472-2, though at even small distances of less than a few kilometres. Given the strong variability of observed ground motions from earthquakes, as well as the influence of factors such as variable stress drops and site conditions, which have not been included in our calculations, the modelled ground motion shown here should be considered as indicative only, rather than encompassing the fully extent of possible ground motions in this magnitude and distance range. However, we do find good general agreement, between our calculations and many observations of small earthquakes in the British Isles.

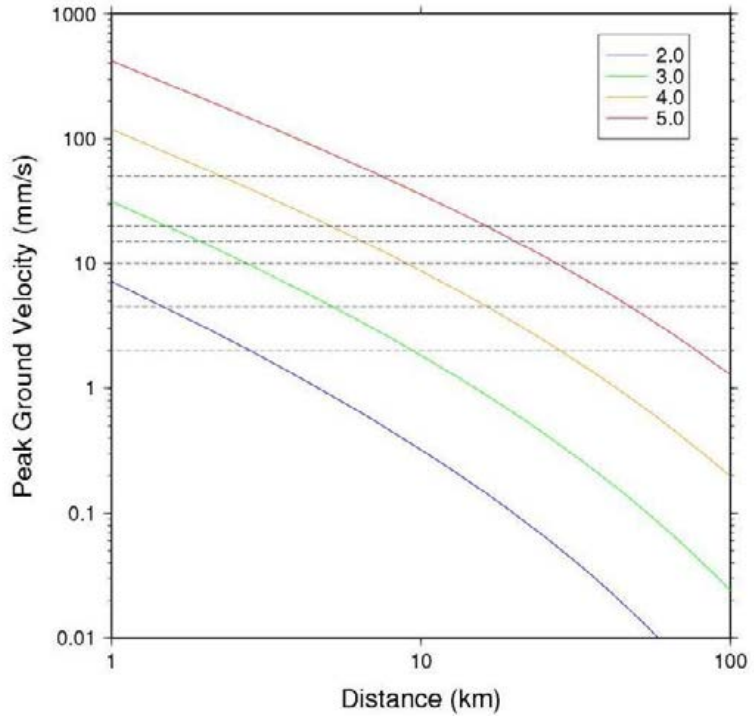

Figure 5.7. Modelled peak ground velocity plotted as a function of hypocentral distance.

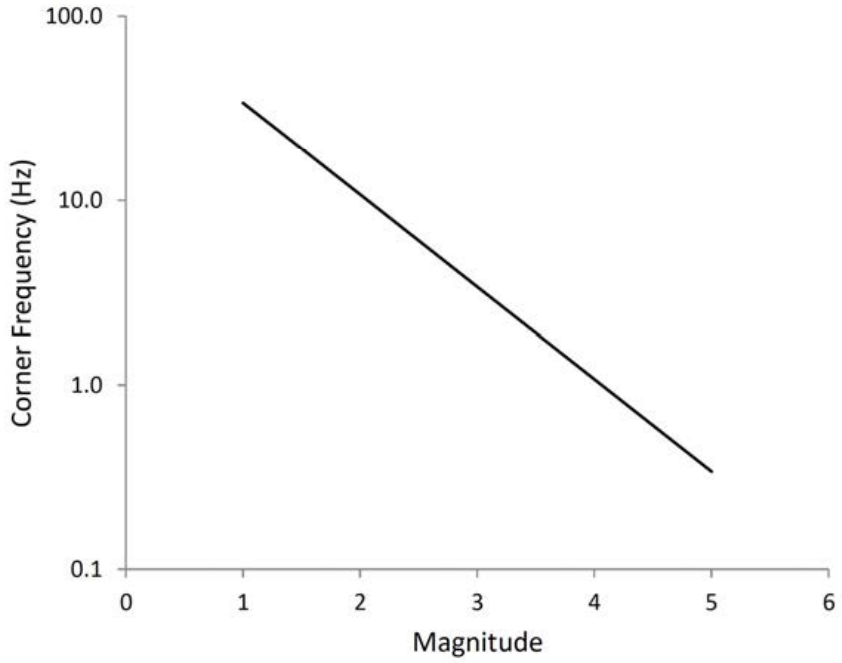

Figure 5.8. Earthquake corner frequencies (equivalent to the peak frequency of (ground velocity) as a function of earthquake magnitude for a fixed stress drop of 1 Mpa.

Figure 5.9 shows peak ground velocities calculated for a range of earthquake magnitudes and hypocentral distances using the same method. The curves show the fixed values of ground velocity given by BS 6472-2 and BS 7385-2. This allows us to estimate the magnitudes and distances at which the model exceeds these limits. Again, it is clear that the limits above which cosmetic damage could occur (BS 7385-2) are only exceeded within a few kilometres of the hypocentre for earthquakes with a magnitude of 3, and within around 10 km of the hypocentre for earthquakes with a magnitude of 4. This seems reasonably consistent

with observations that the largest mining-induced earthquakes, with magnitudes of around 3.0 M_L, caused some superficial damage (Westbrook *et al*., 1980; Redmayne, 1998) including, minor cracks in plaster and harling.

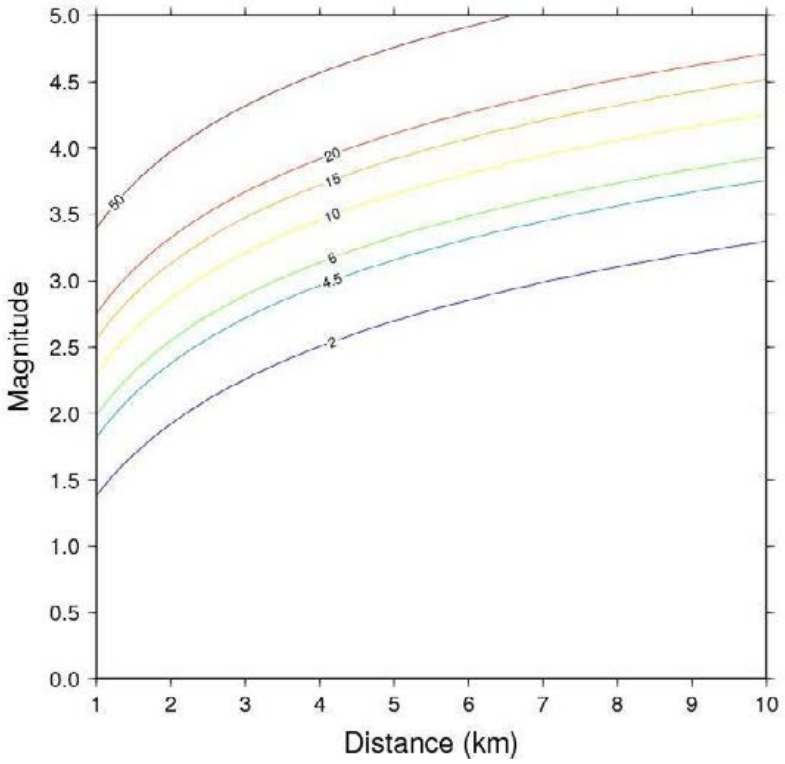

Figure 5.9. Peak ground velocity calculated for a range of earthquake magnitudes and hypocentral distances.

For comparison, Figure 5.10 shows fixed values of macroseismic intensity (EMS) as a function of magnitude and distance. The European Macroseismic scale (EMS) (Grünthal, 1998) is similar to the Modified Mercalli scale. The calculations are based on the intensity attenuation relationship derived for the UK by Musson (2005). The 6 EMS contour, the level at which some slight damage might be occur, appears at magnitudes of just over 2.0, whereas the 15 mm/s limit for cosmetic damage appears at a slightly higher magnitude of 2.5 M_L. This raises the possibility that intensity calculations are overestimated, perhaps, because there are relatively few observations at such small hypocentral distances, which might result in the attenuation function being relatively poorly constrained.

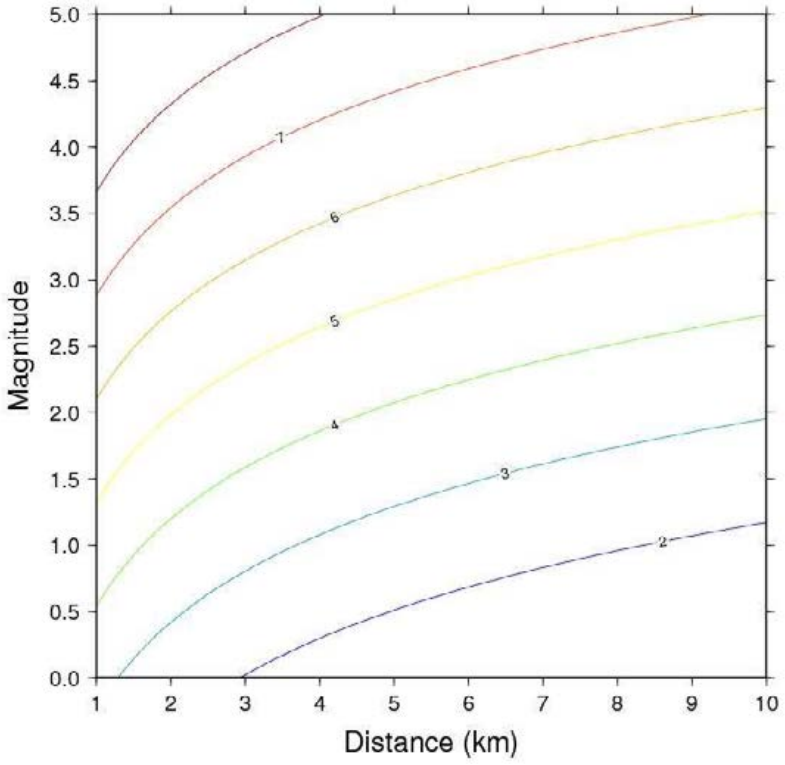

Figure 5.10. EMS intensities for a range of earthquake magnitude and hypocentral distances.

5.6 Public Perception of Potential Damage from Earthquakes

While there has been some research undertaken on assessing the public perception of shale gas extraction in the UK, (O'Hara *et al*., 2013), and the USA (Borick *et al*., 2014) very little documented evidence exists of the public perception to seismic activity alone.

Nottingham University has undertaken 10 surveys on public perception of fracking since March 2012. The possible link between fracking for shale gas and earth tremors has triggered considerable concern and is viewed by some as a potentially dangerous and damaging impact of shale gas exploration. Two small earthquakes in April and May 2011 in the Blackpool area close to where Cuadrilla Resources were fracking for shale gas were widely reported in the media and led to the suspension of fracking at the site pending further investigation. The release of the Preese Hall report in April 2012 and an acknowledgement by Cuadrilla Resources that their activities were the likely trigger for the earth tremors was also widely reported. It is therefore not surprising that the majority of people who correctly identified shale gas also considered it to be associated with earthquakes, with the number of people making this association being high throughout. However, since its peak in April 2012 the association has declined significantly and in September 2014 stood at 49% with the differential being under +20% down significantly from a peak of +58% in April 2012 (O'Hara *et al*., 2013).

An online study by Cardiff University on public attitudes to fracking which used a large and diverse sample found a relatively high degree of ambivalence towards fracking with minor tremors ranking 13th behind other risk factors. When the respondents were asked if they were concerned about earthquake risk 13.2% strongly agreed; 27.2% agreed; 38.7% neither agreed nor disagreed; 14.9% disagreed and 5.9% strongly disagreed (Whitmarsh *et al*., 2014)

5.7 Conclusions

A review of published data confirms that earthquake activity in Ireland is very low. Historical accounts of seismic events felt in Ireland amount to only twenty-six events in the interval 1500 to 1970, which can be

deemed credible. Of these, half of the accounts can be attributed to earthquakes that occurred outside Ireland in England, Scotland or Wales. These were nearly all events of around magnitude 5 M_L or above that occurred in the western part of Britain and were widely felt across Britain and Ireland. The other thirteen events occurred in Ireland and the immediate offshore area. These have low intensities and were only felt over small areas suggesting that these were small earthquakes. Magnitudes have not been determined for these historical Irish earthquakes, except for the magnitude 4.4 M_L earthquake in the Irish Sea in 1951, for which instrumental data from the seismograph at Rathfarnham Castle was available. In addition, the locations remain uncertain, having been assigned directly from the area of maximum felt intensity. These historical earthquakes in Ireland correspond to three localities: Wicklow, Wexford and the Irish Sea on the east coast; Donegal, in the north; and the south coast of Ireland around Cork. The historical reports for the Cavan earthquake in 1756 are unusual and this may have been misinterpreted as an earthquake. Given the good standard of historical records in time period in question, it seems quite unlikely that any significant earthquakes remain undiscovered.

Instrumental data from the DIAS and BGS catalogues confirm these low rates of seismic activity. Ireland had at least one operational seismograph throughout the 20th Century and the first seismograph network was installed in 1977. These networks successfully detected and located a number of earthquakes in the period 1980 to present. Although with lower magnitudes of detection, more earthquakes have been detected. Almost all the instrumental seismicity lies in areas where historical earthquakes have occurred. Mainly, Wicklow and the Irish Sea; Wexford, Waterford and Cork on the south coast of Ireland; and, Donegal in the north. The exception to this is the magnitude 4.0 M_L earthquake off the coast of Mayo in 2012, which is the largest Irish event in the catalogue. It is also notable that nearly all the seismic activity in Ireland, both instrumental and historical, is concentrated around the coast and there is an almost complete absence of seismicity inland, with only two instrumentally recorded earthquakes in County Leitrim and the anomalous Cavan earthquake in historical times.

Comparison of the DIAS and BGS instrumental earthquake catalogues clearly shows that the locations and magnitudes for the common events from each are very similar, although small differences may arise for those earthquakes which are a considerable distance offshore to the west of Ireland.

Calculated earthquake activity rates for Ireland were found to vary depending on the assumed level of completeness of the earthquake catalogue. Using the same catalogue completeness thresholds as for Britain suggests that there should be an earthquake with a magnitude of 4 M_W or greater, somewhere in Ireland and the surrounding offshore area, approximately every 476 years. This is reasonable agreement with the observed data. However, using a more conservative estimate of catalogue completeness leads to a higher activity rate, which would lead to significantly more earthquakes than observed. This highlights the problem of estimating reliable rates in low seismicity regions that allow seismic hazard to be reliably quantified. The average activity rate for Britain suggests that there should be an earthquake with a magnitude of 4 M_W or greater approximately every six years. The reasons for the dramatic difference remain remains poorly understood, given the geological and tectonic similarity between Ireland and Britain.

Modelled ground motions for earthquakes with moderate magnitudes that may occasionally occur in or around Ireland suggest that ground velocities are unlikely to exceed typical levels at which cosmetic damage might occur, except close to the earthquake source.

6 Task 4: Assessment of the Magnitude and Physical Effects of Induced Seismicity That May Be Associated with UGEE Projects/Operations in the Island of Ireland

6.1 Introduction

The injection of fluid under high pressure for the recovery of hydrocarbons by hydraulic fracturing generates two distinct groups of earthquakes:

1. Microseismic events during hydraulic fracturing are the result of deliberate generation and propagation of fractures (by high pressure fluid injection), which increase the rock matrix permeability and allow gas trapped in unconnected pore space to escape to a borehole for collection. These events are an intrinsic part of the hydraulic fracturing process.

2. Larger triggered events can be caused by increased fluid pressure, or stresses caused by pressure induced deformation of the rock volume, on existing faults that have previously been critically stressed by loading external to the fracturing process.

Many thousands of microseismic events can be expected in the course of any injection. Studies examining their size distribution have arrived at a broad consensus that the magnitude probably never exceeds M3.0. Events of this energy, while they are felt locally, are unlikely to cause any structural damage or other social consequences (see for example Green *et al*., 2012). In addition, microseismic events are a direct consequence of the injection process and are therefore, at least in principle, completely controllable. It has been shown that the rate of production of these events is closely related to the injection rate; the induced seismicity rate drops to zero when the injection is stopped (McGarr, 2014). For a review of induced seismicity at UGEE sites globally, see Section 8 of this report for further assessment of damage.

Triggered events on the other hand, whose size is not bounded by the energy of the injection, are the result of interaction between the injection process and unknown pre-stressed faults. They are therefore much more difficult to forecast. Such events can occur even after depressurisation has occurred, as was the case following the Basel geothermal project. This project was abandoned when a M3.4 event occurred when the system was being drained (Bachmann *et al*., 2011). It is also true that a large event may be triggered by a small stress perturbation (e.g. Gupta, 2002; Ellsworth, 2013). For example, the M8.7 Nias earthquake, which occurred 3 months after the great Sumatra-Andaman earthquake of December 2004, was the fourth biggest earthquake every recorded instrumentally and is likely to have been triggered by an interaction stress of less than 0.02MPa, equivalent to the stress of a very gentle handshake (McCloskey *et al*., 2005; Nalbant *et al*., 2005). Such triggered events have been the subject of intensive study, particularly in the field of the Coulomb stress interaction theory (see Section 6.2.1), for some 20 years and an extension of this, the Coulomb Rate-State (CRS) theory, has given very encouraging results in probabilistic forecasts of the triggered distributions.

Since no satisfactory deterministic model for forecasting fluid induced seismicity exists, we have used state-of-the-art insights arising from CRS theory together with the Bayesian statistical techniques developed at the University of Ulster and which are described in this report to develop a model for monitoring and short-term forecasting of fluid induced seismic sequences. This model is then used to illustrate the importance of uncertainty in forecasting such non-linear processes in complex systems and to assist in development of appropriate baseline and ongoing monitoring which is an essential part of any well managed UGEE project.

6.1.1 Organisation of this section

The theoretical background of the forecast model is outlined in Section 6.2. The static Coulomb stress model for the interaction triggering of earthquakes will be outlined briefly. It is shown that forecasts based on the simple Static Coulomb stress model are fraught with data quality issues and fail to predict some obvious features of observed, triggered sequences. This leads into a development of the general CRS theory, which gives time-dependent seismicity rates in a volume, under an arbitrary stressing history and, in particular, assuming a specific reference seismicity model. This section is concluded with a brief overview of the principles of the lattice-Boltzmann coupled fluid-elastic simulator, initially developed in the University of Ulster and subsequently in University College Dublin.

In Section 6.3 the implementation of our CRS based forecast is outlined, given non-ideal baseline estimates. This includes a detailed description of the statistical methods employed.

In Section 6.4 forecasts for a series of scenarios given different reference activity levels and baseline network qualities are presented. For the purposes of this report, the network quality is quantified only by the magnitude of completeness, M_c, defined as the magnitude above which all earthquakes are detected (and located); good quality networks can detect small events and therefore have small M_c (see Section 4.3). The implications for the nature of the uncertainties in the forecasts of increased activity or decreased M_c are illustrated.

In Section 6.5, the consequences of these results are discussed in terms of baseline as well as operational seismic monitoring, Recommendations are presented in Section 6.6.

Note that the social consequences and likely public perception of fluid induced seismicity has been thoroughly covered in Task 3 Sections 5.5–5.6.

6.2 Scientific Background to the Forecasting Protocol

6.2.1 Static Coulomb stress triggering

Deformation of the earth's crust results in a perturbation of the stress in the rock volume; if this deformation can be modelled, the stress perturbation field can be calculated. These stress perturbations are the driving force, for example, for the aftershocks that follow every earthquake. In this case, the deformation is the result of slip on the ruptured mainshock fault plane and it can be estimated by modelling the elastic response of the volume to a set of dislocations on the fault, corresponding to a model of the mainshock slip distribution (see, for example, Figure 6.1a).

The Coulomb Failure Stress perturbation (ΔCFS) at any point in the volume is defined by

$$\Delta CFS = \Delta\tau - \mu(\Delta\sigma - \Delta p) \qquad \text{Equation 6.2.1}$$

(e.g. Cocco and Rice, 2002), where $\Delta\tau$ is the change in shear stress on the failure plane, μ is the coefficient of friction, $\Delta\sigma$ in the change in normal stress and Δp is the change in pore-fluid pressure. It is ΔCFS that is used to describe the stress perturbation, since it includes not only the increase in stress in the direction of failure of a fault $\Delta\tau$, but also the "unclamping" of a fault that occurs when a decrease in $\Delta\sigma$ and/or an increase in Δp reduces the fault friction. An increase in ΔCFS at any point therefore indicates that a fault located there will have been brought closer to failure as a result of the stress perturbation. The mainshock that caused the perturbation is said to "interact" with its aftershocks by this mechanism.

Although this model was developed to explain earthquake aftershock sequences, it is directly applicable to the problem of induced seismicity. The pore fluid pressure change, Δp in Equation (6.2.1), in the context of aftershocks, is the result of deformation of the rock volume and pore space by the mainshock. In the context of induced seismicity, the pore fluid pressure changes are the result of injection of fluid into the crust. In addition, the fluid causes elastic deformation of the earth's crust so that $\Delta\tau$ and $\Delta\sigma$ are non-zero. The problem is more complex because these perturbations are now time-varying. However, if the deformation can be modelled, the Coulomb stress changes can be estimated; a time-dependent form of Equation (6.2.1) holds for the Coulomb stress changes, and the triggering process is the same. The modelling of this deformation field is discussed in Section 6.3.

Much of the research on Coulomb stress interaction has been motivated by the success of early work in explaining the spatial distribution of aftershocks around the 1992 M7.4 Landers earthquake (King *et al*., 1994) in Southern California. The Coulomb stress perturbations in the Landers region resulting from that earthquake (from the slip model in Figure 6.1a) are shown in Figure 6.1b, along with the locations of 1.5 years of aftershocks in Figure 6.1c. The vast majority of aftershocks occurred where the Coulomb stress perturbation was positive. The prominence of the Landers sequence in Coulomb stress studies over the last 20 years is partly because of the success of this paper in explaining the spatial distribution of Landers aftershocks but also because of the quality and availability of the data.

However, while visual inspection of Figure 6.1 appears convincingly to show that the simple Coulomb model explains the locations of the aftershocks well, a detailed examination suggests the triggering is more complex.

Firstly, an examination of the relationship of the seismicity before and after the mainshock (see Figure 6.2, after Nic Bhloscaidh *et al*., 2014) shows how the aftershock locations are controlled to first order, not by the distribution of Coulomb stress change, but by a pre-existing spatial distribution related to the location of major faults. The aftershock rates in Figure 6.2b are much better forecast by the rate of pre-mainshock seismicity (which we refer to as the reference seismicity) in Figure 6.2a than they are by the classic Landers stress map in Figure 6.1b.

This picture is complicated further by the fact that the clusters in activity to the south and west of the main rupture are not direct aftershocks of Landers at all, but aftershocks of the smaller Joshua Tree (marked JT on Figure 6.1c) and Big Bear (BB) earthquakes. Also, the Barstow (B) sequence, to the north of the Landers rupture, is thought to have been triggered by the passage of seismic waves from the mainshock, therefore by dynamic stresses and not static stresses. All these events occurred in regions of positive Coulomb stress change despite not having been directly triggered by the static stress field. They therefore spuriously reinforce the positive picture presented in Figure 6.1.

Another issue is that the size of $\Delta\tau$ and $\Delta\sigma$ are dependent on the orientation of the fault plane onto which they are resolved. Given the large uncertainty in seismological estimates of earthquake failure planes (known as focal mechanisms) in all but the largest earthquakes, the choice of orientation for $\Delta\mathrm{CFS}$ calculations has proved to be one of the most difficult problems in understanding triggered earthquake sequences in this framework.

To compute the shear and normal stress changes, King *et al*. (1994) used the concept of planes that are "optimally orientated" (with respect to the regional stress field) for failure. Thus the map in Figure 6.1 assumes, firstly, that everywhere there is a plane with that orientation and, secondly, that it is this plane that fails in every case. The result is that the impact of the deformation on the calculated Coulomb stress field is maximised everywhere. This implies that the total area modelled to have positive $\Delta\mathrm{CFS}$ is also maximised and it is therefore possible that, just by chance, many aftershocks could occur on red regions of the map, without any real causation.

In fact, it has been shown (McCloskey *et al*. 2003) that the orientations of aftershocks for which we have good quality focal mechanisms are determined, not by the optimal orientation for the regional stress field, but by the orientation of the dominant regional structure (see Figure 6.3), even if this structure is not itself optimally oriented for failure. It seems to be energetically preferable that failure should occur on a pre-existing structure than that new structure should be generated, even if the existing structure is poorly aligned with the regional stress.

This adds a significant complication to the understanding of static stress triggering, since it has been shown (Mallman and Zoback, 2007) that, when these structurally aligned aftershock focal mechanisms are used to inform Coulomb stress calculations, the rate of aftershock production increases even in regions that are modelled to have decreased Coulomb stress as a result of Landers. When the correct failure planes are used, the predicted quiescence of aftershock activity in stress shadows is, in general, not observed (Figure 6.4).

The result is that good quality aftershock forecasts from the Coulomb Failure Stress model rely on well resolved failure plane orientations for triggered events. These are generally not available, even in the best catalogues. This may be to some extent compensated for by accepting the conclusions of McCloskey *et al*., (2003) and replacing seismological focal mechanisms with the orientation of the local structure. This implies that accurate, low-uncertainty modelling of triggered seismicity requires knowledge of the orientation of geological structures in the area.

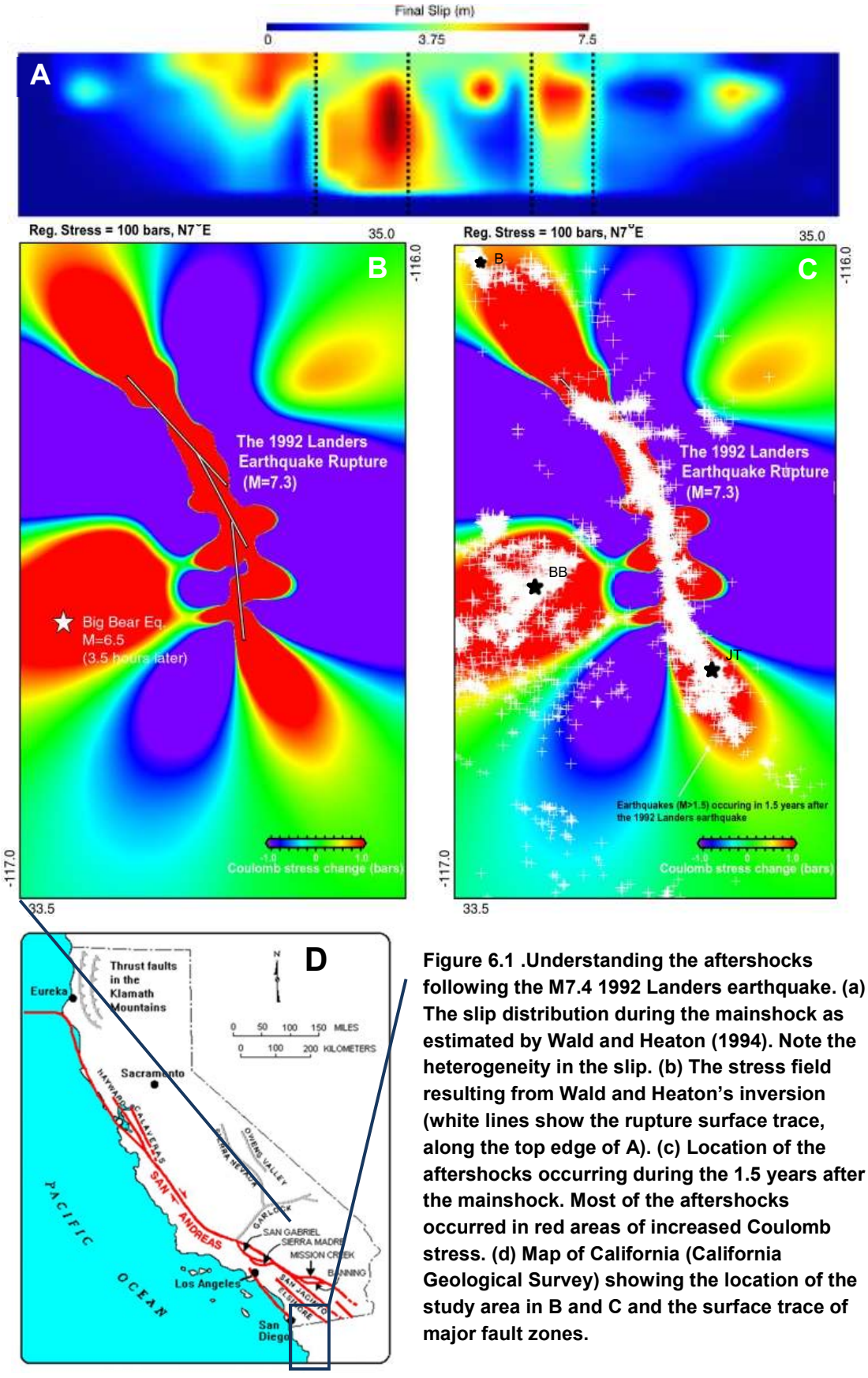

Figure 6.1 .Understanding the aftershocks following the M7.4 1992 Landers earthquake. (a) The slip distribution during the mainshock as estimated by Wald and Heaton (1994). Note the heterogeneity in the slip. (b) The stress field resulting from Wald and Heaton's inversion (white lines show the rupture surface trace, along the top edge of A). (c) Location of the aftershocks occurring during the 1.5 years after the mainshock. Most of the aftershocks occurred in red areas of increased Coulomb stress. (d) Map of California (California Geological Survey) showing the location of the study area in B and C and the surface trace of major fault zones.

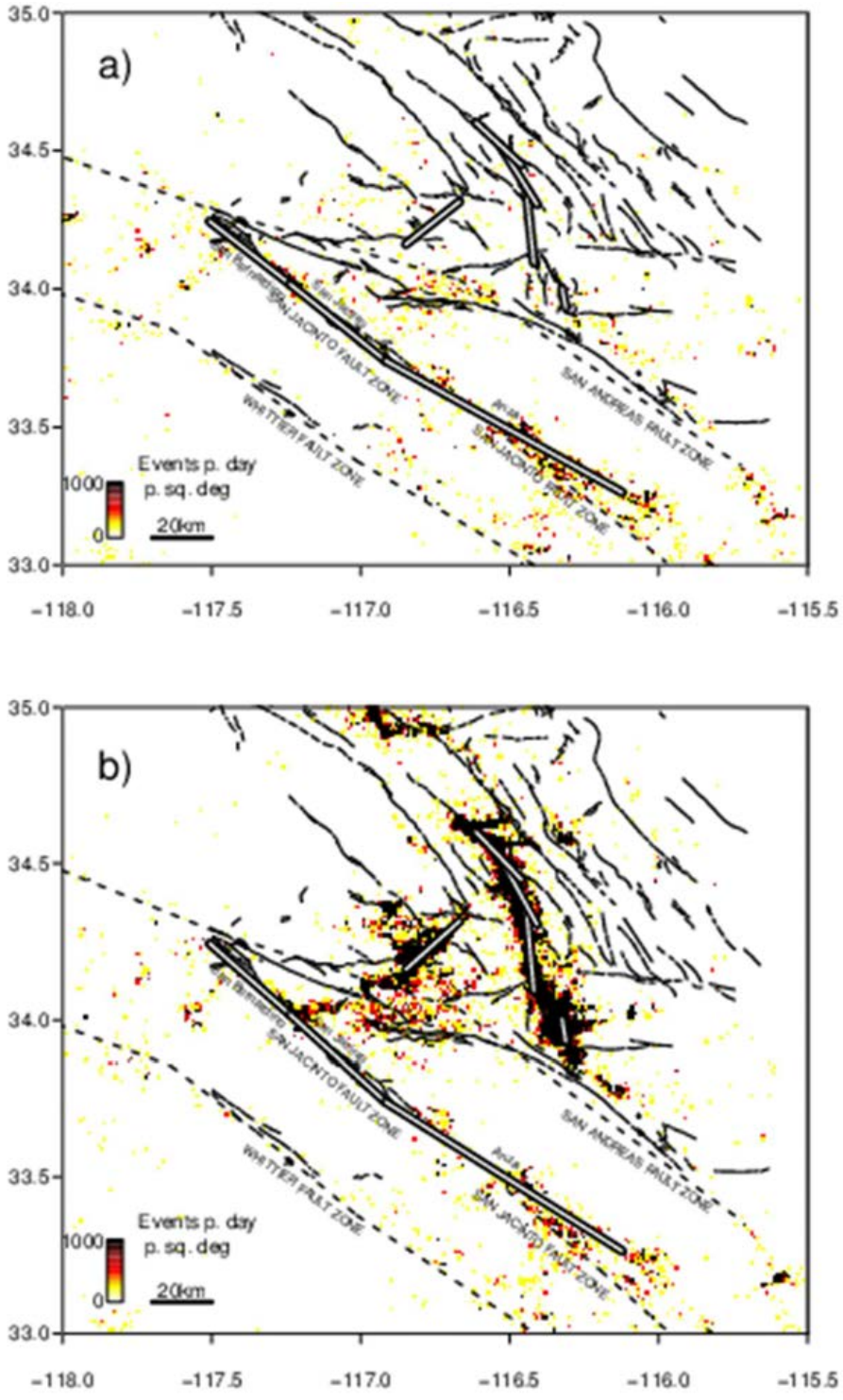

Figure 6.2. Seismic rates. (a) Seismic rate (events/day/deg2) averaged over one year prior to the Landers mainshock. (b) Seismic rate over the year following Landers. (The locations of the ruptured fault planes and major fault zones in the region are shown in white. Other major mapped structures are shown in black. The dashed boxes in both show the map area from Figure 6.1b,c.)

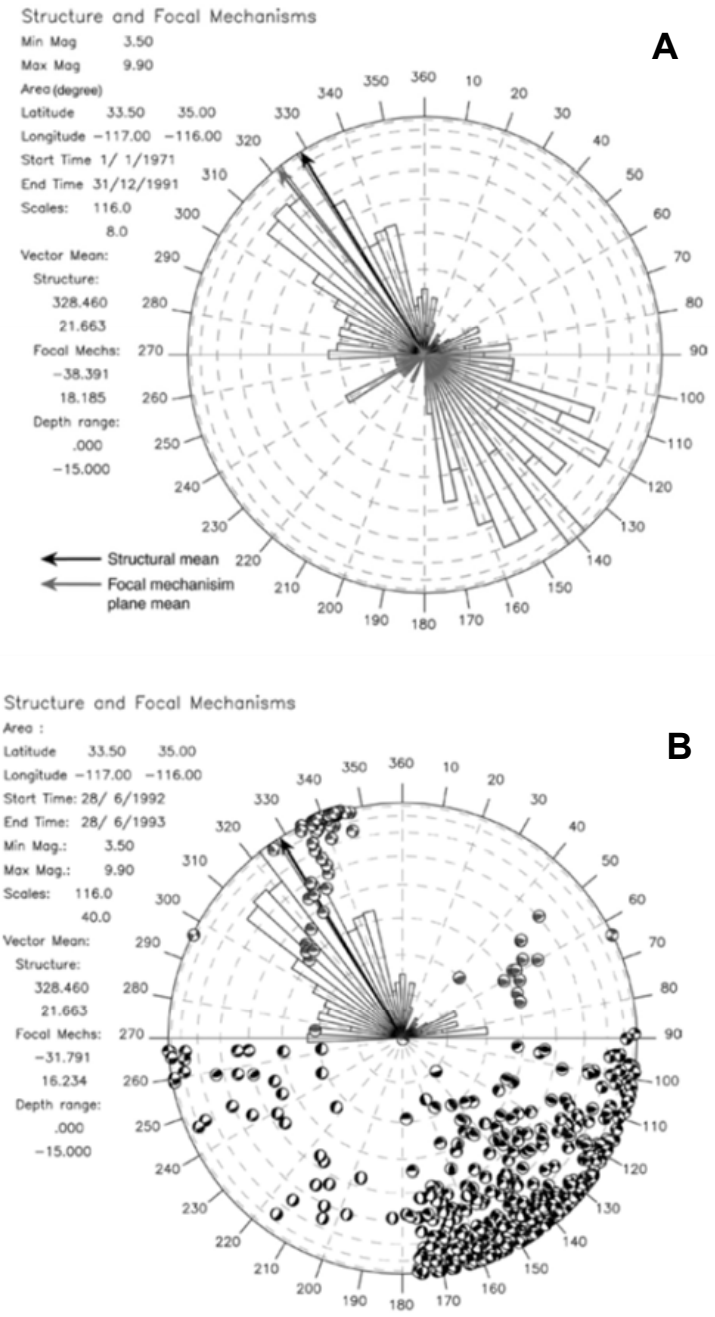

Figure 6.3. Relationships between predicted seismicity, observed seismicity and mapped structure in the Landers source region. Rose diagrams in the upper semicircles of both (a) and (b) represent the distribution of orientations of structure which have experienced recent (Quaternary, Holocene or historical) seismicity. Black arrows show the mean orientation. The rose diagram in the lower left semicircle represents the distribution of earthquake orientations in the 21years preceding Landers; their mean orientation is plotted as a grey arrow on the upper semicircle. The mean orientation of aftershock focal mechanisms is plotted on the upper semicircle of (b); the Landers earthquake did not significantly realign the orientation of seismicity in the region.

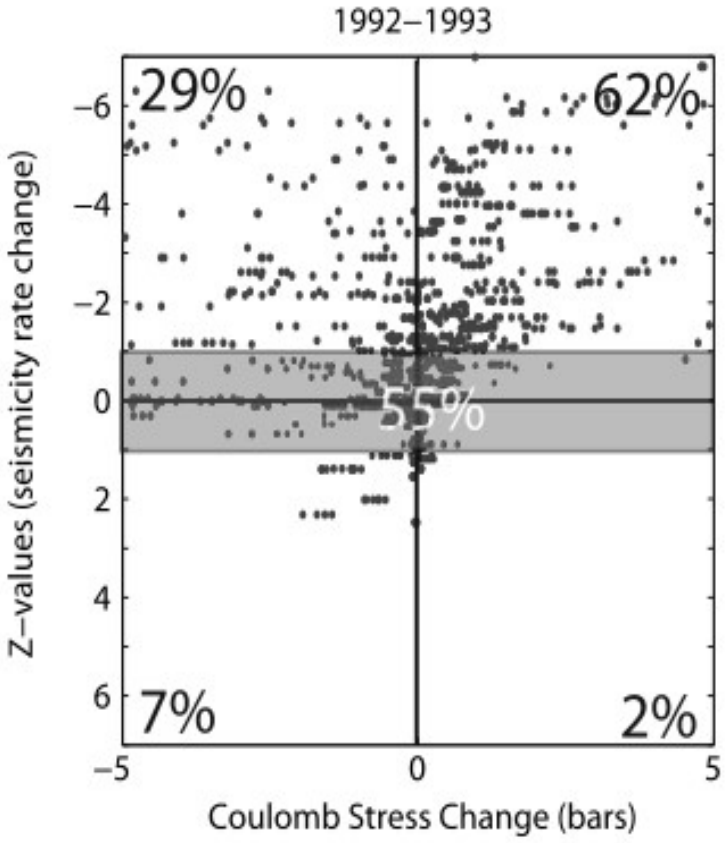

Figure 6.4. The relationship between the applied Coulomb stress and the seismicity rate change for the Landers and Kobe earthquakes (from Mallmann and Zoback, 2007). Most events plot in the top right quadrant as expected. However, the scarcity of the events in the bottom left and the surplus in the top left quadrants respectively show that the simple static stress triggering picture fails quantitative inspection.

6.2.2 The Coulomb Rate-State (CRS) Model

There are a number of other features of aftershock distributions that are not predicted by the simple static stress model, but which are beginning to be understood in the context of a more sophisticated theoretical treatment. These are, in particular, the dependence of the spatial distribution of triggered seismicity on the distribution of previous activity in the region and the time-dependence of the rate of triggered events, which has been determined empirically to decay as a power-law with time after the main shock (Omori-Utsu decay).

Coulomb Rate-State (CRS) models, in which the static stress changes of Equation (6.2.1) act on a population of faults with rate- and state-dependent frictional properties (Dieterich, 1994), have been shown to reproduce some of the temporal and spatial characteristics of aftershock distributions of tectonic earthquakes (see for example, Hainzl *et al*., 2009; Toda *et al*. 2012). This has been demonstrated in some detail (Nic Bhloscaidh *et al*., 2015) for the rate response of the San Jacinto Fault Zone (see Figure 6.5) to Coulomb stress perturbations from Landers: when the distribution of pre-Landers seismicity was taken into account via the CRS model, significant correlation was shown between the rate response and stress perturbation, including evidence of seismicity suppression on stress shadows. Also, according to a Bayesian Information Criterion, the time-

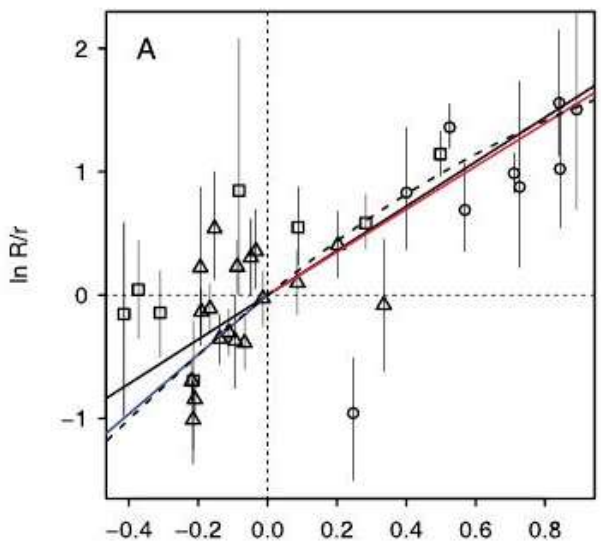

Figure 6.5. The seismicity rate response (points expressed as log of the ratio of pre-mainshock to post-mainshock rate) of the San Jacinto Fault Zone to static stress perturbations from the 1982 Landers earthquake (from Nic Bhloscaidh *et al*., 2014). The predicted rate response according to CRS (dashed lines), a one parameter time-independent exponential model (solid black lines) and a 2 parameter exponential model, (blue and red solid lines).

dependent CRS model explains the rate change data significantly better than simple time-independent models (see Figure 6.5).

Since CRS can be extended to model rate changes from an arbitrary time varying stress field, the model therefore has the potential to provide a framework for quantitative forecasting of rates of seismicity induced from fluid injection. However, the model suffers from uncertainties in input parameters for the Coulomb stress model and others associated with the RS modelling. These include, for example, tectonic stressing rate, fault frictional parameters and, most importantly, the reference seismicity rate. Nic Bhloscaidh *et al*. (2015) concluded that significant errors are introduced into rate estimates when the reference rate is poorly sampled. This is particularly problematic in the context of induced seismicity since, at this much smaller scale, the faults that dominate the seismic activity (the fault zones in the context of the Landers sequence) will not necessarily be able to be identified at the surface. Accurate quantification of the hazards from induced seismicity will therefore depend on estimating the likely magnitudes of the errors associate with poor estimation of the underlying seismicity rates. Details of the implementation of the CRS based scheme are given in Section 6.4.

6.2.3 Coupled Lattice Boltzmann-elastic modelling

The source deformation required to compute the terms in Equation (6.2.1) results from a time dependent fluid injection. The Coulomb stress perturbations may be calculated provided the time varying pressure field $p(t)$ resulting from the flow of injected fluid through the pore spaces is known (this also determines the resulting elastic deformation of the rock volume).

There are two elements to this problem: modelling fluid flow in a complex medium, i.e. a porous rock volume with heterogeneous permeability, and coupling this flow to the rock itself, so that the time-dependent pressure results in realistic deformation of the medium.

The basic method for solving the fluid flow problem is the "lattice gas" model (Frisch *et al*., 1986). Although this model is based on simple rules for the microscopic movement and interaction of particles on a lattice (which conserves mass and momentum), in the macroscopic limit it has been found to reproduce the Navier-Stokes equations for the motion of viscous fluids. This result is important because the lattice used to represent the microscopic physics in the lattice gas model can be populated arbitrarily with solid and void space; a porous medium of arbitrary geometry can be constructed.

Modern implementations of the basic lattice gas model include a number of adjustments.

In Lattice-Boltzmann models (see, for example, Qian ***et al***., 1992), the particle number at each node in the lattice (which is either 0 or 1 in the lattice gas model) is replaced by its ensemble average (calculated from Boltzmann's distribution function). Whereas statistical fluctuations in lattice gas methods (associated with the "Boolean" particle number) mean that long computation times are required to converge on stable values of the ensemble averages, the new Lattice-Boltzmann methods give stable estimates of the flow field after only a small number of iterations.

Since the lattice is also populated by a "Boolean" permeability field, i.e. each node is either solid or void, representing real porous media in a lattice gas model requires massive computational grids. Modifying the Lattice-Boltzmann equations to allow a real-valued solid density at each node (Dardis and McCloskey 1998a, interpreted as the fluid transport properties averaged from the microscopic lattice), allows each node to represent arbitrarily large volumes of real rock. This model reproduces both the predictions of analytical solutions for simple systems and experimentally observed behaviour on complex, dual porosity materials (Dardis and McCloskey 1998b); this is the Lattice-Boltzmann implementation that is now widely used for these applications.

The final step in using the Lattice-Boltzmann scheme in the present context is the full two-way coupling of the fluid flow model with the elastic rock volume (O'Brien ***et al***., 2002 and O'Brien and Bean 2004). The Lattice-Boltzmann lattice is given elastic properties, so that it behaves according to a "lattice spring model", with an additional force to account for the presence of the fluid. The fixed Lattice-Boltzmann nodes are also modified to reflect the motion of the lattice spring model nodes.

This implementation of this fully coupled elastic-lattice and lattice-gas model allows the simulation of the time-dependent stress and pressure fields surrounding a high pressure injection in a complex geologically realistic medium.

However, while the fluid-elastic simulator returns all components of the stress tensor, here, for simplicity, it has been decided to restrict the analysis to changes in the pore fluid pressure only, which dominate the stress perturbations. Thus $\Delta\sigma$ and $\Delta\tau$ are set to zero in Equation (6.2.1). (Note that the software implements the full elastic and pore-fluid pressure solution, so these are easily reintroduced into future calculations if required.) A snapshot of the pressure field resulting from a hypothetical injection is shown in Figure 6.6.

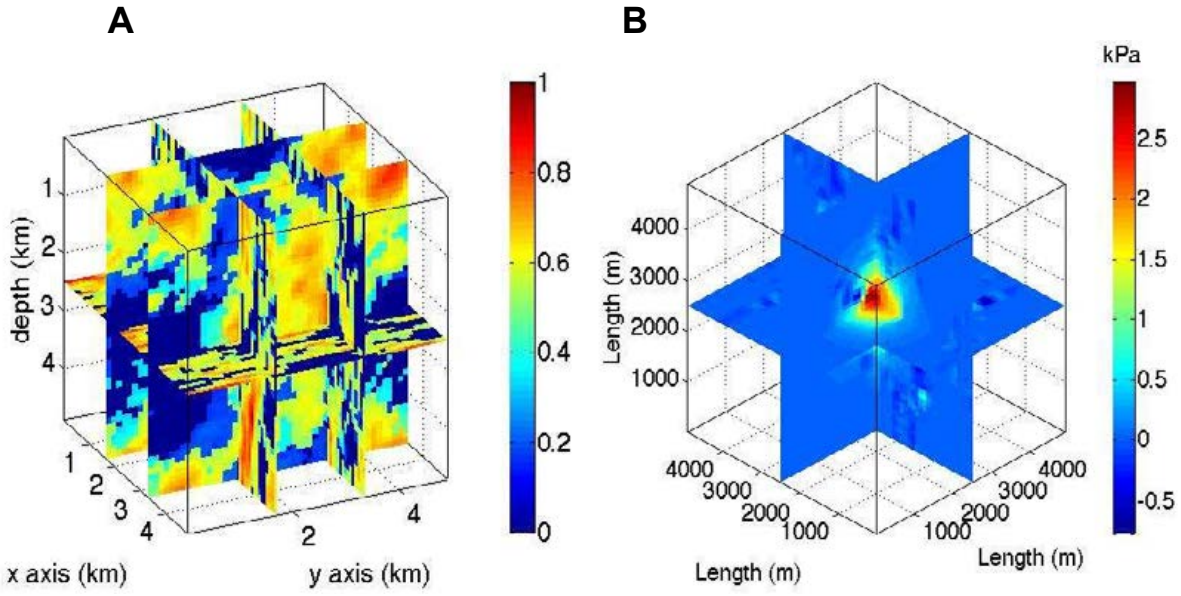

Figure 6.6. Simulation of fluid flow in a complex medium, from a hypothetical injection scenario. (a) the input heterogeneous diffusivity field; (b) the pore fluid pressure.

6.3 Theoretical and statistical basis of the forecasting protocol

6.3.1 The Time-dependent Coulomb Rate-State (CRS) model

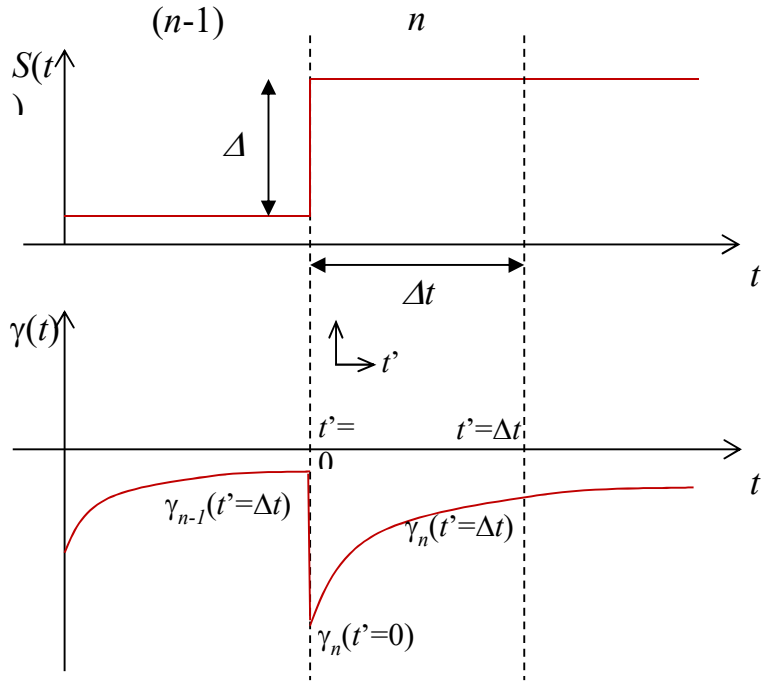

Figure 6.7. Schematic showing the γ-response of a Coulomb Rate-State fault to time dependent stress perturbations.

In the Coulomb Rate-State model, the time-dependent seismicity rate, given some arbitrary stressing history, may be calculated using (Dieterich, 1994)

$$R(t) = \frac{r}{\gamma(t)\dot{\tau}_r} \qquad \text{Equation 6.3.1}$$

where r is a reference seismicity rate, $\dot{\tau}_r$ is the reference shear stressing rate and $\gamma(t)$ is the time-dependent state variable. r and $\dot{\tau}_r$, which are assumed to be time-independent, describe the behaviour of the system at steady state, in the absence of any stress perturbations; they are usually interpreted as the background seismicity rate and the secular loading rate. The response of the seismicity rate to time-dependent stress contributions is therefore described by the evolution of the state-variable γ. To calculate γ, we divide the stress history into small increments (see Figure 6.6)

$$\Delta S_n{}^{3} = \Delta S(t) = S(t + \Delta t) - S(t) = S[n\Delta t] - S[(n-1)\Delta t]$$

Then (see, for example, Toda and Stein, 2003)

$$\gamma_n(t_n{}' = 0) = \gamma_{n-1}(t_{n-1}{}' = \Delta t)e^{-\Delta S_n/A\sigma}$$

where $t_n{}'$ refers to a time system local to the increment, so that $t = (n-1)\Delta t + t_n{}'$, and

$$\gamma_n(t_n{}') = [\gamma_n(t_n{}' = 0) - \gamma_0]e^{-t_n'/t_a} + \gamma_0$$

where $\gamma_0 = 1/\dot{\tau}_r$. The time-dependent rate in time increment n $R(t_n{}')$ is obtained by substituting for $\gamma_n(t_n{}')$ in Equation 6.3.1.

The expected number of induced and reference events in a time increment n is therefore given by

$$\lambda_n = \int_0^{\Delta t} R(t_n')\,\mathrm{d}t$$

$$= rt_a\left[\ln\left(e^{\Delta t/t_a} + \frac{\gamma_{n-1}(\Delta t)}{\gamma_0}e^{-\Delta S_n/A\sigma} - 1\right) - \ln\left(\frac{\gamma_{n-1}(\Delta t)}{\gamma_0}\right) + \frac{\Delta S_n}{A\sigma}\right] \qquad \text{Equation 6.3.2}$$

6.3.2 Generating a synthetic reference distribution

To produce an underlying reference distribution for the scenario, we begin by generating a synthetic set of faults in the study volume.

The main structural trend is defined to be in the y-direction and the centre of the set is offset from the injection point in the positive x-direction. The distance of the fault in the x-direction from the centre of the set is sampled from a power-law distribution, so that

$$f(x) = \begin{cases} C_x 10^{-d_x(x-x_0)}, -D/2 \le x < D/2 \\ 0, \text{otherwise} \end{cases}$$

3 The CRS model requires $\Delta S = \Delta\tau - \mu^*(\Delta\sigma + \Delta p)$ in place of the usual ΔCFS, where μ∗ = (μ − α)(1 − B), α is a positive non-dimensional parameter controlling the normal stress dependence of the shear strength (Linker and Dieterich, 1992; Dieterich *et al.*, 2000) and B is the Skempton coefficient (see Cocco and Rice, 2010).

where D is the length of the study volume in the x-direction. To obtain the fault lengths, the maximum magnitude for a fault is defined to be (Wells and Coppersmith, 1994)

$$M^*(L) = 1.61(\log_{10} L + 2.57)$$

Therefore, only faults of length $L > l_0 = 10^{0.62Mc-2.57}$ km, are considered where M_c is the magnitude of completeness of the catalogue. The lengths are then sampled from the power law:

$$f(L) = \begin{cases} 0, L < l_0 \\ C_L 10^{-d_L L}, L \geq l_0 \end{cases}$$

A fault can be considered to be composed of $(L/l_0)^2$ fault units of length l_0, each with a nucleation rate of

$$r_0(L) = 10^{a_0 - b[M_c - M^*(L)]}$$

events per unit time and a cumulative frequency-magnitude relation,

$$N(M, L) = \begin{cases} 10^{a_0 - bM_c}, & M < M_c \\ 10^{a_0 - bM}, & M_c \leq M \leq M^*(L) \\ 0, & M > M^*(L) \end{cases}$$

or, in the form of a probability density function,

$$g(m|L) = \begin{cases} 0, & m < M_c \\ A10^{-bm}, & M_c \leq m \leq M^*(L) \\ 0, & m > M^*(L) \end{cases} \quad \text{Equation 6.3.3}$$

where the constant A is obtained by setting

$$A \int_{M_c}^{M^*(L)} 10^{-bm} \, \mathrm{d}m = 1$$

to obtain

$$A = \frac{\ln 10}{b} \left[10^{-bM^*(L)} - 10^{-bM_c}\right]$$

Each fault unit, therefore, nucleates events according to a stationary Poisson distribution with expected value $r_0 l_0^2$ per unit time and obeys the same frequency-magnitude law, except that the maximum magnitude of the distribution depends on the dimensions L of the whole fault (i.e. a fault unit can only nucleate a large event if it is part of a larger fault).

The reference seismicity rate at any grid location ijk in the study volume is given by

$$r_{ijk} = \frac{1}{\Delta V} \sum_{f \in \mathbb{f}(ijk)} {v_f}^{ijk} r_0(L_f)$$

events per unit time and volume, where $\Delta V = \Delta x \Delta y \Delta z$, $\mathbb{f}(ijk)$ is the set of faults that pass through ijk and ${v_f}^{ijk} l_0^2$ is the area of the section of fault f that passes through element ijk.

The expected number of events in element ijk and time interval n after the injection is given by substituting for r in Equation 6.3.2. This distribution is referred to as the induced model distribution: it is the projected distribution of induced seismicity without any sampling errors in the reference seismicity rate.

In order to estimate the likely errors in the projected properties of the induced seismicity associated with poor sampling of the reference seismicity, we Monte Carlo sample from the reference population with a completeness threshold applied to the synthetic data. The rates and parameters of the frequency-magnitude distribution are then recalculated so that the forecasts are made with pseudo-realistic *a priori* information. Finally, the projected distributions for different reference rate are compared to completeness magnitude scenarios and the samples from the induced model distribution compared to with the projected distributions.

6.3.3 Sampling from the reference distribution

Samples from the reference distribution are drawn so that $F\left(n_{ijk}^{l}|\lambda_{ijk}\right) = u$, where n_{ijk}^{l} is the number of events in the lth sample at volume element ijk, F is the cumulative mass function for the Poisson distribution, u is a random deviate from the uniform distribution on the interval (0,1), $\lambda_{ijk} = r_{ijk}T_r$ and T_r is the duration of the reference catalogue. For each event in ijk its magnitude is sampled according to the distribution function

$$g_{ijk}(m) = \frac{1}{\sum_f {v_f}^{ijk}} \sum_{f \in \mathbb{f}(ijk)} {v_f}^{ijk} g\left(m, L_f\right)$$

where $g\left(m, L_f\right)$ is the probability density function in Equation 6.3.3.

We assume that, in general, seismicity rates are not high enough to resolve a spatially heterogeneous rate, so we use the sample to define a homogeneous rate

$$\rho_l = \frac{1}{\Delta t \Delta V} \sum_{ijk} n_{ijk}^{l}$$

6.3.4 Maximum likelihood estimation of the Gutenberg-Richter parameters

To construct the likelihood for the sample, given the parameters of the frequency-magnitude distribution, the Gutenberg-Richter density function is used

$$g(m) = 10^{a' - bm} \qquad \text{Equation 6.3.4}$$

where a' is related to the a-value from the cumulative form by $a' = a \log_{10}(\ln 10 \,/b)$. The magnitude data is divided into increments of Δm, so that the data $n_i = n(m_i, m_i + \Delta m)$ are frequencies in the ith interval. It is assumed the n_i are distributed as count data, with a Poisson probability mass function given by

$$f(n_i|\lambda_i) = \frac{{\lambda_i}^{n_i} e^{-\lambda_i}}{n_i}$$

The expected number of events in each interval, given a' and b is given by integrating Equation 6.3.4 over the interval to give

$$\lambda_i = \lambda(m_i, m_i + \Delta m) = \int_{m_i}^{m_i + \Delta m} g(m)\, \mathrm{d}m$$

$$= -\frac{b10^{a'}}{\ln 10}(1 - 10^{-b\Delta m})10^{-bm_i}$$

The likelihood may then be calculated using

$$\mathcal{L}(\mathbf{n}|a', b) = \prod_i f(n_i|\lambda_i) = \exp\left\{\sum_i \ln f(n_i|\lambda_i)\right\}$$

where

$$\ln f(n_i|\lambda_i) = n_i \ln \lambda_i - \lambda_i - \ln n_i!$$

Although the maximum likelihood estimates $\widehat{a'}$and $\hat{b}$ do not depend on the log-factorial term, this is retained for weighting samples during Bayesian Monte Carlo estimation of the posterior density functions for $a'$and b; it is evaluated using

$$\ln n_i! = \sum_{k=1}^{n_i} \ln k$$

Defining $w_k = \mathcal{L}(\mathbf{n}_k|\widehat{a'_k}, b)$ (see Nic Bhloscaidh *et al.*, 2015, in review), we can estimate the posterior distribution functions for the a'- and b- values using

$$p(a'|\mathbf{n}_k)\delta a' = \frac{1}{\sum_l w_l}\sum_{l\in R} w_l$$

where $R = \{l: a' \leq \widehat{a'_l} < a' + \delta\ '\}$. The expectation value for a' is estimated using

$$\mathrm{E}(a'|\mathbf{n}_k) = \frac{1}{\sum_l w_l}\sum_{l\in R} w_l a'$$

The variance can then be constructed from

$$\mathrm{Var}(a'|\mathbf{n}_k) = \mathrm{E}(a'^2|\mathbf{n}_k) - [\mathrm{E}(a'|\mathbf{n}_k)]^2$$

6.3.5 The properties of the projected induced seismicity

Finally, the expected number of induced and reference events in each volume element ijk and time increment n is calculated according to Equation 6.3.2, substituting ρ_l for r_{ijk}. Using $\widehat{b_l}$ and $\widehat{a_l} = \log_{10}\Lambda_l + \widehat{b_l}M_c$, where $\Lambda_l = \Lambda_l(M_c) = \Delta t\Delta V \sum_{ijkn}\lambda_{ijkn}$, the probability for a magnitude greater than some threshold M_t can be calculated

$$p_l(M > M_t) = 1 - e^{-\Lambda_l(M_t)}$$

where

$$\Lambda_l(M_t) = 10^{\widehat{a_l} - \widehat{b_l}M_t}$$

is the expected number of events above M_t.

Since there would have been a non-zero probability for $M > M_t$ with reference seismicity rates, i.e. had the injection not occurred, the relative probability, defined to be the ratio of $p_l(M > M_t)$ to this reference probability are also discussed.

6.4 Parameters of the Simulations and Results

The review of Irish background seismicity rates in Task 3 (Section 5.4) has shown that underlying seismic activity is not high enough to enable reliable estimates of rates local to the study areas to be made using national networks. Deployment of local dense seismic networks (Section 7) will be required for baseline monitoring before any preliminary estimates of induced rates can be made. Since there is not, as yet, any dependable baseline data, several scenarios have been explored based on synthetic reference catalogues (see Section 6.4 for details of the generation of these catalogues) to illustrate the effect of a few of the key factors governing the nature of the induced seismicity and the quality of the forecasts.

Specifically, the effect of varying the reference seismic activity (parameterised by r_o, the number of events per second per fault unit, see Section 6.3.2) in the region and also the magnitude of completeness M_c of the network have been explored.

While many aspects of this network will be governed by economic, as much as seismological, considerations, a clear picture of the impact of the choice of M_c on the uncertainty in the estimates of the potential induced seismicity will help to inform decision making.

Uncertainties will be estimated by a Monte Carlo method: the reference distribution was sampled (in this case we use 5000 samples), to produce a catalogue defined by r_o and M_c; the reference rate was then re-estimated from the sample and forward model from the estimate to produce a population of induced rates.

In what follows, all parameters of the modelling except r_o and M_c remain constant (see Table 6.1 for their values). It is stressed however, that the protocol and software were developed as a generic tool that could be applied to the seismicity in any injection project. The scenarios the tool can accommodate are completely flexible as far as injection pressure, depth and duration, fault network model, fault frictional parameters and rock properties are concerned.

Table 6.1. The key fixed parameters of the simulations in Section 6.4. See Section 6.3 for the mathematical and statistical description of the protocol

$\dot{\tau_r}$	1×10^3	Pa/yr
A	0.005	
σ	1×10^7	Pa
d_x	3.0	
d_L	1.0	
b	1.0	
$\Delta x = \Delta y = \Delta z$	100	M
T_r	115	Days
T_R	5.7	Days
Δt	5000	seconds

In Sections 6.4.1 - 6.4.3 the choices of parameters controlling the fault network, the properties of the seismicity catalogue and the fluid injection are discussed. Results of the simulations are presented in Section 6.4.4.

6.4.1 The fluid injection simulation

The generic study region modelled is a 5km cube, with the injection at the centre and the surface at $z = 0$km. The lattice (see Section 6.3.1) contains $50\times50\times50$ nodes at 100 m spacing. Injection takes place into a fractured horizontal reservoir in the volume, at a depth of 2.5km, with a scale invariant matrix diffusivity field. The values used for the diffusivities are within the general range of fractured igneous rocks, sandstones/siltstones and intact carbonates (Roeloffs 1996). A layer with very low permeability (i.e. $D_{xx} = D_{yy} = 0.05$ m^2s^{-1}, $D_{zz} = 0.1$ m^2s^{-1}) has been placed around the boundary so as to reduce leakage from the volume. Anti-symmetric components of the diffusivity tensor are zero on all nodes.

The input for the (LB) model is the pressure rate at the bottom of the borehole. The pumping rate used results in a peak pressure of 58.24MPa, with the average pressure in the reservoir increasing by 2.1MPa by the end of the simulation at 15 days. This value is comparable to the peak wellhead pressures observed at a number of different injection projects (see

Table 6.2). Active injection takes place over the first 6.37 days.

For clarity we present results for rate simulations for a single time slice $\Delta t = 5000s$, so that the stress perturbations are integrated over Δt and the study period for the induced seismicity $T_R = \Delta t$ is about 1.5 hours. The simulation may, in principle, be run forward for an arbitrary time after the injection (of the order of months, for example), and at arbitrarily small time increments, in order to study the time evolution of the seismicity in detail, as might be required at the beginning of the injection.

Table 6.2. Peak wellhead pressures at a number of induced seismicity projects and experiments (after Evans et al. 2012). For hydraulic fracturing peak pressures are typically in the range 50–60MPa

Project	Type	Peak pressure (MPa)
Gross Schönebeck	Hydraulic fracturing	59
KTB	Hydraulic fracturing	55
Basel	Enhanced geothermal	3
Paradox Valley	Waste brine disposal	33.8
Soultz	Enhanced geothermal	10–18

6.4.2 The active fault model

A single shear zone was modelled, oriented parallel to $x = 0$, whose centre is located at $x = 100$m, i.e. the injection takes place 100m from the major structural trend in the region. The shear zone is comprised of 5000 individual faults with a power-law scaling exponent for the fault length of $d_f = 1.0$. The fault spacing distribution decays with distance from the centre of the shear zone according to a power-law with an exponent of $d_x = 3.0$. This choice, as will be seen, produces a very spatially focused fault population. Smaller values of the exponent would produce a more distributed fault population and, consequently, a more distributed induced seismicity.

In practice, the parameters of the fault model will, where the data allows, be inverted from the observed seismicity using a Markov Chain Monte Carlo (MCMC) solution to the inverse problem. Prior information for the MCMC algorithm will include detailed structural geology and good quality focal mechanisms to constrain the geometry of the main active fault sets, and an empirical value for the scaling exponent of the fault spacing distribution.

6.4.3 The seismicity

A reference rate of $r_0 = 1\times10^{-10}$ events per fault unit per second was chosen for Scenarios 1 and 2. For Scenario 3, the reference rate was halved to so $r_0 = 5\times10^{-11}$. Given the fault network described in Section 4, this gives 20 and 10 $M > 0$ events respectively in the study period. For Scenarios 1 and 3 $M_c = 0.0$. For Scenario 2, it was increased to $M_c = 1.0$.

6.4.4 Scenario Results

Results from Scenarios 1–3 are presented in Figure 6.8, Figure 6.9 and Figure 6.10. The layout of these figures is the same in each case: the top panel shows a sample catalogue from the scenario, with event locations plotted in the study volume, coloured by their time and sized by their magnitude. The faults are marked by open circles, showing their approximate dimensions and orientations. The bottom panel has five plots labelled A-E, which show some statistics of the Monte Carlo sampled reference and induced seismicity distributions.

Figure 6.8 shows the results from Scenario 1, with $\mathrm{r_0} = 1\times10^{-10}$ and $\mathrm{M_c} = 0.0$: Figure 6.8a shows a histogram of the numbers of events in the sample reference catalogue. The vertical line shows the total expected number of events in the reference catalogue, given the underlying distribution, i.e. it is the "correct" result, with no sampling error. The standard deviation is as for a Poisson distribution and goes as the square root of the total number of events; in this case it is about 40 events, or 2% of the total.

The sample value for $\mathrm{N_r}$ is used to estimate a homogeneous reference rate for the volume, which is substituted into Equation 6.3.2 to forecast the expected number of induced events in the study window. Figure 6.8b shows a histogram of the modelled expected number of events in the $\mathrm{T_R} = 5000\mathrm{s}$ after the injection begins. The random errors that have propagated through the forecast from the sampling errors in the reference can be seen; the forecasts are scattered, with a standard deviation of about 15 events. These errors are distributed as a Poisson distribution and their magnitude is predictable.

However, there is an additional systematic error that has been introduced into these forecasts. In fact, the expected number of events calculated from the underlying distribution is 124, whereas from our simulations it appears much larger at 195. The CRS model responds very differently depending on whether the underlying reference seismicity is correlated with the stress perturbations. This systematic error results from the approximation of the spatially heterogeneous reference seismicity rate with a homogeneous field, which misrepresents this correlation between the fields for the CRS calculations.

In this case, the underlying reference seismicity is very strongly concentrated around the centre of the shear zone. This centre is 100m away from the injection point, so the underlying rate is very small there. In fact, by approximating the reference with a homogeneous distribution, the model overestimates the reference rate at the injection point, where the largest stress changes are. This leads to an overestimate in the forecast rates.

For relatively large $\mathrm{d_x}$ values, where the underlying seismicity distributions are concentrated on a very narrow shear zone, the injection needs to be very close to the shear zone before the stress begins to be correlated with the reference seismicity and this method begins to underestimate the induced rates. However, in this case rates are very significantly underestimated, since the reference rates are so high on the main structures. This is a general issue with CRS: predicted rates are underestimated by homogeneous reference models, when the true reference distribution is correlated with the stress perturbations and vice-versa (Nic Bhloscaidh et al., 2014). The implications of this feature of the calculations will be discussed in Section 6.5.

Figure 6.8c,d show posterior density functions, calculated using the Bayesian Monte Carlo methodology outlined in Section 6.3.2, for the Gutenberg-Richter (density) a- and b- values respectively of the reference catalogue. Well sampled density functions indicate good convergence of the BMC solution for the parameters.

Small errors in the parameters are indicated by narrow peaks in these density functions; for Scenario 1, the parameters are well resolved.

For real baseline catalogues, these density functions can be estimated by re-sampling many times real catalogue values of $\mathbf{n}_k$ (i.e. the number of events in each magnitude increment) from Section 6.3.2 and repeating the procedure to estimate the parameter values and densities.

The final plot Figure 6.8e, shows a histogram of the probabilities of a $\mathrm{M} > 4$ event occurring in the study period after the start of the injection (red) and the corresponding values had there been no injection (i.e. the reference probabilities). Although there is some overlap between the distributions, there is, in general, a clear probability increase.

Furthermore, the ratio between $\mathrm{p}(\mathrm{M} > 4)$ and the reference probability is approximately constant between pairs (i.e. pairs belonging to the same Monte Carlo sample) at 2.37+\–0.003, suggesting that this number is a constant of the interaction between the stress perturbation and the reference seismicity, i.e. it does not seem to be susceptible to random errors. However, we note that the underlying value for this relative probability (i.e. from the underlying input reference and induced distributions) is only 1.5. This is again a consequence of overestimating the reference rate at the injection point by using a homogeneous approximation. It is also noted that this relative probability depends, in general, on the magnitude of interest (i.e. calculations from Section 6.4 should be repeated for $\mathrm{p}(\mathrm{M} > 3)$, for example), though for very small probabilities, it may be approximately constant over a small range of magnitudes.

Scenario 2 has the same reference rate, but the completeness threshold of the catalogue increases to 1.0. The seismicity is the same; it is the quality of the observations that change. Figure 6.9a shows the numbers of events in the sample reference catalogues; there are now a tenth of the events overall compared to Scenario 1. The standard deviation is 12.8, which is almost 4 times larger as a percentage of the total at 7.8%. This propagates through into the random errors in the forecast number of events (Figure 6.9b), which now have a standard deviation of 22% of the mean number of events. Again there is a large systematic error in the forecast rates: the correct value is 12 events, whereas the mean forecast value is 19 events.

The BMC posterior density functions for the GR parameters are clearly less peaked around the correct values. When there are few events in the catalogue, such as when the activity is low or $\mathrm{M_c}$ is large, methods to identify moments of the underlying distributions typically perform poorly. The advantage of Monte Carlo methods, such as BMC, in these circumstances is that the errors are apparent from the estimated density functions.

The larger random errors in the rates and the GR b-value lead to large errors in the estimated values of $\mathrm{p}(\mathrm{M} > 4)$. Despite Scenarios 1 and 2 having the same underlying seismicity, in Scenario 1 very few simulations estimated probabilities of greater than about 0.03, whereas in Scenario 2 there are simulations with $\mathrm{p}(\mathrm{M} > 4)$ values greater than 0.04.

Finally, Scenario 3 uses $\mathrm{r_0} = 5{\times}10^{-11}$ events per fault unit per second, and $\mathrm{M_c} = 0.0$. In this scenario, the network has the same detection capability as Scenario 1, but the study area has much lower underlying rates. Random errors in the sampled reference rates (Figure 6.10a) are large at 11% of the underlying rate, despite the low completeness threshold. This is reflected in a standard deviation of 33% of the mean forecast rate (Figure 6.10b). There is, as before, a systematic overestimate of the rates, but the underlying induced number of events is quite close to the noise in the forecast in this case, because of the large errors.

The GR parameters are very poorly resolved (Figure 6.10c and d), the b-value in particular. However, the scatter in the forecast probabilities $\mathrm{p}(\mathrm{M} > 4)$ (Figure 6.10e) is smaller than in Scenario 2. This is the result of the smaller underlying rates; the probabilities, while relatively poorly resolved, are much smaller than in the

previous scenarios (and they cannot be less than zero). We suggest that, despite the large errors associated with small reference seismicity rates, the hazard from larger events could, in some cases, still be demonstrated to be small.

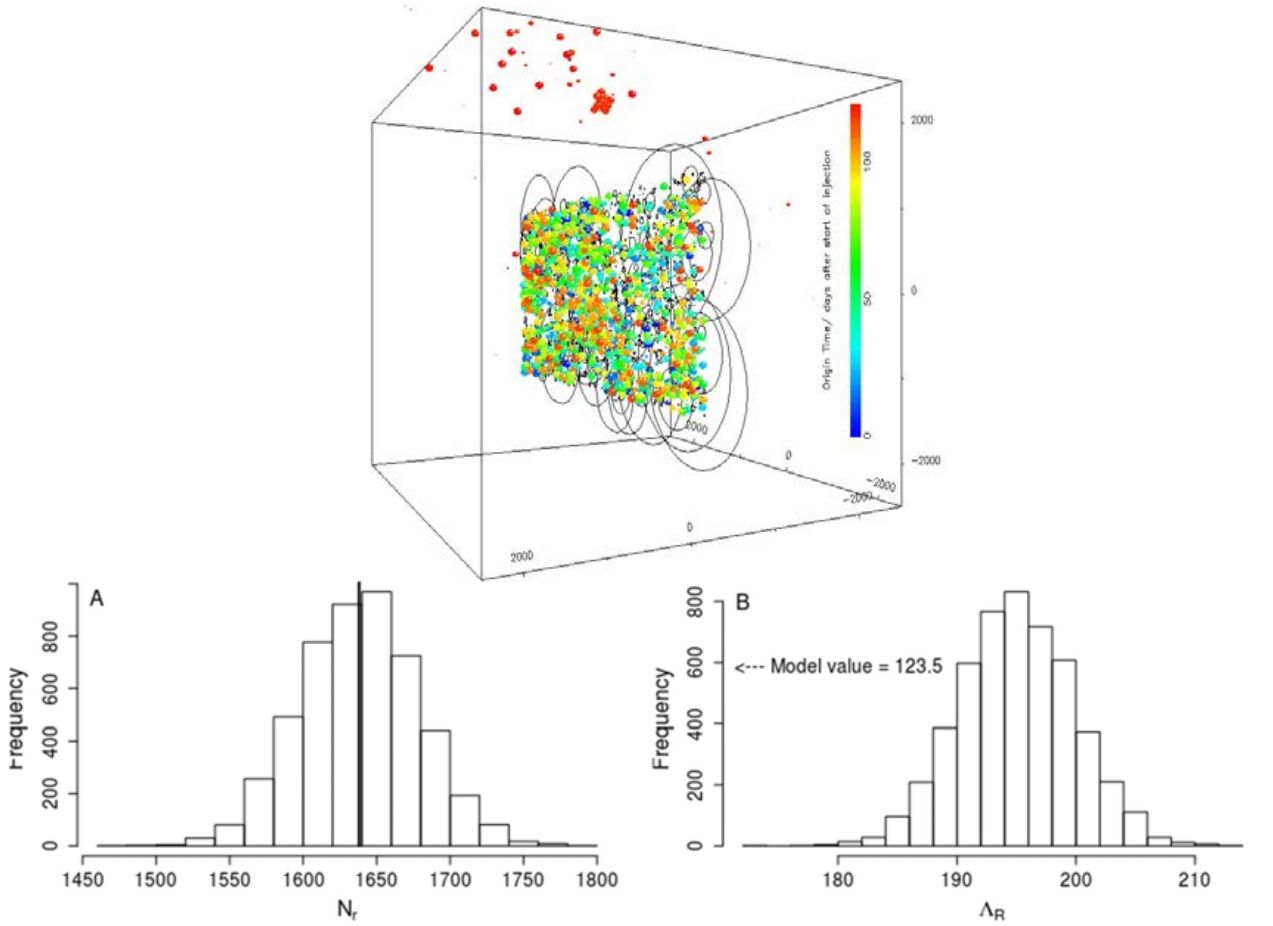

Figure 6.8. Results from Scenario 1: $r_0 = 1{\times}10^{-10}$ and $M_c = 0.0$.

Top panel: one example catalogue, with event locations plotted in the study volume, along with circles representing the fault locations and dimensions. Time from the beginning of the reference catalogue is shown in colour and the event magnitude is shown by the size of the point. Bottom panel: A Histogram of the number of events in the reference catalogue (the value corresponding to the underlying distribution shown by a vertical line) B. Histogram of the number of events in the induced catalogue (the value corresponding to the underlying distribution is off the scale and is shown by an arrow). C) and D) The BMC estimates for the posterior density functions for the GR a- and b-values. The correct values are shown as vertical lines. E Histograms of the values of the induced $p(M > 4)$ (red) and the reference probability (black). The correct values are shown as vertical lines.

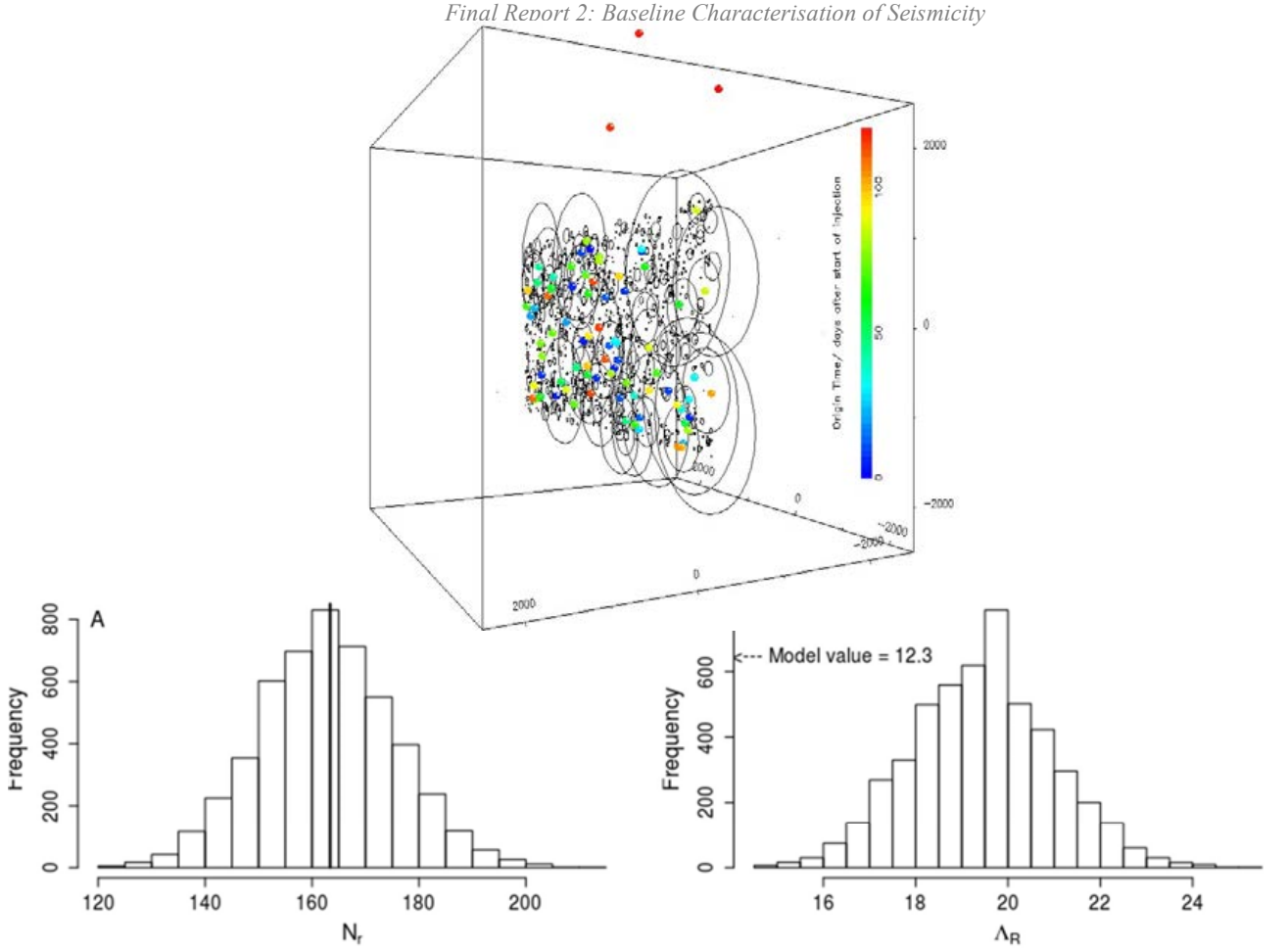

Figure 6.9. Results from Scenario 2: $r_0 = 1{\times}10^{-10}$ and $M_c = 1.0$.

Top panel: one example catalogue, with event locations plotted in the study volume, along with circles representing the fault locations and dimensions. Time from the beginning of the reference catalogue is shown in colour and the event magnitude is shown by the size of the point. Bottom panel: (a) Histogram of the number of events in the reference catalogue (the value corresponding to the underlying distribution shown by a vertical line). (b) Histogram of the number of events in the induced catalogue (the value corresponding to the underlying distribution is off the scale and is shown by an arrow). (c, d) The BMC estimates for the posterior density functions for the GR $\boldsymbol{a}$- and $\boldsymbol{b}$- values. The correct values are shown as vertical lines. (e) Histograms of the values of the induced $\boldsymbol{p(M > 4)}$ (red) and the reference probability (black). The correct values are shown as vertical lines.

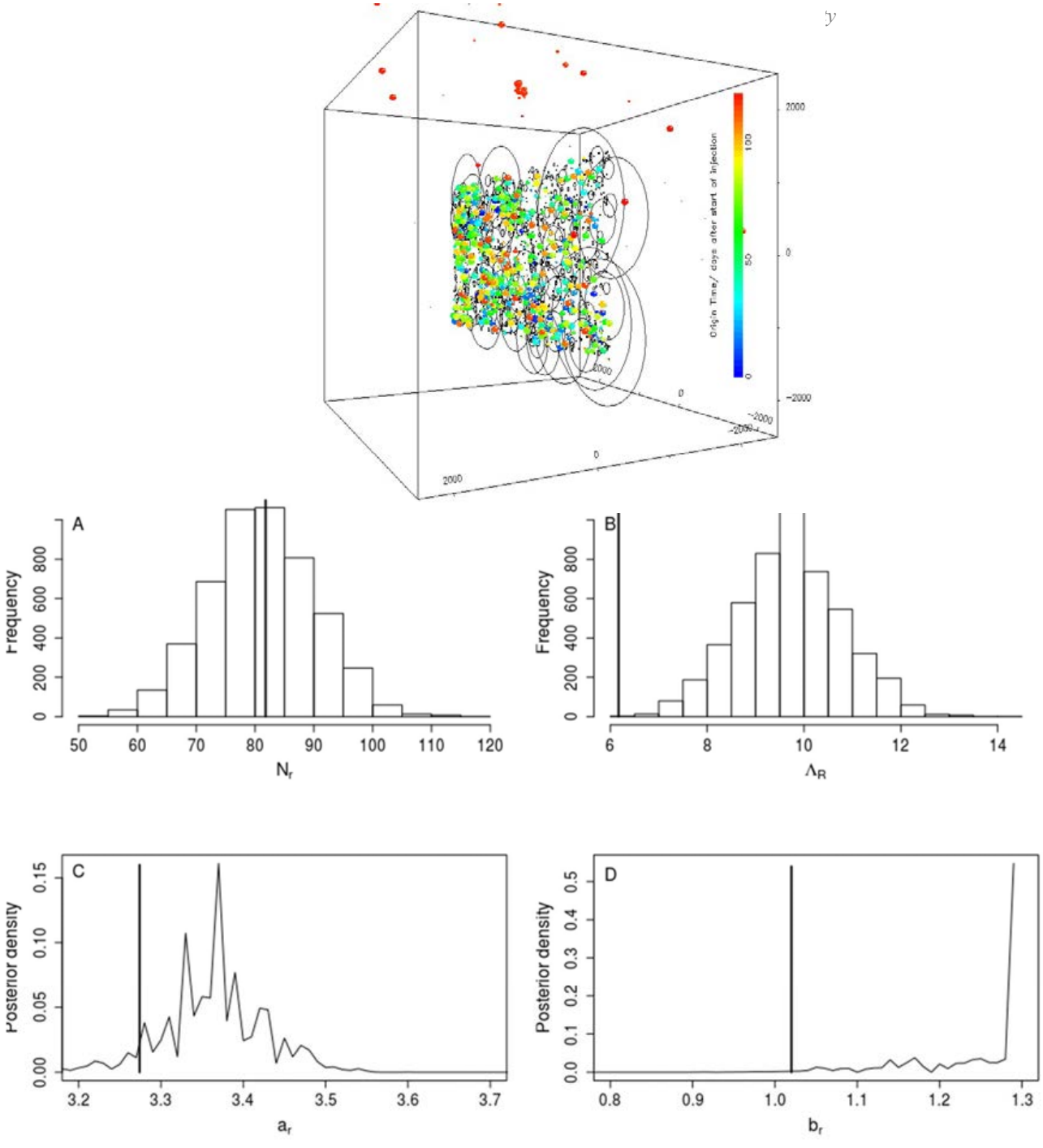

Figure 6.10. Results from Scenario 3: $r_0 = 5\times10^{-11}$ and $M_c = 0.0$.

Top panel: one example catalogue, with event locations plotted in the study volume, along with circles representing the fault locations and dimensions. Time from the beginning of the reference catalogue is shown in colour and the event magnitude is shown by the size of the point. Bottom panel: (a) Histogram of the number of events in the reference catalogue (the value corresponding to the underlying distribution shown by a vertical line) (b) Histogram of the number of events in the induced catalogue (the value corresponding to the underlying distribution is off the scale and is shown by an arrow). (c, d) The BMC estimates for the posterior density functions for the GR a- and b- values. The correct values are shown as vertical lines. E Histograms of the values of the induced $p(M > 4)$ (red) and the reference probability (black). The correct values are shown as vertical lines.

6.5 Discussion

A rigorous statistical forecast model has been developed based on state of the art understanding of triggering of induced seismicity. The model presented here is newly developed and undergoing further statistical evaluation. We are, however, confident that the results are essentially correct, even if the choices of parameter values are the subject of future consideration. Some important general features of the results may be identified.

The uncertainties presented here mean that robust estimates for basic hazard parameters are likely to be high in an area of very low seismicity; this will be the case even for the best realistic baseline. The quality of all the estimates of the moments of the important hazard-relevant distributions deteriorates as the number of earthquakes on which the simulations are based decreases. High completeness thresholds for the networks and low underlying seismicity rates both contribute to large uncertainty; both are likely to be significant problems in applying any statistical forward modelling in the Irish context.

The use of a homogeneous reference catalogue generates systematic errors in the parameter estimates. In certain extreme cases, where the fluid injection occurs on an active fault, this could lead to very significantly under-prediction of induced rates. More generally, however, it will lead to moderate over-prediction of rates. This problem can be minimised (but not solved) by a good quality baseline deployment and data analysis, to generate the best reference model possible. However, ultimately, detailed subsurface structural information will be required to understand this problem completely since a) ideally, we need to localise the reference seismicity on arbitrarily narrow structures (at least down to the resolution of the stress calculations) b) the permeability field will be, in general, an unknown. It is the interaction between the stress perturbation field (controlled in part by the permeability) and the reference that determines the induced rates. At present, there are good models of the statistical properties of both these variables, so Monte Carlo methods may allow progress in this aspect of the problem, once preliminary catalogues are available to inform the simulations.

Note that the model does not include uncertainties in earthquake locations and magnitudes or, for example, in any of the parameters of the CRS model, such as the fault frictional constants. The uncertainties presented here can therefore be considered as lower bounds on the uncertainties that can be expected from real seismic catalogues. While we consider these errors to be relatively minor compared to the issues discussed in this report, every effort to minimise them should be made from the best seismological and structural data. Any remaining uncertainties can then be incorporated into the Monte Carlo sampling to estimate their effect on the forecast.

The data requirements for good quality forecasts are significant and the specification of baseline networks are subject to external considerations; whether it is will be possible to constrain the uncertainties well enough for acceptable forecasting will probably only be known after preliminary seismic data has been collected, so that we have a better idea of underlying, ambient seismicity rates in Ireland. While this will be subject to underlying seismicity rates in the study areas, we expect to be able to make some progress with $M_c = 0.5$ for 2 years, which will be discussed in Section 7: Task 5: Technical specification for baseline monitoring.

6.6 Conclusions

This section has several important implications for baseline and production monitoring:

1. The choice of fault network model has a first order effect on the success of the seismicity forecasts. Important information on the active structure could be obtained from detailed structural studies and also from any available high quality focal mechanisms of very well recorded earthquakes in the area;

2. Robust forecasts of the hazard-relevant parameters of induced catalogues can only be made using a high-quality network and current best practice in data analysis;

3. Significant systematic errors are introduced into induced rate estimates by assuming homogeneous reference rates. Networks should ideally be designed to resolve heterogeneous baseline rates in detail. However statistical models for fault distributions in the region would potentially allow these uncertainties to be estimated, using an extension of the Monte Carlo methodology employed here; and

4. Current catalogues are completely inadequate for forecast modelling on these spatial scales and up to the standard required for this application. Here, the use of synthetic catalogues to represent hypothetical baseline scenarios allows us to illustrate the nature of the uncertainties that might be expected, but does not allow us to make a specific forecast from an injection at present.

It is recommended that:

1. Detailed structural mapping form part of the baseline studies (examination of any available good quality focal mechanisms might be used to supplement this information);

2. A high-quality seismic network with good location capabilities, state of the art data analysis and a low completeness magnitude is essential during the baseline monitoring phase. This should be augmented by local denser networks, possibly including borehole instruments, deployed during extraction operations; and

3. Estimating uncertainty is a necessary part of any assessment of seismic hazard. Uncertainties must be treated rigorously using current statistical techniques such as those employed in this study.

Finally, perhaps the most important general conclusion is that the low background rates of seismicity observed in current Irish catalogues has two contrasting implications:

1. From a scientific perspective the data is unlikely to allow robust forecasts of the main parameters

2. In terms of impacts it means that hydraulic fracturing projects in Ireland are extremely unlikely to have any potentially troublesome seismic consequences. However, this conclusion will require confirmation by examination of good quality baseline catalogues.

7 Task 5: Technical Specification for Sub-regional Seismic Baseline Monitoring

7.1 Introduction

The main goal of seismic baseline monitoring is to establish the rate of naturally occurring seismicity in an area. Any seismicity induced in the future can then be quantified by comparing the seismicity recorded during the operational phase with the baseline seismicity. In addition, a baseline study is useful to locate active faults and to map seismic noise levels in detail.

The aim of this task is to answer two questions:

1. Is the detection threshold of existing seismic networks in Ireland sufficient to detect and to determine the location and magnitude of all local earthquakes with magnitudes ML ≥ 0.5 in the two study areas?

2. What kind of local seismic network is required if existing seismic networks in Ireland are insufficient for baseline monitoring of all local earthquakes with ML ≥ 0.5?

The detection threshold value of ML = 0.5 is chosen because events with ML < 0.5 are unlikely to be felt by humans or to cause any structural damage. Considering a detection threshold value of ML = 0.5 is consistent with the limit recommended for cessation of injection in the UK traffic light scheme proposed by Green *et al*. (2012). Dependent on hypocentral depth and local ground properties in general only events with magnitudes ML ≥ 2 are perceptible to humans (Musson, 2007) and only events with magnitudes ML ≥ 2.7 are thought to potentially cause minor damage (Baisch and Voros, 2011).

Seismic data from the Irish National Seismic Network (INSN) and the Science Foundation Ireland (SFI) funded UCD project Waveobs are available to this study. The INSN is operated by the Dublin Institute for Advanced Studies (DIAS) and INSN data were downloaded for this study from the European Integrated Data Archive using the network protocol arclink. The Waveobs project has the goal to develop new techniques to characterise sea state in the Atlantic offshore Ireland using an onshore system of seismometers. Seismic recordings started in October 2011 and the temporary nature of the project means that data will not be available long term. The seismic station locations of the two networks are shown in Figure 7.1. Also shown are all regional epicentre locations for the time period 1.10.2011 to 30.9.2014, sourced from http://earthquakes.bgs.ac.uk/earthquakes/dataSearch.html and https://www.dias.ie/irish_seismicity/, see Table 7.1 for a list of the earthquake parameters.

Table 7.1. List of earthquake parameters for all significant earthquakes in Ireland for the time period 1.10.2011 to 30.9.2014

Date	Time	Latitude	Longitude	Depth	ML	Location
[yyyy-mm-dd]	[hh:mm:ss.ss]	[degrees N]	[degrees E]	[km]		
2012-01-26	01:04:31.40	55.157	-7.619	3.3	2.2	Donegal
2012-03-13	21:22:03.10	55.112	-7.529	3.4	1	Donegal
2012-03-14	00:01:48.00	55.096	-7.557	2.9	0.7	Donegal
2012-06-06	07:58:13.90	54.151	-10.904	3.4	4	Off Mayo
2012-09-08	19:02:54.50	55.029	-7.573	1.3	1.1	Donegal
2012-11-21	09:08:22.90	55.851	-10.313	34.3	2.7	NNW of Co. Donegal
2013-12-04	07:57:26.00	51.45	-8.72		2.6	off County Cork coast
2014-03-18	20:45:16.00	52.319	-6.305	9.7	2.2	off Wexford coast
2014-04-29	04:02:00.80	55.05	-7.363	7.2	0.6	Donegal

The first step in evaluating the detection threshold of the INSN and Waveobs network is to quantify typically observed seismic noise levels in Ireland, see section 7.2. From these noise levels detection threshold functions are determined as a function of seismic noise amplitude, local magnitude ML and hypocentral distance, see section 7.3. Then the calculated detection thresholds are compared with the actual detectability of local earthquakes in recordings from the Irish seismic networks, see section 7.4. It becomes clear that smaller local networks with inter-station spacing of the order of 15 to 25 kilometres are required to detect and locate the totality of events with magnitudes ML ≥ 0.5 in the two study areas, which have an approximate size of 500 and 2,500 km^2, see Figure 7.1. The requirements that such local networks have to meet are discussed in section 7.7, and findings are summarised in section 7.6.

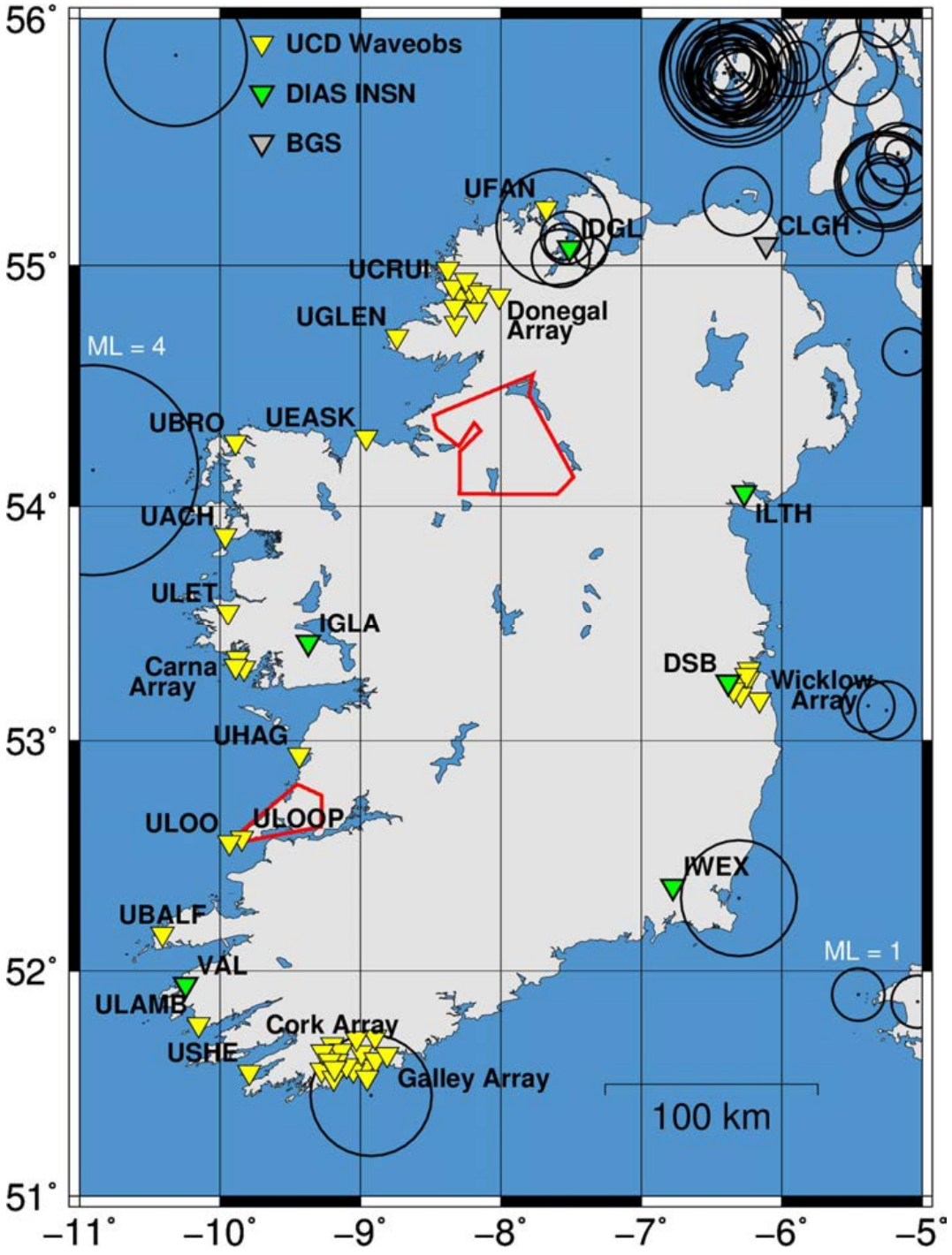

Figure 7.1. Map of seismic station locations in Ireland.

7.2 Quantification of Seismic Noise Levels in Ireland

Seismometer recordings are a function of ground vibrations at the installation site and instrumental noise. The ground vibrations are a mixture of continuous signals and event signals which are time limited. Typical sources of event type signals are earthquakes and explosions. Because continuous signals can mask the detection of event signals they are often referred to as seismic noise. Seismic noise varies in amplitude and frequency content and is best quantified in the frequency domain by calculating power spectral densities (PSD). PSD were calculated for all available seismic station data in 1-hour data segments and derived the frequency distribution as power density functions (PDF) according to McNamara and Boaz (2011). The PDF were derived by binning the data in 1/8 octave period intervals and 1 dB power intervals and normalising by the total number of PSDs. The probability of occurrence of a given power at a particular period is plotted in a colour code. See Figure 7.2 for an example of the vertical component (channel HHZ) of station UACH, located on Achill Island in Co. Mayo, West of Ireland.

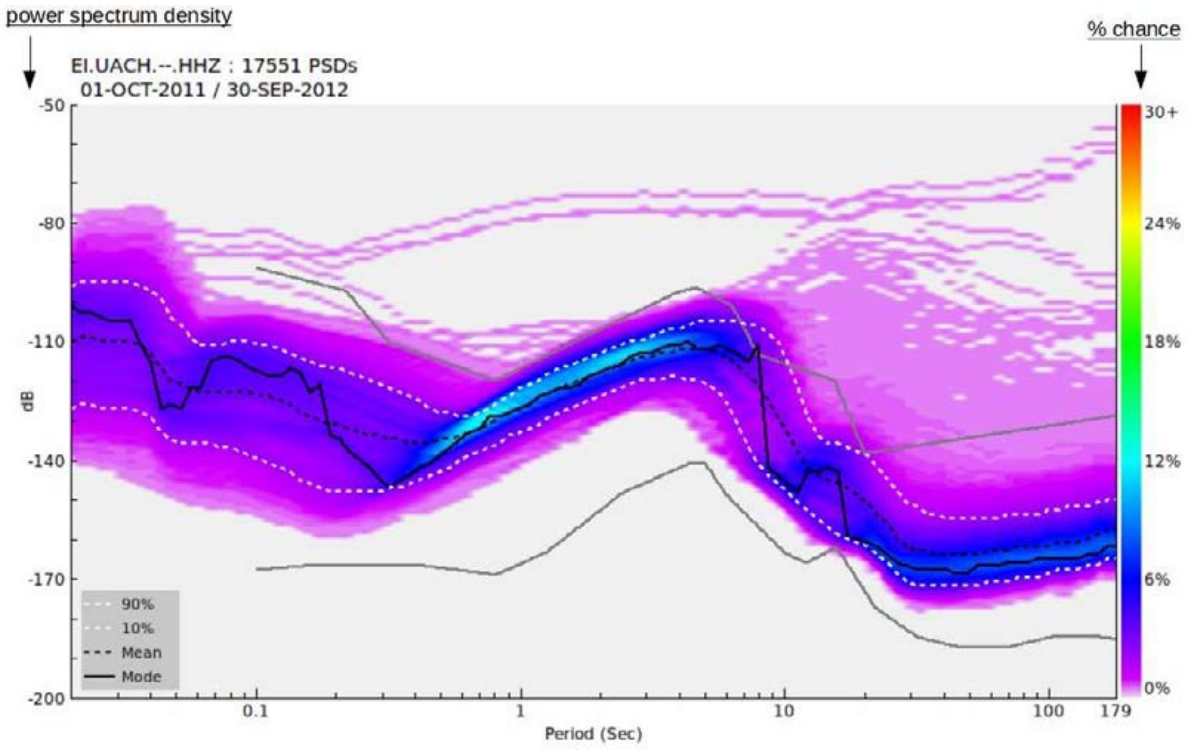

Figure 7.2. PDF for station UACH, component HHZ (calculated from 17,551 PSDs for the time period 1 October 2011 to 30 September 2012).

Also shown are the statistical quantities mode (black solid line), mean (black dotted line), 90 percentile (P90, upper dashed white line) and 10 percentile (P10, lower dashed white line). The Peterson New High and Low Noise Models (NHNM and NLNM) are shown as grey solid lines. These two models were derived by Peterson (1993) from high-quality installations distributed world-wide and are widely used in the seismological community to compare station site characteristics. The NLNM represents the lowest PSD observed at continental interior stations during quiet periods. The NHNM represents maximum noise levels typically observed with high quality installations when cultural or seismic activity is absent.

The calculated PSD values are based on acceleration power spectra P_a. However, because ML is determined from ground displacements, see section 7.3, it is necessary to convert P_a values to ground displacements in

the time domain. This can be achieved by considering a narrow frequency band of interest using the relationship between average peak amplitude displacement *d* and displacement power spectra P_d (Havskov and Alguacil, 2006)

$$d = 1.25\sqrt{P_d(f_2 - f_1)} \quad \text{Equation 7.1}$$

where f_2 and f_1 are the upper and lower limits of the chosen frequency band. P_d can be calculated from P_a using the relationship

$$P_d = \frac{P_a}{(2\pi f_0)^4} \quad \text{Equation 7.2}$$

where f_0 is the geometric centre frequency of the frequency band. Using these relationships, we calculated for each seismic station the most likely average peak ground amplitude d_{mode} from the PSD mode value at the frequency of interest. The resulting values are then used to calculate event detection thresholds, see Section 7.3.

7.3 Calculation of Earthquake Detection Thresholds and Network Capability

The local magnitude ML of earthquakes is defined as a function of the hypocentral distance *R* (Richter, 1935)

$$ML = \log(A) + alog(R) + bR + c \quad \text{Equation 7.3}$$

where *A* is the maximum ground displacement amplitude measured with a Wood-Anderson (W-A) seismometer and *a*, *b* and *c* are constants representing geometrical spreading, attenuation and base level respectively. The parameters *a, b* and *c* depend on local conditions, resulting in different ML scales for different geographical regions. For regions with similar attenuation characteristics the parameters are similar. Hence for Ireland, as the geological setting is similar, we here adopt the ML scale defined for the UK (Ottemöller and Sargeant, 2013)

$$ML = \log(A) + 0.95\log(R) + 0.00183R - 1.76 \quad \text{Equation 7.4}$$

If no measurements of a W-A seismometer are available the maximum ground displacement amplitude *A* can be approximated by removing the instrument response and then convolving with the response of a W-A seismometer (Havskov and Ottemöller, 2010). Originally *A* was measured from the two horizontal components, but current practice is often to use maximum vertical component amplitude which on a bedrock site is quite similar to maximum horizontal component amplitude. Horizontal components are affected more strongly by amplification if a station is located on soil rather than bedrock. Usage of vertical component data results in more consistent ML estimation amongst stations located on different ground conditions than using horizontal component data (Havskov and Ottemöller, 2010).

Figure 7.3 shows that the same maximum event amplitude *A* can be caused by earthquakes with different magnitudes *ML* and different hypocentral distances *R*. For example, a recorded amplitude *A* = 6 nm could be observed for an earthquake with magnitude *ML* = 0.4 and a hypocentral distance of 25 km as well as for an

earthquake with *ML* = 0.9 and a hypocentral distance of 70 km. Figure 7.3. also shows that at a fixed hypocentral distance larger magnitude earthquakes cause larger ground displacements. At a hypocentral distance of 70 km for example the ground displacement *A* is 1.5 nm for earthquakes with *ML* = 0.3 and 6 nm for earthquakes with *ML* = 0.9. Depending on the background noise amplitude *d* at event time, the earthquake signal can become masked by the noise. It is usually assumed that a signal-to-noise ratio (SNR) of 3 is sufficient for earthquake detection and location (Baillard *et al*., 2014; Gaci, 2014; Stork *et al*., 2014). Therefore, assuming *A* = 3*d*, the curves in Fig. 7.3 also give information on the smallest earthquakes that can be detected in environments with different background noise levels.

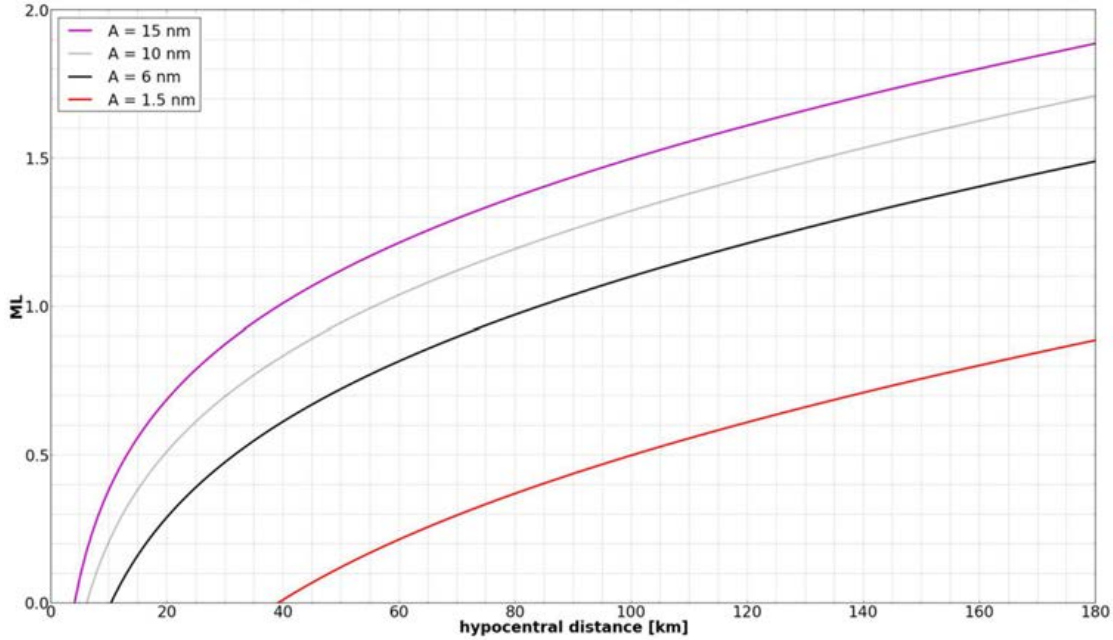

Figure 7.3. Magnitude ML versus hypocentral distance R (for different maximum earthquake amplitudes A, based on Equation 7.2)

To calculate an average background noise level for Ireland the 2 Hz P_a value of each INSN station's PDF mode curve was picked and converted to an average peak ground amplitude d_{mode} by using equations 2.1 and 2.2 (see section 7.2). The average of the d_{mode} values for all INSN stations is 0.5 nm. Because *A* = 3*d* corresponds to the amplitude of the smallest event detectable for background noise with amplitude *d*, the red curve (*A* = 1.5 nm) in Figure 7.3 represents a detection threshold curve for the calculated average noise level *d* = 0.5 nm (i.e. *d* = 1.5 nm/3). The curve for *A* = 6 nm corresponds to the detection threshold of a higher noise level with *d* = 2 nm and is based on the largest P90 value observed in the INSN. Because seismic noise levels are highly time dependent it is prudent to assume high noise levels when calculating the detection capability of a network. Hence curves are also presented with values of *A* = 10 nm and *A* = 15 nm representing noise levels d = 3.3 nm and d = 5 nm respectively, exceeding the P90 value. The latter value was chosen as a detection threshold in the seismic monitoring study for Balcombe in West Sussex, UK by Horleston *et al*. (2013).

The earthquake detection capability for the permanent seismic stations that are currently installed in Ireland was calculated as follows. This virtual network is referred to as the all-Ireland Network, consisting of six INSN installations and the BGS station CLGH in Northern Ireland, see Figure 7.1. The earthquake location capability of a network depends on the station density, the detection thresholds at the individual stations and the minimum number of earthquake station records required for a reliable estimation of earthquake location. A

minimum of four phase picks is required to determine the four unknowns of an earthquake location, which are latitude, longitude, depth and origin time (Havskov and Ottemöller, 2010). In principal one 3-component seismometer is sufficient to provide this information, for example from three p-arrivals and one s-arrival time. However, in practice event detection on several stations is desirable because locations can be better estimated automatically when more detections are available and hence fewer false detections have to be reviewed. A minimum of four seismic station detections is frequently recommended in the literature (e.g. Deichmann and Giardini, 2009; Horleston *et al*., 2013; Stork *et al*., 2014). Baptie *et al*. (2015) recommend detections on at least five stations and Trnkoczy *et al*. (2009b) state that detections on at least six stations "provide scientifically credible evidence of an event's location". In practice a distinction has to be made between automatic earthquake detections, i.e. observations of energy exceeding a given SNR, and manual phase picks, required to accurately locate an event. In the following we assume that six detections of an event are needed for a reliable event location. This conservative approach allows for the fact that six detections do not necessarily result in six clear manual phase picks.

The earthquake location capability of the all-Ireland network was calculated based on the Richter relationship between magnitude and hypocentral distance for the UK, see Equation 7.4. For the calculation it was assumed that earthquake recordings with a SNR of at least 3 are required on a minimum of six stations, see above. Noise amplitudes at the seven stations are derived from their PSD mode values as described above for the estimation of the average background noise level for Ireland. Figure 7.4a presents the resulting location capability plot for average noise conditions while Figure 7.4b shows the corresponding plot for high noise conditions, based on P90 PSD values, see above. From Figure 7.4b it can be concluded that the all-Ireland network is expected to provide reliable locations for all events with ML ≥ 1.5 in the CB area and for all events with ML ≥ 1.2 in the NCB area. Considering additional stations from the BGS network, situated on the west coasts of Scotland, Wales and England, does not improve the network capability in the two study areas significantly (not shown here). Overall it can be concluded that the all-Ireland network is clearly incapable of providing a baseline catalogue with a magnitude of completeness ML ≥ 0.5 for the two study areas and that this would require denser sub-networks in each study area.

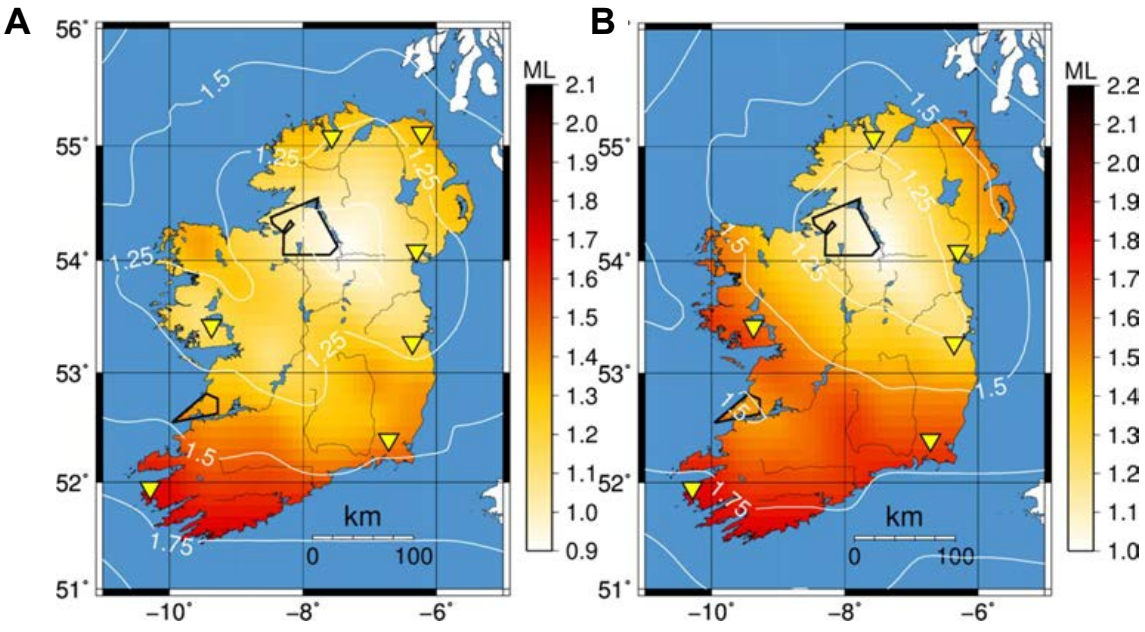

Figure 7.4. Earthquake detection capability plots (assuming earthquake recordings with SNR > 3 on at least 6 stations, for station noise levels based on (a) mode PSD and (b) P90 PSD, representing average and high noise conditions respectively).

7.4 Comparison between Calculated and Observed Detection Thresholds

In this section the detection thresholds derived in section 7.3 are compared with actual detections of earthquakes recorded in Ireland. The goal is to identify the maximum hypocentral distance for which good quality seismometer installations in the two study areas can reliably detect all events with ML ≥ 0.5. In section 7.5 five earthquakes with epicentres in Co. Donegal and local magnitudes between 0.6 and 2.2 are analysed, see Figure 7.5 for the epicentre locations. The effect of high noise levels on event detection is demonstrated with recordings from the ML = 2.2 earthquake. This event occurred during a storm period and it is shown that noise levels are especially high for stations close to the Atlantic coast. This is relevant to this study because both study areas are located on the West coast of Ireland (see section 5). In order to improve reliability of the comparison between theoretical and observed detection thresholds additional earthquake detections are presented in section 7.6, mainly for earthquakes with epicentres in Scotland and Wales. Finally, the influence of station installation quality on detection thresholds was investigated and a threshold value that is suitable for baseline monitoring in the two study areas identified, assuming good quality installation methods.

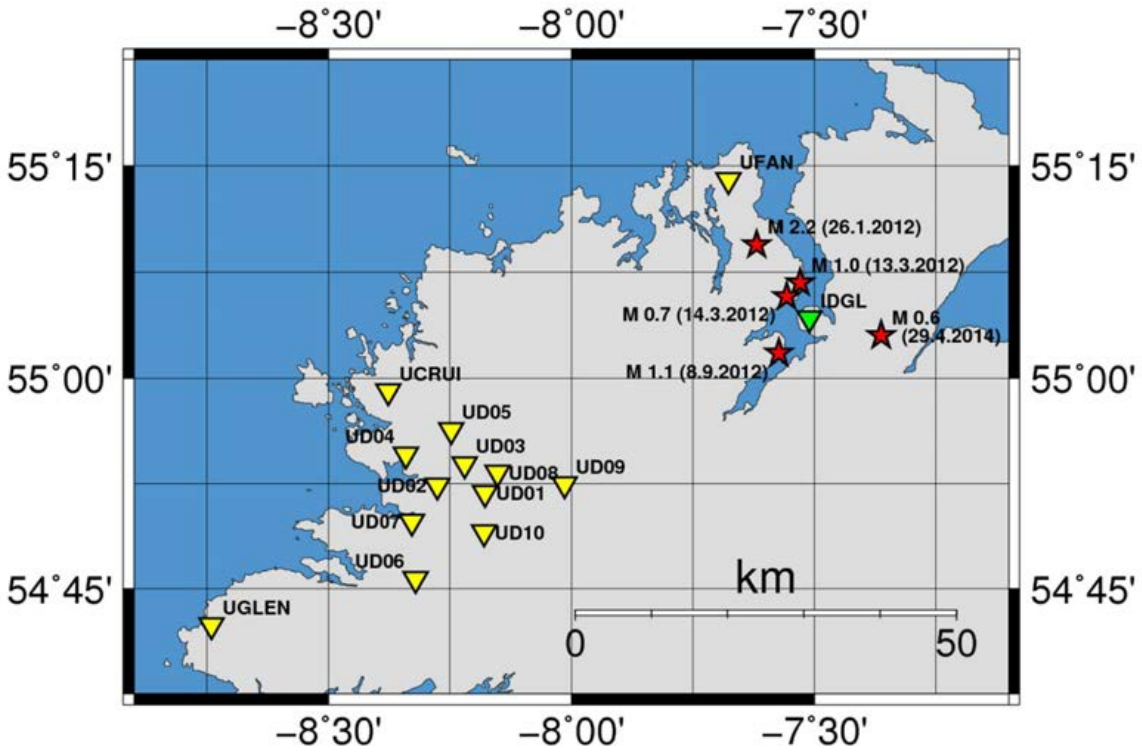

Figure 7.5. Epicentre locations of earthquakes in Donegal (for the time period 1.10.2012 to 30.9.2014 (red stars) and locations of nearby seismic stations (triangles)).

7.5 Detection of Donegal Earthquakes

The INSN data for the ML = 2.2 Donegal earthquake of 26th January 2012, see Figure 7.5 for the epicentre location, demonstrate that detectability can be significantly reduced if station noise is high. Figure 7.6 shows that the earthquake arrival at station VAL, which is located about 400 km from the epicentre and only 140 m from the coast, is barely detectable because the background noise level is high. The root mean square (rms)

amplitude of noise at event time was on the order of 3 nm. The seismogram is restituted to the displacement response of a W-A seismometer and filtered with a 2 Hz high pass filter. The theoretical ML(R) curves in Figure 7.7 predict for an earthquake with ML = 2.2 and a hypocentral distance of 400 km a signal amplitude *A* of about 6 nm, see black line. Thus the expected SNR for the ML = 2.2 signal at VAL is about 2, which agrees with the observation in the bottom panel of Figure 7.6. The yellow square marker in the top right of Figure 7.7 summarises the information we obtained from the recording of the ML = 2.2 event at VAL, namely RMS noise amplitude at the time of the recording (shape of marker) and observed SNR (colour of marker). The three blue circular markers at smaller hypocentral distances signify that the noise level at stations IDGL, DSB and IWEX were below 0.5 nm and that the earthquake signal was recorded with SNR larger than 5. Before considering the markers for the lower magnitude events in Figure 7.7 the Waveobs station recordings of the ML = 2.2 event are discussed.

The elevated noise level at station VAL on the 26.1.2012 is due to a storm system and the stations proximity to the coast. Möllhoff and Bean (2016) have shown that in Ireland seismic noise in the frequency band 1 to 2 Hz is generally elevated in coastal zones, especially on the western sea board. This effect is enhanced during storm conditions as is observed for the ML = 2.2 Donegal earthquake at the coastal station VAL and also several Waveobs stations, depending on their distance from the Atlantic shoreline. The Waveobs stations with the highest noise levels during the time of the ML = 2.2 Donegal earthquake are UACH, UGAL and USHE, see Figure 7.9 for the seismic waveform data. These stations are located only 70 to 330 metres from the Atlantic shoreline and recorded RMS noise amplitudes *d* larger than 3.3 nm, represented by the three star symbols in the top of Figure 7.8. Detection of the ML = 2.2 earthquake at these stations required a signal amplitude of at least 10 nm (grey line), achieved only at station UACH because it is much closer to the epicentre than UGAL and USHE. The lowest RMS noise amplitudes at event time were observed at stations UFAN, UCRUI and ULET, see Figure 7.9, because they are located further inland between 1.5 and 4.2 km from the shoreline. The noise levels at these stations were between 0.7 and 1.1 nm, represented by the triangular markers at ML = 2.2 in Figure 7.8. This leads to the conclusion that in order to obtain noise levels not much larger than 1 nm seismic stations in the baseline study should be located at least 4 km from coastlines directly open to the Atlantic Ocean.

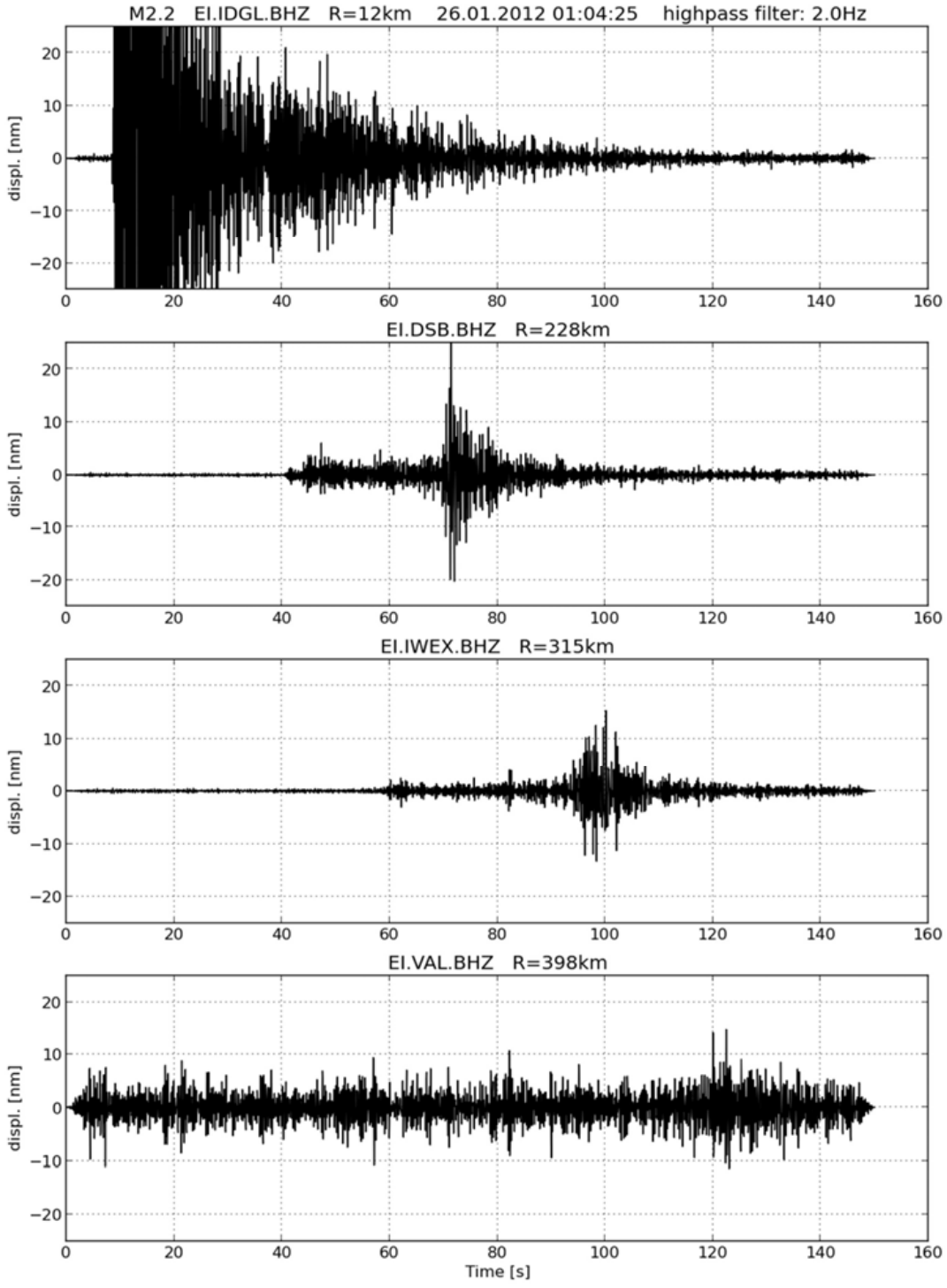

Figure 7.6. INSN recordings of the M=2.2 Donegal earthquake, 26.1.2012 (restituted to the displacement recording of a Wood-Anderson seismometer. Station names and hypocentral distances R are given above each subfigure. Note that the recording of station IDGL is not clipped, but displayed with the same displacement amplitude range as the recordings at the other stations).

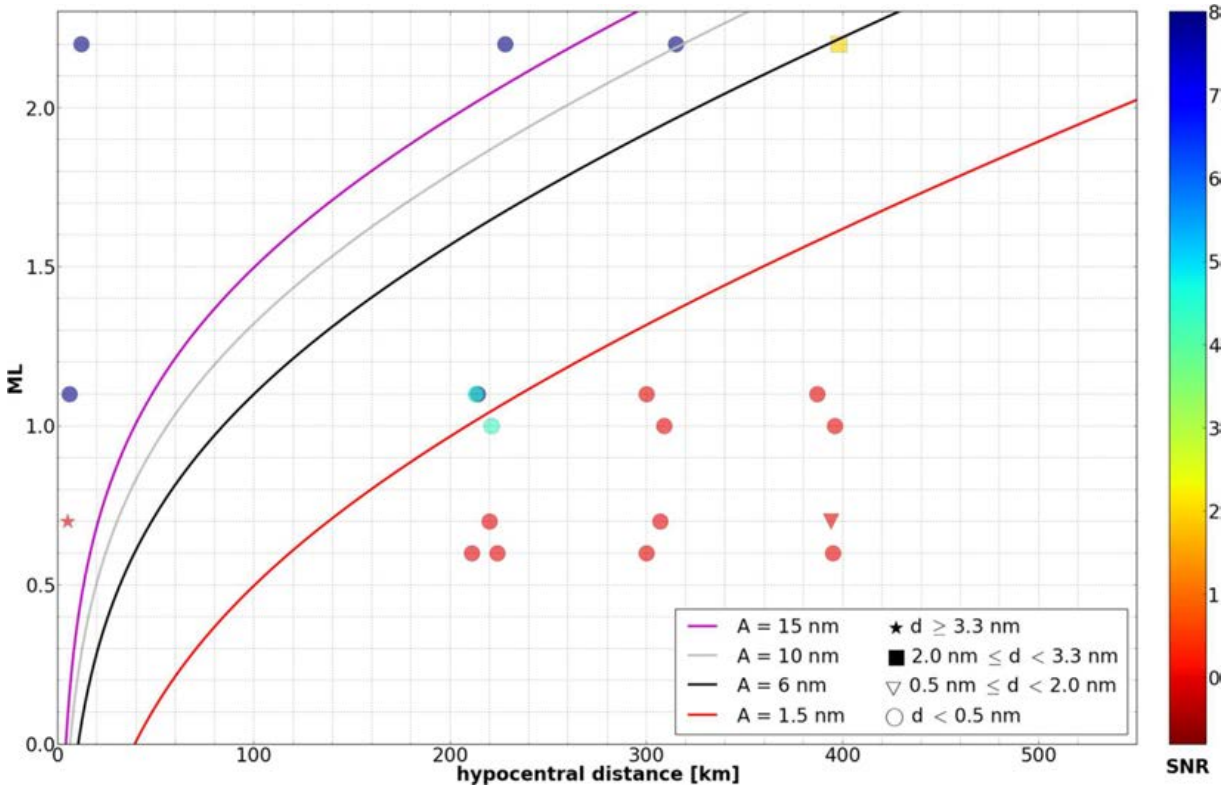

Figure 7.7. INSN station detectability of earthquakes in Donegal, see Figure 7.1 (Marker colours indicate the SNR for each recording. Marker shapes indicate the RMS noise amplitude (d) at the relevant station just before arrival of the earthquake signal. Also shown are theoretical curves of ML versus hypocentral distance R for different maximum W-A signal amplitudes A).

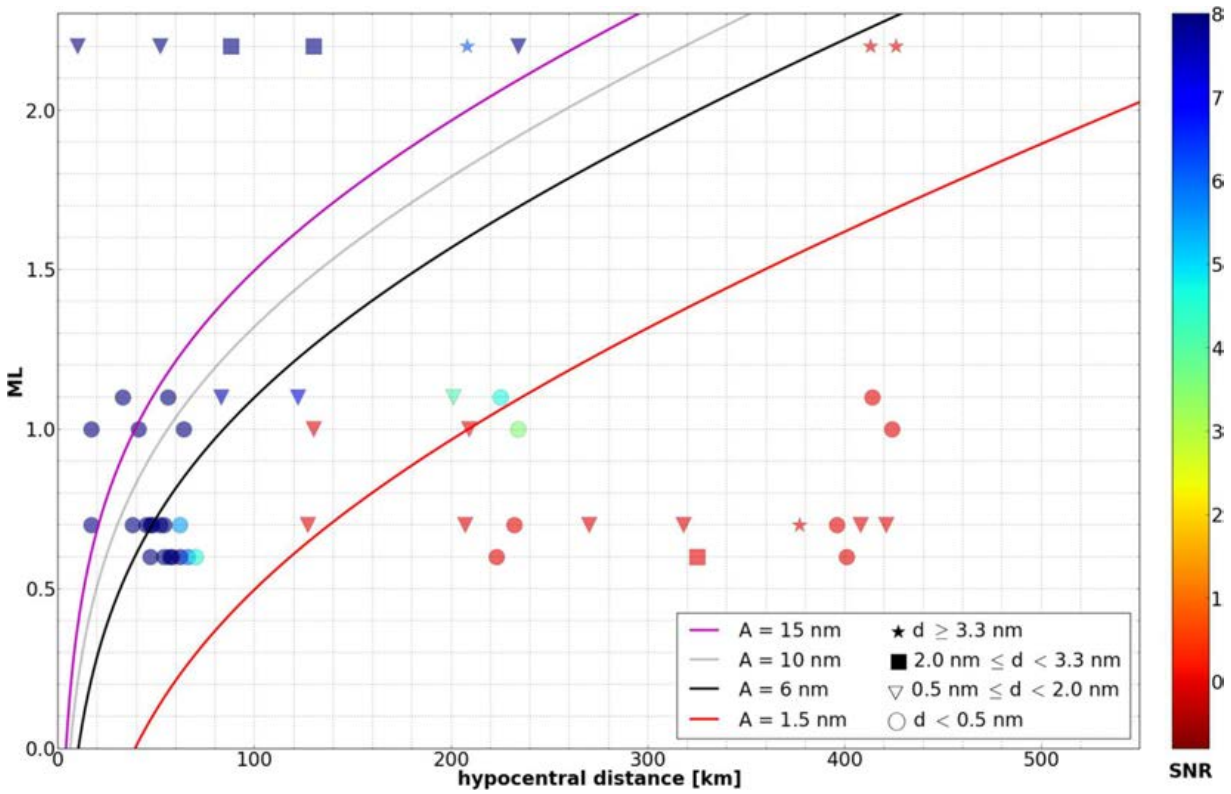

Figure 7.8. Waveobs station detectability of earthquakes in Donegal, see Figure. 7.5 (Marker colours indicate the SNR for each recording. Marker shapes indicate the RMS noise amplitude (d) at the relevant station just before arrival of the earthquake signal. Also shown are theoretical curves of ML versus hypocentral distance R for different maximum W-A signal amplitudes A).

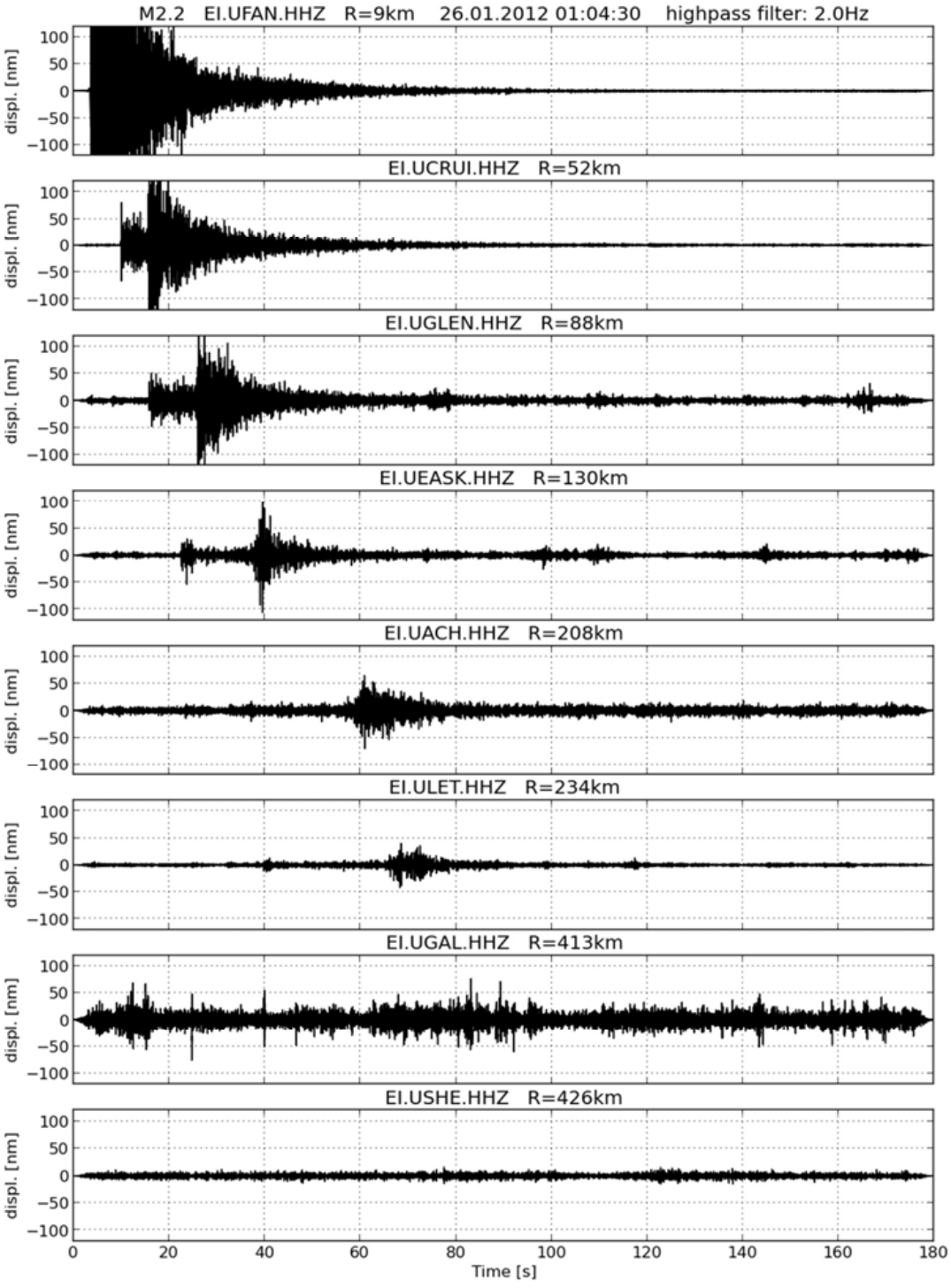

Figure 7.9. Waveobs recordings of the ML=2.2 Donegal earthquake, 26.1.2012 (restituted to the displacement recording of a Wood-Anderson seismometer. Station names and hypocentral distances R are given above each subfigure. Note that the recording of station UFAN is not clipped, but displayed with the same displacement amplitude range as the recordings at the other stations).

Figure 7.10 shows Waveobs station recordings of the magnitude 1.1 Donegal event, 8.9.2012. The earthquake was detected on all stations that were operating at the time, except USHE. The event was also detected in the data streams from the INSN stations IDGL, DSB and IGLA, but not on IWEX and VAL, see Figure 7.11. These detection results are summarised in Figures 7.7 and 7.8, which also show detectabilities for the Donegal events with magnitude 1.0 (13.3.2012), magnitude 0.7 (14.3.2012) and magnitude 0.6 (29.4.2012), see Figures 7.12 to 7.14 for the corresponding seismic recordings from the Waveobs network.

A perfect match between theory and observation in Figures 7.7 and 7.8 would result in only red or yellow circular markers to the right of the red curve and only green or blue circular markers to the left. Correspondingly for a perfect match all triangular markers to the right of the black curve would be red or yellow and all to the left would be green or blue. Square and star markers would lie similarly with respect to the grey and the magenta line. Theory and actual observations show a good qualitative match. In order to achieve a more reliable comparison we present an analysis of additional earthquakes in the next section. The increased number of detection observations allows us to study the influence of installation quality on detection thresholds and to identify a threshold value that is suitable for baseline monitoring in the two study areas.

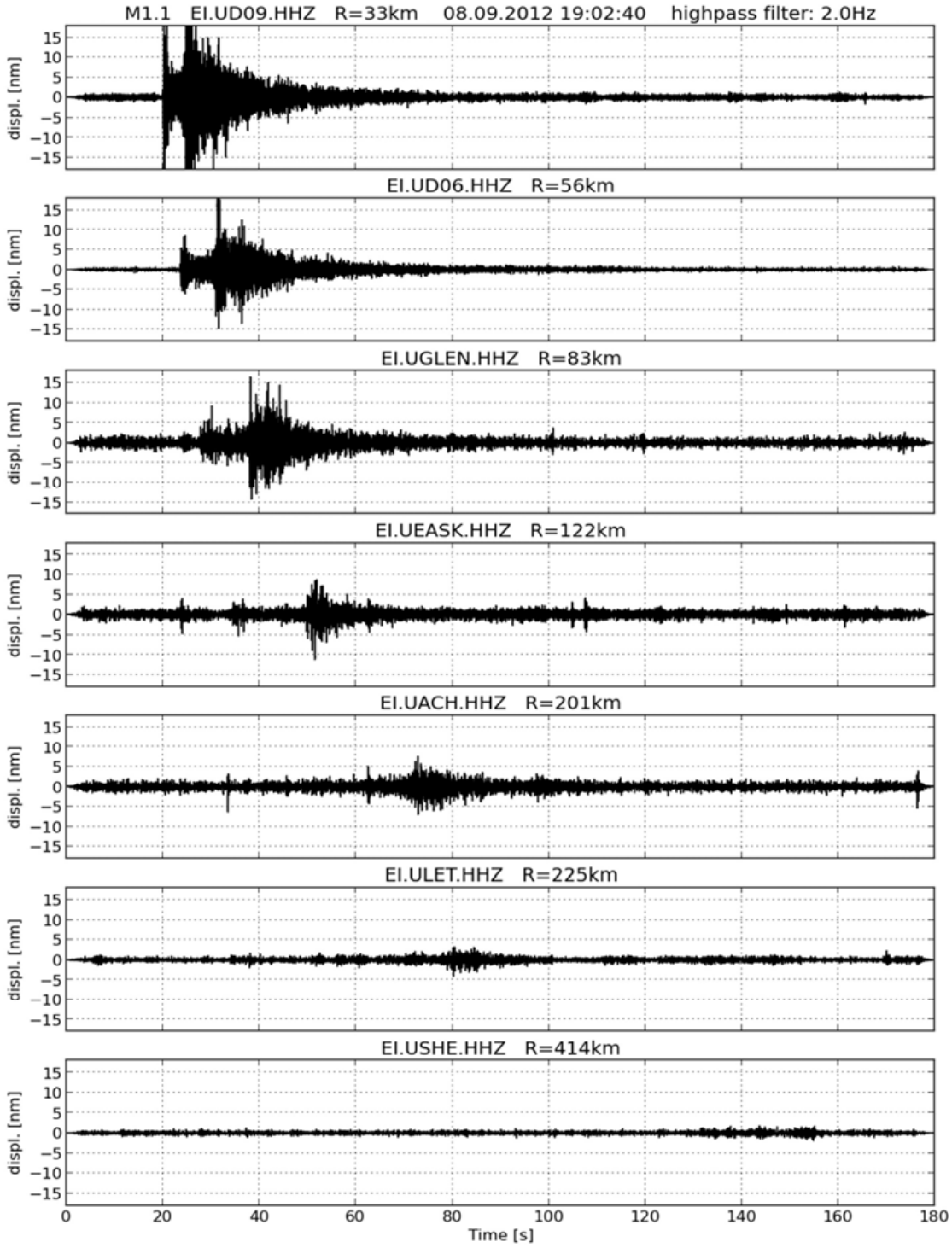

Figure 7.10. Waveobs recordings of the ML=1.1 Donegal earthquake, 8.9.2012 (restituted to the displacement recording of a Wood-Anderson seismometer. Station names and hypocentral distances R are given above each subfigure).

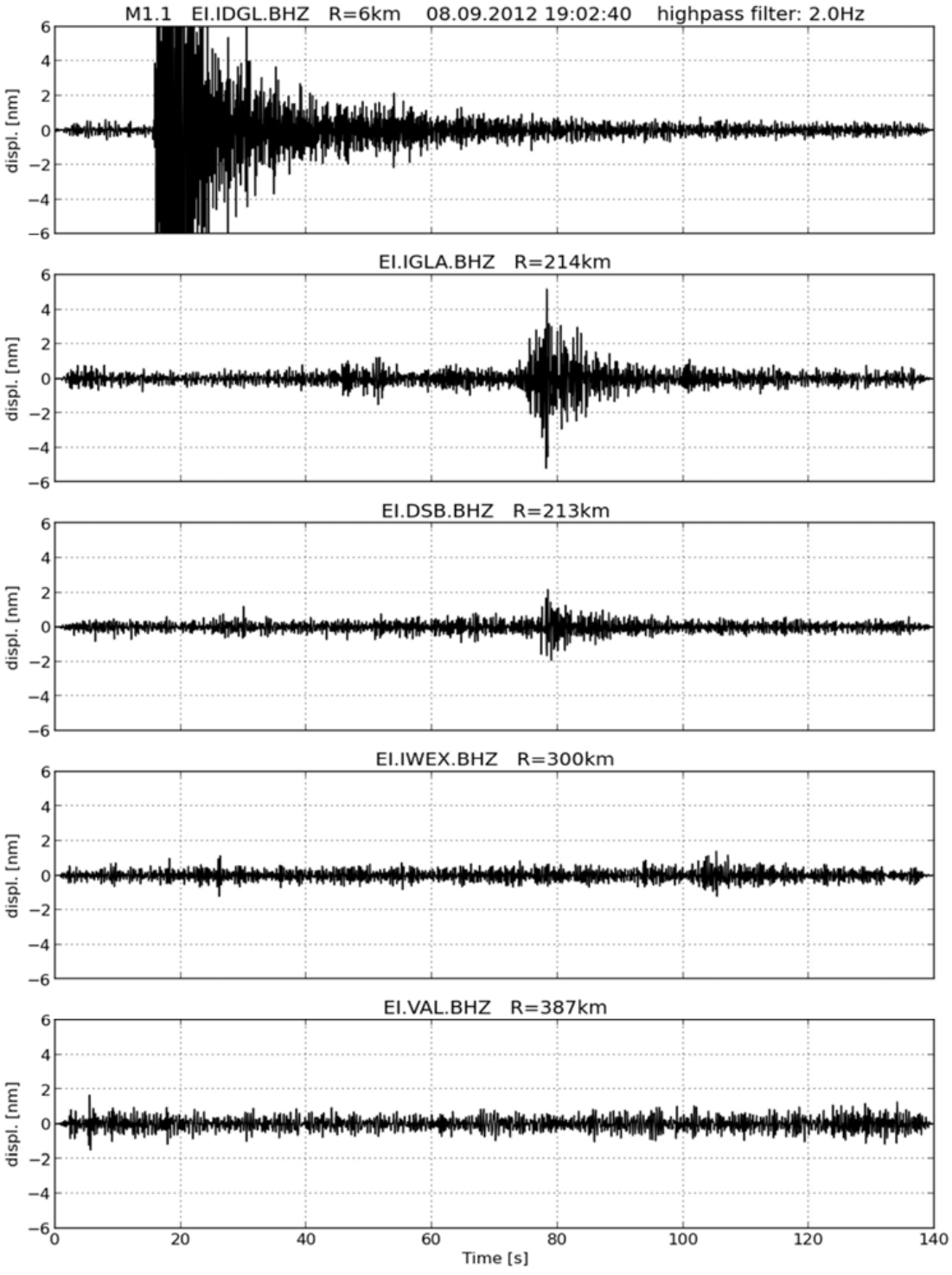

Figure 7.11. INSN recordings of the ML=1.1 Donegal earthquake, 8.9.2012 (restituted to the displacement recording of a Wood-Anderson seismometer. Station names and hypocentral distances R are given above each subfigure).

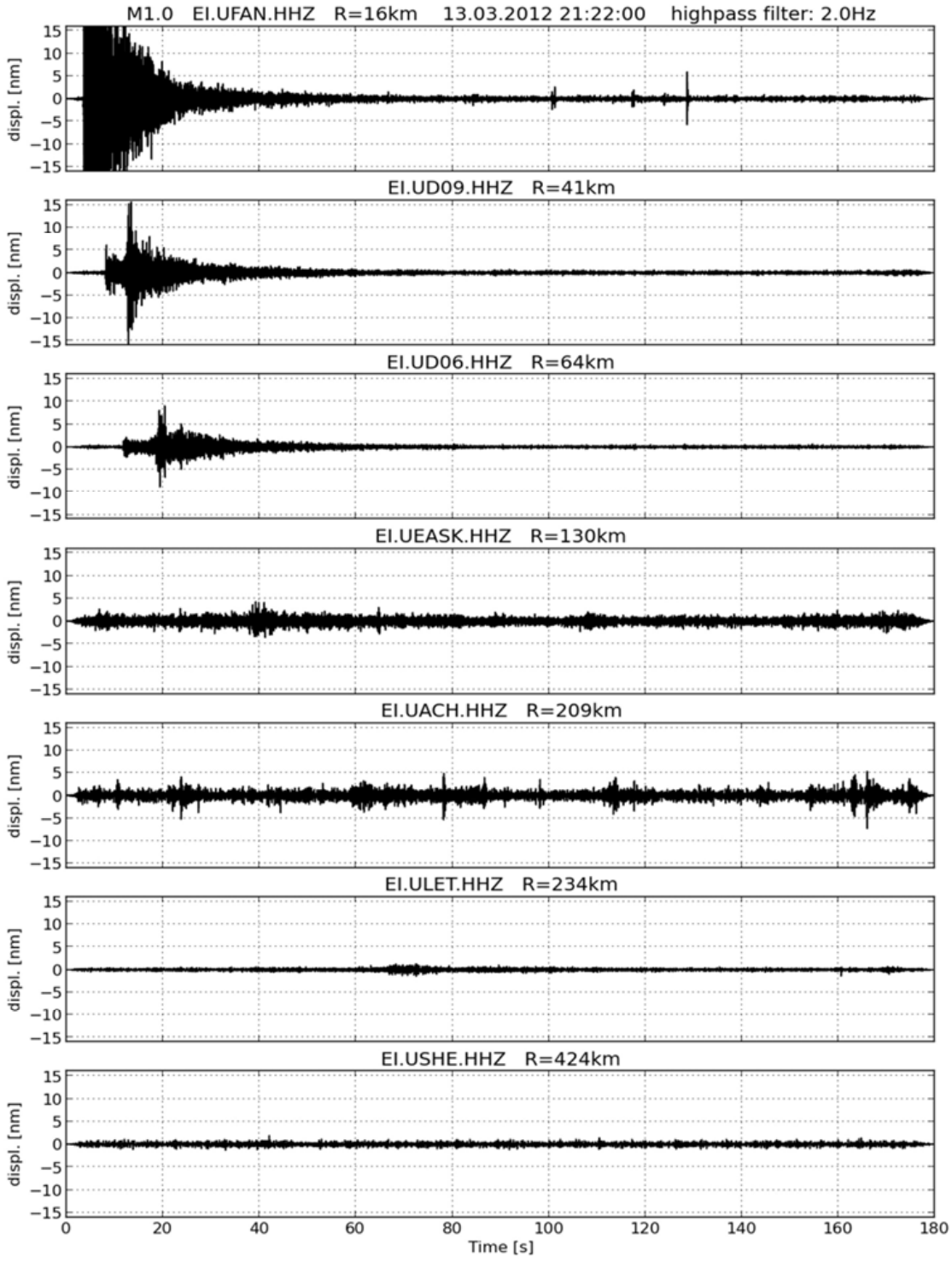

Figure 7.12. Waveobs recordings of the ML=1.0 Donegal earthquake, 13.3.2012 (restituted to the displacement recording of a Wood-Anderson seismometer. Station names and hypocentral distances R are given above each subfigure).

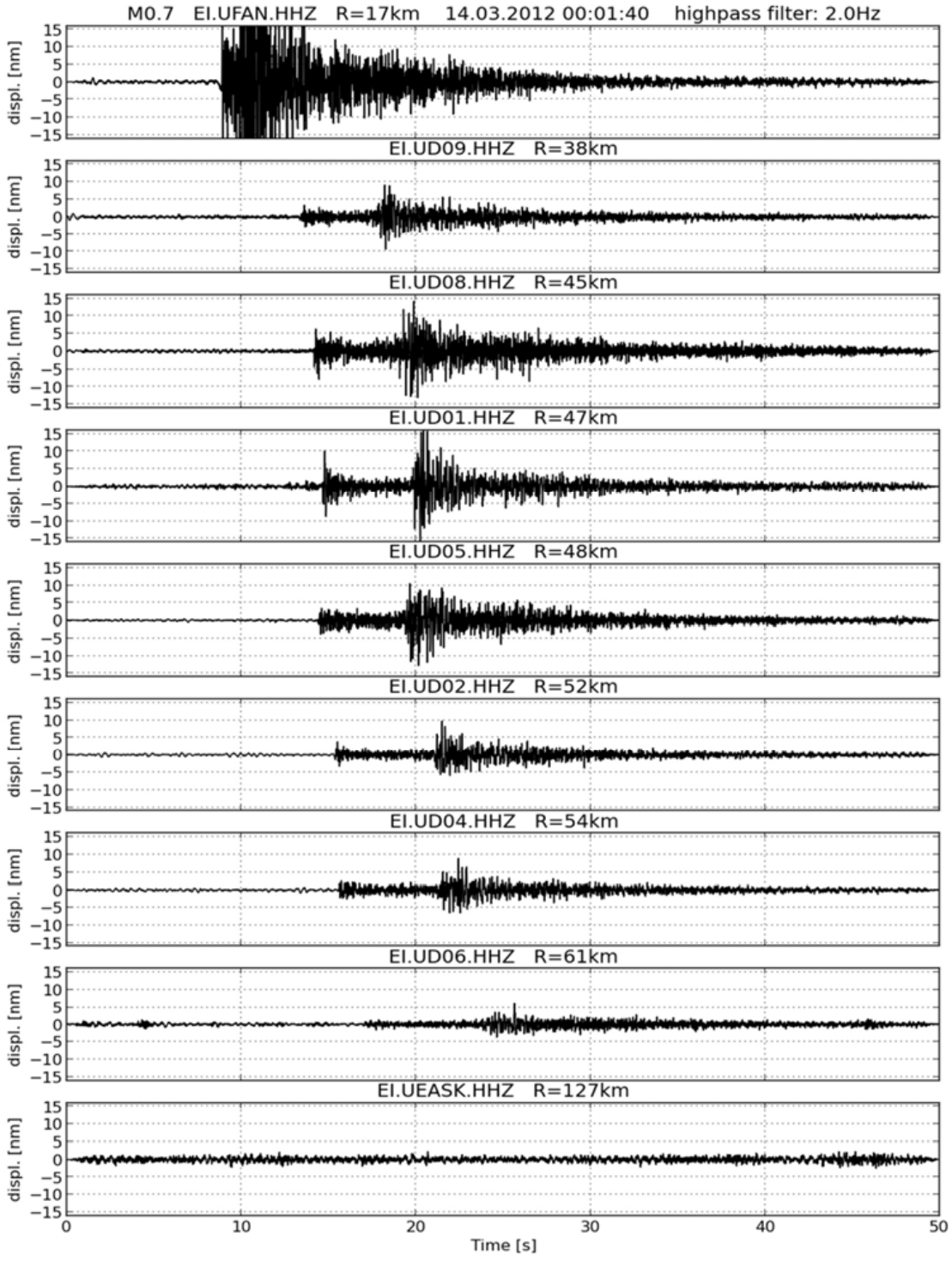

Figure 7.13. Waveobs recordings of the ML=0.7 Donegal earthquake, 14.3.2012 (restituted to the displacement recording of a Wood-Anderson seismometer. Station names and hypocentral distances R are given above each subfigure).

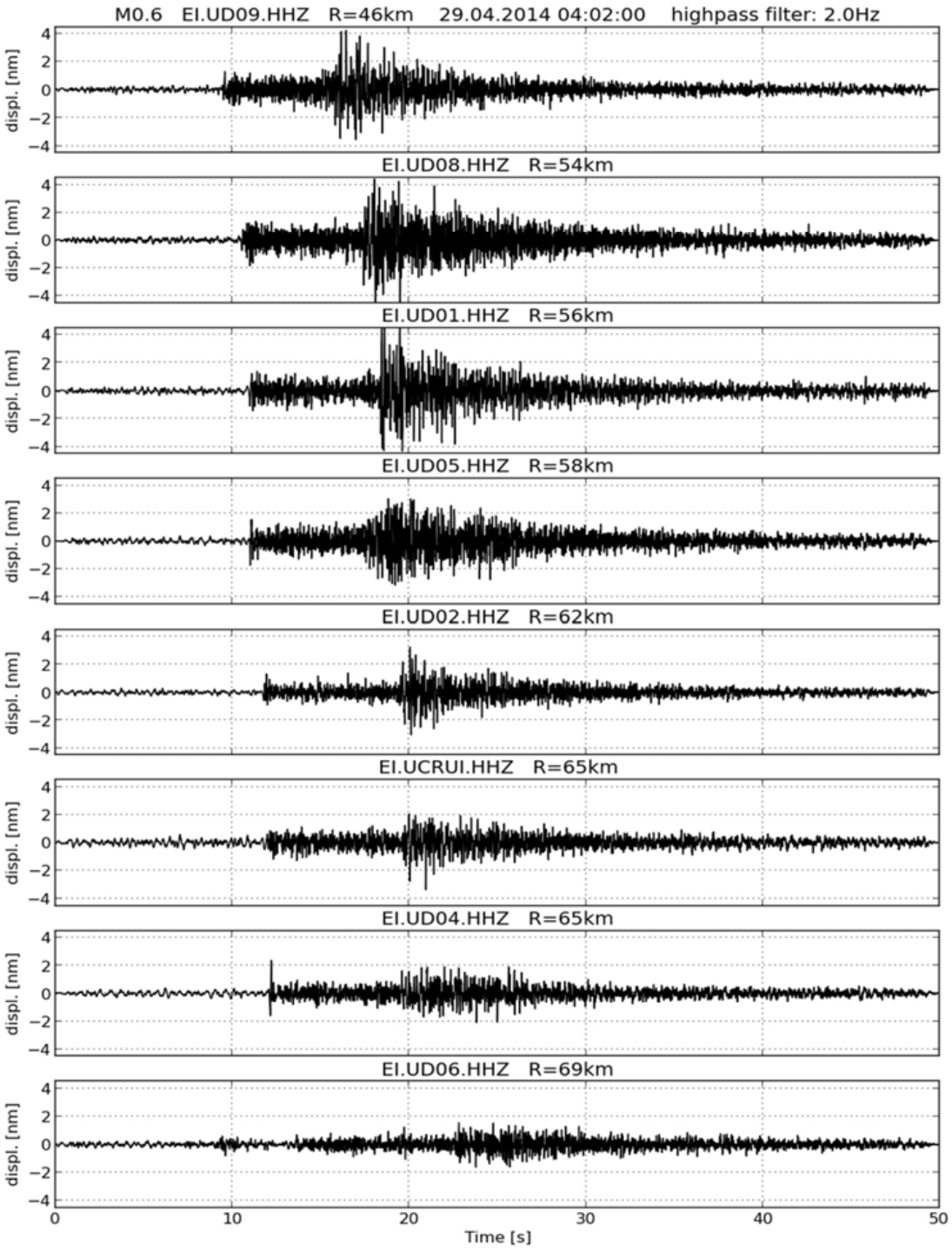

Figure 7.14. Waveobs recordings of the ML=0.6 Donegal earthquake, 29.04.2012 (restituted to the displacement recording of a Wood-Anderson seismometer. Station names and hypocentral distances R are given above each subfigure).

7.6 Influence of Installation Details on Observed Detection Thresholds

Further earthquakes with suitable hypocentral distances and magnitudes have been analysed to provide more detectability observations. Most of the epicentres of these earthquakes are located in Scotland and Wales. In Fig. 7.15 theoretical ML(R) curves are compared with all INSN and Waveobs earthquake detections considered in this study. Each marker in this figure refers to the seismic recording of an earthquake with the hypocentral distance and magnitude values given by the x- and y-axis respectively. The marker colour represents the SNR, with red and yellow signifying SNR values smaller than 3 and hence no reliable earthquake signal observed. The shape of each marker represents the RMS noise level d at the relevant station at the time of the earthquake. A perfect match between theory and observation in Fig. 7.15 would result in circular markers that are red or yellow to the right of the red curve and green or blue to the left. The colour of the triangular markers would be red or yellow to the right of the black curve and green or blue to the left. Square and star markers would lie similarly with respect to the grey and the magenta curve. Generally, theory and observation in Figure 7.15 agree well, especially for magnitudes smaller than ML = 1.6.

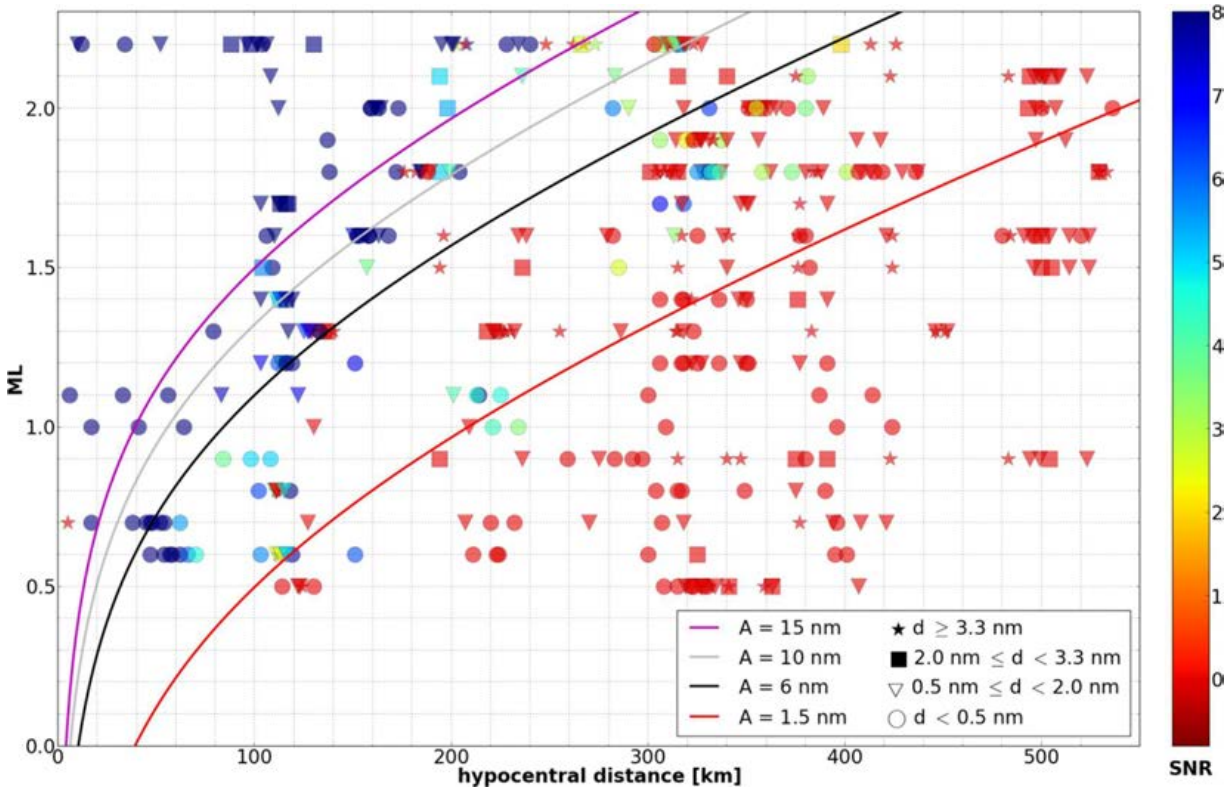

Figure 7.15. INSN and Waveobs earthquake detectabilities (compared with theoretical curves of ML versus hypocentral distance R for different maximum W-A signal amplitudes A of earthquakes. Marker colours indicate the SNR for each recording. Marker shapes indicate the RMS noise amplitude (d) at the relevant station just before arrival of the earthquake signal).

Therefore, theoretical detection thresholds based on the UK ML scale (Equation 7.4) are determined as suitable for calculation of the detection capability of the example baseline network geometries calculated in Section 7.9. These calculations require expected station noise levels as an input. In order to estimate the noise levels that can be expected for good quality installations in the two study areas the noise levels that were

observed in the above analysis for INSN and Waveobs stations were compared. Figure 7.16a shows that the INSN high quality, permanent installations on bedrock in concrete vaults result in RMS noise amplitudes most often between 0.1 and 0.5 nm. Larger noise amplitudes are usually due to weather systems that cause strong winds and rough sea states, but can also be caused by anthropogenic noise sources or local interference at a station.

The temporary Waveobs installations are of lower quality, with seismometers either installed in outbuildings and domestic garages or in field vaults constructed out of small (25 litre) or large (65 litre) plastic bins. Figure 7.16b shows that these lower quality installations result in noise amplitudes that are most often between 0.2 and 1 nm, but frequently up to 4 nm or even higher. In addition, some of the Waveobs stations are very close to the Atlantic sea shore, where noise amplitudes are elevated. If only stations that are deployed inland and in the larger bins are considered, then the observed noise amplitudes are significantly lower, almost as good as INSN installations, see Figure 7.17. It was concluded that good quality installations can be expected to have average noise levels of around 0.5 nm. During time periods with strong winds and rough sea states the noise levels of such installations are expected to increase to no more than 2 nm. Achieving these noise levels does not necessarily require the construction of concrete vaults in order to house seismometers, good quality field installations in large plastic bins with a concrete base on bedrock can be expected to be sufficient.

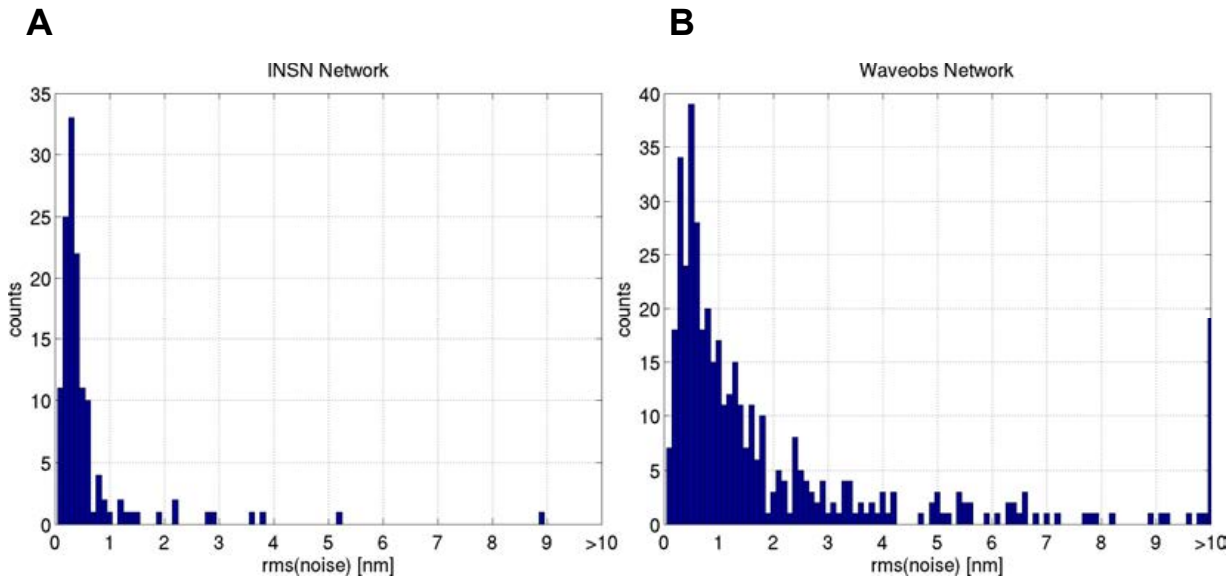

Figure 7.16. Seismic noise amplitudes observed in the detectability analysis of this study for (a) INSN installations and (b) Waveobs installations.

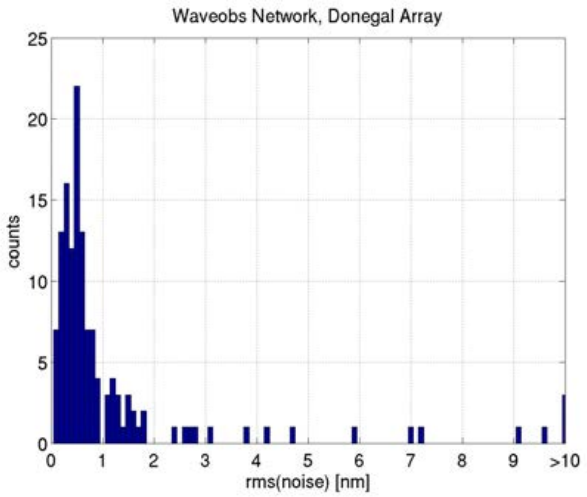

Figure 7.17. Seismic noise amplitudes observed in the detectability analysis of this study for Waveobs installations that are inland and in vaults constructed with the larger plastic bins.

7.7 Local Seismic Network Specifications

In this section we discuss what local network specifications are required for the baseline monitoring of naturally occurring seismicity in the Northwest Carboniferous Basin (NCB) and the Clare Basin (CB).

7.8 Deployment Length

The number of earthquakes recorded with a baseline network, and hence the reliability of the obtained seismicity rate, depends on the seismic activity, the sensitivity of the network and the deployment duration of the network. Gutenberg and Richter (1956) proposed the following linear relationship for the number of events N with magnitude M or higher in a given region and for a given time

$$\log N = a - bM \qquad \text{Equation 7.5}$$

where *a* and *b* are constants. The constant *a* is known as the rate parameter and corresponds to the number of earthquakes with magnitude zero or higher, usually normalised to a period of one year. The constant *b* is called *b*-value and gives the proportion between large and small events. *b* is usually around 1. As part of the European SHARE project Giardini *et al*. (2013) determined a rate parameter of *a* = 2.1756 for a source zone covering Ireland including offshore areas, a total area of about 200,000 km^2. Based on the seismicity actually observed in the SHARE zone, Baptie *et al*. (2015) estimated *a* = 2.1673 and *b* = 1, using the magnitude of completeness observed for offshore areas around Britain. Considering Equation 7.5 this means that about 47 earthquakes with a magnitude of 0.5 or larger can be expected to occur per year in the Ireland SHARE zone. Baptie *et al*. (2015) point out that this estimate for offshore areas around Britain is based on only 2 earthquakes. Using instead the catalogue completeness for onshore Britain they derive *a* = 1.4142 and *b* = 1.023. Using these parameters, the number of expected earthquakes with a magnitude of 0.5 or larger in the Ireland SHARE zone decreases to about 8 per year.

The seismicity rate for a sub-zone can be estimated using its relative size compared to the Ireland SHARE zone. The NCB for example has an area of about 2,500 km^2, which is 80 times smaller than the Ireland SHARE area. Assuming that the seismicity distribution in the SHARE area is homogenous and *a* = 2.1673, about 0.6

earthquakes with a magnitude of 0.5 or larger can be expected to occur per year, which corresponds to about one event every two years. In reality the seismicity distribution in the Ireland SHARE zone is not homogenous with less events onshore than offshore (Baptie *et al.*, 2015). The actual seismicity rate in the NCB is therefore expected to be less than one event with a magnitude of 0.5 or larger every two years. The CB is about 500 km^2 in size, which is five times smaller than the NCB which results in an estimate of a five times lower seismicity rate as calculated for the NCB.

The seismicity rates for the two study areas are expected to be so low that a reliable estimation of these rates could not be achieved even with a baseline network that is deployed for several decades. The upper estimate for the occurrence of earthquakes with a magnitude of 0.5 or larger in the NCB is one event every two years. Therefore, in order to determine if there is any unexpected seismicity in the study areas, the baseline network should be deployed for at least two years, though a longer deployment is very likely to be required to determine reliable statistics.

7.9 Network Geometry

In the following the station density required for baseline monitoring in the NCB and the CB is determined. An example network geometry for the NCB was designed by dividing the region into equally sized triangles and assigning station locations to the triangle corners. Network detection capability was then calculated based on the Richter relationship between magnitude and hypocentral distance for the UK, see Equation 7.4. For the calculation it was first assumed that earthquake recordings with a SNR of at least 3 are required on a minimum of six stations (see Section 7.3) and that RMS noise amplitudes at the stations are between 1 and 2 nm. The latter assumption reflects relatively high noise levels expected for good quality installations only during windy to stormy weather conditions, see section 7.2. The size of the triangles and hence the station density is varied until a detection threshold of at least ML = 0.5 is achieved throughout the area of interest. The station locations are then fine-tuned to allow for a good detectability at the network fringes by complying with the azimuthal gap rule, see next paragraph. Satellite imagery was employed to confirm that potential locations are not obstructed by lakes, towns or other large scale structures and change locations accordingly if required. The resulting example network has an inter-station spacing between 15 km and 25 km. Figure 7.18a shows the network detection capability for a focal depth of 0 km and

Figure 7**.18**b shows the corresponding result for a focal depth of 10 km. While considering a focal depth of 10 km decreases the detection sensitivity inside the NCB somewhat, the area covered by the ML = 0.5 contour does not change significantly. An analysis of the BGS earthquake catalogue shows that less than 10% of all earthquakes recorded with epicentres in or near Ireland had a focal depth of more than 10 km. It should be noted that the depth estimates of events in or near Ireland are very unreliable because network coverage in Ireland is sparse. However, lacking more detailed information a focal depth of 10 km was assumed in all following network detection capability calculations, underestimating network performance slightly for all events with focal depths less than 10 km.

Two rules of thumb in seismic network design should also be considered at this point. The first rule states that ideally epicentres should be inside the network and the azimuthal gap (the largest of all angles among the lines connecting a potential epicentre with all the stations in the network) should be less than 180 degrees (Baptie *et al.*, 2015) or 200 degrees (Havskov and Ottemöller, 2010). The example network geometry in Figure 7.18 fulfils this rule throughout the entire study area. The second rule of thumb states that for an accurate focal depth estimate the nearest station should be no further away than 1 to 2 times the hypocentral depth (Havskov and Ottemöller, 2010). Because inter-station spacing in the example network are between 15 and 25 km accurate depth estimates cannot be expected for events with focal depths less than about 10 km, unless an event occurs close to a station.

Depth accuracy is further compromised by the lack of high resolution seismic velocity models for the study areas. It is suggested that increasing station density in order to improve the depth accuracy is not practical for a baseline network. It was concluded from Figures 7.18a and 7.18b that 12 seismic stations are sufficient to detect and locate all events with ML ≥ 0.5 in the NCB. While earthquake recordings at six stations with SNR > 3 are required for a scientifically credible location estimation (Trnkoczy *et a*l., 2009b), it was assumed in the following that three such recordings are sufficient to reliably detect that an earthquake occurred. Figure 7.19a shows that assuming again noise levels of 1 to 2 nm the example network geometry is expected to detect all events in the NCB with ML ≥ 0.25. However, events with ML <= 0.5 cannot be properly located.

A requirement of 10 to 15 event recordings is usually required for more sophisticated studies of earthquake source properties (Trnkoczy *et al*., 2009b). A large number of earthquake recordings is also of benefit for mapping active faults, identifying seismicity variations within a study area and for attenuation and crustal studies (Havskov and Ottemöller, 2010). The network capability for the requirement that all 12 stations provide earthquake recordings with SNR > 3 is shown in Figure 7.19b. A large part of the area is covered by a magnitude detection limit of ML ≥ 0.75 while the southeast corner of the network only provides detectability in the range between 0.75 and 1.

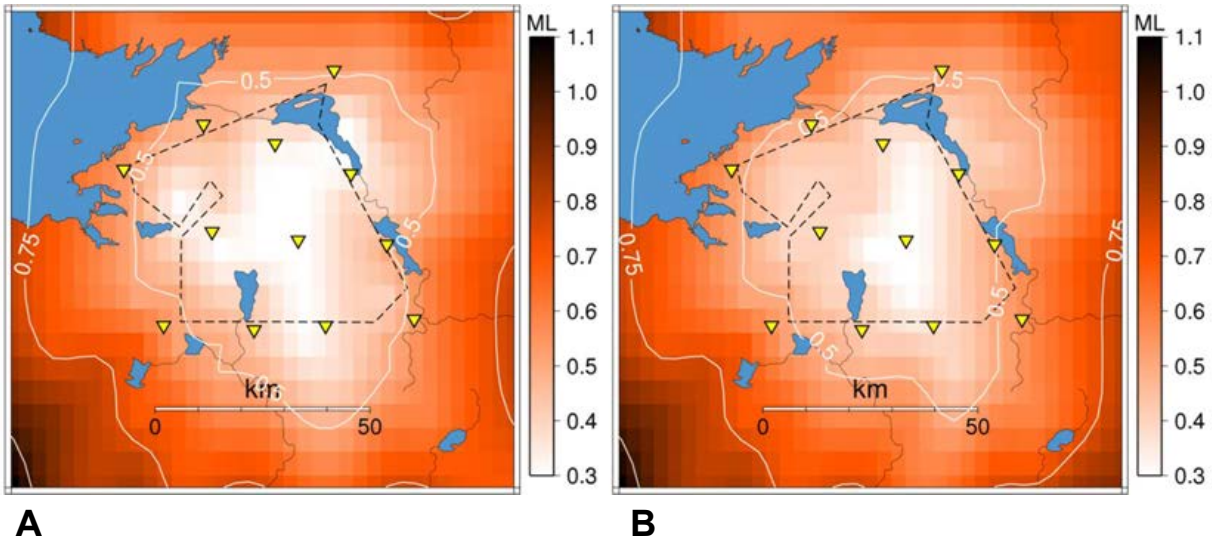

Figure 7.18. Example network detection capability plots (assuming earthquake recordings with SNR > 3 on at least 6 stations, station noise levels between 1 and 2 nm and a focal depth of (a) 0 km and (b) 10 km. The dashed black line shows the approximate outline of the NCB).

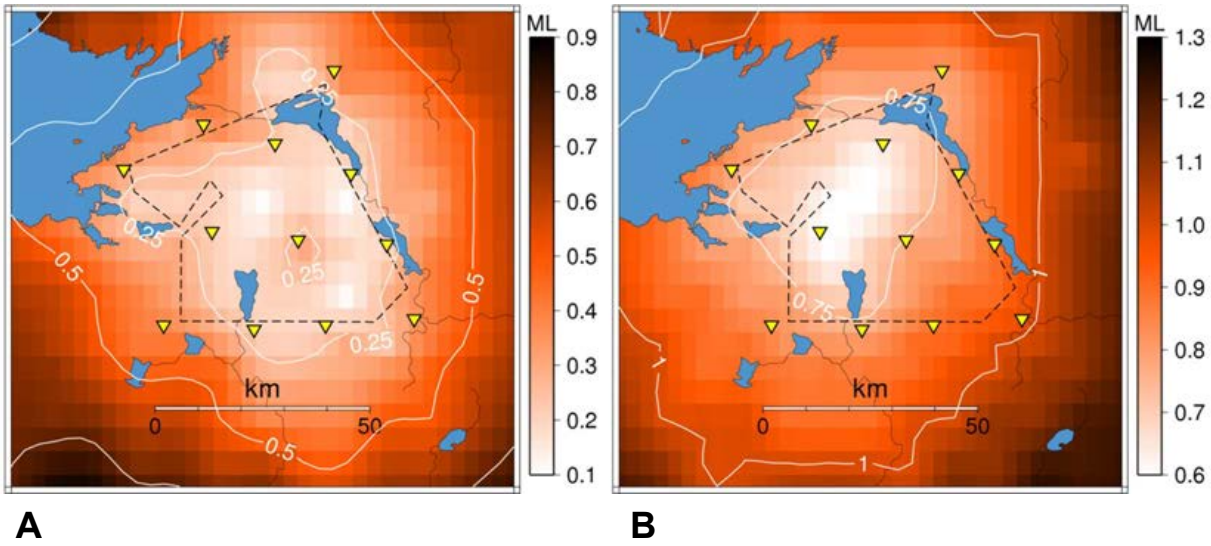

Figure 7.19. Example network detection capability plots (assuming earthquake recordings with SNR > 3 on at least (a) 3 stations and (b) 12 stations, station noise levels between 1 and 2 nm and a focal depth of 10 km. The dashed black line shows the approximate outline of the NCB).

The network detection capability plots presented above assume noise levels of 1 to 2 nm, which is probably a worst case scenario, for example if meteorological conditions are unfavourable or if local ground conditions are poor. The observations in Section 7.6 show that in Ireland noise levels at good quality installations are frequently in the range 0.2 to 0.5 nm, but can increase during stormy conditions up to 2nm. In order to investigate the network performance under favourable conditions detection capabilities were calculated for station noise levels between 0.2 and 0.5 nm. Figures 7.20a and 7.20b show the results assuming at least 6 and 12 earthquake detections respectively. It follows that for these lower noise levels, the example network geometry can provide good location and magnitude accuracy throughout the NCB for all events ML ≥ 0. For more sophisticated studies that require more than 10 detections the detection threshold of the network increases for the NCB to about ML = 0.3.

In the following the impact of station location flexibility on network performance is estimated. The latitude and longitude positions of the individual station locations are changed independently by random values between –2 km and +2 km (Figure 7.21a) and random values between –4 km and +4 km (Figure 7.21b). A comparison with Figure 7.18a shows that the changes in station locations have only a small impact on network capability. Because regular station distributions result in more uniform location accuracies (Trnkoczy *et al*., 2009b) a station location accuracy of +/- 2 km is suggested for the baseline network. In addition, good station coverage around the network's fringes should be ensured to comply with the azimuthal gap rule, see above.

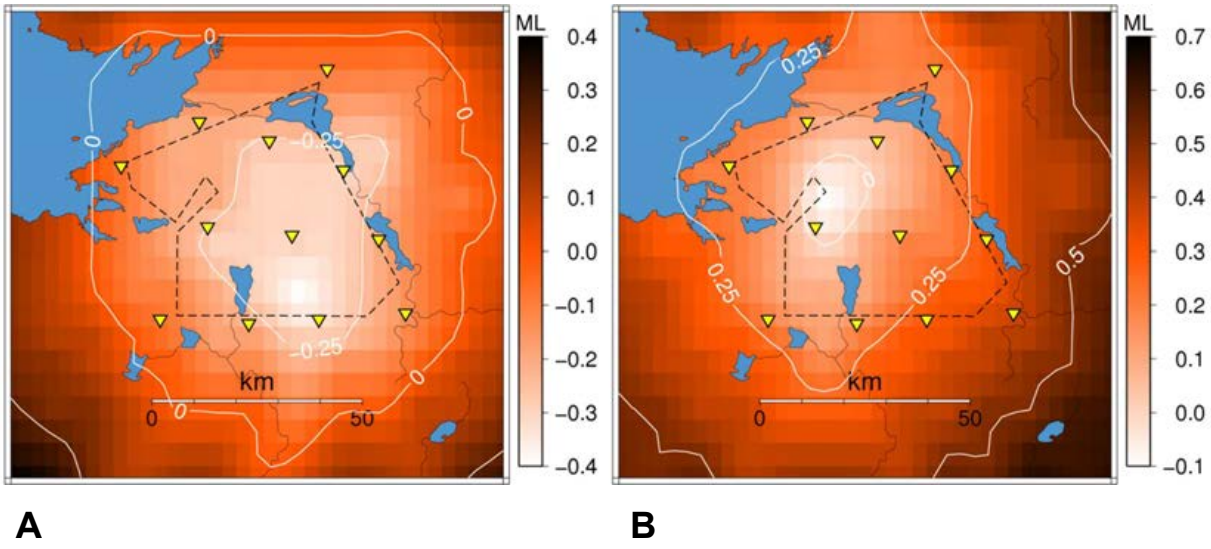

Figure 7.20. Example network detection capability plots (assuming earthquake recordings with SNR > 3 on at least (a) 6 stations and (b) 12 stations, station noise levels between 0.2 and 0.5 nm and a focal depth of 10 km. The dashed black line shows the approximate outline of the NCB).

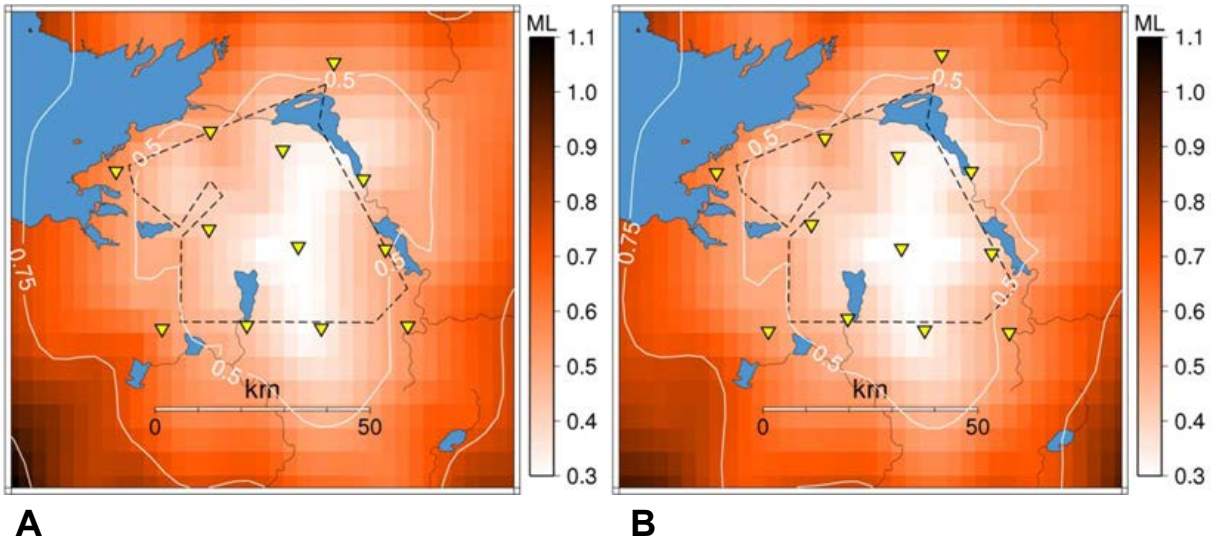

Figure 7.21. Example network detection capability plots (assuming earthquake recordings with SNR > 3 on at least 6 stations, station noise levels between 1 and 2 nm and a focal depth of 10 km. Compared to the network geometry presented in previous figures the latitude and longitude positions of the individual station locations are changed independently by random values between (a) –2 km and +2 km and between (b) –4 km and +4 km. The dashed black line shows the approximate outline of the NCB).

The narrow Loop Head peninsula in the CB has a strong influence on the network design for that area. Ideally seismic stations should be located at least 4 km from coastlines directly open to the Atlantic Ocean, see section 7.5. However, in order to ensure coverage around the network fringes it is necessary in this case to have stations along the coast on the northwest side of the CB, see Figure 7.22a for the example station network for the CB. Because these stations are expected to have relatively high noise levels they have reduced inter-

station spacing of about 15 km. In addition, high noise levels are considered for these stations in the calculation of the network detection capability. Further stations are placed around the study area and two inside it. Figure 7.22a shows that the example network provides the capability of locating all events in the study area with ML ≥ 0.5, assuming that noise amplitudes are between 1 and 2 nm. These noise levels are expected when meteorological conditions are unfavourable or local ground conditions are poor. Figure 7.22b shows that for more favourable conditions with noise levels between 0.2 and 0.5 nm the network capability improves to ML ≥ –0.25 throughout most of the study area.

Experience shows that up to 20% of stations in a temporary network experience technical problems at any one time. Because six station recordings are required to provide reliable location parameters it is suggested that temporary networks should consist out of at least eight seismic stations. It was found that determining the location of all local earthquakes with magnitudes ML ≥ 0.5 requires 12 stations in the NCB and 10 stations in the CB. Based on the calculated example network geometries and the required station location accuracy, example deployment target zones are presented with a radius of 2 km for each seismometer location, see Figures 7.23 and 7.24 and the list of centre coordinates for the example target zones in Table 7.2.

It is not feasible to propose more detailed station locations as part of this report. Finding suitable locations requires a professional site selection procedure that involves several site visits to address many factors, e.g. unexpected man-made or natural noise sources (machines, pumps, streams, exposure to wind etc.), local ground and soil conditions, lack of power (or solar/wind exposure at remote sites), inaccessibility, topographical features, wildlife, lightning threat, future capability for telemetric data transmission, land ownership and future developments or changes in land usage. It should be noted that the calculated network configurations are just examples and were designed in order to estimate the required number of seismic stations in each of the two baseline networks. Many other configurations would also satisfy the basic requirements described above. If the presented configurations were used for an actual network deployment, flexibility to make significant adjustments to station target zones might be required, for example if site permission cannot be obtained or to allow for optimal station locations e.g. on bedrock. In such a case the detection and location capability of the changed network geometry would have to be reassessed.

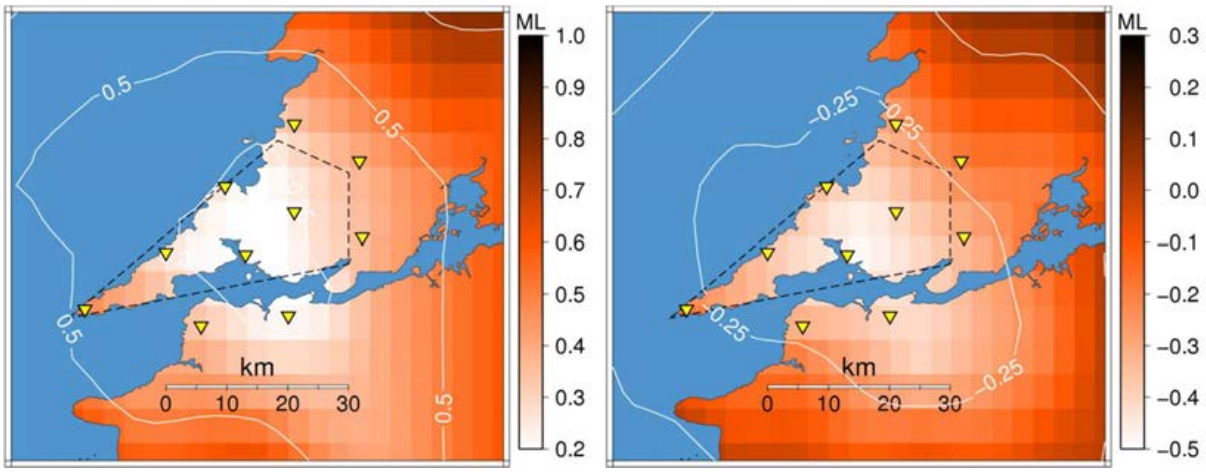

Figure 7.22. Example network detection capability plots (for the CB assuming earthquake recordings with SNR > 3 on at least 6 stations, station noise levels between (a) 1 and 2 nm and between (b) 0.2 and 0.5 nm. The dashed black line shows the approximate outline of the CB).

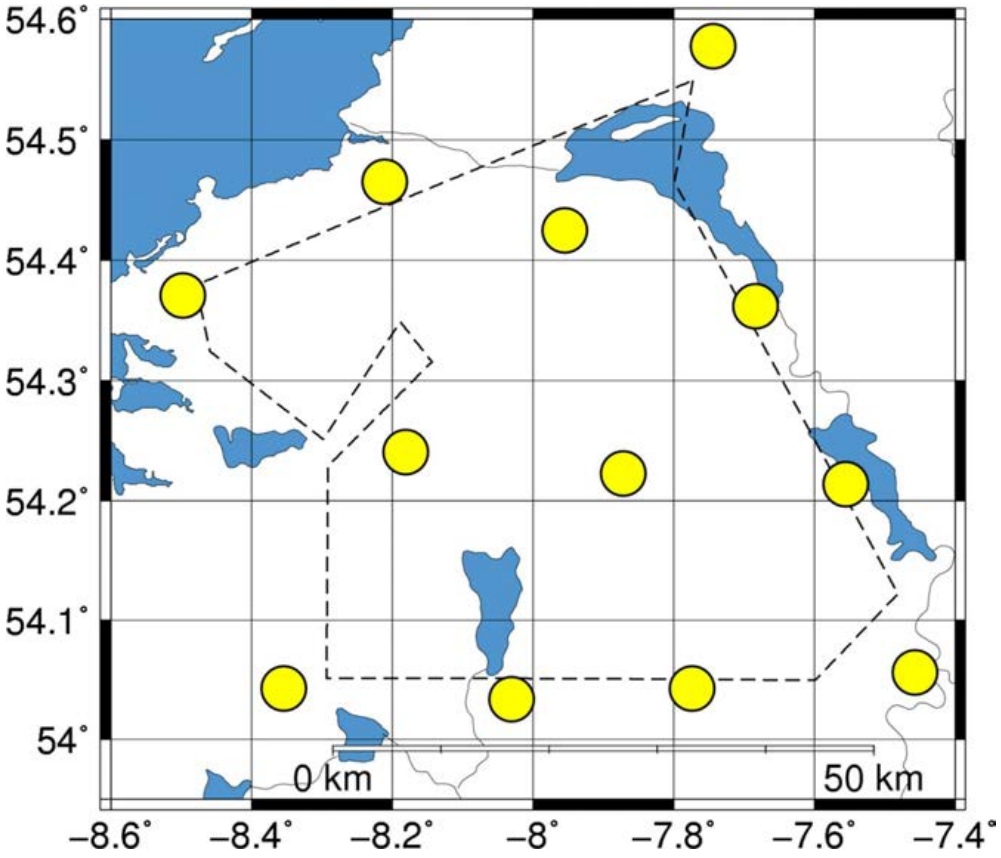

Figure 7.23. Example deployment target zones for the NCB.

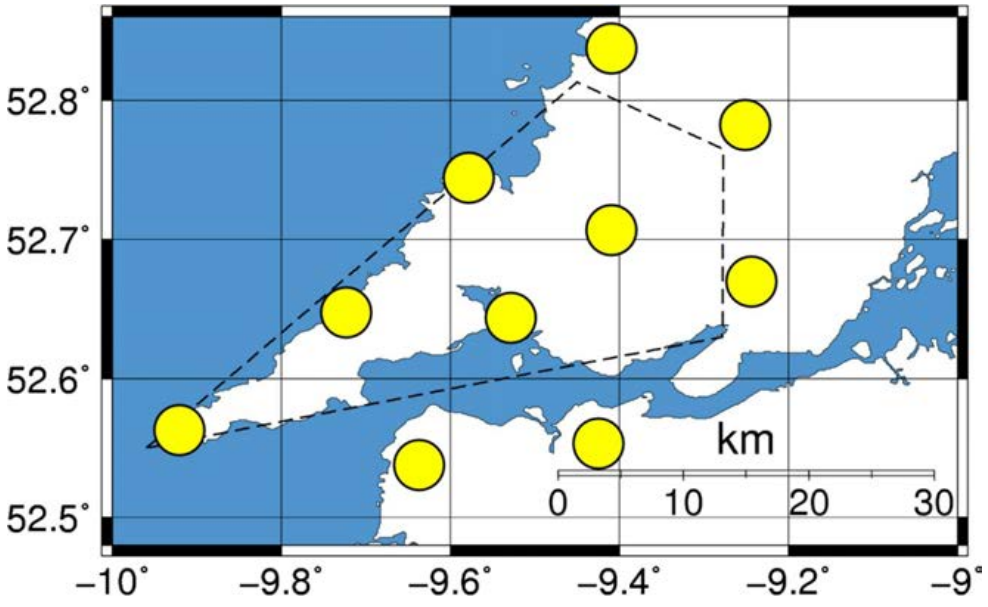

Figure 7.24. Example deployment target zones for the CB.

Table 7.2. Centre coordinates for the example installation target zones

NCB	Latitude	Longitude		CB	Latitude	Longitude
station no.	degrees [N]	degrees [E]		station no.	degrees [N]	degrees [E]
01	54.043	-8.354		01	52.563	-9.921
02	54.034	-8.030		02	52.538	-9.637
03	54.043	-7.774		03	52.648	-9.723
04	54.056	-7.457		04	52.553	-9.425
05	54.240	-8.181		05	52.670	-9.244
06	54.222	-7.872		06	52.745	-9.578
07	54.213	-7.555		07	52.782	-9.251
08	54.371	-8.497		08	52.837	-9.410
09	54.465	-8.211		09	52.644	-9.529
10	54.425	-7.955		10	52.707	-9.410
11	54.362	-7.683				
12	54.577	-7.744				

7.10 Instrumentation Specifications

It is important to identify the seismic frequency range of interest when considering instrumentation specifications. The frequency content of an earthquake signal is band-limited and depends in addition to path (in particular distance) and site effects on the source dimensions and hence the event magnitude. The typical spectral range of interest in micro-earthquake studies is usually from 1 Hz to several tens of Hz, where micro-earthquakes are considered to have magnitudes ML < 3 (Aki and Richards, 2002) or ML < 2 (Havskov and Ottemöller, 2010). In order to obtain good quality data, the seismic system should be able to provide an undistorted recording of ground motion in the main frequency range of local earthquakes. In other words, the range of frequencies created by the earthquake at the recording location should lie within the corner frequencies of the sensors frequency response function. Thus, for the recording of micro-earthquakes, the system should at least have a flat response in the frequency range from 1 Hz to several tens of Hz. However, the baseline network should also provide for the undistorted recording of earthquakes with magnitudes up to ML ≈ 4 ([4]) and this requires a low frequency corner that is smaller than 1 Hz. Viegas *et al*. (2012) have shown that for earthquakes larger than Mw = 3 the long-period spectral plateau can fall completely outside the recording bandwidth of a sensor with a low frequency corner of 0.7Hz, causing an underestimation of the real magnitude.

The two main types of seismic sensors that have a flat response in the frequency range from 1 Hz to several tens of Hz are short period (SP) seismometers and broadband (BB) seismometers. The upper frequency limits for SP and BB seismometers are usually 100 Hz and 50 or 100 Hz respectively. The low frequency corner of SP seismometers is typically 1 Hz or higher while for BB seismometers it is typically between 0.01 and 0.03 Hz.

Besides the ability to record larger magnitude events undistorted, using BB instruments for the proposed baseline study would bring several additional advantages. Several techniques require the measurement of long-period spectral amplitudes, for example moment magnitude (Mw) estimates which provide a more accurate magnitude measure for small earthquakes than using ML (Deichmann, 2006). Another advantage is that BB instruments have not only larger bandwidth than SP instruments, but also larger dynamic range, higher resolution, lower self-noise, lower noise induced by variations in air pressure or temperature and analytically better known transfer functions. This results in more complete seismic information bringing important advantages over SP instrumentation, for example improvement of event characterisation and the capability to employ modern seismological analysis techniques (Havskov and Alguacil, 2006; Trnkoczy *et al*., 2009b) as well

4 The largest instrumentally recorded earthquake with epicentre in Ireland's territory had a magnitude ML = 4, see Table 7.1.

as higher accuracy and stability when carrying out instrument simulations (Bormann *et al*., 2009). These simulations involve the mapping of a given seismogram into the seismogram of another type of seismometer and build an important step in the determination of local magnitude ML and also body- and surface-wave magnitudes.

While historically many seismic stations were equipped with only one-component SP sensors, most modern installations use 3-component BB sensors which cost in the same order as a 3-component SP installation, hence 3-component BB sensors are recommended for the baseline network. The technical specifications of the seismic sensors and recorders should allow for the generation of high quality earthquake catalogues for the two study areas that include locations and accurate magnitude estimations in the range –0.5 <= ML <= 4. While equipment with a very high dynamic range is recommended for production monitoring installations close to UGEE operations, standard good quality broadband sensors with a dynamic range of at least 140 dB at 1Hz are considered adequate for the baseline study. The instruments should feature automatic or remote mass centring functionality and the associated data acquisition system should feature 24-bit digitizers, a sampling rate of at least 100 Hz, GPS time stamping, a storage capacity of at least 16 GB and support for standard seismological community data formats. While real-time data transmission is not necessarily required for the baseline monitoring period, the recorders should be transmission capable in case this might be needed later. The instrument self-noise should be below the Peterson NLNM for signal frequencies between 0.017 and 10 Hz. Specifying more detailed instrument specifications than given here would limit the choice unnecessarily, especially considering that only a small number of manufactures worldwide are able to provide such systems.

7.11 Installation Specifications

The seismometers should be installed directly on bedrock to minimise the effect of seismic noise. Sites in stiff overburden should be chosen if bedrock sites cannot be realised. Installation methods should follow international best practice to ensure good data quality. This includes a pit with solid concrete base, water proofing, thermal insulation and low sensitivity to wind, see Trnkoczy *et al*. (2009a) and Havskov and Alguacil (2006) for details. RMS noise amplitudes of the seismic data simulated to the response of a W-A seismometer should not exceed 2 nm, even during stormy weather conditions. This corresponds to an acceleration PSD value of about –131 dB (relative to 1 $(m/s^2)^2$/Hz) at 2Hz. For frequencies ≥ 2Hz the 90 percentile of the acceleration PSD power density function should be at least 18 dB lower than the Peterson New High Noise Model (Peterson, 1993).

7.12 Data Analysis and Management

It is recommended that data from the proposed baseline network should be integrated with the National Data Centre (NDC) operated as part of the Irish National Seismic Network (INSN). The UCD Waveobs project is of temporary nature and ends in 2016; therefore, Waveobs data will not be available long term. For logistical reasons the baseline network should be site selected, permissioned, deployed and operated by a commercial entity. The network operation includes data management and should provide for adequate documentation of network operation parameters (station calibrations, station downtimes, technical problems, details of maintenance and service work etc.) and archiving of continuous seismic data, response files and other relevant metadata in standard seismological community formats. The data analysis should follow international best practice in routine seismological observatory operation. The resulting earthquake catalogue together with the seismic raw data should be made publicly available via the NDC to ensure transparency. The main steps to determine the location and magnitude of local earthquakes are:

- Signal filtering, restitution and simulation;
- Signal detection (trigger algorithm to discriminate between seismic events and seismic noise);

- Automatic and manually reviewed phase picking and identification;
- Manual determination of onset times, polarities, maximum ground displacement and related period;
- Automatic and manual determination of source parameters (hypocentre location, origin time, magnitude determination and source mechanism); and
- Manual discrimination between natural earthquakes and man-made seismic events (e.g. quarry blasts).

More advanced data processing could include relative location methods, improvement of the seismic velocity model for the region over time and moment magnitude (Mw) estimations. However, defining more detailed data processing and data management specifications or specific software would limit the choice in a future tender unnecessarily. Instead, here we provide the broad principles of what is required; the details of how they are achieved should form part of a future tender.

8 Task 8: Examination of Global Experience of Seismic Events Stimulated by UGEE Operations

8.1 Introduction

It is relatively well-known that anthropogenic activity can result in man-made or "induced" earthquakes. Although such events are generally small in comparison to natural earthquakes, they are often perceptible at the surface and some have been quite large. Underground mining, deep artificial water reservoirs, oil and gas extraction, geothermal power generation and waste disposal have all resulted in cases of induced seismicity. Davies *et al*. (2013) presented a review of published examples of earthquakes induced by a variety of activities. There are numerous examples of induced earthquakes in hydrocarbon fields related to oil and gas production (e.g. Suckale, 2010). These are often a response to long-term production, where the extraction related subsidence is compensated by, for example, normal faulting on existing faults near or inside the reservoir (Van Eijs *et al*., 2006). For example, in 2001 a magnitude 4.1 Mw earthquake occurred in the Ekofisk field in the central North Sea (Ottemöller *et al*., 2005). The earthquake was thought to be related to the injection of around $1.9x10^6$ m^3 of water.

Induced earthquakes with magnitudes as large as 3.5–4.0 ML are well documented in Enhanced Geothermal Systems (EGS) (e.g. Majer *et al*., 2007), in which injected fluids are heated by circulation through a hot fractured region of crystalline rocks and then brought back to the surface for power generation. A series of magnitude 3+ earthquakes induced during an EGS project in Basel, Switzerland resulted in the suspension of the project, which was ultimately abandoned almost 3 years later following further study and risk evaluation after these seismic events (Giardini, 2009).

Earthquakes can also be induced by the injection of brines from oil and gas production into wells that are drilled to dispose of large volumes of waste water over many years (e.g. Frohlich *et al*., 2011). Induced seismicity caused by long term disposal of large volumes of waste fluid in deep boreholes is suspected to be partially responsible for a significant increase in seismicity rate that has been observed in Eastern North America (Ellsworth, 2013). In addition, several of the largest earthquakes in the US midcontinent in 2011 and 2012 may have been triggered by nearby disposal wells (e.g. Horton, 2012; Kim, 2013), suggesting that wastewater disposal by injection to deep wells poses a significant seismic risk. The largest of these was a magnitude 5.7 event in central Oklahoma that destroyed 14 homes and injured two people (Kerenan *et al*., 2013).

The process of hydraulic fracturing in order to increase the permeability of reservoir formations and stimulate the recovery of hydrocarbons is also generally accompanied by microseismicity, commonly defined as earthquakes with magnitudes of less than 2.0 that are too small to be felt. Mapping the microseismicity during hydraulic fracturing operations is widely acknowledged as the best means of characterising stimulated fracture networks in unconventional reservoirs (Maxwell, 2010). Induced seismicity during hydraulic fracture operations has been discussed by a number of authors in the last few years, including Shemeta *et al*. (2012), Warpinski *et al.* (2012) and Ellsworth (2013). Extensive experience in the US, where over 100,000+ stimulations have been carried out suggest that the magnitudes of the induced earthquakes in reservoirs such as the Barnett Shale (Maxwell *et al*., 2006) and the Cotton Valley (Holland, 2011) are typically less than 1 Mw, and that felt seismicity is almost unheard of. However, it should be pointed out that most sites of UGEE operations lack independent instrumentation for monitoring induced seismicity and that earthquakes with magnitudes of 2.5 or less will fall below the detection thresholds of regional seismic monitoring networks. There have also been three documented examples of rather larger induced earthquakes during hydraulic fracturing operations. In the Etsho and Tattoo fields in Horn River, Canada, 216 earthquakes were detected during in 2009–2011 (BC Oil and Gas Commission, 2012). Twenty-one of these earthquakes had magnitudes of 3.0 or greater, and the

largest event had a magnitude of 3.8 ML, which is, to date, the largest known earthquake induced by hydraulic fracture operations in a hydrocarbon field anywhere in the world. In the Eola Field, Garvin County, Oklahoma, 86 earthquakes were detected during hydraulic fracturing in 2011 with magnitudes up to 2.9 ML (Holland, 2013).

In Lancashire, UK, 58 earthquakes were linked to fluid injection during hydraulic fracturing at the Preese Hall well in 2011 (de Pater and Baisch, 2011). The largest had a magnitude of 2.3 ML and was felt locally. These hydraulic fracture treatments were carried out during exploration of a shale gas reservoir in the Bowland basin, Lancashire. As a result of the earthquakes, operations were suspended at Preese Hall, and the operator, Cuadrilla Resources Ltd, commissioned a number of studies (Baisch and Voros, 2011; de Pater and Pellicer, 2011; Eisner *et al*., 2011; GMI, 2011; Harper, 2011) into the relationship between the earthquakes and their operations. An overall summary or synthesis of the findings was also published (de Pater and Baisch 2011).

Despite these examples of earthquakes induced by hydraulic fracturing, the process appears to pose a low risk of inducing destructive earthquakes. A report by the National Research Council in the US (NAS, 2012), which examined the scale, scope and consequences of seismicity induced during fluid injection and withdrawal related to energy technologies, concluded that the process of hydraulic fracturing a well as presently implemented for shale gas recovery does not pose a high risk for inducing felt seismic events. A Royal Society and Royal Academy of Engineering report (2012) also examined the risks associated with hydraulic fracturing during shale gas exploration and production, concluding that the surface impacts of any seismicity induced by hydraulic fracturing would be negligible. A report commissioned by the Department of Energy and Climate Change in the UK (Green *et al*., 2012) set out a number of recommendations for the mitigation of seismic risk in future hydraulic fracture operations for shale gas, and these recommendations were adopted as part of the regulatory framework for future operations.

This task comprised: an extensive review of induced seismicity in UGEE operations; an assessment of examples of recent seismicity related to waste water disposal in the eastern United States; examination of available UGEE data from recent examples, such as the induced seismicity in Blackpool, UK, as well as data from other analogues to investigate the controlling factors on induced seismicity during fluid injection and the relationships between injection volume and pressure and induced seismicity; and finally, assessment of measures suggested for mitigating the risk of induced earthquakes, specifically for UGEE operations and for energy technologies in general.

8.2 Mechanisms for Seismicity Induced by Fluid Injection

The aim of hydraulic fracturing is to improve fluid flow in an otherwise impermeable volume of rock. This is achieved by injecting fluid at a sufficient pressure to cause tensile failure (cracking of the rock) and develop a network of connected fractures to increase permeability and provide conduits for gas flow. The method is not new and has in fact been in use since the 1940s (Montgomery and Smith, 2010). The injection of fluids under high pressure generates new cracks and fractures in a previously intact rock mass. As these new fractures grow and spread through the previously intact rockmass they are accompanied by brittle failure of the rock and corresponding microseismicity, usually defined as earthquakes with magnitudes of less than 2.0 that are too small to be felt. This can involve both shear and tensile failure (crack opening), which occurs when fluid pressure exceeds the minimum compressive stress, σ_3, allowing a fracture to open in the plane normal to direction of σ_3. In this report, these are referred to as “fracked” events. Mapping the hydraulic-fracture induced microseismicity is widely acknowledged as the best means to image fracture networks and estimate the orientation and size of a stimulated volume (Maxwell, 2010). The size of these “fracked” events is constrained by the energy of the injection process, and, as a result, the observed magnitudes for these are generally less than 1 Mw.

However, both presence of high pressure fluid and the stress perturbation in the rockmass caused in by the fluid can change the effective stress on pre-existing faults, causing them to fail. In this report, these events are referred to as “triggered” events. Since small stress perturbations can cause relatively large earthquakes the size of these events depends largely on the amount of stored up elastic strain energy already in the rocks. Slip on a pre-existing fault is triggered when the stress acting along the fault exceeds the frictional resistance to sliding. The critical conditions are quantified by the Coulomb criterion, which embodies two fundamental concepts, friction and effective stress. This can be illustrated by considering the shearing of a split block, (Figure 8.1).

The block is subjected to a normal force, F_n, and a shear force, F_s, which can be translated into a normal stress, σ, and the shear stress, τ, acting across and along the fault at *A*. Both the normal stress, σ, and the shear stress, τ, are a result of the pre-existing state of stress on the fault. Slip is triggered when the shear stress T is equal to the frictional strength $\mu(\sigma - p)$, where $(\sigma - p)$ is the effective stress and μ is the coefficient of friction. The presence of fluid at pressure, *p*, on the fault surface will reduce the effective stress on the fault. This means that the injection of fluids into the Earth can increase fluid pressures on existing fault zones, reducing effective stress and move faults closer to failure. In addition, fluid injection also causes deformation of the solid rock mass which can directly perturb the stress field for many hundreds of metres from the point of injection. This stress change may also move faults closer to failure and lead to induced seismicity. Conversely, it can also move the fault further from failure. The pre-existing state of stress on most faults is unknown, though if a fault is close to failure it may only require a small stress perturbation to cause it to fail. These faults would fail at some point in future as more stress accumulates, but the reduction in the effective stress caused by an increase in pore fluid pressure or a change in the shear stress moves that failure forward.

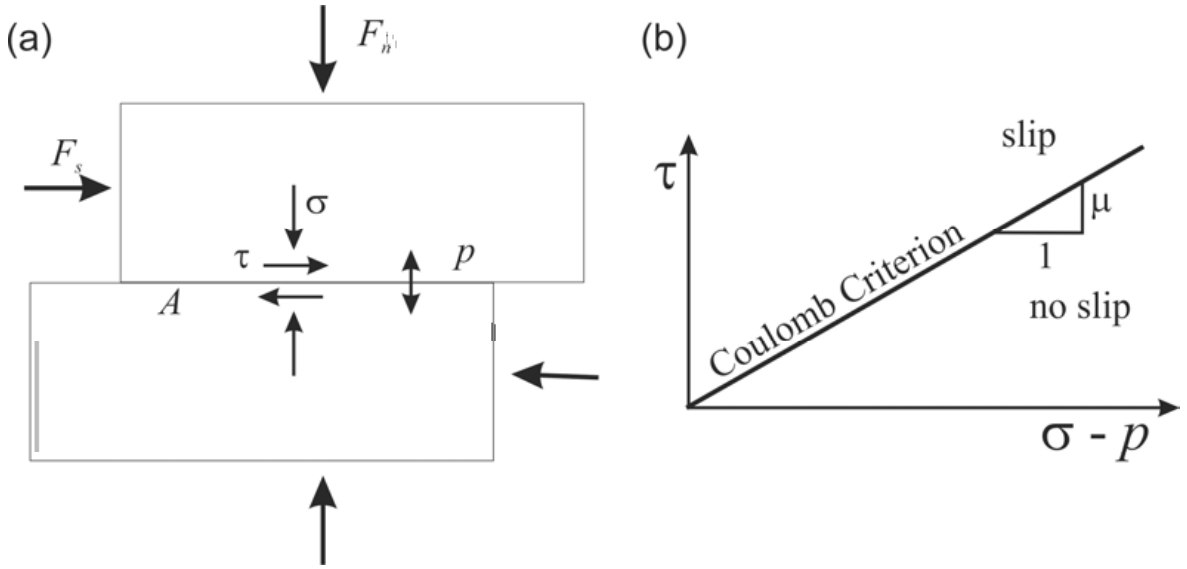

Figure 8.1. Shearing of a jointed block (subjected to normal force, F_n and shear force F_s, with fluid inside the joint at pressure p. Slip along the joint is triggered when the shear stress T is equal to the frictional strength $\mu(\sigma-p)$, where $(\sigma-p)$ is the effective stress and μ is the coefficient of friction).

8.3 Examples of Seismicity Induced by Hydraulic Fracturing in UGEE Operations

Over the past few decades, observations during over 100,000 hydraulic fracture treatments in the U. S. A. suggest that the magnitudes of the seismic events induced by these fracture treatments are generally very small (Warpinski *et al*., 2012). Magnitudes of the induced microseismicity recorded during monitored hydraulic

fracture stages in the Barnett Shale, Texas, typically lie in the range –3.0 to 1.0 Mw, making them unlikely to be felt, or even recorded unless a specific monitoring network is in place. Again, it should be noted that most sites of UGEE operations lack independent instrumentation for monitoring induced seismicity and that earthquakes with magnitudes of 2.5 or less will fall below the detection thresholds of regional seismic monitoring networks. Magnitudes of microseismicity recorded during monitored stages in the Marcellus shale, Pennsylvania, lie in the range –3.0 to –0.5 Mw, although fewer fracture stages have been monitored the maximum observed magnitude is less than –0.5 Mw. These can all be considered as "fracked" events. As a result, hydraulic fracturing for shale gas development was not thought to pose a high risk for inducing felt seismic events.

However, there have also been three instances of earthquakes with magnitudes greater than 2 induced during hydraulic fracturing operations for UGEE: Blackpool, UK (Clarke *et al.*, 2014); Garvin County, South-Central Oklahoma (Holland, 2013): and, Horn River, Canada (BC Oil and Gas Commission, 2012). These remain the only documented examples of earthquakes of these magnitudes that were induced by UGEE operations.

8.3.1 Earthquakes induced by hydraulic fracturing operations near Blackpool, UK

In Lancashire, UK, 58 earthquakes were linked to fluid injection during hydraulic fracturing at the Preese Hall well in 2011 (de Pater and Baisch, 2011). The largest, on 1 April 2011, had a magnitude of 2.3 and was felt locally. These hydraulic fracture treatments were carried out during exploration of a shale gas reservoir in the Bowland basin, Lancashire. A further magnitude 1.5 ML earthquake was felt on 27 May, 2011 and also linked to hydraulic fracture treatments, leading to the suspension of operations at Preese Hall.

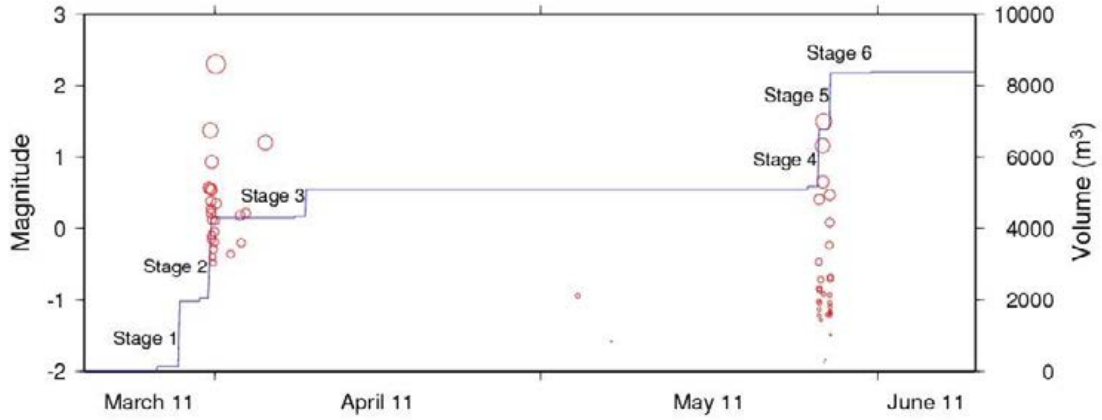

Figure 8.2. Volume of injected fluid and earthquakes at Preese Hall, Blackpool (Volume of injected fluid (blue line) and earthquakes (red circles, scaled by magnitude) during hydraulic fracturing operations at Preese Hall, Blackpool, between March and June 2011 (from de Pater and Baisch, 2011). There are five distinct treatment stages. Earthquake activity closely correlates with stages 2 and 4. The largest event with 2.3 ML at 02:34 on 1/4/2011 occurred shortly after stage 2.).

The unusual seismicity led to a number of detailed studies of the relationship between the earthquakes and hydraulic fracturing operations (for example, de Pater and Baisch 2011; Eisner *et al.*, 2011). In total, 58 earthquakes were detected in the time period between 31 March and 30 August 2011, nearly all of these occurred either during or within a few hours of fracturing operations at Preese Hall. De Pater and Baisch (2011) concluded that the earthquake activity was caused by fluid injection directly into a nearby fault zone, which reduced the effective normal stress on the fault and caused it to fail repeatedly in a series of small earthquakes.

A possible causative fault was later identified following a detailed 3-D seismic reflection study (Clarke *et al.*, 2014).

Figure 8.2 shows the injected volume of fluid as a function of time in each of the hydraulic fracture stages carried out at Preese Hall along with the recorded earthquake activity (from de Pater and Baisch, 2011). It is clear that the earthquakes correlate strongly with stages 2, 4 and 5, in which the largest amount of fluid was injected. In two of the hydraulic fracture treatments, stages 2 and 4, the largest earthquakes occurred approximately ten hours after the start of injection, while the well was shut-in under high pressure. These events were preceded by smaller events, which started immediately after injection, the largest of which was a magnitude 1.4 ML event on 31 March.

No seismicity was observed during stages 1 and 3, and only very weak seismicity occurred during stage 5. The lack of seismicity in stage 3 can be attributed to the smaller pumped volume and aggressive flowback. The pumped volume in stage 5 was similar to stages 2 and 4, but there was also flowback, which could explain the lack of larger events. The results show that injected volume and flowback timing are an important controlling factor in the level of seismicity, as evidenced from the lack of seismicity during and after stage 3, suggesting that seismicity can be mitigated by modifying job procedure.

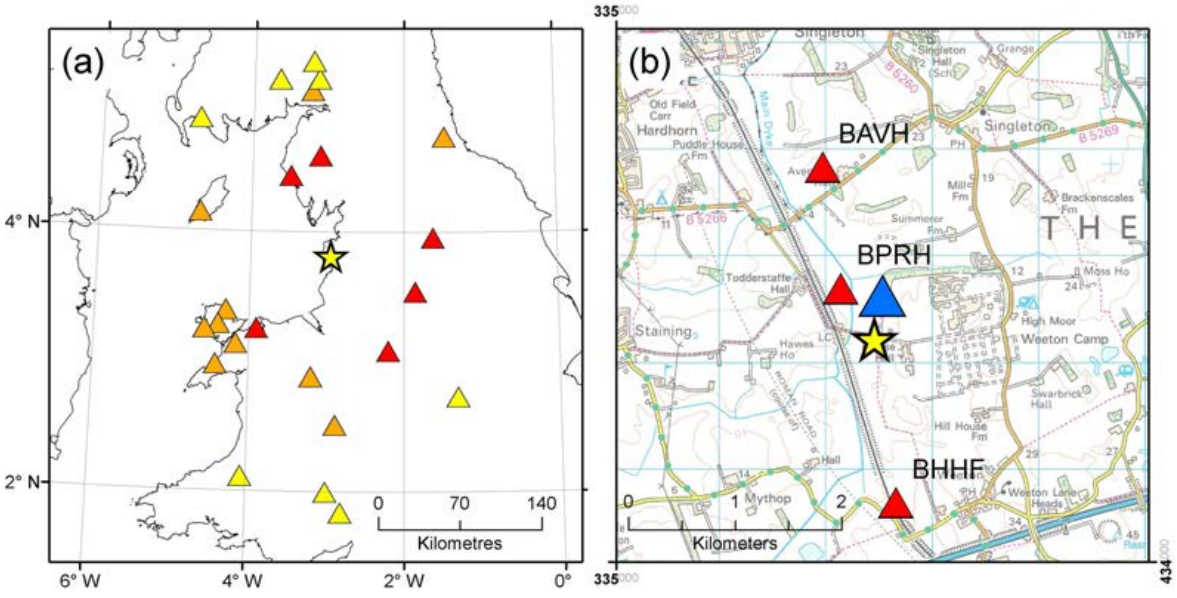

Figure 8.3. Locations of Preese Hall events (The yellow star shows the epicentre for the Blackpool earthquakes in April and May, 2011, as determined by Eisner *et al.* (2011). The coloured triangles in (a) show permanent monitoring stations operated by the British Geological Survey at epicentral distances of 75 to 99 km (red), 100 to 149 km (orange) and greater than or equal to 150 km (yellow). The red triangles in (b) show temporary stations deployed after the initial earthquakes on 1 April 2011. The blue triangle shows the location of the Preese Hall well).

Locations for the Blackpool earthquakes were determined by Eisner *et al.* (2011) and Clarke *et al*. (2014) among others. Similarity between the recorded events suggested that all the events were from the same location and had the same mechanism. The location is shown in Figure 8.3. It is clear that the location is less than 0.5 km from the well head. In addition, the depths of 3.6 km and 2.9 km, estimated by Eisner *et al.* (2011) and Clarke *et al*. (2014) are close to the point of injection (2.3 – 2.7 km) for all 6 stages.

8.3.2 Earthquakes induced by hydraulic fracturing in the Horn River Basin, British Columbia

Over 200 earthquakes were induced during hydraulic fracturing operations in the Etsho and Tattoo fields in the Horn River Basin, British Columbia, during 2009–2011 (BC Oil and Gas Commission, 2012). The Horn River Basin lies in northeast British Columbia, between Fort Nelson and the Northwest Territories border. The Horn River Group shales occur throughout the basin and are a target for hydrocarbon extraction and exploitation.

Thirty-eight earthquakes were detected by the regional seismic monitoring network operated by Natural Resources Canada (NRCan) between 8/4/2009 and 13/12/2011. Twenty-one of the earthquakes had magnitudes of 3.0 or greater, and the largest event had a magnitude of 3.8 ML, to date, the largest known earthquake induced by hydraulic fracture operations in a hydrocarbon field anywhere in the world. This event was also felt by workers in the area. The earthquakes occurred in an area where no previous seismicity had been recorded and a report by the BC Oil and Gas Commission (2012) concluded that the earthquakes were caused by fluid injection during hydraulic fracturing in proximity to pre-existing faults.

Hydraulic fracturing operations in the Etsho area took place between February 2007 and July 2011. During this period, over 90 wells were drilled from 14 different locations, with more than 1,600 hydraulic fracturing stages completed. Twenty-seven of the earthquakes detected by NRCan occurred within 10 km of the Etsho area. Seven drilling pads were located within the same area, five of where were conducting hydraulic fracturing operations when events occurred. All seven of the earthquakes detected by NRCan in the Tattoo area occurred within 10 km of wells in which there were hydraulic fracturing operations when the seismicity occurred.

A dense array consisting of 20 seismometers was deployed by the operator in the Etsho area to study the seismicity in greater detail than was possible with NRCan data. This array operated from 16 June to 15 August 2011 and detected 216 earthquakes ranging from magnitude –0.8 to 3.0 ML, with 19 events greater than 2.0 ML. These earthquakes were interpreted to be related to fault movement and a report by the operator concluded that magnitudes from 0.5ML to 1.0ML indicate the transition from fracture driven seismicity to seismicity driven by fault movement. The four earthquakes detected by NRCan in the same time period were relocated by the operator using data from the dense array. The results suggested that the earthquakes were located within 200 m of hydraulic fracturing stages.

At both Etsho and Tattoo, all 38 NRCan reported events occurred either during a hydraulic fracturing stage or sometime after one stage ended and another began. No events were recorded before hydraulic fracturing operations began or after the last hydraulic fracturing operations ended.

The average volume of fluid injected into wells for hydraulic fracturing in the Etsho area was approximately 60, 000 m^3, with a maximum of 138,000 m^3 and a minimum of 11,000 m^3, with corresponding flow rates of 0.2 m^3/s, 0.25 m^3/s and 0.13 m^3/s, respectively.

In British Columbia, the only previously documented case of induced seismicity, linked to oil and gas activity, occurred in the Eagle Field area, approximately five km north of Fort St. John. Twenty-nine earthquakes with magnitudes from 2.2 to 4.3 ML were recorded from November 1984 to May 1994. Horner (Horner, 1994) used the Davis and Frohlich criteria (Davis and Frohlich, 1993) to conclude that the events were induced. High pressure fluid injection for secondary oil recovery was identified as a possible cause. High volume hydraulic fracturing was not employed in the area at that time.

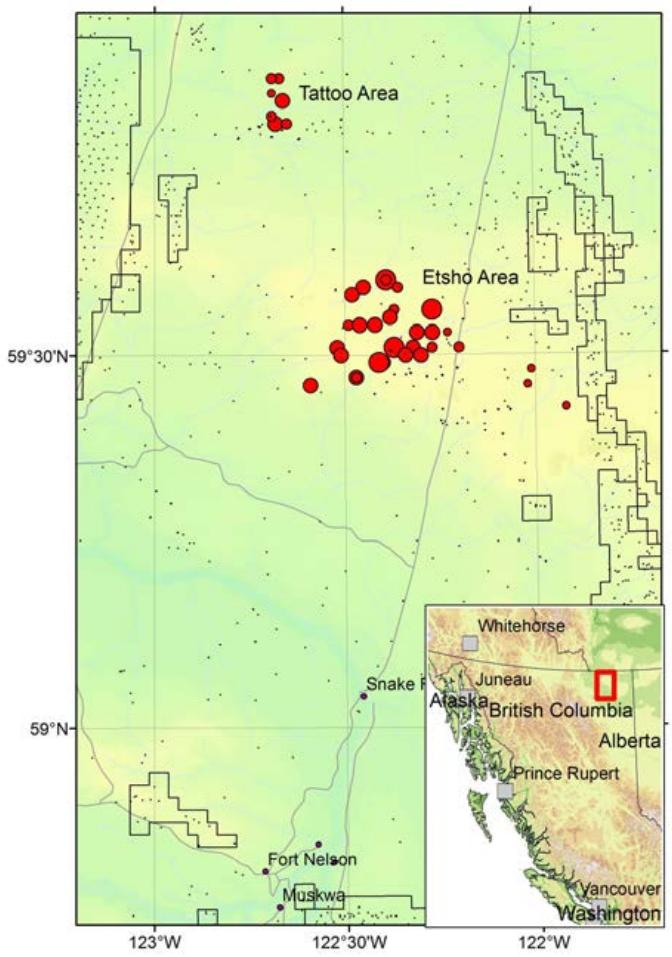

Figure 8.4. Location of the Etsho and Tattoo areas in the Horn River Basin (from BC Oil and Gas Commission, 2012). Red circles show the NRCan reported epicentres (scaled by magnitude). Small black dots show well positions.

8.3.3 Earthquakes in the Eola Field, Oklahoma

In January 2011, a sequence of earthquakes occurred in close proximity to a well, which was being hydraulically fractured in the Eola-Robberson oil field, south-central Oklahoma (Holland, 2013). A total of 116 earthquakes were detected by Holland (2013) between 17/01/2011 at 19:06 and 23/01/2011 at 3:13 GMT. Hydraulic fracturing operations in the Picket Unit B Well 4–18 took place between 16/01/2011 at 18:43 and 22/01/2014 at 16:54 GMT. Earthquake magnitudes varied from 0.6 to 2.9 ML, with 16 earthquakes having magnitudes of 2.0 ML or greater. The locations calculated by Holland (2013) suggest that the earthquakes occurred at shallow depths from 2 to 3 km and within ~2.5 km of the well. The alignment of the hypocentres suggests that the earthquakes occurred on a fault striking N166°E, subparallel to the mapped faults in the area. The first earthquake occurred ~24 hours after hydraulic fracturing began at the well. This delay is consistent with the diffusion of pore pressure in the subsurface over a distance of ~2 km. The strong spatial and temporal correlation between hydraulic fracturing and earthquakes suggests that the earthquakes were induced. This correlation is strengthened because hydraulic fracturing operations ceased for ~2 days due to bad weather, and earthquakes can be observed to cease during this period and resume after hydraulic fracturing had

resumed. In addition, no other similar earthquakes were identified at other times before to or after hydraulic fracturing.

8.4 Induced Seismicity and Waste Water Disposal

By contrast with hydraulic fracturing itself, the subsequent disposal of the waste water from hydraulic fracturing operations can lead to significantly larger earthquakes because of the larger volumes of fluid that are injected into sedimentary strata over long periods of time during this process. There are numerous examples of earthquakes induced by disposal of waste fluids from the hydrocarbon industry in deep injection wells (e.g. Frohlich *et al*., 2011). Ellsworth (2013) shows that that numbers of earthquakes in central and eastern US have increased dramatically in the last few years. This is demonstrated in Figure 8.5, which shows that more than 300 earthquakes with M ≥ 3 occurred in the 3 years from 2010 to 2012, whereas the average number/year from 1967 to 2000 is 21. In addition, several of the largest earthquakes in the US midcontinent in 2011 and 2012 may have been triggered by nearby disposal wells, and of the seven earthquakes of magnitude 4.0 or greater that occurred east of the Rocky Mountains, six are thought to have been induced. The magnitude 4.0 Mw earthquake on 31 December 2011 in Youngstown, Ohio, appears to have been induced by injection of wastewater in a deep well (Kim, 2013). The magnitude 4.7 earthquake in central Arkansas in 2011 has also been linked to deep injection of wastewater wells (Horton, 2012). The magnitude 4.4 Mw earthquake on 11 September 2011, near Snyder, Texas, occurred in an oil field where injection for secondary recovery has been inducing earthquakes for years (Davis and Pennington, 1989). The largest of these was a magnitude 5.7 earthquake in Prague, central Oklahoma that was located close to active wastewater-injection wells, which destroyed 14 homes and injured two people (Kerenan *et al*., 2013).

These results have added to a significant body of evidence suggesting that wastewater disposal by injection to deep wells poses a significant seismic risk. The report by the National Research Council in the USA (NAS, 2012), which examined the scale, scope and consequences of seismicity induced during fluid injection and withdrawal related to energy technologies, concluded that Injection for disposal of wastewater derived from energy technologies into the subsurface does pose some risk for induced seismicity, but very few events have been documented over the past several decades relative to the large number of disposal wells in operation.

The recent increases in earthquake rates and significant earthquakes in many areas of the Central and Eastern United States that have been linked to wastewater injection in deep disposal provide a considerable body of evidence that this activity has a non-negligible contribution to the seismic hazard. Seismic hazard forecasts for the Central and Eastern United States now include contributions from both induced and natural earthquakes and show increases in earthquake hazard by a factor of 3 or more in some areas of induced earthquake activity. If wastewater disposal on this scale were to proceed in Ireland then increases in seismic activity may also be observed, however, background earthquake activity in Ireland is lower than in Central and Eastern United States, so the probability of earthquakes with similar magnitudes should be less and will depend on the state of stress on existing faults. It should also be noted that although many wastewater injection wells can be associated with earthquakes, the majority are not. Additionally, the nature of the wastewater injected into deep wells varies; while some comes from hydraulic fracturing used in unconventional oil and gas production, many wastewater injection wells are used to dispose of produced water from conventional hydrocarbon production.

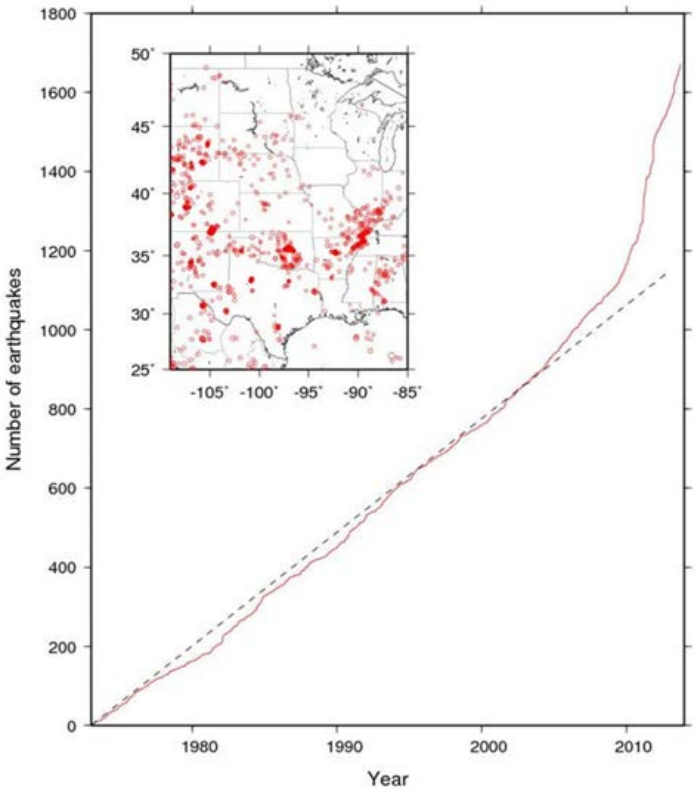

Figure 8.5. Cumulative count of earthquakes with M ≥ 3 in the central and eastern United States, 1967–2012 (from Ellsworth, 2013). Reproduced with permission from the American Association for the Advancement of Science.

8.5 Controlling factors

In general, the seismicity induced by hydraulic fracturing depends on a number of factors. The first of these is the strength of rocks in the geological formations of interest. Most potential shale gas reservoirs occur at shallow depths in relatively weak rocks, whereas the larger tectonic events tend to nucleate at much greater depths where the Earth's crust is significantly stronger.

A second factor is the size and state of stress of any faults in the area likely to be affected by fluid injection. Earthquake magnitude scales with fault area, for example, an earthquake with a magnitude of 2 might typically occur on a fault that is 100m long, whereas magnitude 5 earthquakes require fault dimensions of several kilometres. The pre-existing state of stress on a fault determines how close it is to failure. Faults that are critically stressed may require only a small stress perturbation to cause them to fail. A critical state of stress is widely expected at depth and observed throughout the Earth's crust (Townend and Zoback, 2000). Evidence for this comes from three sources: seismicity induced by reservoir impoundment (e.g. Gupta, 1985) or fluid injection (Frohlich *et al*., 2011; Ellsworth, 2013); earthquakes triggered by stress changes caused by other earthquakes (e.g. Stein *et al*., 1997); and, *in situ* stress measurements in deep wells and boreholes (e.g. Brudy *et al*., 1997).

A third factor is the pressure change induced by the hydraulic fracture process (Zoback, 2012). In turn, this is affected by the volume of injected fluid and the rate of injection. Larger volumes and higher injection rates

generate higher pressures. For the volumes of fluid used in shale gas exploration and production, the pressurization during hydraulic fracturing affects only limited volumes of rock (typically several hundred metres in extent) and pressurization typically lasts only a few hours. This restricts the spatial extent to the volume affected by a pressure change, to a region close to the point of injection. More distant faults are unlikely to be affected by such operations.

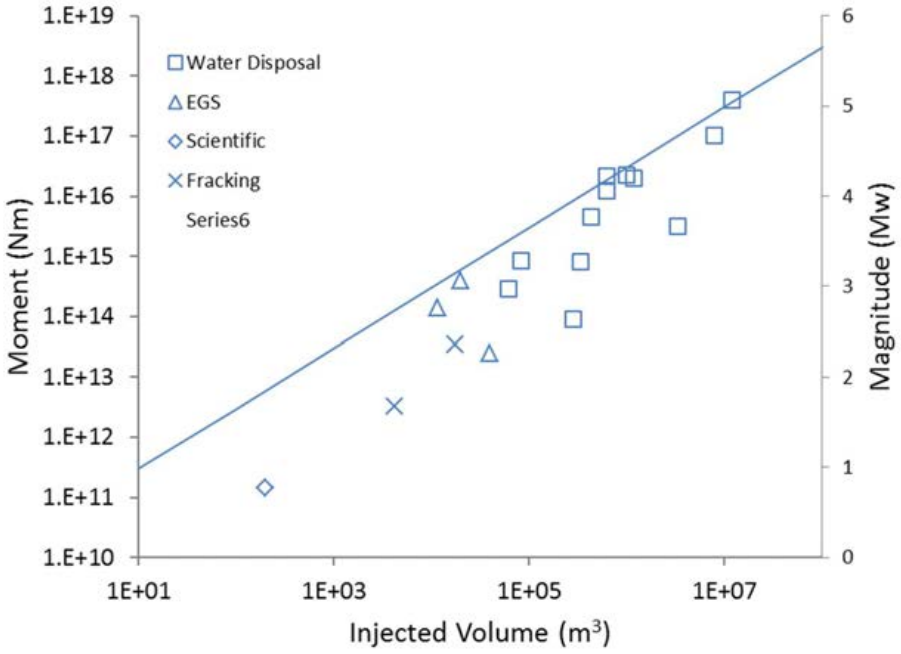

Figure 8.6. Maximum seismic moment and as a function of total volume of injected fluid (from the start of injection until the time of the largest induced earthquake for a number of different examples of induced earthquakes (from McGarr, 2014). The solid line shows a possible upper bound determined from the product of the modulus of rigidity and the total volume of injected fluid).

McGarr (2014) uses a number of examples of earthquakes induced by hydraulic fracturing, disposal of waste water in wells and enhanced geothermal systems to suggest that maximum magnitude is related to the total volume of injected fluid. The results of this analysis are summarised in Figure 8.6, which shows maximum seismic moment and as a function of total volume of injected fluid for different induced earthquakes. Seismic moment (and therefore earthquake magnitude) can be seen to increase with injected volume. It is also clear from Figure 8.6 that the activities that involve the largest injected volumes, i.e. waste water disposal are associated with the largest earthquakes. The solid line in Figure 8.6 shows a possible upper bound determined from the product of the modulus of rigidity, here assumed to be 3 GPa, and the total volume of injected fluid. However, McGarr (2014) notes that in view of the uncertainties, this should not be regarded as an absolute physical limit. Note also that the Horn River basin earthquakes are not included in the data set as it was not possible to determine injection volume responsible for the largest event.

The number of fluid injection induced earthquakes above a given magnitude is also seen to increase approximately proportionally to the injected fluid volume (Shapiro *et al.*, 2003; 2012), consistent with the Gutenberg-Richter law (Gutenberg and Richter, 1954). It is clear from the observations of the induced seismicity at Preese Hall, Blackpool in 2011 (Figure 8.2) that earthquake activity closely correlates with stages 2 and 4. No observed seismicity was associated with those stages in which smaller volumes of fluid were used.

8.6 Mitigation

Extensive experience of induced seismicity in Enhanced Geothermal Systems have led to a series of measures to address induce seismicity that may be considered as “industry best practice”. For example, the US Department of Energy “Protocol for Addressing Induced Seismicity Associated with Enhanced Geothermal Systems” (Majer *et al*., 2012) list seven steps for mitigating seismic risk. These are listed in Table 8.1 and include establishment of seismic monitoring and quantify the hazard from natural and induced seismic events.

Table 8.1. The US Department of Energy Protocol for Addressing Induced Seismicity Associated with Enhanced Geothermal Systems (steps are listed in the order expected to be followed)

Step 1	Perform a preliminary screening evaluation.
Step 2	Implement an outreach and communication programme.
Step 3	Review and select criteria for ground vibration and noise.
Step 4	Establish seismic monitoring.
Step 5	Quantify the hazard from natural and induced seismic events.
Step 6	Characterise the risk of induced seismic events.
Step 7	Develop risk-based mitigation plan.

Experience of induced seismic activity in Enhanced Geothermal Systems (EGS) has led to the development of so-called “traffic light systems” linked to real-time monitoring of seismic activity (e.g. Bommer *et al*., 2006; Majer *et al*., 2012). These are essentially control systems for management of induced seismicity that allow for low levels of seismicity but add requirements when seismic events may result in a concern for public health and safety. Table 8.2 shows the traffic light system used in Basel, Switzerland and adapted from Bommer *et al*. (2006). This has four levels: green, where injection proceeds as planned; yellow/orange, injection proceeds with caution, possibly at a reduced rate; and, red, injection is suspended immediately. However, any such system requires the definition of acceptable limits for the cessation and recommencement of operations. In addition, an effective monitoring system needs to provide reliable automatic locations and magnitudes in near real-time for very small events in the magnitude range –1 to >1 ML. It is also worth noting that in some cases, the cessation of operations may not be sufficient to preclude further seismicity. For example, Basel in 2006 (Giardini, 2009) although operations were stopped when the traffic light threshold was exceeded, this was still followed by a much larger magnitude 3.4 event. Bachmann *et al*. (2011) present an alternative probability based statistical approach that is used to describe and forecast features of the observed induced seismicity at Basel in 2006. This approach has the advantage of not being dependent on a single magnitude threshold but on many small events, which increases robustness. It also integrates injection rates and allows forecasts of the hazard/risk to be made.

Table 8.2. Seismic response procedure used in Basel, Switzerland (and adapted from the traffic light system proposed by Bommer *et al*. (2006). The system is based on three independent parameters: (1) public response; (2) local magnitude (ML); and, peak ground velocity (PGV))

Traffic light	Earthquake activity	Earthquake magnitude	Ground velocity	Action
Green	None	ML < 2.3	< 0.5 mm/s	Regular operation. Continue pumping.
Yellow	Some	ML ≥ 2.3	≤ 2.0 mm/s	Continue pumping but do not increase flow rate
Orange	Many	ML ≤ 2.9	≤ 5.0 mm/s	Maintain well head pressure below stimulation pressure
Red	Widely Felt	ML > 2.9	> 5 mm/s	Stop pumping. Bleed off to minimum wellhead pressure

Given the rather more limited number of examples of earthquakes that have been large enough to be felt that were induced by hydraulic fracturing and that the process appears to pose a low risk of inducing destructive earthquakes (NAS, 2012), there are relatively few published measures for mitigation of seismic risk specifically for this activity. However, both the BC Oil and Gas Commission (2012) and the UK Department of Energy and Climate Change (Green *et al*., 2012) set out a number of recommendations for the mitigation of seismic risk in future hydraulic fracture operations for shale gas. The latter have now been adopted as part of the regulatory framework for future hydraulic fracturing operations in shale gas exploration and production in the UK These recommendations are summarised in Tables 8.3 and 8.4.

Table 8.3. Recommendations investigation of observed seismicity in the Horn River Basin (BC Oil and Gas Commission, 2012)

1	Improve the accuracy of the Canadian National Seismograph Network in northeast B.C.
2	Perform geological and seismic assessments to identify pre-existing faulting.
3	Establish induced seismicity monitoring and reporting. Suspend operations on detection of a 4.0 ML or greater event
4	Install ground motion sensors to quantify risk from ground motion
5	Characterisation of any possible active faults in the region using all available data.
6	Submission of micro-seismic reports to monitor hydraulic fracturing for containment of micro fracturing and to identify existing faults

Table 8.4. Recommendations for future hydraulic fracturing operations in the UK, from Green *et al*. (2012)

1	Hydraulic fracture growth should be monitored during future treatments using microseismic.
2	Future fracture treatments should be modified to reduce the probability of induced earthquakes
3	A suitable traffic light system linked to real-time monitoring of seismic activity
4	Appropriate baseline seismic monitoring to establish background seismicity in the area of interest.
5	Characterisation of any possible active faults in the region using all available geological and geophysical data.
6	Application of suitable ground motion prediction models to assess the potential impact of any induced earthquakes

From both these studies, it is clear that avoiding injection into active fault zones and faults in brittle rock is likely to reduce the possibility of significant induced seismicity. However, identifying such faults may require a more

accurate model of the sub-surface geology than is presently available in some areas. Secondly, seismic monitoring should be used both to establish reliable baselines for background activity and as an essential part of a traffic light system.

The limit for cessation proposed by the BC Oil and Gas Commission (4.0 ML) and Green *et al*. (0.5 ML) differ greatly. The value of 0.5 ML proposed by Green *et al*. (2012) allowed for the observation that post injection seismicity may increase by one order of magnitude. However, this may still be considered a rather conservative threshold that may prove difficult to implement in practice. By contrast, the limit proposed by the BC Oil and Gas Commission seems rather high for areas of higher population density such as Ireland, where such earthquakes are likely to be strongly felt.

Green *et al*. (2012) also suggest that since the number of fluid injection induced earthquakes depends on the injected fluid volume and formation pressure, reducing the volume of fluid and implementing flow back, where appropriate, is also likely to reduce the probability of significant earthquakes.

The National Research Council in the US (NAS, 2012) compiled a list of questions (

Figure 8.7) that can be used to understand and possibly quantify the hazard and risk associated with induced seismicity associated with energy technologies. These primarily relate to the strength of the ground shaking and whether it can be felt and if it might represent nuisance to people or a risk to structures. This suggests that microseismicity, with magnitudes of less than 2, does not pose a risk. Earthquakes that result in weak or moderate shaking, while they are unlikely to result in damage to structures, may represent a nuisance if they occur frequently.

In all the published examples of seismicity associated with hydraulic fracturing in the hydrocarbon industry only the three examples presented above have led to felt seismicity. Of these, it is possible that an earthquake with a similar magnitude to the largest observed in Horn River Basin would be strongly felt at intensities of 4–5 EMS at small epicentral distances, and could cause some alarm to local residents. However, such an earthquake would be unlikely to cause structural damage. There are examples of mining-induced earthquakes with magnitudes of 3.0 ML in the UK that reportedly caused superficial damage (Westbrook *et al*., 1980; Redmayne, 1998), however, there have been no reports of structural damage from mining-induced earthquakes in the UK in the past forty years.

8.7 Discussion

Our knowledge of fault systems in the sub-surface is generally limited to areas where detailed geophysical surveys have been carried out. In intraplate areas such as the British Isles, it is often difficult to associate earthquakes with specific faults given the uncertainties in both the earthquake location estimates and our lack of knowledge of sub-surface faulting. For example, in the case of the Blackpool earthquake activity, the existing legacy geophysical data was unable to identify any faulting close to the Preese Hall well prior to UGEE operations. Clarke *et al*. (2014) subsequently identified a possible causative fault close to the well using data from a detailed 3-D seismic reflection study. It is clear that high resolution monitoring of background seismicity in Ireland is required prior to commencement of any UGEE operations, so that the low seismic activity rates suggested by existing instrumental monitoring data and historical data can be confirmed, and also so that unusual seismicity can be identified.

In addition, the pre-existing state of stress and pore pressure acting on a fault are also usually unknown. So although effective-stress models provide a basis for modelling induced earthquakes, the initial conditions to constrain this model are generally lacking. We also often lack knowledge about the hydrological properties of

the sub-surface. This limits the use of geomechanical modelling methods. Measuring the initial stress state and pore pressure, tracking the injection history, and careful seismic monitoring may help improve understanding.

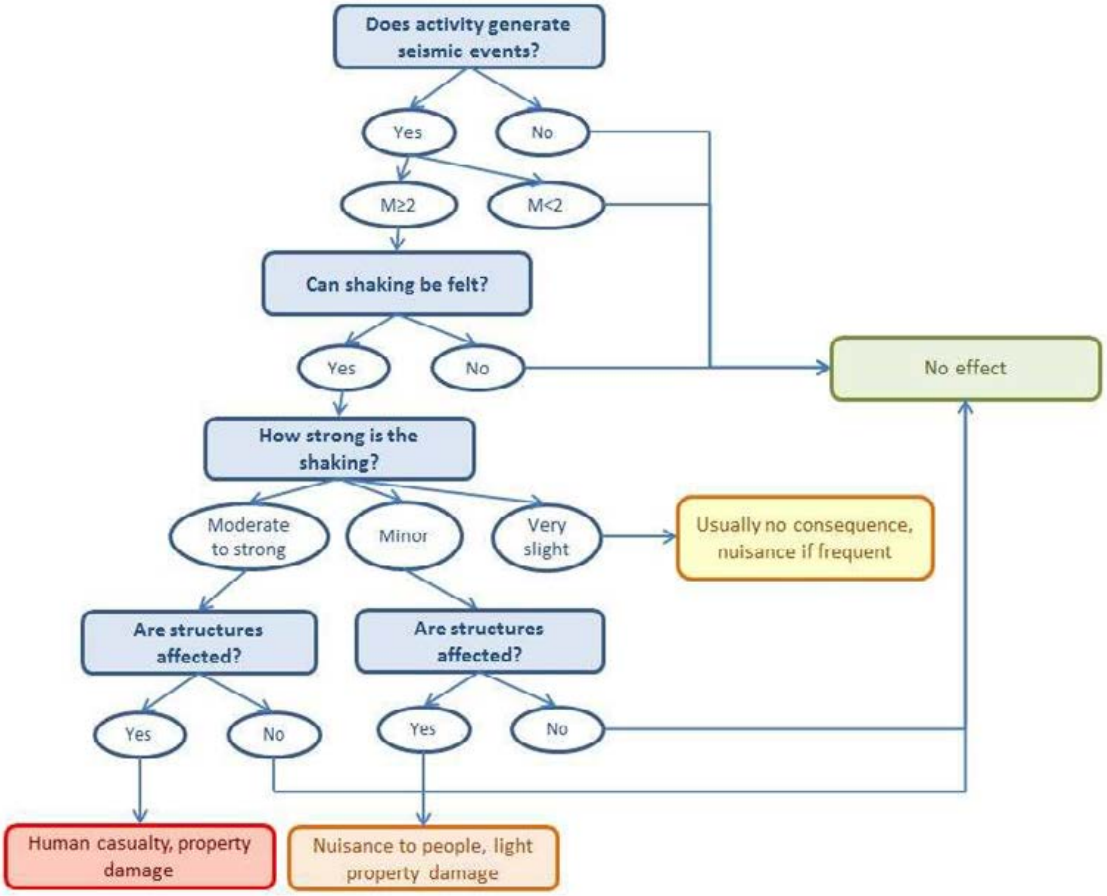

Figure 8.7. Questions to be addressed to understand and quantify the hazard and risk associated with induced seismicity associated with energy technologies (adapted from Committee on Induced Seismicity Potential in Energy Technologies *et al*., 2012).

The statistical relationships observed in natural seismicity may not necessarily apply to induced seismicity. This has implications for maximum expected magnitudes and more research is needed to better understand this. Although both numbers and magnitudes of induced earthquakes are observed to increase with the volume of injected fluid (McGarr, 2014; Shapiro *et al*., 2007), this relationship can be complex, and more research is needed to better understand this. For example, Brodsky *et al*. (2013) show that seismicity rate positively correlates with the net volume of produced fluid (extraction minus injection) rather than the total injected volume. More work is also required to better understand the relationship between well pressures and seismicity induced in shale.

A traffic light system linked to real-time monitoring of seismic activity is an essential mitigation strategy that will also need to accompany any UGEE operations in Ireland. This requires the definition of acceptable thresholds for the cessation and recommencement of operations. Published recommendations for these thresholds in

UGEE operations differ widely (the BC Oil and Gas Commission, 2012; Green *et al*., 2012). It seems clear that any thresholds should be based on levels of ground motion which may represent a hazard or a public nuisance. For example, Bommer *et al*. (2006) use peak ground velocity thresholds based on both human response to ground shaking and vulnerability curves defined for local buildings. Existing regulatory guidelines for ground vibrations caused by blasting could also provide a useful framework for this purpose. The British Standards BS 6472-2 and BS 7385-2 define limits for ground vibrations caused by blasting which are acceptable for human exposure and above which cosmetic damage could take place. The equivalent German DIN4150-Part 3 (Effects of Vibration on Structure) also examines levels of vibration at which building damage may occur. Empirical relationships between earthquake intensity and peak ground motions based on observed data, such as Wald *et al*. (1999) may provide a useful alternative means for comparing the effects of ground shaking.

Baptie *et al*. (2015) use stochastic modelling (Boore, 1983, 2003) to simulate ground motions for small to moderate earthquakes that might occur in Ireland, and compare these with British Standards BS 6472-2 and BS 7385-2. Figure 8.8 shows peak ground velocities calculated for a range of earthquake magnitudes and hypocentral distances where the coloured contours show the values of ground velocity given by BS 6472-2 and BS 7385-2. This allows the magnitudes and distances at which the model exceeds these limits to be estimated. In this case, the limit of 15 mm/s, above which cosmetic damage could occur (BS 7385-2) is only exceeded for earthquakes with magnitudes of 3 or above within a few kilometres of the hypocentre. However, ground motions from earthquakes typically show large aleatory variability, and, in the face of this uncertainty, it would seem prudent to make conservative decisions on any thresholds. These results suggest that an upper magnitude threshold for the cessation of operations in the range 2–2.5 may be practical. Direct use of a ground motion threshold, such as peak ground velocity, may be preferable to magnitude threshold, since this avoids the issue of magnitude calculation and the averaging of a number of ground motion values. Also, the use of peak ground velocity would allow thresholds to be directly linked to existing guidelines.

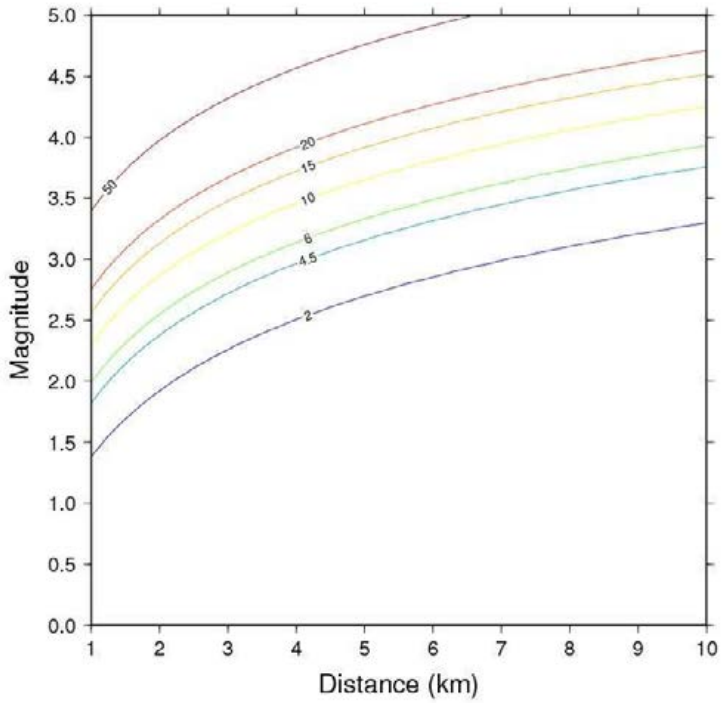

Figure 8.8. Peak ground velocity (mm/s) calculated for a range of earthquake magnitudes and hypocentral distances (from Baptie *et al*., 2015). The coloured contours show the fixed values of peak ground velocity given by BS 6472-2 and BS 7385-2).

The number of natural earthquakes in this magnitude range in Ireland is expected to be low. For example, the recent SHARE project (Giardini *et al*., 2013) determined an activity rate parameter for earthquakes in the source zone containing Ireland of a = 2.1756, i.e. approximately three earthquakes with a magnitude of 2 or above every two years. Scaling this for the larger of the two study areas in this project, which has an area of approximately 2,200 km^2, and assuming that seismicity is homogeneous, we might only expect an earthquake with a magnitude of 2 or greater roughly every 60 years. There will be even fewer earthquakes in the smaller study area. Such low expected activity rates suggest that it should not be difficult to identify earthquakes related to UGEE operations. However, seismological methods alone cannot discriminate between man-made and natural tectonic earthquakes. In some cases, induced earthquakes may occur close to the source of the pressure perturbation, but at other times, they may take place many kilometres away. Similarly, the delay times between the start of fluid injection and the induced earthquakes may vary from minutes or hours to days or weeks, and, in some cases have continued to occur long after injection has ceased.

In the case of Blackpool, seismicity was detected close to the start of injection during stages 2, 4 and 5. Figure 8.9 shows the injected volume as a function of time together with the earthquakes. This continued throughout injection, and, in the case of stages 2 and 5 for several hours after shut-in. The largest earthquakes occurred approximately ten hours after shut-in, when earthquakes with magnitudes of 2.3 ML and 1.5 ML were observed following stages 2 and 5 respectively. Very few earthquakes were detected following these two events. The lack of seismicity during stage 3 (Figure 8.2) can perhaps be explained by the reduced injection volume and the use of flowback. The use of flowback may also explain the relatively weak seismicity observed during stage 5. The reason for the lack of seismicity during stage 1 is unclear.

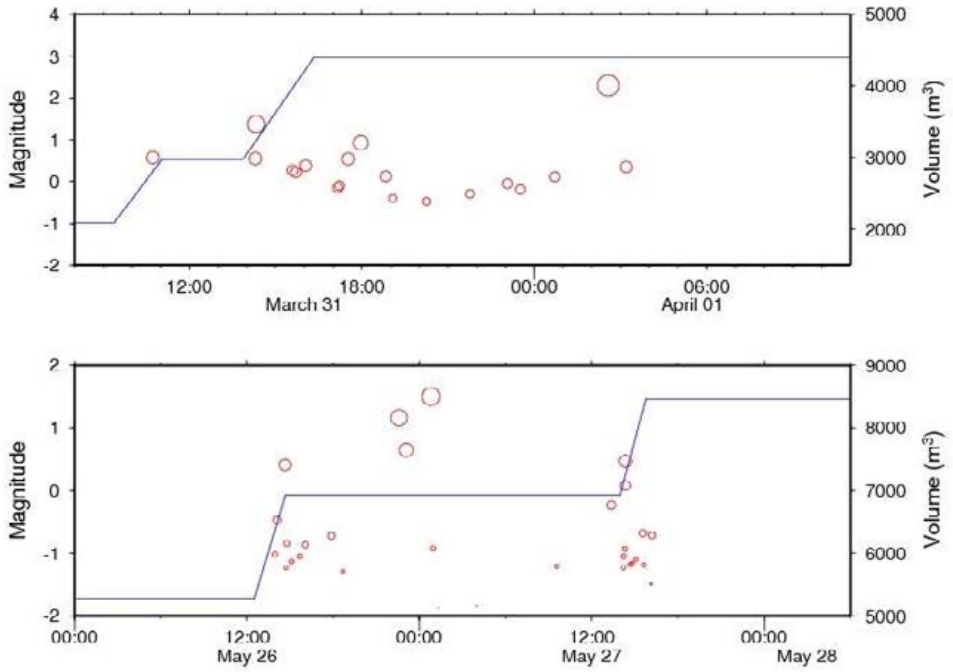

Figure 8.9. Volume of injected fluid (blue line) and earthquakes (red circles, scaled by magnitude) during hydraulic fracturing operations at Preese Hall, Blackpool (during treatment stages 2 (a) and 4 and 5 (b) (from de Pater and Baisch, 2011)).

In the Eola field, South Central-Oklahoma (Holland, 2013) the first earthquakes occurred approximately 24 hours after the first hydraulic fracturing stage began and almost immediately after the start of the second stage. Holland (2013) suggests that this delay is consistent with diffusion of pore pressure.

In Basel, Switzerland, seismicity started immediately after fluid injection started on 2 December 2006 (Haering *et al*., 2008). The number of events was observed to increase as flow rate and well head pressure increased. Injection was reduced then stopped on 8 December as the seismicity was at an unacceptably high level. The largest earthquake, with a magnitude of 3.4 ML, occurred 5 hours after shut-in. Sporadic seismicity continued inside the stimulated volume for years after.

In the case of seismicity related to long term disposal of waste water in deep injection wells, such as Rocky Mountain Arsenal (Hsieh and Bredehoeft, 1981) or Paradox Valley (Ake and Mahrer, 2005) earthquakes were observed to occur many kilometres from the point of injection, many years after injection stopped, again, as a result of diffusion of pore pressure.

A growing body of evidence of changes in observed seismicity rates and significant earthquakes linked to Deep Water Injection (DWI) of waste water from the hydrocarbon industry suggests that this activity may pose a rather greater seismic risk. Reports from Project B of this research programme discuss the possibility that DWI could be one of several potential ways of dealing with waste water. However, currently, the practice is not legal under EU law, as explained in project C of this research programme (Calero *et al*., 2015). The Commission has confirmed that used fracturing fluid in UGEE operations is to be considered as extractive waste and that flowback water must be treated according to the requirements of the Mining Waste Directive.

8.8 Recommendations

1. Follow the seven steps for mitigating seismic risk identified in the US Department of Energy "Protocol for Addressing Induced Seismicity Associated with Enhanced Geothermal Systems" (Majer *et al.*, 2012) and listed in Table 8.1;

2. A traffic light system linked to real-time monitoring of seismic activity is an essential mitigation strategy that will also need to accompany any UGEE operations in Ireland. Thresholds for the cessation and recommencement of operations should be based on levels of ground motion which may represent a hazard or a public nuisance. An upper magnitude threshold for the cessation of operations in the range 2–2.5 may be practical;

3. Direct use of a ground motion threshold, such as peak ground velocity, may be a suitable alternative to earthquake magnitude. This would allow thresholds to be directly linked to existing guidelines for ground vibrations caused by blasting such as the British Standards BS 6472-2 and BS 7385-2, and the equivalent German DIN4150-Part 3; and

4. Characterise of any possibly active faults in the area of interest using all available geological and geophysical data.

8.9 Conclusions

The process of hydraulic fracturing in order to increase the permeability of reservoir formations and stimulate the recovery of hydrocarbons is generally accompanied by microseismicity, usually defined as earthquakes with magnitudes of 2 or less, that are too small to be felt. Two types of induced events can be defined: "fracked" events, whose size is constrained by the energy of the injection process; and "triggered" events, whose size depends largely on the amount of stored up elastic strain energy already in the rocks. The "fracked" events are caused by the formation and growth of new cracks and fractures in a previously intact rock mass as a result of the injection of high pressure fluids. The "triggered" events are a result of both presence of high pressure fluid and the stress perturbation caused by the fluid, which changes the effective stress on pre-existing faults, causing them to fail. These earthquakes can be "triggered" by very small stress perturbations, however, the potential for such events depends very much on the geological context and, given the low levels of background seismicity, the probability of large triggered in Ireland can be considered as small.

The general consensus among most authors is that the process of hydraulic fracturing a well as presently implemented for shale gas recovery does not pose a high risk for inducing either felt, damaging or destructive earthquakes. Experience in the USA, where many thousands of stimulations have been carried out suggest that the magnitudes of the induced earthquakes in reservoirs such as the Barnett and Marcellus Shales are typically less than 1 Mw. However, it should be pointed out that most sites of UGEE operations lack independent instrumentation for monitoring induced seismicity and that earthquakes with magnitudes of 2.5 or less will fall below the detection thresholds of regional seismic monitoring networks. Earthquakes of this size are unlikely to be felt or even detected unless local seismic monitoring networks are in place.

There are only three documented examples of earthquakes with magnitudes greater than two that have be conclusively linked to hydraulic fracturing for shale gas exploration/recovery: a magnitude 2.3 ML earthquake in Blackpool, UK in 2011; from 86 earthquakes in Garvin County, South-Central Oklahoma in 2011, 16 had a magnitude of greater than 2.0 ML and the largest had a magnitude 2.9 ML; in a sequence of over 200 earthquakes in Horn River, Canada, also in 2011, 21 had magnitudes of 3 ML or greater and the largest had a magnitude of 3.8 ML. It is likely that an earthquake similar in magnitude to the largest that occurred in Horn River, Canada, could be strongly felt and could even cause some superficial damage. In addition, if an earthquake of such a magnitude were to occur in Ireland where felt seismicity is very rare it would be likely to

cause rather more concern among the local population than it would in other parts of the world where earthquakes of this magnitude are more frequent, However, the maximum magnitudes observed in Blackpool and Garvin County would be unlikely to cause any damage, although they could be felt by people close to the epicentre and may cause some concern.

Section 5 (Task 3) of this project discusses the large uncertainties in forecasting seismicity in areas such as Ireland where the background activity rates are low. However, although it is difficult to quantify, the probability of significant triggered seismicity depends strongly on the prior activity of the area. As a result, significant events are very unlikely in areas such as Ireland where the background seismicity rate is extremely low, and there is no evidence to suggest that the process of hydraulic fracturing for shale gas recovery poses a higher risk for inducing earthquakes than in other parts of the world. This risk may be further reduced by effective mitigation.

By contrast, the growing body of evidence of changes in observed seismicity rates and significant earthquakes linked to long term disposal of waste water from the hydrocarbon and other industries, suggests that this activity may pose a rather greater seismic risk. Earthquakes with magnitudes comparable to the magnitude 5.7 earthquake in Prague, central Oklahoma have a non-negligible contribution to the seismic hazard in such regions and should be considered in any long term assessments of seismic hazard.

Experience of induced seismicity in Enhanced Geothermal Systems have led to a series of measures to address induced seismicity that may be considered as “industry best practice”, and, as such, may be considered appropriate for mitigating the risk of induced seismicity in UGEE operations. For example, an operational traffic light system linked to real-time monitoring of seismic activity is an essential mitigation strategy that will also need to accompany any UGEE operations in Ireland. This will require the definition of acceptable thresholds for the cessation and recommencement of operations and these should be based on levels of ground motion which may represent a hazard or a public nuisance. Existing regulatory guidelines for ground vibrations caused by blasting could also provide a useful framework for this purpose. The direct use of ground motion thresholds rather than derived magnitudes may, in some case, be preferable. Other means of mitigating earthquake risk may require improved understanding of the Earth’s sub-surface in areas of unconventional hydrocarbon potential, such as better characterisation of existing fault zones, which may be difficult to achieve without detailed geophysical surveying.

Controlling factors on seismicity induced by hydraulic fracturing include: the strength of rocks in the geological formations of interest; the size and state of stress of any faults in the area likely to be affected by fluid injection; and, the pressure change induced by the hydraulic fracture process. The pre-existing state of stress on a fault determines how close it is to failure, so faults that are critically stressed may require only a small stress perturbation to cause them to fail. The pressure change induced by the hydraulic fracture process is mainly controlled by the volume of injected fluid and the rate of injection, where larger volumes and higher injection rates generate higher pressures. Recent work suggests that maximum magnitude is related to the total volume of injected fluid.

There remain a number of gaps in our existing knowledge of induced seismicity. For example, pre-existing state of stress and pore pressure acting on a fault are usually unknown. We also often lack knowledge about the hydrological properties of the sub-surface. Measuring the initial stress state and pore pressure, tracking the injection history, and careful seismic monitoring may help improve understanding.

Finally, it should be noted that seismological methods alone cannot discriminate between man-made and natural tectonic earthquakes. This strengthens the case for site specific seismic monitoring and detailed recording of injection parameters, to reduce uncertainties in earthquake locations and to compare the temporal evolution of seismic activity with any hydraulic fracture operations.

9 Task 9: Assessment of Pre-fracturing Modelling Techniques

9.1 Introduction

The physical properties of rocks control the propagation of fractures in the subsurface via contrasts between an array of petrophysical properties. Variations in these properties produce complex environments through which fractures must propagate; realistic modelling of them is a vital prerequisite for accurate forecasting of distributions of fracture length and orientation. For many years it was thought that these properties were well described by Gaussian distributions, which would have allowed modelling of the spatial extent by upscaling localised measurements, to form so called "representative elemental volumes". Since the 1980s this view has become increasingly discredited and it is now accepted that elastic moduli (Bean and McCloskey, 1993; Dolan and Bean, 1997) the spatial and length distributions of existing fractures (Barton and Scholz 1993; Barton *et al.*, 1993), the porosity–permeability relations and the volume of fluid transported per unit volume (Hsieh *et al.*, 1993; Barton *et al.*, 1995), are all invariant to changes in scale from a few mm to many kilometres. These observations have been confirmed by many subsequent studies.

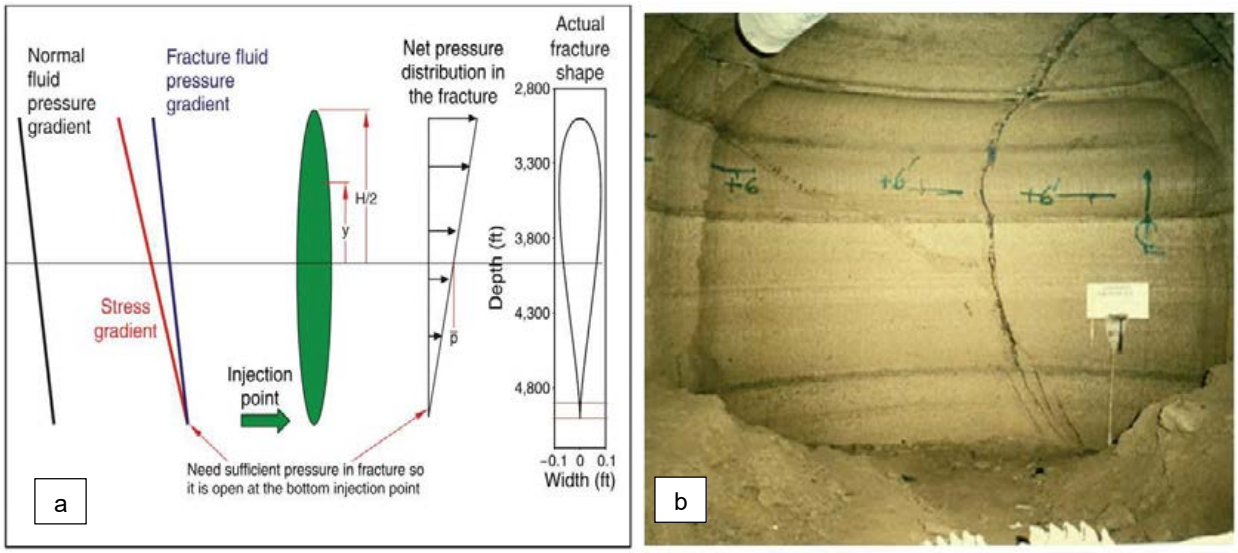

Figure 9.1. Typical geometry used in fracture height calculations compared to fractures observed in mineback experiments (both from Fisher and Warpinski, 2011). Reproduced with permission from the Society of Petroleum Engineers.

This fact has some problematic, and unavoidable, issues for the forecasting of fracture populations in the hydraulic fracturing environment (note that this forecasting addresses “fracked” rather than “triggered” events). Firstly, traditional fracture-mechanical methods become intractable when the scale invariance of petrophysical properties is included in the prior description of the material. Secondly, while the parameters of the appropriate scaling distributions, such as the fractal dimension, can be estimated, the fractures do not propagate through a statistical distribution but through a physical field which happens to be well described by this distribution. In other words, only through the understanding of the physical state of the rock mass and how it is responding to a particular set of forcing conditions can a useful estimate be made of how the fracture set is developing and how this might continue to develop through the injection. Exponential divergence of initially similar initial

conditions, which is an essential feature of such strongly non-linear systems, ensures that such measurements must be made and updated continuously if we are to understand and forecast the fracture propagation.

Another problem renders fracture mechanical models for the forward modelling of fracture length distributions is the simplification of fracture geometry required to provide tractable analytic, or even numerical simulations of fracture growth. Typically, models assume some simple shape for the fracture (see for example Figure 9.1a) which allows the modeller to solve the appropriate equations in a medium with an assumed homogeneous set of physical properties for fracture growth. So-called mineback experiments where rock, previously fractured by fluid injection was excavated to reveal the fractures induced show that these simple geometries have no relationship to the fractures observed in these experiments (Figure 9.1b).

Fortunately, modern seismological and geodetic instrumentation and analytical techniques for the near-real-time monitoring of seismicity and deformation offer the real possibility of empirically tracking and forecasting the development of fractures before and during any potential fracking operation. Here we will briefly review the main observations relevant to forecasting the likely maximum fracture length distributions in Ireland. We show that, while published results from mineback experiments, laboratory rock mechanics experiments and field tiltmeter deployments are unlikely to assist n forecasting likely fracture lengths, published microseismic data may provide a workable guide. We show, however, that published estimates make unreasonable assumptions about the likely maximum event size which in turn would lead to a significant underestimate of the maximum vertical length of fractures in previous frack treatments. We then develop a general framework by which we provide a more robust forecast of the possible vertical height of fractures by modelling of the formation of fractures from widely accepted seismological scaling relations. Thus we avoid the problems associated with the scale invariance of rock properties and approach the problem on a purely observational and well-established theoretical basis.

In Section 9.2 we briefly critically review the literature relevant to forecasting possible height of fractures from unconventional gas exploration and extraction in Ireland using observations from previous UGEE operations. In section 3.3 the methodology and theoretical framework for the estimation of the length of fracture associated with each microseismic event is described. This must be added to the vertical distance of the event from the perforation to provide an estimate of the vertical extent of fractures. In Section 3.4 we present a set of results for a synthetic scenario. We stress that the modelling parameters leading to these results can be updated in near-real-time during any fracking operation. In Section 3.5 we discuss the method in the context of the problem. In Section 3.6 we draw some conclusions and make some recommendations for possible future developments of the technique. We refer the reader to Interim Report A2.1 for a detailed description of the nomenclature for seismic events adopted in this report. In brief, we use “fracked” to define those events whose energy arises predominantly from the high pressure fluid injection, “triggered” to define those events whose energy arises from external (e.g. tectonic or glacial) forces, and “induced” to describe all the events recorded during a given project.

9.2 Observational Estimates of Fracture Length

There is a wealth of literature on the vertical propagation of fractures resulting from the injection of high pressure fluid into low permeability rocks. This literature covers a wide range of information sources spanning mineback and coring evidence, laboratory testing, analytical models and numerical models. It is our view that none of these methods provide compelling evidence on which general statements can be made about likely fracture lengths or the possibility of contamination of aquifers in the Irish context. Much of this literature results largely from the analysis of industry data by scientists and technicians who have been directly employed by the various major players in the extraction of hydrocarbons from UGEE operations. Nonetheless, while many of these publications are selective in their choice of data and make assumptions which are contradictory to more

objective observations, it is our view that some published data do provide a reasonable basis on which to place a lower bound on the possible fracture heights which might result from UGEE operations in Ireland.

9.2.1 Direct observations of fractures

Direct observations of fractures can be made by mineback experiments, in which previously fracked rocks are excavated to expose the fractures generated. The main objective of this work, however, is to improve hydraulic fracture technology rather than to estimate the maximum fracture height. Thus while mechanisms for the prevention of fracture propagation, such as termination of fracture propagation by geological layering can be clearly seen in mineback data, the entire experiment never completely samples the fracture field and therefore the maximum fracture height can never be observed. It is also clear that lithological control of fracture development is not uniform and there are many observations of mineback and laboratory experiments in which fractures propagate across lithological boundaries (e.g. Daneshy, 1978; Gillespie *et al.*, 2001). The technique is therefore explicitly biased towards providing evidence for fracture termination rather than propagation. Current mineback experiments are focused on fluid flow through the created fractures with a view to the better control of permeability enhancement and do not generally attempt to elucidate maximum fracture lengths. Evidence from coring, provides no possible evidence of fracture length and instead is again focused mainly on fracture development better to understand permeability enhancement.

Laboratory testing is frequently used to explore the fractures generated by the differential stressing of rocks by various mechanisms. We are not aware, however, of any laboratory experiments which have been carried out to explore the maximum fracture height induced in the laboratory sample and it is unclear how observations from such experiments could be upscaled to provide estimates of real fracture populations produced in industrial scale hydraulic fracture stimulation.

9.2.2 Indirect observations of fracturing

The two main methods for the indirect observation of fracturing are by the use of tiltmeters to observe deformation and by microseismic observations. The former is integrative and provides evidence of the bulk properties of the fracture field where the latter, arguably provides information about the formation of individual fractures.

9.2.2.1 Using tiltmeters to observe fracture development

Tiltmeters very accurately measure the slope of a surface. A model is assumed for the developing fracture and the characteristics of the assumed model are investigated by solving the inverse problem for the resulting slope distributions. They can be deployed in two ways to investigate the development of fractures during hydraulic fracture stimulation. Surface arrays record changes in surface slope due to deformation of the ground by the production of fractures and it is argued that they are sensitive to the orientation of the generated fractures. Downhole tiltmeter arrays record the internal deformation of the rock volume and, while they are much more sensitive than surface arrays due to their proximity to the fractures being observed, they are less sensitive to fracture orientation. In both cases, it is our view that while the assumptions associated with overly simplistic forward model might usefully help to model the permeability at depth which is of most interest to oil industry, they are singularly inappropriate technology for elucidating maximum fracture height.

Tiltmeter data provides a clear illustration of selective analysis of data employed by industrial scientists to argue that induced fractures are unlikely to contaminate near surface reservoirs. Figure 9.2 shows the components of deformation recorded by a surface array as a function of fracture depth. It is frequently argued that this distribution shows that near-surface fractures are predominantly horizontal (e.g. Fisher and Warpinski, 2011) leading to the conclusion that fractures cannot propagate into the shallow subsurface. In fact, these data show that while horizontal fractures are rare (but not non-existent) at depth, vertical fractures are dominant at

all depths. This data provides clear evidence that vertical fractures do propagate into shallow depths where they might interact with reservoirs. Of course they do not indicate that they will do so from any particular treatment.

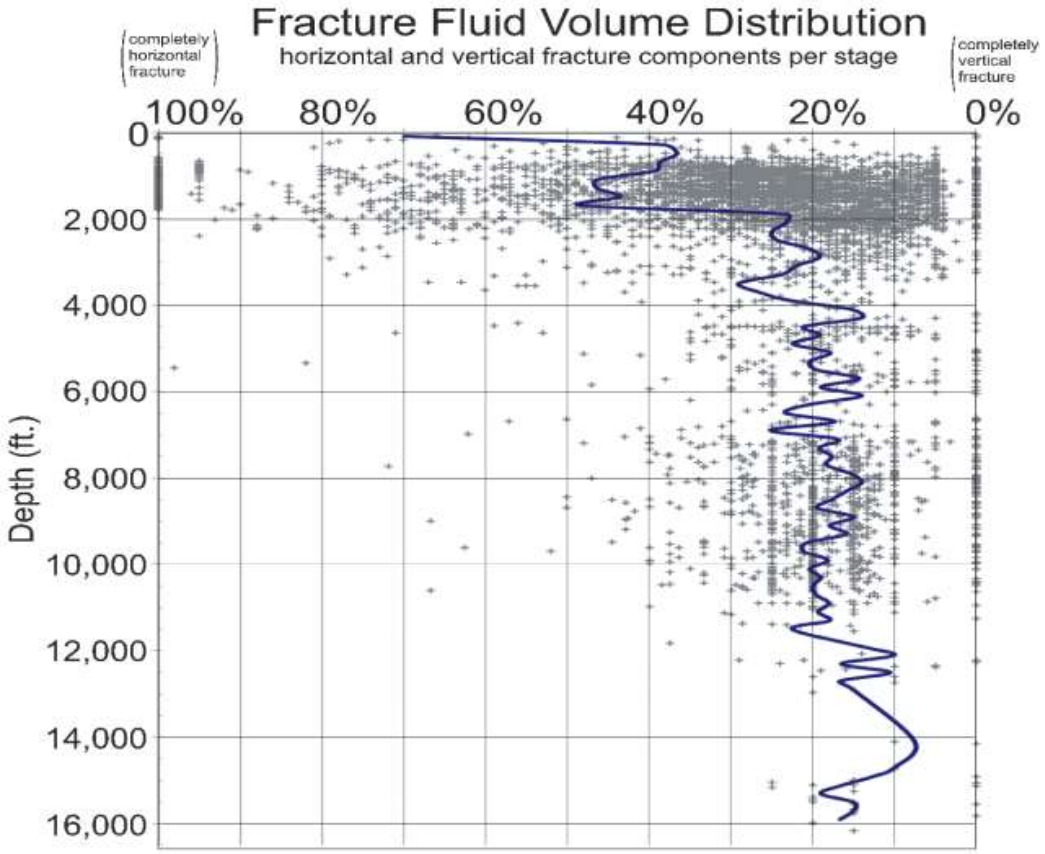

Figure 9.2. Variation of orientation of fracture length with depth. Note the great density of the data for the horizontal component <40% (i.e. dominantly vertical elongation) for depths of less than 2500ft (about 750m).

9.2.2.2 Using seismicity to observe fracture development

Generation of fractures progresses by the sequential brittle fracture of rock. Each brittle failure generates seismic waves in the rock volume which can be detected using seismometers deployed either in surface or in downhole arrays. While there are significant differences in the detection capabilities of these array geometries, each is capable of producing estimates of the location of the causative fracture which can be interpreted as the generation of an element of fracturing at depth. Taken in the whole the data produces an image of the entire fractured volume.

Figure 9.3 shows the type of seismicity which is typically recorded during a frack treatment. The data shown here was collected from two neighbouring wells in the Marcellus Shale which extends throughout much of the Appalachian Basin in NW USA and has been heavily fracked over the last 3 decades. The data show a deepest microseismic event at around 300ft below the perforation and a shallowest some 400ft above. Thus if we assume that each event represents a small fracture increment then the worst case maximum height of fractures consistent with these data is on the order of 700ft or some 215m. Clearly this particular measurement is representative of this pair of wells, any inference about the general maximum fracture height requires data from many such treatments. Additionally, while a microseismic event is located at points in 3 dimensions,

known as the hypocentre, its source is actually extended in space. Furthermore, the tiltmeter data shown in Figure 9.2 shows that the causative fractures are generally dominated by vertical fracture extension. An assessment of the maximum possible fracture height must therefore involve two separate lines of evidence:

1. The maximum likely vertical extent of the microseismicity; and

2. The length of the longest fracture associated with the seismicity which should be assumed to be vertical.

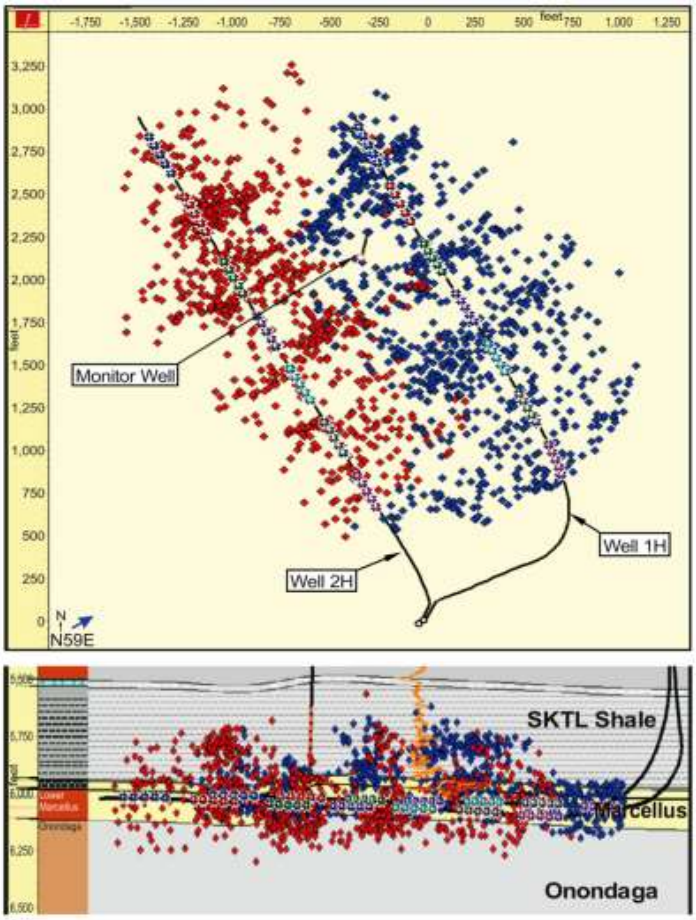

Figure 9.3. Seismicity due to two sub-horizontal wells in the Marcellus shale. A) map view and B) vertical section. In this case the shallowest microseismic event is located at about 5,600ft, some 400ft above the perforation whereas the lowest is 6300ft, some 300ft deeper than the perforation.

Several studies (e.g. Fisher and Warpinski, 2012; Flewelling *et al.*, 2013) have reviewed data from many thousands of treatments across the major tight gas formations in North America. Figure 9.4 show one such review. Some features are important. Firstly, it has been argued by the oil industry scientists that the vertical extent of microseismicity is smaller at shallower depths. We have examined many published examples such as Figure 9.4 and find that in general there is little if any systematic relationship between vertical extent of seismicity with depth of the perforation. We therefore conclude that the likely vertical extent of fracturing is likely to be insensitive to frack depth. The separation between the wells and the seismicity in all the cases we have

examined is large so assuming no pre-existing through-going fractures or faults then it is unlikely that any contamination has occurred due to the data which is publically available. This of course is entirely site dependent and no general case can be made for the safety of this operation on the basis of these data.

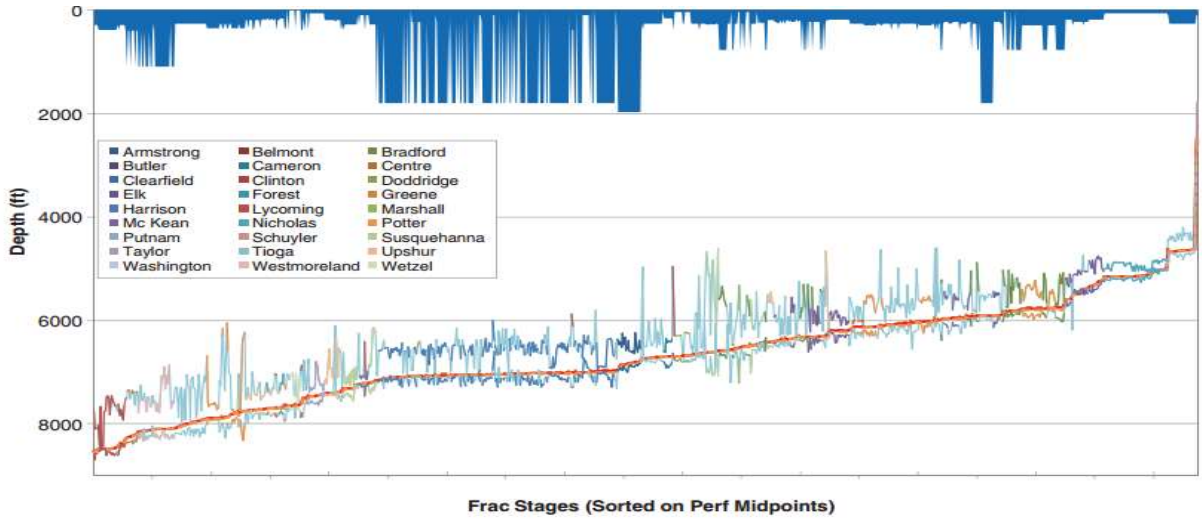

Figure 9.4. Shallowest and deepest microseismic events for treatments n the Marcellus shale. Orange curve indicates the mid-perforation depth for each of several thousand stages. The coloured lines on either side show the shallowest and deepest microseismic events coloured by the county in which they occurred. Blue lines at the top indicate the depth of potable water wells in the region. The large separation between the microseismic activity and the deepest well suggests that there is no possibility of contamination from the treatments to the wells.

Maxwell (2011) systematically examined the published data on the vertical extent of frack-induced microseismicity. The data examined are slightly skewed to the shallow depth, but, assuming a normal distribution, Maxwell estimates the standard deviation at 87 m. We note, however, that this is an optimistic assessment of the data (7 of the 48 data points would exceed 2σ) and we argue that the data are more consistent with 2σ around 300 m. Thus 1 in 20 projects in N. America produced recorded seismicity approaching 300 m shallower than the perforation.

This does not of course show that the maximum upward fracture extent in these treatments was 300m above the perforation. We must also include an additional component which relates to the finite extent of the fractures associated with each event. This is more complicated since it depends on several assumptions and expectations. In the first instance we note that the length of the failing patch associated with a given seismic source is related to the magnitude of the event; large events occur on larger slip patches. Seismologists have made many observations concerning this relationship which we develop in some detail in Section 9.3 below. Secondly, we must elucidate and systematic variation of magnitude with depth. The literature provides several studies of this variability which are summarised in Figure 9.5. The diagram shows a slight increase in maximum magnitude with depth but there is no notable systematic variation; variability appears to be controlled by sub-horizontal layering rather than depth. We therefore assume here that the probable maximum magnitude does not vary with depth.

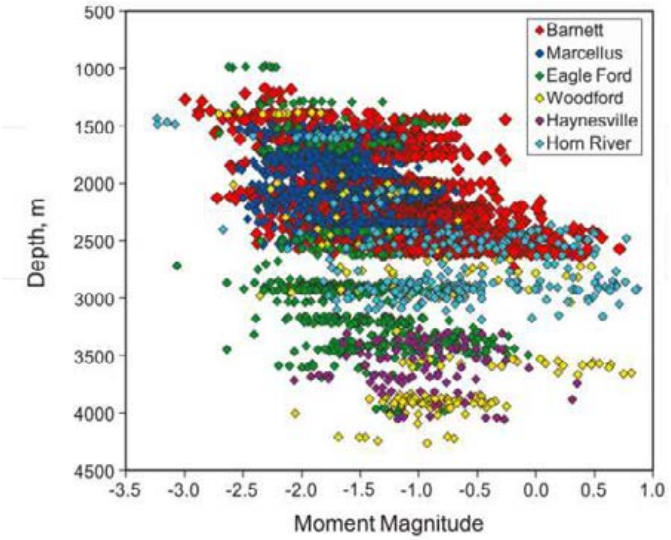

Figure 9.5. Variation of magnitude with depth for frack basins in USA.

9.3 Fracture Length Distribution Due to Seismicity

9.3.1 Introduction

Having provided estimates of the likely vertical extent of microseismic activity above a given perforation level, we now must make an estimate of the likely size of fractures which are formed during this seismicity. It has been argued (e.g. Flewelling *et al.*, 2013) that the fractures associated with the largest events are on the order of 10m long and therefore that this contribution can be ignored. To arrive at this estimate they make two assumptions which are questioned here. Firstly, they assume that the maximum fracked event size is M_L=0.86. Results presented in Section 9.2 above show that a more reasonable maximum magnitude for these events approaches ML=3.0. Secondly they make no allowance ether for the uncertainty in either the location of the events, their estimated magnitude or for the parameters of the seismicity distributions. Here we address these issues to provide, we believe a more realistic worse-case estimate.

Our aim is to use scaling relations between event magnitude and fracture length to forecast the distribution of hydraulic fracture dimensions from a known magnitude distribution. However, while there have been a number of studies of empirical relations for the scaling of earthquake magnitude and rupture length for tectonic earthquakes (Wells and Coppersmith, 1994; Henry and Das, 2003; Leonard, 2010), no corresponding relations exist for hydraulic fracturing. In what follows, we demonstrate that tectonic scaling relations should also apply for hydraulic fracturing. We then outline the methodology.

Since we are dealing with newly generated fractures, we approach the problem from the perspective of fracture mechanics and not fault friction (though Kanamori and Brodsky (2004) show that these perspectives are consistent). Crack propagation models for the earthquake rupture process (see Pollard and Segall (1987) for a review) are based on three "modes" of rupture (see Figure 9.6 for a schematic representation). In the coordinate system where the normal to the crack surface is in the y-direction and the crack propagates in the x-direction, Modes I, II and III describe components of displacements in the y-, x- and z- directions respectively: Mode I is an opening of the crack, where the crack displacement is normal to the crack surface; Mode II is a longitudinal shear mode, where the displacement is in the plane of the crack, parallel to the propagation

direction and; Mode III is a transverse shear mode, where the displacement is in the plane of the crack, normal to the propagation direction. Tectonic earthquakes are therefore usually modelled using some mixture of shear Mode II and III displacements, whereas the generation of fractures by hydraulic fracturing includes a significant Mode I component due to tensile opening of cracks.

Pollard and Segal (1987) define a scalar moment for each mode

$$M_0^l = \mu \iint_S \Delta u_v \, \mathrm{d}S$$

where $l = \mathrm{II}$, for example, corresponds to $\Delta u_{\mathrm{II}} = \Delta u_x = u_x(x = 0^+) - u_x(x = 0^-)$ in the coordinate system of Figure 9.6.

The Mode II/III moments of a double couple tectonic earthquake are equivalent to off-diagonal components of the moment tensor in the coordinate system defined by the rupture surface and propagation direction; Mode I fractures have an exactly analogous definition for moment and moment magnitude to tectonic earthquakes.

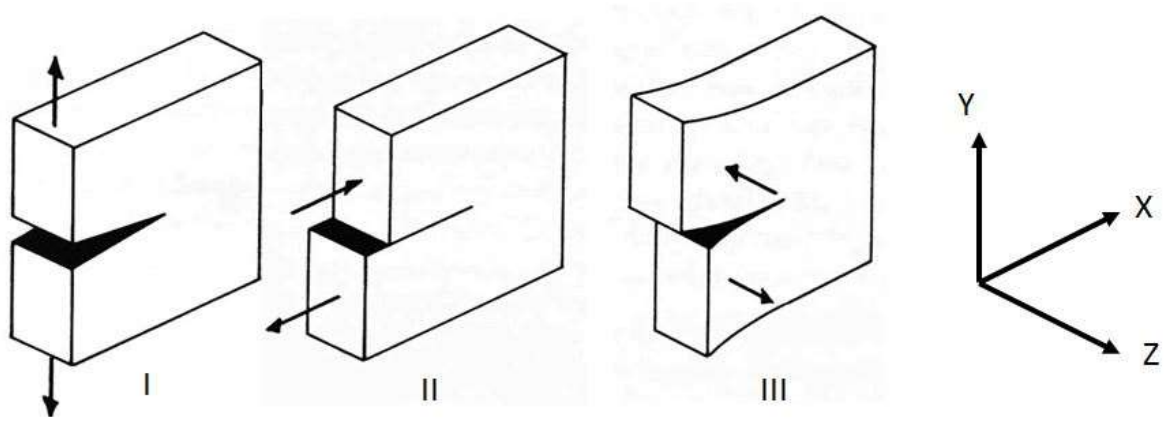

Figure 9.6. Schematic diagram showing the modes of crack. The crack or rupture propagates along the *x*-direction. The normal to the crack surface is in the *y*-direction. Arrows show the direction of displacement across the crack surface for each mode (adapted from Kanamori and Brodsky, 2004).

For a crack of dimension L in an elastic body subjected to uniform stresses, it can be shown (Scholtz, 2002) that the Mode l displacement across the crack surface is

$$\Delta u_l = \Delta \sigma_l \frac{2(1-\nu)}{G} (L^2 - x^2)^{1/2}$$

where the $\Delta \sigma_l$ refers to the relevant "driving stress" for the mode (normal stress less the pore-fluid pressure for Mode I and shear stress less the friction for Mode II and III). Since the equation applies for all modes, we can expect the displacement across Mode I to scale in the same way with crack dimensions as for Mode II and III, provided the driving stresses are the same. From the definition of the moment, this implies therefore that the rupture dimension should scale with the moment in the same way for all modes.

Therefore, we suggest that scaling relations between magnitude and rupture dimensions of tectonic earthquakes are also applicable here. The most widely used of these relations were developed by Wells and

Coppersmith (1994, WC94). Although there is a more recent study (Leonard, 2010), which includes the dataset of WC94 and data from other sources, it does not have uncertainties in both parameters of the scaling relation. We consider that WC94 will, therefore, give a more realistic estimate of the uncertainties for this application. The scaling relation we use is

$$\log_{10} L = 0.59(\pm 0.02) M_w - 2.44(\pm 0.11) \qquad \text{Equation 9.1}$$

which is for all earthquakes in the WC94 dataset. The uncertainty σ_L is calculated by propagation of the parameter uncertainties in brackets through Equation 9.1 and is therefore a function of M_w. We note that, although WC94 gives different values for the parameters for strike-slip, reverse and normal events, they are broadly consistent with the values calculated for all events. We therefore consider this to be the most reasonable choice for the scaling of fracked events. However, we should point out that Leonard (2010, see Table 4 in that paper) finds that strike-slip and dip-slip earthquakes have precisely the same $M_0 - L$ scaling for small (L<3.5 km) interplate earthquakes (consistent with rupture widths much smaller than the seismogenic width); for intraplate events the scaling is the same within the published uncertainties. This suggests that if the Leonard (2010) analysis could be repeated to include uncertainty analysis comparable to WC94, the uncertainties in our calculations could be reduced further.

In order to estimate the distribution of fracture lengths, we therefore require an estimate of the distribution of event magnitudes for the fracked events. The appropriate model for the frequency-magnitude scaling of fracked events is still under discussion. There seems to be significantly different behaviour between different fracking projects, some exhibiting Gutenberg-Richter scaling, i.e. perfect power law behaviour, with large values of the scaling exponent b, and others showing a clear roll off at higher magnitudes. In order to reflect as wide a range as possible of frequency-magnitude scaling, we use the Gutenberg-Richter relation with an exponential tail (Main and Burton, 1984), or a gamma distribution, given by

$$f(M_0|M_0^*) = A M_0^{-\beta} e^{-M_0/M_0^*} \qquad \text{Equation 9.2}$$

where M_0 is the seismic moment and M_0^* is the moment at which the exponential function is equal to $1/e$ (and therefore allows the upper magnitude roll-off for the distribution to be adjusted). The gamma distribution approaches perfect power law behaviour when $M_0 \ll M_0^*$.

M_0 (in Nm) is related to the moment magnitude by

$$M_w = \frac{2}{3}\log_{10} M_0 - 6.07$$

This definition allows us to calculate M_0^* from a threshold moment magnitude for the fracked seismicity. The scaling exponent in Equation 9.2 is related to the traditional Gutenberg-Richter b-value by $\beta = \frac{2}{3}b$ and A is a normalising constant, which can be obtained by setting[5]

$$A \int_{M_{0,\min}}^{\infty} M_0^{-\beta} e^{-M_0/M_0^*} \, \mathrm{d}M_0 = 1$$

The total expected number of fracked events allows the full expected distribution of magnitudes to be forecast. The gamma distribution needs to be fitted to real fracked seismicity data from the site before it will provide realistic estimates of the parameters. A frequency-magnitude fit to a test catalogue will also allow the likely rate of fracked seismicity to be estimated.

5 This integral, with the exponential tail, cannot be evaluated analytically. However, our method of sampling, outlined below, does not require a value for A.

However, it is important to point out that seismicity rates are likely to be time varying, not only depending on the injection itself, but also on the diffusion of fluid though an unknown permeability field. Operational monitoring and real-time re-estimation of local seismicity rates and frequency magnitude scaling is therefore essential and is assumed in what follows. Also, we reiterate that the work in this task does not relate to the seismic hazard, which comes almost completely from "triggered" seismicity, and not "fracked" seismicity; different rates and magnitude distributions apply for the seismic hazard problem.

For a typical catalogue from a hydraulic fracturing project (with very small numbers of larger magnitude events), the distribution around M_w^* is very poorly sampled and the magnitude distribution does not reflect the (potentially large) variability in the rupture dimensions at a given magnitude.

Our approach is to estimate the distribution of fracture lengths by Monte Carlo methods: we generate a large number of synthetic fracked catalogues of events with moment magnitudes (large enough that the distributions are well sampled, and the distributions at large magnitudes have converged); we use the empirical relation in Equation 9.1, with a random error added, to assign fracture lengths to these events; and we use the mean properties of all the Monte Carlo simulations to determine the distribution function for fracture length for the hydraulic fracturing scenario.

Based on the discussion above, the algorithm for generating a single synthetic fracked seismicity catalogue is:

1. Generate a random sample n from a Poisson distribution, with expected value equal to the number of events above $M_{w,\min}$.
2. Set $i = 0$.
3. Generate a random sample u from a uniform distribution on the interval $(0,1)$.
4. Generate a samples from a pure GR distribution with a minimum magnitude $M_{w,\min}$ using $M_w = M_{w,\min} - \frac{\log_{10} u}{b}$
5. Generate a second uniform random variable u on the interval $(0,1)$. If $u > e^{-M_0/M_0^*}$, set $i = i + 1$ and continue to step 6. Otherwise return to step 3.
6. Using E2.1, calculate the expected rupture dimension μ_L of the event, given its magnitude (from step 4)
7. Generate a random sample u from a normal distribution with mean 0 and standard deviation 1.
8. Set the length of the event to $L = \mu_L + u\sigma_L$.
9. If $i = n$ then finish. Otherwise, return to step 2.

9.3.2 Results

We implement the above algorithm for 10,000 Monte Carlo samples. We set the parameters of the Gutenberg-Richter relation to $a = 0.0$ and $b = 1.0$, and the roll-off magnitude $M_w^* = -0.5$. This gives a total expected number of events for the catalogue of $\langle N \rangle = 990$ above $M_{w,\min}$,which we set to -3.0. Figure 9.7a shows a histogram of the number of events (sampled from a Poisson distribution with expected value $\langle N \rangle = 990$) in each of 10,000 Monte Carlo samples.

Note that, as we mentioned in Section 9.2, the total number of events will, in practice, have to be inferred from fracked rates as observed on site and scaled to reflect the time window of interest (i.e. the duration of the injection). The values we have chosen here reflect typical rates of fracturing that might be expected based on a few hours of injection. Roll off magnitudes are very difficult to estimate robustly from existing fracked seismicity frequency magnitude distributions and physical arguments for upper limits to the moments of fracked events

typically indicate much larger values than we have used here. The value we have chosen for M_w^* here is therefore for illustration only; in practice, a Gutenberg-Richter distribution with no exponential tail may be the best distribution to use until enough data exists to demonstrate that such a roll off really exists. Also note that, for decreasing $M_{w,\min}$, the number of events in the catalogue diverges, but the total fractured length (i.e. the sum of the lengths of all fractures) does not.

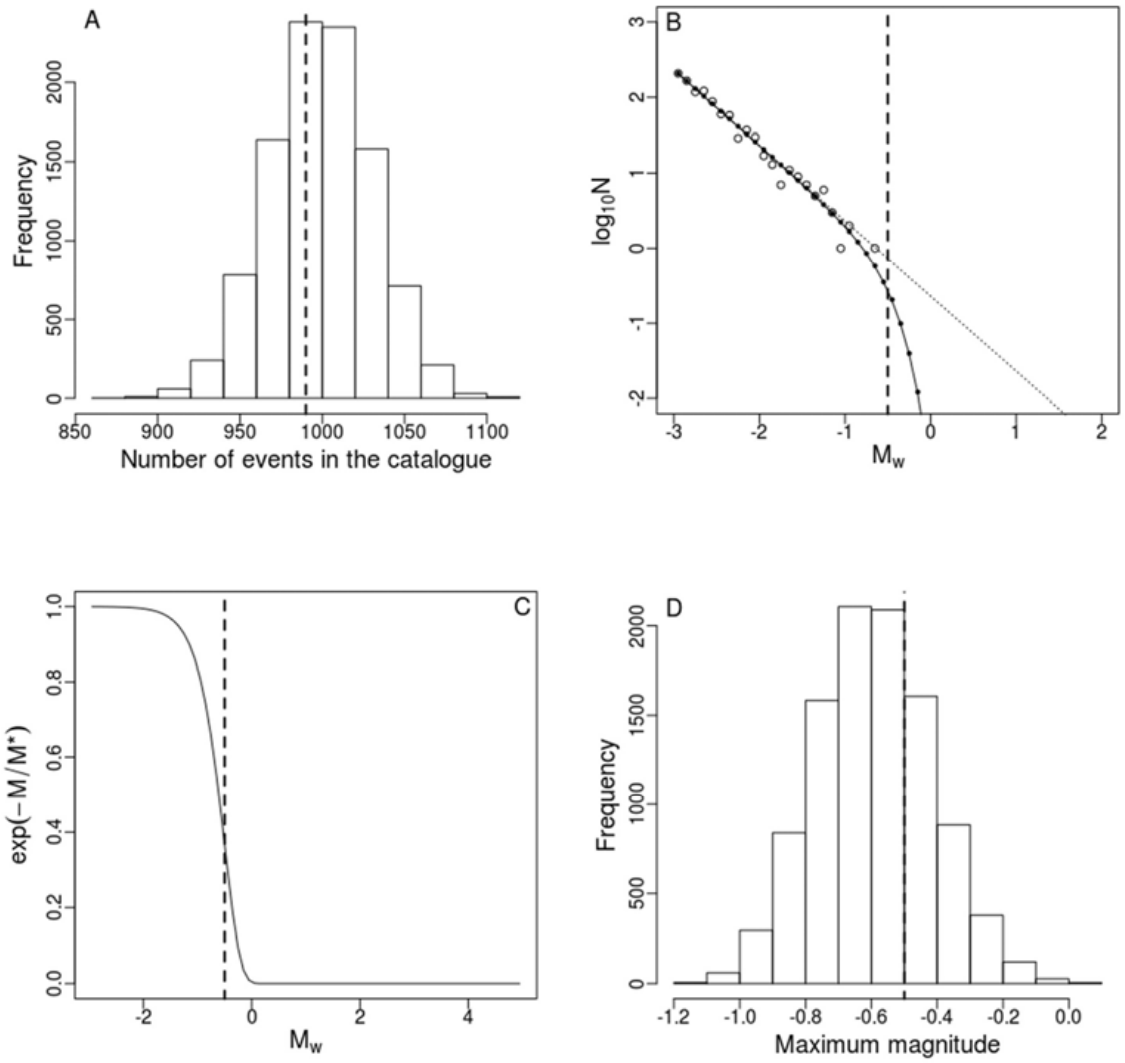

Figure 9.7. Monte Carlo Simulations. (a) Histogram showing the number of events in each of 10,000 Monte Carlo simulations $\langle N \rangle = 990$ events. (b) The model used for the distribution of magnitudes. The Gutenberg-Richter distribution has $a = 0.0$ and $b = 1.0$ and the exponential distribution has $M_w^* = -0.5$. We consider events above $M_{w,min} = -3$.The solid line shows the model frequency magnitude distribution (E2.2). The dotted line shows the perfect power law Gutenberg-Richter relation, without the roll off. The solid points show the mean of 10,000 Monte Carlo simulations of the number of events per magnitude interval in each synthetic catalogue. The open points show one sample catalogue from this distribution. The vertical dashed line shows M_w^*. (c) The solid line shows the value of the exponential function with magnitude. The vertical dashed line shows M_w^*. (d). A histogram of the maximum observed magnitude in each of 10,000s.synthetic catalogue.

We can see the gamma distribution (Equation 9.2) diverges from the GR distribution above about $M \sim -1$ FIgure 9.7a) and the expected number of events falls very quickly to zero, below $M = 0$. The form of the exponential function is shown in Figure 9.7c. A particular advantage of using a gamma distribution is that the distribution does not have a sharp cut-off at M_w^*. It is more realistic that the events should be "thinned" with respect to GR than that there should be no events above M_w^* at all.

While the individual synthetic catalogue in B shows a lot of scatter, particularly at larger magnitudes (which is what we are interested in), the mean values for all the samples converge to the model values; the distribution is well sampled by 10,000 Monte Carlo simulations.

Finally, we can see from Figure 9.7d that the maximum magnitudes in the catalogues show a distribution around M_w^*. We would expect some scatter of maximum magnitudes below M_w^* even with a sharp magnitude cut-off, since the larger magnitudes are so poorly sampled in each catalogue (not all catalogues reach the maximum possible magnitude). The scatter above M_w^* in this case, however, is a feature of the "soft" cut-off of the gamma distribution; we consider this to be the more realistic scenario of the two. Note that despite the scatter, there is a well-defined peak around M_w^* in the simulations. The probability of large events gets very small quickly above M_w^*. For the GR distribution the maximum magnitude is distributed as a power law above about $M = M^{*GR} \approx a/b$, the magnitude at which the expected frequency is only 1. There is no well-defined maximum magnitude in the GR. Conversely, if we were to reduce the magnitude roll-off to some value where the number of GR expected events is significantly greater than 1, so that the roll-off has a very obvious effect on samples at larger magnitudes, we would find the maximum observed magnitude is well-defined, with a small uncertainty.

For these simulated catalogues, we now investigate the distribution of fracture lengths. These lengths cannot be forecast individually, since they depend on unknowns such as local heterogeneity or anisotropy in the material properties. This method allows us to account for uncertainties due to this unknown variability in the rupture lengths of events of a given magnitude. The variability is reflected in the uncertainties in the parameters of the WC94 empirical relations. Monte Carlo methods allow us to estimate the effect of these uncertainties on estimates of the fracture lengths.

Figure 9.8a shows the frequency-fracture length distribution for the simulation. Again we see that individual catalogues do not sample the distribution well, but the mean properties of all the Monte Carlo simulations do much better. The roll-off above $L^* = 1.84\mathrm{m}$ (calculated by substituting M_w^* into the empirical relation in E3.1) is clear. However, there is still some noise in the mean values for the frequency of very large fracture lengths. This is a result of both the small numbers of large magnitude events and the increasing uncertainties with large L. Larger numbers of Monte Carlo simulations would improve the convergence, but the probabilities are very low, so this is unlikely to be worth the extra computation.

To produce the cumulative distribution (in probability density form) in Figure 9.8b, we take the mean number of events n_i in each interval i of fracture length in 3.2A and calculate $\Lambda_i = \sum_{k=i}^{\infty} n_k$ (analogous to the cumulative frequency magnitude distribution). Then,

$$\Pr(L_i | M_w^*) = 1 - \mathrm{e}^{-\Lambda_\mathrm{i}}$$

We find that probabilities approach 1 for very small fracture lengths; many small fractures are generated in every injection. This probability falls off rapidly to less than 0.3 above L^* and is close to zero above $L = 5\mathrm{m}$ (we say close to zero, since the Monte Carlo sampling has not resolved probabilities for extremely rare, very large fractures). The histogram of the maximum fracture length in Figure 9.8c shows a long tail above the value of L^*, resulting both from the tail in the distribution of maximum magnitude and in the additional uncertainties in the fracture length scaling relations.

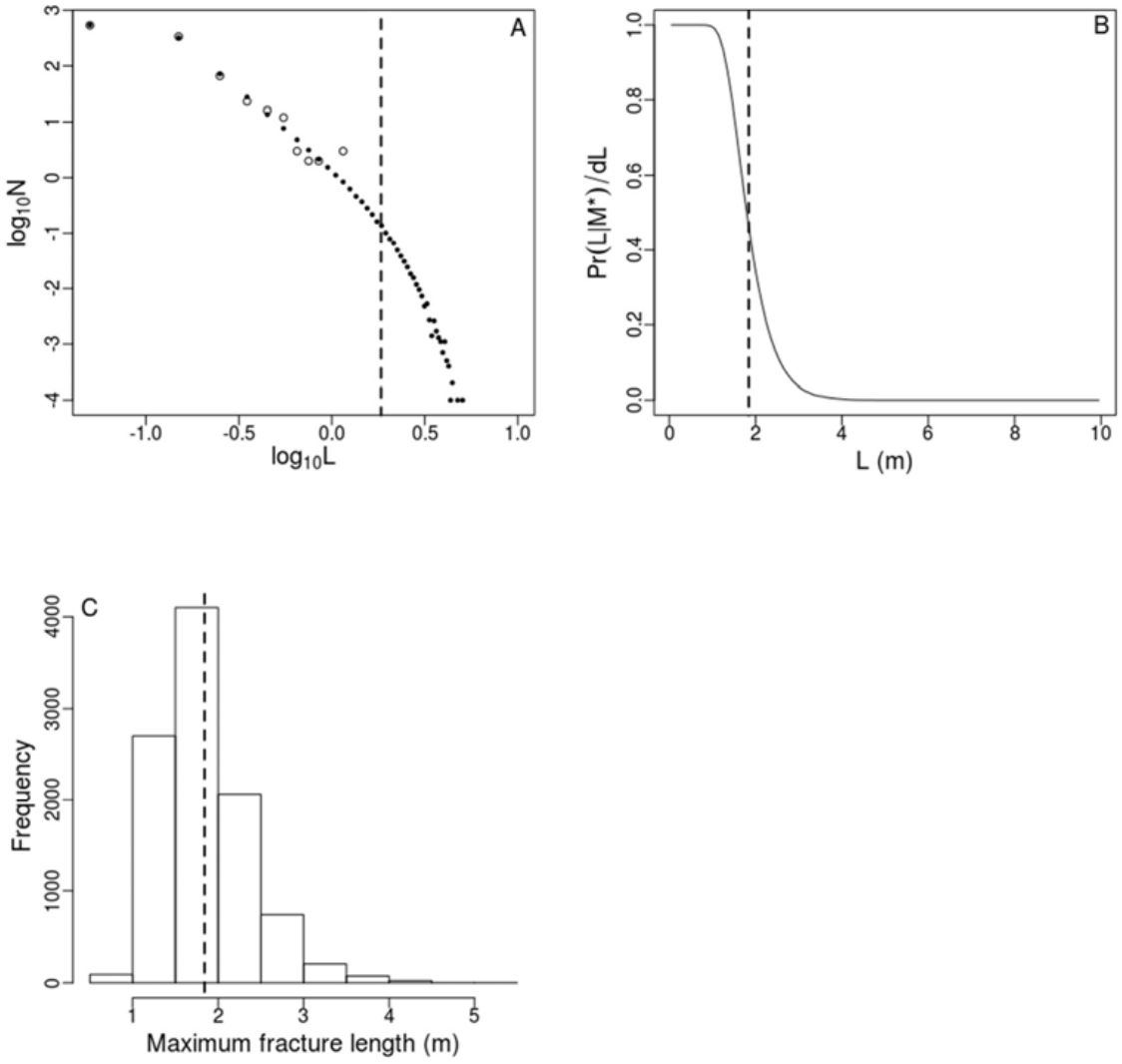

Figure 9.8. Monte Carlo Simulations. (a) Solid points show the mean of 10,000 Monte Carlo simulations of the number of events in each interval of fracture length, in each synthetic catalogue. The open points show one sample catalogue from this distribution. The vertical dashed line shows the value of L^*, calculated by substituting M_w^* into Equation 9.1. (b) The solid line shows the probability for the fracked seismicity catalogue to have an event of greater than length L, as a function of L.

A key conclusion is that there is a well-defined upper bound on the fracture length because there is a roll-off in the frequency magnitude distribution. This would not be clear with GR distributed fractures.

Finally, these results can be scaled up to larger projects, for example, if the same conditions were maintained for a longer duration. If this synthetic project were extended for several thousand hours at constant seismicity rate, for example, there would be around a million events of $M > -3$ expected (we would not simulate all these, necessarily, since the small events do not contribute significantly to the total fractured length). For $M_w^* = 3.0$ ($L^* = 220\mathrm{m}$), which is closer to what is expected for the upper magnitude limit on real fracked events, and $M_{w,\min} = 0.0$, the fracture distributions look qualitatively similar to those in Figure 9.8, but with a shift upwards in length, so that the maximum fracture lengths are as large as several hundred metres.

9.3.3 Discussion

Again, since forecasts depend on detailed local knowledge of the relevant geology and underlying seismicity rates, much of which will not be available on the short term, we have been able to go only as far as developing the protocol for a forecast. These results do not therefore constitute a forecast for fracture lengths from hydraulic fracturing in Ireland.

We have dealt only with fracked earthquakes in this report and not with triggered events. This report does not say anything about maximum magnitudes for triggered events and therefore does not relate to the seismicity hazard from fracking. There is no evidence that triggered seismicity has a definable maximum magnitude at any scale relevant to hydraulic fracturing projects.

The well-defined upper magnitudes and fracture lengths in this report result from the magnitude roll-off introduced into the Gutenberg-Richter relation for the frequency-magnitude scaling. In reality, the nature of the frequency magnitude distribution at the upper magnitude limits is not well understood. There are physical reasons to suggest there should be an upper magnitude for fracked seismicity. However, in practice, it is very difficult to demonstrate robustly from the data that this is a good model for the magnitudes of real events, partly because of the difficulties in separating triggered from fracked earthquakes. It may be that GR is the better model on the short term and in the early stages of projects, until the frequency magnitude scaling is clearer. This would result in higher forecast probabilities for large fracture lengths for a given injection.

We note that where large events have occurred in previous projects, they have been attributed to triggering of frictional sliding on faults which have been identified retrospectively (e.g. Clarke *et al*., 2014) thus retrospectively introducing a deterministic component to make the large event "special". In general, while anecdotal reports suggest a break in scaling between fracked events, which are not reported, and triggered events which occasionally are, it is only by the careful examination of the full frequency magnitude distribution for a project that any conclusion can be drawn. These are not normally published and the data are not normally available. We therefore include estimates from two scenarios M*=1.0 and M*=3.0. Observations from many treatments in the US would suggest the former, where the length of individual fractures makes little contribution to the upward extent of fracture permeability; reports of large events associated with specific fracking projects, however, allow the later. The roll-off in the frequency magnitude scaling here has not been clearly demonstrated in either case though is more feasible for M*=1.0.

We have assumed throughout that values for $\langle N \rangle$, a, b and M_0^* will come from real-time operational monitoring of the fracked seismicity (with possible initial estimates from the baseline). This is important a) because of the time dependence of the injection and of the diffusion of fluid through an unknown pre-existing fracture network, which determine the seismicity rates and b) because the frequency-magnitude scaling is likely to be difficult to determine robustly.

9.4 Conclusions and Recommendations

We have reviewed the literature on the fractures associated with unconventional hydrocarbon recovery by fracking and have shown that microseismic observations are likely to provide a reasonable guide to the distribution of fracturing activity surrounding any particular well. We then argue that estimates of likely fracture heights are given by the addition of the likely length of fractures associated with these microseismic events. We then developed a protocol to forecast the distribution of hydraulic fracture dimensions from a known magnitude distribution using empirically determined scaling relations between earthquake magnitude and rupture length. The parameters used for the stochastic model here are for illustration; they should be replaced by values determined firstly from the baseline survey and then further updated in near-real-time during any fracking operation.

There are a number of key conclusions from the results:

- Data from tiltmeters provides clear evidence that vertical fractures can propagate into shallow depths where they might interact with aquifers;
- Inspection of the vertical extent of microseismic activation shows that the vertical extent of fracturing is likely to be insensitive to frack depth;
- Data show that the distribution of distance of microseismic events from the perforation is skewed to shallow depths but support the conclusion that 95% of N. American projects had worst case events less than 300m above the perforation;
- Variability in microseismic magnitude appears to be controlled by sub-horizontal layering and is largely insensitive to frack depth;
- There is no well-defined maximum magnitude for events following a GR frequency magnitude distribution for all seismicity induced by fracking;
- If, as is suggested for fracked (not triggered) seismicity which is responsible for increased vertical permeability, there is a roll-off in the frequency magnitude distribution, a well-defined upper magnitude limit exists. However, this limit is, in general, "soft", meaning that for any particular project, there will be an uncertainty in the maximum observed magnitude;
- The nature of these uncertainties depend on the value of M^*. If M^* is small, then the upper limits of the magnitude distribution will be well sampled and the maximum observed magnitude will have small uncertainty. Large values of M^*, on the other hand, lead to GR behaviour, with no definable maximum magnitude;
- As well as the uncertainties from poor sampling of the upper magnitudes in power law distributions, the rupture lengths have additional large uncertainties from the empirical relations, which reflect, mainly, unknown variability in the material properties;
- Fracture lengths show a strong decrease in probability above L^*, suggesting that gamma distributed magnitudes lead to well-defined (although "soft") upper limits on the fracture length (again, depending on the size of M^*). However, there is a relatively long tail on the distribution, suggesting that there are very rare large events;
- Published data on fracked events resulting from thousands of treatments in the US suggest that M*=1.0 might be a realistic model for fracked seismicity. In this case the worst-case fractures would be on the order of 10m which implies a worst case vertical fracture extent of some 300m above the perforation;
- Results suggest that for $M^* = 3$ (which would be consistent with close to the worst case events in other areas), fracture lengths of up to several hundred metres are possible implying worst case vertical extent of some 500m above the perforation;
- The expectation value for the longest fracture would become more certain quickly after commencement of fracking, could be updated in near real time thereafter and could be included in any proposed traffic light system for governing the extraction;

- The top of a lithological unit, such as the top of the shale, would expect to provide a significant, though not impenetrable, barrier to upward fracture propagation particularly at shallow depths. This definitely moderates the threat of extreme fractures propagating to an aquifer far above the shale top;
- Given the unpredictability both of the location and magnitude of the worst microseismic event (in the sense that it produces the shallowest fracture) and the associated uncertainty in the length of the fracture it generates, the expected worst case vertical extent of fracturing is very uncertain;
- On the basis of this study, and remembering that the joint probability of a large event occurring at a great distance from the perforation, we conclude that we would have a realistic expectation ($p \approx 0.05$) of fractures approaching 300m but that fractures extending more than 500m above the perforation could occur in extremely rare cases.

9.5 Caveat

The arguments advanced in this section assume that the formation to be fracked does not contain permeable faults which connect the stimulated fractured rock volume with an overlaying aquifer. The argument used to support this assertion is that should such a fault exist there would be unlikely to be any gas remaining in the reservoir since it would have long since escaped through the open fracture. It seems to us that this is a spurious argument. Any open fault would only drain that volume of the rock to which it was connected either by connected porosity or by other fractures, providing the matrix permeability was very low this would likely only represent a very small percentage of the reservoir. During fracking the permeability of the entre volume is increased by a set of fractures whose density by design exceeds the percolation threshold (see for example Stauffer and Aharony, 1994) connecting any permeable thoroughgoing fault to the fracked volume and thereby potentially connecting the fracked volume to the surface. This potentially troublesome process has not been addressed in this study. We note, however, that the presence of such faults in the study areas cannot be determined from the available geological and geophysical, including seismic, data. The acquisition of 3D seismic data, detailed structural studies and the establishment of a high resolution seismic monitoring network may help to identify such faults and quantify the associated risks.

10 Conclusions

Unconventional Gas Exploration & Extraction (UGEE) involves hydraulic fracturing (fracking) of low permeability rock to permit the extraction of natural gas on a commercial scale from unconventional sources, such as shale gas deposits, coal seams and tight sandstone. The main aim of the UGEE Joint Research Programme is to further the understanding of potential impacts on the environment and human health from UGEE projects/operations.

Project A2: Seismicity of the JRP dealt with the baseline characterisation of seismicity, which is required to enable potential impacts to be assessed and involved 7 tasks.

10.1 Task 1: Assessment of Existing Baseline Monitoring Operated Worldwide for UGEE Projects/Operations

Assessing existing experience in UGEE projects suggests that baseline monitoring should be a basic key requirement of any future exploration and extraction, enabling background levels of seismicity to be reliably characterised and any unusual seismicity or active faults that could potentially be affected by operations identified. Baseline monitoring is essential to be able to differentiate between natural background earthquake activity and UGEE induced activity, allowing seismicity rates before, during and after operations to be reliably compared and any differences to be identified.

It is critical that baseline monitoring must be established prior to the commencement of any activity that is known to induce earthquakes. With the expected seismicity rate in Ireland to be low this presents a significant challenge, since it may require many decades of baseline monitoring to reliably determine the rates in each of the two study areas. However, it is important to test the assumption that seismicity rates are uniform across Ireland. Therefore, detailed monitoring will be required in each study area to detect any unusual seismicity that may suggest that seismicity rates are higher in the study areas, or that there is seismicity associated with any specific fault structure. One to two years may be an appropriate monitoring period for this purpose.

If an accepted level of confidence in data produced is to be gained than at least some of the background monitoring stations should remain installed through all phases of monitoring to ensure continuity and allow relative re-locations of seismicity and analysis of waveform similarity.

To enable a reliable and uniform detection of seismic events across a given area of interest requires a uniform distribution of monitoring stations. The density of the stations along with the noise levels at each station control the lowest magnitudes that can be reliably detected. Higher station densities will be required to detect and locate lower magnitudes. Noise levels at individual stations also affect detection capability, and these should be low in order to maximise detection potential. In addition, a monitoring network must also extend beyond the limits of the area of interest in order to be able to reliably detect earthquakes that occur close to these limits.

Reliable location and magnitude measurement places additional constraint on network design, since measurements at more stations are needed than for detection alone. In addition, location errors depend on the distribution and density of the recording stations. These errors may be large if the station density is insufficient, or if the closest stations are far from the earthquake source, which may limit the capability to discriminate between induced and natural earthquakes. Again, a uniform station density is required to ensure comparable location accuracy across the region of interest, with monitoring stations extending beyond the area of interest.

Extensive experience of seismic monitoring in the geothermal industry may be considered as “best practice” for UGEE. This will allow many of the methods used for the monitoring of earthquake activity along with

appropriate control measures for the mitigation of risks associated with induced earthquakes to be readily adopted. The case studies discussed in this report highlight the importance of an appropriate monitoring network for reliable detection and location of any seismic events before, during and after any operations that may induce seismic activity

10.2 Task 2: Evaluation of Methodologies for the Monitoring of Ground Deformation That May Be Associated with UGEE Projects/Operations

The factors affecting InSAR for ground motion monitoring in Ireland were addressed and the assessment has concluded that the technique is valid for the island of Ireland, and the study sites in Co. Clare and the Northwest Carboniferous Basin, in particular.

Ground deformation from UGEE projects/operations will not necessarily result in damage to structures but it is important to quantitatively monitor the motion at surface in order to gauge potential damage to structures, and to address potential concerns of the public and policy makers regarding impacts to the environment.

Available records indicate that PSI or SBAS methodologies should be viable. However, further analysis of the normal and temporal baselines of the image stacks should be done to verify whether interferometric phase correlation can be guaranteed.

Ongoing monitoring using InSAR techniques can be facilitated by a recently launched ESA satellite with a C-band radar sensor on board. It is acquiring data at the time of writing, and a sufficient volume will be available for InSAR analysis of Ireland by end 2015.

Visibility of the terrain by the satellite sensor is acceptable, with less than 0.01% of the landmass would be affected by shadow, and layover would affect 0.4% in each acquisition mode. Therefore >99.9% of the landmass is visible to the SAR satellites in at least one acquisition mode.

Over 90% of the island of Ireland consists of predominantly rural land cover types and would therefore have approximately relatively low numbers of persistent scatters which are essential for data interpretation. This would mean that InSAR would only be partly successful. Nevertheless, new analysis techniques, such as ISBAS, in non-urban environments are showing very positive results, increasing the number and density of scatterers. The increase offers significant advantages for the interpretation of ground motion and allows the identification of small areas of motion and also allows the edges of displacement areas to be more accurately defined (and interpreted). This makes it easier to relate the results to other datasets and hence increases understanding of the ground motion.

It was concluded that any UGEE projects operating in Ireland should be monitored using historic and current satellite radar data, processed to provide InSAR results with a technique such as ISBAS. The historic data will provide a baseline of surface millimetric motions back to 1992, confirming stability or otherwise of the surface prior to UGEE operations.

In combination with the InSAR technique, complementary *in situ* methods such as GNSS and tiltmeters could be deployed; research has shown that integrating the monitoring techniques provides better and more detailed information on deformation characteristics since each technique has advantages. A network of GNSS stations would provide data on regional surface motion, from the time at which the instruments are installed. Tiltmeters would provide complementary data on local micro-deformation and fracture propagation (if installed on the surface and downhole).

10.3 Task 3: Assessment of Existing Data on Natural Seismicity in the Island of Ireland

A review of published data confirmed that earthquake activity in Ireland is very low. Historical accounts of seismic events felt in Ireland amount to only twenty-six events in the interval 1500 to 1970 occurring in three localities: Wicklow, Wexford and the Irish Sea on the east coast; Donegal, in the north; and the south coast of Ireland around Cork.

Instrumental data confirm these low rates of seismic activity. Almost all the instrumental seismicity records are in areas where historical earthquakes have occurred. The exception to this is the magnitude 4.0 M_L earthquake off the coast of Mayo in 2012, which is the largest Irish event in the catalogue.

Calculated earthquake activity rates for Ireland were found to vary depending on the assumed level of completeness of the earthquake catalogue. Using the same catalogue completeness thresholds as for Britain suggests that there should be an earthquake with a magnitude of 4 M_W or greater, somewhere in Ireland and the surrounding offshore area, approximately every 476 years. This is reasonable agreement with the observed data. However, using a more conservative estimate of catalogue completeness leads to a higher activity rate, which would lead to significantly more earthquakes than observed. This highlights the problem of estimating reliable rates in low seismicity regions that allow seismic hazard to be reliably quantified. The average activity rate for Britain suggests that there should be an earthquake with a magnitude of 4 M_W or greater approximately every six years. The reasons for the dramatic difference remain remains poorly understood, given the geological and tectonic similarity between Ireland and Britain.

Modelled ground motions for earthquakes with moderate magnitudes that may occasionally occur in or around Ireland suggest that ground velocities are unlikely to exceed typical levels at which cosmetic damage might occur, except close to the earthquake source.

10.4 Task 4: Assessment of the Magnitude and Physical Effects of Induced Seismicity That May Be Associated with UGEE Projects/Operations in the Island of Ireland

A rigorous statistical forecast model has been developed based on state of the art understanding of triggering of induced seismicity. Current catalogues are completely inadequate for forecast modelling on these spatial scales. Here, the use of synthetic catalogues to represent hypothetical baseline scenarios allows the illustration of the nature of the uncertainties that might be expected, but does not allow specific forecasts from an injection at present. The uncertainties presented mean that robust estimates for basic hazard parameters are likely to be high in an area of very low seismicity; this will be the case even for the best realistic baseline.

The use of a homogeneous reference catalogue generates systematic errors in the parameter estimates. This problem can be minimised (but not solved) by a good quality baseline deployment and data analysis, to generate the best reference model possible. However, ultimately, detailed subsurface structural information will be required to understand this problem completely. The choice of fault network model has a first order effect on the success of the seismicity forecasts. Important information on the active structure could be obtained from detailed structural studies and also from any available high quality focal mechanisms of very well recorded earthquakes in the area. Monte Carlo methods may allow progress in this aspect of the problem, once preliminary catalogues are available to inform the simulations.

The model does not include uncertainties in earthquake locations and magnitudes or, for example, in any of the parameters of the CRS model, such as the fault frictional constants. The uncertainties presented here can therefore be considered as lower bounds on the uncertainties that can be expected from real seismic catalogues. While these errors are considered to be relatively minor compared to the issues discussed in this report, every effort to minimise them should be made from the best seismological and structural data.

The data requirements for good quality forecasts are significant and the specification of baseline networks are subject to external considerations; it is expected that some progress can be made with 2 years of monitoring data. Robust forecasts of the hazard-relevant parameters of induced catalogues can only be made using a high-quality network and current best practice in data analysis;

The low background rates of seismicity observed in current Irish catalogues has two contrasting implications:

- From a scientific perspective the data is unlikely to allow robust forecasts of the main parameters; and
- In terms of impacts it means that any hydraulic fracturing projects in Ireland are extremely unlikely to have any potentially troublesome seismic consequences.

However, this conclusion will require confirmation by examination of good quality baseline catalogues.

10.5 Task 5: Technical Specification for Sub-regional Seismic Baseline Monitoring

The study evaluated the detection threshold of existing seismic networks in Ireland to assess if they are sufficient to detect and locate all local earthquakes with magnitudes ML ≥ 0.5 in the NW Carboniferous Basin (NCB) and the Clare Basin (CB). If the existing seismic networks are insufficient for baseline monitoring in these two areas the characteristics of suitable local seismic networks were to be identified.

It was concluded that the Irish National Seismic Network (INSN) and the UCD Waveobs network are not sufficient to detect and locate all local earthquakes with magnitudes ML ≥ 0.5 in the two study areas.

Local networks with inter-station spacing between 15 and 25 km are required to reliably locate all such events during the proposed baseline study, which should operate for at least two years. This would require the deployment of at least 12 seismometers in the NCB and 10 seismometers in the CB.

Example network geometries were designed to enable the detection and location of all events with ML ≥ 0.5 during periods of elevated seismic background noise conditions, for example during stormy weather. The network capability is expected to yield a threshold between ML = –0.25 and ML = 0 during periods of average seismic noise levels.

Unless an event occurs within a distance of less than two focal depths from a station, reliable focal depth estimations are expected only for events with depths larger than 10km. Improving the depth accuracy by increasing network station density is not practical for a baseline network. Such an effort would also be hampered by the lack of high resolution seismic velocity models for the two study areas.

The network should comprise good quality 3-component broadband seismometers with a flat velocity response up to 100 Hz, a dynamic range of at least 140 dB at 1Hz and instrument self-noise below the Peterson New Low Noise Model (NLNM; Peterson, 1993) for signal frequencies between 0.017 and 10 Hz. The seismometer installations should comply with international best practice.

Borehole seismometer installations were not recommended for the baseline study. However, in the complete absence of bedrock or stiff soil over a significant part of the area of interest, some shallow borehole sensors may be required. The seismometers should be installed directly on bedrock to minimise the effect of seismic noise. Sites in stiff overburden should be chosen if bedrock sites cannot be realised. Installation methods should follow international best practice to ensure good data quality.

It was recommended that the network should be deployed and operated by a commercial entity.

Data from the proposed baseline network should be integrated with the National Data Centre (NDC) operated as part of the Irish National Seismic Network (INSN). The data analysis should follow international best practice in routine seismological observatory operation. The resulting earthquake catalogue together with the seismic raw data should be made publicly available via the NDC to ensure transparency.

10.6 Task 8: Examination of Global Experience of Seismic Events stimUlated by UGEE Operations

The process of hydraulic fracturing in order to increase the permeability of reservoir formations and stimulate the recovery of hydrocarbons is generally accompanied by microseismicity, usually defined as earthquakes with magnitudes of 2 or less, that are too small to be felt. Two types of induced events can be defined: “fracked” events, whose size is constrained by the energy of the injection process; and “triggered” events, whose size depends largely on the amount of stored up elastic strain energy already in the rocks. The “fracked” events are caused by the formation and growth of new cracks and fractures in a previously intact rock mass as a result of the injection of high pressure fluids. The “triggered” events are a result of both presence of high pressure fluid and the stress perturbation caused by the fluid, which changes the effective stress on pre-existing faults, causing them to fail. These earthquakes can be “triggered” by very small stress perturbations, however, the potential for such events depends very much on the geological context and, given the low levels of background seismicity, the probability of large triggered in Ireland can be considered as small.

The general consensus among most authors is that the process of hydraulic fracturing a well as presently implemented for shale gas recovery does not pose a high risk for inducing either felt, damaging or destructive earthquakes. Experience in the USA, where many thousands of stimulations have been carried out suggest that the magnitudes of the induced earthquakes in reservoirs such as the Barnett and Marcellus Shales are typically less than 1 Mw. However, it should be pointed out that most sites of UGEE operations lack independent instrumentation for monitoring induced seismicity and that earthquakes with magnitudes of 2.5 or less will fall below the detection thresholds of regional seismic monitoring networks. Earthquakes of this size are unlikely to be felt or even detected unless local seismic monitoring networks are in place.

There are at least five documented examples of earthquakes with magnitudes greater than 2 that have been conclusively linked to hydraulic fracturing for shale gas exploration/recovery. These were in: Blackpool, UK in 2011; Garvin County, South-Central Oklahoma in 2011; Horn River, Canada in 2011; Montney Trend in 2013/14 where the largest had a magnitude of 4.4 Mw and to date, is the largest known earthquake triggered by hydraulic fracture operations in a hydrocarbon field anywhere in the world; and near Crooked Lake, Alberta, Canada in 2013/14 (earthquake activity has continued in this region and a magnitude 4.4 earthquake in 2016 is also suspected to be due to hydraulic fracturing).

It is likely that an earthquake similar in magnitude to the largest such events (4.4 MW) would be strongly felt and could even cause some superficial damage. In addition, if an earthquake of such a magnitude were to occur in Ireland where felt seismicity is very rare it would be likely to cause rather more concern among the local population than it would in other parts of the world where earthquakes of this magnitude are more frequent, However, the maximum magnitudes observed in Blackpool and Garvin County would be unlikely to cause any damage, although they could be felt by people close to the epicentre and may cause some concern.

There are large uncertainties in forecasting seismicity in areas such as Ireland where the background activity rates are low. However, although it is difficult to quantify, the probability of significant triggered seismicity depends strongly on the prior activity of the area. As a result, significant events are very unlikely in areas such as Ireland where the background seismicity rate is extremely low, and there is no evidence to suggest that the process of hydraulic fracturing for shale gas recovery poses a higher risk for inducing earthquakes than in other parts of the world. This risk may be further reduced by effective mitigation.

By contrast, the growing body of evidence of changes in observed seismicity rates and significant earthquakes linked to long term disposal of waste water from the hydrocarbon and other industries, suggests that this activity may pose a rather greater seismic risk. Earthquakes with magnitudes comparable to the magnitude 5.7 earthquake in Prague, central Oklahoma have a non-negligible contribution to the seismic hazard in such regions and should be considered in any long term assessments of seismic hazard.

Experience of induced seismicity in Enhanced Geothermal Systems have led to a series of measures to address induced seismicity that may be considered as "industry best practice", and, as such, may be considered appropriate for mitigating the risk of induced seismicity in UGEE operations. For example, an operational traffic light system linked to real-time monitoring of seismic activity is an essential mitigation strategy that will also need to accompany any UGEE operations in Ireland. This will require the definition of acceptable thresholds for the cessation and recommencement of operations and these should be based on levels of ground motion which may represent a hazard or a public nuisance. Existing regulatory guidelines for ground vibrations caused by blasting could also provide a useful framework for this purpose. The direct use of ground motion thresholds rather than derived magnitudes may, in some case, be preferable. Other means of mitigating earthquake risk may require improved understanding of the Earth's sub-surface in areas of unconventional hydrocarbon potential, such as better characterisation of existing fault zones, which may be difficult to achieve without detailed geophysical surveying.

Controlling factors on seismicity induced by hydraulic fracturing include: the strength of rocks in the geological formations of interest; the size and state of stress of any faults in the area likely to be affected by fluid injection; and, the pressure change induced by the hydraulic fracture process. The pre-existing state of stress on a fault determines how close it is to failure, so faults that are critically stressed may require only a small stress perturbation to cause them to fail. The pressure change induced by the hydraulic fracture process is mainly controlled by the volume of injected fluid and the rate of injection, where larger volumes and higher injection rates generate higher pressures. Recent work suggests that maximum magnitude is related to the total volume of injected fluid.

There remain a number of gaps in our existing knowledge of induced seismicity. For example, pre-existing state of stress and pore pressure acting on a fault are usually unknown. We also often lack knowledge about the hydrological properties of the sub-surface. Measuring the initial stress state and pore pressure, tracking the injection history, and careful seismic monitoring may help improve understanding.

10.7 Task 9: Assessment of Pre-fracturing Modelling Techniques

The literature on the fractures associated with unconventional hydrocarbon recovery by fracking was reviewed and it was shown that microseismic observations are likely to provide a reasonable guide to the distribution of fracturing activity surrounding any particular well. Estimates of likely fracture heights are given by the addition of the likely length of fractures associated with these microseismic events.

A protocol was developed to forecast the distribution of hydraulic fracture dimensions from a known magnitude distribution using empirically determined scaling relations between earthquake magnitude and rupture length. The parameters used for the stochastic model are for illustration and should be replaced by values determined firstly from the baseline survey and then further updated in near-real-time during any fracking operation.

Data from tiltmeters provides clear evidence that vertical fractures can propagate into shallow depths where they might interact with aquifers. Inspection of the available data shows that the vertical extent of fracturing is likely to be insensitive to frack depth. The distribution of distance of microseismic events from the perforation is skewed to shallow depths but support the conclusion that 95% of N. American projects had worst case events less than 300m above the perforation.

Variability in microseismic magnitude appears to be controlled by sub-horizontal layering and is largely insensitive to frack depth. There is no well-defined maximum magnitude for all seismicity induced by fracking. If, as is suggested for fracked (not triggered) seismicity which is responsible for increased vertical permeability, there is a roll-off in the frequency magnitude distribution, a well-defined upper magnitude limit exists. However, this limit is, in general, "soft", meaning that for any particular project, there will be an uncertainty in the maximum observed magnitude. As well as the uncertainties from poor sampling of the upper magnitudes in power law distributions, the rupture lengths have additional large uncertainties from the empirical relations, which reflect, mainly, unknown variability in the material properties.

The modelling suggests a well-defined (although "soft") upper limit on the fracture length. However, there is a relatively long tail on the distribution, suggesting that there are very rare large events. Based on parameters derived from data on thousands of fracked events in the USA the worst-case fractures would be on the order of 10m which implies a worst case vertical fracture extent of some 300m above the perforation.

Using parameters from close to the worst case events results in fracture lengths of up to several hundred metres being possible, implying worst case vertical extent of some 500m above the perforation. The expectation value for the longest fracture would become more certain quickly after commencement of fracking, could be updated in near real time thereafter and could be included in any proposed traffic light system for governing the extraction.

The top of a lithological unit, such as the top of the shale, would expect to provide a significant, though not impenetrable, barrier to upward fracture propagation particularly at shallow depths. This definitely moderates the threat of extreme fractures propagating to an aquifer far above the shale top. Given the unpredictability both of the location and magnitude of the worst microseismic event (in the sense that it produces the shallowest fracture) and the associated uncertainty in the length of the fracture it generates, the expected worst case vertical extent of fracturing is very uncertain. On the basis of this study, and remembering that the joint probability of a large event occurring at a great distance from the perforation, it was concluded that there is a realistic expectation of fractures approaching 300m above the perforation, but that fractures extending more than 500m above the perforation could occur in extremely rare cases.

Finally, it should be noted that seismological methods alone cannot discriminate between man-made and natural tectonic earthquakes. This strengthens the case for site specific seismic monitoring and detailed recording of injection parameters, to reduce uncertainties in earthquake locations and to compare the temporal evolution of seismic activity with any hydraulic fracture operations.

10.8 Data Gaps

It should be noted that seismological methods alone cannot discriminate between man-made and natural tectonic earthquakes. This strengthens the case for site specific seismic monitoring and detailed recording of injection parameters, to reduce uncertainties in earthquake locations and to compare the temporal evolution of seismic activity with any hydraulic fracture operations. Understanding of the hazard from induced earthquakes for a specific site would benefit from the following additional data:

- Improved earthquake catalogues that can be used to determine reliable estimates of background activity rates and that allow the discrimination and forecasting of induced seismic activity. This will require improved monitoring and observation;
- Geological and geophysical data that can be used to map sub-surface fault systems in high resolution, measure the orientation and magnitude of the stress field, and determine the hydrological properties of the sub-surface. This would be expected to be part of the operator’s exploration activities.

- Industrial data from proposed hydraulic fracturing operations such as injection rates, volumes and downhole pressures. Again, this would be expected to be part of the operator's exploration activities.

Operational monitoring arrays could be implemented independently, but the data should be openly available to maintain public confidence and form part of the national database.

References

Abrahamson, N.A., Atkinson, G.M., Boore, D.M. *et al*., 2008. Comparisons of the NGA ground–motion relations. *Earthquake Spectra* 24: 45–66.

Ake, J. and Mahrer, K., 2005. Deep-injection and closely monitored induced seismicity at Paradox Valley, Colorado. *Bulletin of the Seismological Society of Am*erica 95: 664–683.

Aki, K. and Richards, P.G., 2002. *Quantitative Seismology*. University Science Books, Sausalito, CA.

Akkar, S. and Bommer, J.J., 2010. Empirical equations for the prediction of PGA, PGV and spectral acceleration in Europe, the Mediterranean region and the Middle East. *Seismological Research Lett*ers 81: 195–206.

Bachmann, C.E., Wiemer, S., Wössner, J. *et al*., 2011. Statistical analysis of the induced Basel2006 earthquake sequence: introducing a probability-based monitoring approach for Enhanced Geothermal Systems, *Geophysical Journal International* 186: 793–807.

Baillard, C., Crawford, W.C., Ballu, V. *et al*. 2014. An automatic kurtosis-based P- and S-phase picker designed for local seismic networks. *Bulletin of the Seismological Society of America* 104: 394–409.

Baisch, S. and Voros, R., 2011. *Geomechanical Study of Blackpool Seismicity*. Q-Con report for Cuadrilla.

Barton, C.C. and Scholz, C.H., 1993. *The Fractal Size and Spatial Distribution of Hydrocarbons: Implications for Resource Assessment and Exploration Strategy*. US Geological Survey Administrative Report. Springer US, Springer Science+Business Media, New York NY.

Barton, C.C., Larsen, E., Page, W.R. *et al*., 1993. *Characterizing Fractured Rock for Fluid-flow, Geomechanical, and Paleostress Modeling: Methods and Results from Yucca Mountain, Nevada*. US Geological Survey Open-File Report 93-269. USGS, ESIC, Reston, VA.

Barton, C.A., Zoback, M.D. and Moos, D., 1995. Fluid flow along potentially active faults in crystalline rock. *Geology* 23: 683–686.

Baptie, B., 2010. Seismogenesis and state of stress in the UK. *Tectonophysics* 482: 150–159.

Baptie, B., 2012. *UK Earthquake Monitoring 2011/2012: Twenty-third Annual Report*. British Geological Survey Commissioned report, OR/12/092, British Geological Survey, Edinburgh.

Baptie, B., Jordan, C., Mosca, I. *et al*., 2015. *Project A2: Interim Report A2.1 (Tasks 1, 2, 3 and 4)*. 2014-W-UGEE-1. Environmental Protection Agency, Johnstown Castle, Ireland.

Baria, R. and Green, A.S.P., 1990. Microseismics: a key to understanding reservoir growth. In *Proceedings, Camborne School of Mines International Hot Dry Rock, Conference, 27–30 June 1989*. Robertson Scientific Publications, London, pp. 363–377.

Bateson, L., Cigna, F., Boon, D. *et al*., 2014. The application of the Intermittent SBAS (ISBAS) InSAR method to the South Wales Coalfield, UK*. International Journal of Applied Earth Observation and Geoinformation* 34: 249–257.

Båth, M., 1965. Lateral inhomogeneities in the upper mantle. *Tectonophysics* 2: 483–514.

BC Oil and Gas Commission, 2012. *Investigation of Observed Seismicity in the Horn River Basin.* Available online: https://www.bcogc.ca/node/8046/download (accessed May 2016).

Bean, C.J. and McCloskey, J., 1995. Seismic constraints on statistical models for upper crustal heterogeneity. *First Break* 13: 105–110.

Bean C.J. and McCloskey, J., 1993, Power-law random behaviour of seismic reflectivity in boreholes and its relationship to crustal deformation models. *Earth and Planetary Science Letters* 117: 423–429.

Berardino, P., Fornaro, G., Lanari, R. *et al*., 2002. A new algorithm for surface deformation monitoring based on small baseline differential SAR interferograms. *IEEE Transactions on Geoscience and Remote Sensing* 40: 2375–2383.

Bommer, J.J., Oates, S., Cepeda, J.M. *et al.*, 2006. Control of hazard due to seismicity induced by a hot fractured rock geothermal project. *Engineering Geology* 83: 287–306.

Bommer, J.J., Stafford, P.J., Alarcón, J.E. *et al*., 2007. The influence of magnitude range on empirical ground-motion prediction. *Bulletin of the Seismological Society of America* 97: 2152–2170.

Boore, D.M., 1983. Stochastic simulation of high-frequency ground motion based on seismological models of the radiated spectra. *Bulletin of the Seismological Society of America* 73: 1865–1894.

Boore, D.M., 2003. Simulation of ground motion using the stochastic method, *Pure and Applied Geophysics* 160: 635–675.

Boore, D.M., 2005. *SMSIM – Fortran Programs for Simulating Ground Motions from Earthquakes: Version 2.3 – A Revision of OFR 96-80-A*. Technical report, US Department of the Interior, US Geological Survey, Menlo Park, CA.

Borick, C., Lachapelle, E. and Rabe, B. (eds), 2014. *Proceedings from IPSA World Congress – Montréal 2014: The great divide: An examination of public perceptions of shale gas extraction and hydraulic fracturing in New York and Pennsylvania*. IPSA, Montréal. Available online: http://paperroom.ipsa.org/papers/view/31102

Bormann, P., Klinge, K. and Wendt, S., 2009. Data analysis and seismogram interpretation. In Bormann, P. (ed), *New Manual of Seismological Observatory Practice (NMSOP-2)*. IASPEI, GFZ German Research Centre for Geosciences, Potsdam, Chapter 11.

Bradley, S.L., Milne, G.A., Teferle, F.N. *et al*., 2009. Glacial isostatic adjustment of the British Isles: new constraints from GPS measurements of crustal motion. *Geophysical Journal International* 178: 14–22.

Brodsky, E.E. and Lajoie, L.J., 2013. Anthropogenic seismicity rates and operational parameters at the Salton Sea Geothermal Field. *Science* 341(6145): 543–546.

Brudy, M., Zoback, M.D., Fuchs, K. *et al*., 1997. Estimation of the complete stress tensor to 8 km depth in the KTB scientific drill holes: implications for crustal strength. *Journal of Geophysical Research* 102: 18453–18475.

Brune, J.N., 1970. Tectonic stress and the spectra of seismic shear waves from earthquakes. *Journal of Geophysical Research* 75: 4997–5009.

Calero, J., De Carlos, A., Fretwell, B., *et al*., 2015. *Interim Report for Project C: Regulatory Framework for Environmental Protection, Environmental Impacts of Unconventional Gas Exploration & Extraction (UGEE), Prepared for the Environmental Protection Agency*. Environmental Protection Agency, Johnstown Castle, Ireland.

Castellaro, S., Mulargia, F. and Kagan, Y., 2006. Regression problems for magnitudes. *Geophysical Journal International* 165: 913–930.

Chiou, B.S.-J. and Youngs, R., 2008. A NGA model for the average horizontal component of peak ground motion and response spectra. *Earthquake Spectra* 24: 173–215.

Cigna, F., Bateson, L., Jordan, C.J. *et al*., 2014. Simulating SAR geometric distortions and predicting Persistent Scatterer densities for ERS-1/2 and ENVISAT C-band SAR and InSAR applications: nationwide feasibility assessment to monitor the landmass of Great Britain with SAR imagery. *Remote Sensing of Environment* 152: 441–466.

Clarke, H., Eisner, L., Styles, P. *et al*., 2014. Felt seismicity associated with shale gas hydraulic fracturing: the first documented example in Europe. *Geophysical Research Letters* 41: 8308–8314.

Cocco, M. and Rice, J.R., 2002. Pore pressure and poroelasticity effects in Coulomb stress analysis of earthquake interactions. *Journal of Geophysical Research* 107: 2156–2202,

Committee on Induced Seismicity Potential in Energy Technologies, Committee on Eart Resources, Committee on Geological and Geotechnical Engineering *et al*., 2012. *Induced Seismicity Potential in Energy Technologies.* National Academy of Sciences, Washington, DC. DOI: 10.17226/13355.

Cooper, M.A., Collins, D.A., Ford, M. *et al*., 1986. Structural evolution of the Irish Variscides. *Journal of the Geological Society of London* 143: 53–61.

Crosetto, M., Monserrat, O., Iglesias, R. *et al*., 2010. Persistent scatterer interferometry: potential, limits and initial C- and X-band comparison. *Photogrammetric Engineering and Remote Sensing* 76: 1061–1069.

Daneshy, A.A., 1978. Hydraulic fracture propagation in layered formations. *Society of Pertoleum Engineers Journal* 18.

Dardis, O. and McCloskey, J., 1998a. Lattice Boltzmann with real numbered solid density for the simulation of flow in porous media. *Physical Review E* 57: 4834–4837.

Dardis, O. and McCloskey, J., 1998b. Permeability porosity relationships from numerical simulations of fluid flow. *Geophysical Research Letters* 25: 1471–1474.

Davis, S.D. and Frohlich, C., 1993. Did (or will) fluid injection cause earthquakes? Criteria for a rational assessment. *Seismological Research Letters* 64: 207–224.

Davis, S.D. and Pennington, W.D., 1989. Induced seismic deformation in the Cogdell oil field of west Texas. *Bulletin of the Seismological Society of America* 79: 1477–1495.

Davies, R., Foulger, G., Bindley, A. *et al*., 2013. Induced seismicity and hydraulic fracturing for the recovery of hydrocarbons. *Marine and Petroleum Geology* 45: 171–185.

Davison, C., 1919. The Stafford earthquakes of January 14–15, 1916 and the relations between twin earthquakes of the Midland counties. *Geological Magazine* Decade VI, 6: 302–312.

Davison, C., 1924. *History of British Earthquakes*. Cambridge University Press, Cambridge.

de Pater, H. and Baisch, S., 2011. *Geomechanical Study of Bowland Shale Seismicity*. Synthesis Report. British Geological Survey, Nottingham, UK.

de Pater, H. and Pellicer, M., 2011. Geomechanical Study of Bowland Shale Seismicity – Fracture Geometry and Injection Mechanism. Cuadrilla Resources, Preston, UK.

Deichmann, N., 2006. Local magnitude, a moment revisited. *Bulletin of the Seismological Society of America* 96: 1267–1277.

Deichmann, N. and Giardini, D., 2009. Earthquakes induced by the stimulation of an enhanced geothermal system below Basel (Switzerland). *Seismological Research Letters* 80: 784–798.

Dieterich, J.H., 1994. A constitutive law for rate of earthquake production and its application to earthquake clustering. *Journal of Geophysical Research* 99: 2601–2618.

Dieterich, J.H., Cayol, V. and Okubo P., 2000. The use of earthquake rate changes as a stress meter at Kilauea volcano. *Nature* 408: 457–460.

Dolan, S.S. and Bean, C.J., 1997. Some remarks on the estimation of fractal scaling parameters from borehole wire-line logs. *Geophysical Research Letters* 24: 1271–1274.

Dost, B., Caccavale, M., van Eck, T. *et al*., 2013. *Report on the Expected PGV and PGA Values for Induced Earthquakes in the Groningen Area*. KNMI. Available online: http://bibliotheek.knmi.nl/knmipubDIV/Report_on_the_expected_PGV_and_PGA_values_for_induced_earthquakes.pdf (accessed May 2016).

Douglas, J., 2007. On the regional dependence of earthquake response spectra. *ISET Journal of Earthquake Technology* 44: 71–99.

Duncan, P.M. and Eisner, L., 2014. Reservoir characterization using surface microseismic monitoring. *Geophysics* 75: 75A139–75A146.

Eisner, L., Janska, E. and Matousek, P., 2011. *Seismic Analysis of the Events in the Vicinity of the Preese Hall Well*. Seismic Report for Cuadrilla Resources, Prague, Czech Republic.

Ellsworth, W.L., 2013. Injection-induced earthquakes. *Science* 341: 142–151.

Evans, K.F., Zappone, A., Kraft, T. et al., 2012. A survey of the induced seismic responses to fluid injection in geothermal and CO_2 reservoirs in Europe. *Geothermics* 41: 30–54.

Evernden, J.F., 1969. Precision of epicenters obtained by small numbers of world-wide stations. *Bulletin of the Seismological Society of America* 59: 1365–1398.

Ferretti, A., Prati, C., and Rocca, F., 2001. Permanent scatterers in SAR interferometry. *IEEE Transactions on Geoscience and Remote Sensing* 39: 8–20.

Fisher, K. and Warpinski, N.R., 2011. Hydraulic fracture growth: real data, SPE 145949.Conference paper from SPE Annual Technical Conference and Exhibition, Denver, CO, 30 October–2 November.

Fisher, K. and Warpinski, N., 2012, Hydraulic fracture-height growth: Real data. *Society of Petroleum Engineers* 27: 8–19.

Flewelling, S.A., Tymchak, M.P. and Warpinski, N., 2013. Hydraulic fracture height limits and fault interactions in tight oil and gas formations. *Geophysical Research Letters* 40: 3602–3606.

Flinn, E.A., 1965. Confidence regions and error determinations for seismic event location. *Reviews of Geophysics* 3: 157–185.

Frisch, U., Hasslacher, B. and Pomeau, Y., 1986. Lattice-gas automata for the Navier–Stokes equation. *Physical Review Letters* 56: 1505–1508.

Frohlich, C., Hayward, C., Stump, B. *et al*., 2011. The Dallas–Fort Worth earthquake sequence: October 2008 through May 2009. *Bulletin of the Seismological Society of America* 101: 327–340.

Gaci, S., 2014. The use of wavelet-based denoising techniques to enhance the first-arrival picking on seismic traces. *IEEE Transactions on Geoscience and Remote Sensing* 52: 4558–4563.

Galloway, D.D., 2006. *Bulletin if British Earthquakes 2005*. British Geological Survey Internal Report IR/06/047. British Geological Survey, London.

Geiger, L., 1912. Probability method for the determination of earthquake epicenters from the arrival time only (translated from German). *St. Louis University Bulletin* 8: 56–71.

Giardini, D., 2009. Geothermal quake risks must be faced. *Nature* 462: 848–849.

Giardini, G., Woessner, J., Danciu, L. *et al*., 2013. Seismic Hazard Harmonization in Europe (SHARE): Online Data Resource. doi:10.12686/SED-00000001-SHARE. Available online: http://www.share-eu.org/node/57

Gill, W.D., 1962. The Variscan fold belt in Ireland. In Coe, K. (ed.), *Some Aspects of the Variscan Fold Belt*. Manchester University Press, Manchester, pp. 49–64.

Gillespie, P.A., Walsh, J.J, Watterson, J. *et al*. 2001. Scaling relationships of joint and vein arrays from the Burren, Co. Clare, Ireland. *Journal of Structural Geology* 23: 183–201.

GMI Geomechanics Services, 2011. Wellbore failure analysis and geomechanical modelling in the Bowland Shales, Blackpool, UK. Cuadrilla Resources, Preston, UK.

Gölke, M. and Coblentz, D., 1996. Origins of the European regional stress field. *Tectonophysics* 266: 11–24.

Green, C.A., Styles, P. and Baptie, B., 2012. *Preese Hall Shale Gas Fracturing Review and Recommendations for Induced Seismic Mitigation Report*. Report for DECC. Available online: https://www.gov.uk/government/uploads/system/uploads/attachment_data/file/15745/5075-preese-hall-shale-gas-fracturing-review.pdf (accessed May 2016).

Grejner-Brezzinska, D.A., Toth, C.K., Moafipoor, S. *et al*., 2005. Volcano deformation monitoring in Indonesia: status, limitations and prospects. In Tregoning, P. and Rizos, C. (eds), *Dynamic Planet: Monitoring and Understanding a Dynamic Planet with Geodetic and Oceanographic Tools*. IAG Symposium, Cairns, Australia, 22–26 August 2005. Springer, New York.

Grünthal, G. (ed.), 1998. *European Macroseismic Scale 1998*. Cahiers du Centre Européen de Géodynamique et de Séismologie Volume 15, Luxembourg.

Gupta, H.K., 1985. The present status of reservoir induced seismicity investigations with special emphasis on Koyna earthquakes. *Tectonophysics* 118: 257–279.

Gupta, H.K., 2002. A review of recent studies of triggered earthquakes by artificial water reservoirs with special emphasis on earthquakes in Koyna, India. *Earth-Science Reviews* 58: 279–310.

Gutenberg, B. and Richter, C.F., 1954. *Seismicity of the Earth and Associated Phenomena*, 2nd ed. Princeton University Press, Princeton, NJ..

Gutenberg, B. and Richter, C.F., 1956. Magnitude and energy of earthquakes. *Annals of Geophysics* 9: 1–15.

Hainzl, S., Enescu, B., Cocco, M. *et al*., 2009. Aftershock modelling based on uncertain stress calculations. *Journal of Geophysical Research* 114: 2156–2202.

Hanks, T.C. and Kanamori, H., 1979. A moment magnitude scale, *Journal of Geophysical Research* 84: 2348–2350.

Häring, M.O., Schanz, U., Ladner, F. *et al*., 2008. Characterisation of the Basel 1 enhanced geothermal system. *Geothermics* 37: 469–495.

Harper, T., 2011. Geomechanical analysis of the Worston Shale Microseismicity. Geosphere Report. Cuadrilla Resources, Preston, UK.

Havskov, J. and Alguacil, G., 2006. *Instrumentation in Earthquake Seismology*. Modern Approaches in Geophysics vol. 22, Springer, New York.

Havskov, J. and Ottemöller, L., 2010. *Routine Data Processing in Earthquake Seismology*. Springer, London.

Haering, D.K., Schanz, M.O., Ladner, U. *et al*., 2008. Characterisation of the Basel 1 enhanced geothermal system. *Geothermics* 37(5): 469–495.

Henry, C. and Das, S., 2002. Aftershock zones of large shallow earthquakes: fault dimensions, aftershock area expansion and scaling relations. *Geophysical Journal International* 147: 272–293.

Holland, A., 2011. Examination of possibly induced seismicity from hydraulic fracturing in the Eola Field, Garvin County, Oklahoma. Oklahoma Geological Survey, Norman, OK.

Holland, A., 2013. Earthquakes triggered by hydraulic fracturing in South-Central Oklahoma. *Bulletin of the Seismological Society of America* 103: 1784–1792.

Horleston, A., Stork, A., Verdon, J. *et al*., 2013. *Seismic Monitoring of Drilling Operations in Balcombe, West Sussex*. University of Bristol, Bristol.

Horner, R.B., Barclay, J.E. and MacRae, J.M., 1994, Earthquakes and hydrocarbon production in the Fort St. John area of northeastern British Columbia. *Canadian Journal of Exploration Geophysics* 30: 38–50.

Horton, S., 2012. Disposal of hydrofracking waste fluid by injection into subsurface aquifers triggers earthquake swarm in central Arkansas with potential for damaging earthquake. *Seismological Research Letters* 83: 250–260.

Hsieh, P.A. and Bredehoeft, J.S., 1981. A reservoir analysis of the Denver earthquakes: a case of induced seismicity. *Journal of Geophysical Research* 86: 903–920.

Hsieh, P.A., Shapiro, A.M., Barton, C.C. *et al*., 1993. Methods of characterizing fluid movement and chemical transport in fractured rock. In *Geological Society of America Field Trip Guidebook for the Northeastern United States*, vol. 2. Geological Society of America, Boston, pp. R1–R30.

Johnston, A.C., Coppersmith, K.J., Kanter, L.R. *et al*., 1994. *The Earthquakes of Stable Continental Regions*. TR-102261-V4, Electric Power Research Institute, Palo Alto, CA.

Kanamori, H. and Brodsky, E.E., 2004. The physics of earthquakes. *Reports on Progress in Physics* 67: 1429–1496.

Keilis-Borok, V.I., 1960. Investigation of the mechanism of earthquakes (translated from Russian). *Soviet Research in Geophysics* 4: 29.

Kerenan, K.M., Savage, H.M., Abers, G.A. *et al*., 2013. Potentially induced earthquakes in Oklahoma, USA: links between wastewater injection and the 2011 Mw 5.7 earthquake sequence. *Geology* 41: 699–702.

Kim, W.-Y., 2013. Induced seismicity associated with fluid injection into a deep well in Youngstown, Ohio. *Journal of Geophysical Research* 118: 3506–3518.

King, G., Stein, R. and Lin, J., 1994. Static stress changes and the triggering of earthquakes. *Bulletin of the Seismological Society of America* 84: 935–953.

Leonard, M., 2010. Earthquake fault scaling: self consistent relating of rupture length, width average displacement and moment release. *Bulletin of the Seismological Society of America* 100: 1971–1988.

Linker, M.F. and Dieterich, J.H., 1992. Effects of variable normal stress on rock friction: observations and constitutive equations. *Journal of Geophysical Research* 97: 4923–4940.

Lomax, A., Virieux, J., Volant P. *et al*., 2000. Probabilistic earthquake location in 3D and layered models: Introduction of a Metropolis-Gibbs method and comparison with linear locations. In Thurber, C.H. and Rabinowitz, N. (eds.), *Advances in Seismic Event Location*. Kluwer, Amsterdam, pp. 101–134.

Lomax, A., Michelini, A. and Curtis, A., 2009. Earthquake location, direct, global-search methods. In *Encyclopedia of Complexity and Systems Science, Part 5*. Springer, New York, pp. 2449–2473.

McCloskey, J., Nalbant, S., Steacy, S. *et al*., 2003. Structural constraints on the spatial distribution of aftershocks. *Geophysical Research Letters* 30: 1610.

McCloskey, J., Nalbant, S. and Steacy, S., 2005. Indonesian earthquake: earthquake risk from co-seismic stress. *Nature* 434: 291.

McGarr, A., 2014. Maximum magnitude earthquakes induced by fluid injection, *Journal Geophysical Research* 119: 1008–1019.

McNamara, D.E. and Boaz, R.I., 2011. *PQLX: A Seismic Data Quality Control System Description, Applications and User Manuals*. Open-File Report 2010-1292. US Geological Survey, Reston, VA.

Main, I.G. and Burton, P.W., 1984. Information theory and the earthquake frequency-magnitude distribution. *Bulletin of the Seismological Society of America* 74: 1409–1426.

Majer, E.L., Baria, R., Stark, M. *et al*., 2007. Induced seismicity associated with Enhanced Geothermal Systems. *Geothermics* 36: 185–222.

Majer, E.L., Nelson, J., Robertson-Tait, A. *et al*., 2012. *Protocol for Induced Seismicity Associated with Enhanced Geothermal Systems*. DOE/EE-0662. Available online: https://www1.eere.energy.gov/geothermal/pdfs/geothermal_seismicity_protocol_012012.pdf (accessed May 2016).

Mallet, R. and Mallet, J.W., 1858. *The Earthquake Catalogue of the British Association: With the Discussion, Curves and Maps, etc.; Transactions of the British Association for the Advancement of Science*. Taylor and Francis, London.

Mallman, E.P. and Zoback, M.D., 2007. Assessing elastic Coulomb stress transfer models using seismicity rates in southern California and southwestern Japan. *Journal of Geophysical Research* 112 (B3): 2156–2202.

Masson, F., Hauser, F. and Jacob, A.W.B., 1999. The lithospheric trace of the Iapetus suture in SW Ireland from teleseismic data. *Tectonophysics* 302: 83–98.

Mathieson, A., Midgley, J., Wright, I. *et al*., 2010. In Salah CO_2 Storage JIP: CO_2 sequestration monitoring and verification technologies applied at Krechba, Algeria. *Energy Procedia* 4: 3596–3603.

Maxwell, S.C., 2010. Microseismic: growth born from success. *Leading Edge* 29: 338–343.

Maxwell, S.C., 2011. Hydraulic fracture height growth. *Canadian Society of Exploration Geophysicists Recorder* 39: 18–22.

Maxwell, S.C., Waltman, N., Warpinski, M. *et al*., 2006. Imaging seismic deformation induced by hydraulic fracture complexity. SPE paper 102801. *Society of Petroleum Engineers* 12(1).

Maxwell, S.C., Rutledge, J., Jones, R. *et al*., 2010. Petroleum reservoir characterization using downhole microseismic monitoring. *Geophysics* 75: 75A129–75A137.

Möllhoff, M. and Bean, C.J., 2016. Seismic noise characterization in proximity to strong microseism sources in the northeast Atlantic. *Bulletin of the Seismological Society of America* 106: 464–477.

Montgomery, C.T. and Smith, M.N., 2010. Hydraulic fracturing: history of an enduring technology. *Journal of Petroleum Technology* 62(12): 26–32.

Musson, R.M.W., 1989. *Seismicity of Cornwall and Devon*. BGS Global Seismology Report WL/89/11. British Geological Survey, London.

Musson, R.M.W., 1994. *A Catalogue of British Earthquakes*. British Geological Survey Global Seismology Report WL/94/04. British Geological Survey, London.

Musson, R.M.W., 2005. Intensity attenuation in the UK. *Journal of Seismology* 9: 73–86.

Musson, R.M.W., 2007. British earthquakes. *Proceedings of the Geologists Association* 118: 305–337.

Musson, R.M.W., 2012. *The Effect of Magnitude Uncertainty on Earthquake Activity Rates*. British Geological Survey. Available online: http://nora.nerc.ac.uk/500525/1/BSSANoteV4b.pdf (accessed 17 October 2016).

Musson, R.M.W. and Sargeant, S., 2007. *Eurocode 8 Seismic Hazard Zoning Maps for the UK*. British Geological Survey Technical Report CR/07/125N. British Geological Survey, London.

Nalbant, S.S., Steacy, S., Sieh, K. *et al*., 2005. Seismology: earthquake risk on the Sunda trench. *Nature* 435(7043): 756–757.

NAS (National Research Council), 2012. *Induced seismicity potential in energy technologies*. National Academies Press. Available online: http://www.nap.edu/catalog.php?record_id=13355 (accessed May 2016).

Naylor, D. and Shannon, P., 2009. The geology of offshore Ireland. In Holland, C.H. and Sanders, I.S. (eds), *The Geology of Ireland*, Dunedin Academic Press, Edinburgh, pp. 405–460.

Neale, C. and Smith, P., 2009. The use of large aperture buried geophone arrays for high efficiency stimulation and production microseismic monitoring. Paper presented at the Annual Convention and Exhibition of the American Association of Petroleum Geologists, AAPG Search and Discovery No. 90090.

Nic Bhloscaidh, M., McCloskey, J. and Bean, C.J., 2014. Response of the San Jacinto Fault Zone to static stress changes from the 1992 Landers earthquake. *Journal of Geophysical Research: Solid Earth* 119: 8914–8935.

Nic Bhloscaidh, M., McCloskey, J., Naylor, M. *et al*., 2015. Bayesian Monte Carlo reconstruction of the slip distributions in historical earthquakes on the Sunda megathrust, W. Sumatra. *Geophysical Journal International* 202: 1339–1361.

O'Brien, G.S., Bean, C.J. and McDermott, F., 2002. A comparison of published experimental data with a coupled lattice Boltzmann-analytic advection–diffusion method for reactive transport in porous media. *Journal of Hydrology* 268: 143–157.

O'Brien, G.S. and Bean, C.J., 2004. A 3D discrete numerical elastic lattice method for seismic wave propagation in heterogeneous media with topography. *Geophysical Research Letters* 31.

O'Hara, S., Humphrey, M., Jaspal, R. *et al*., 2013. *Public Perception of Shale Gas Extraction in the UK: How People's Views Are Changing*. Available online: http://ground-gassolutions.co.uk/wp-content/uploads/2013/03/Nottm_PublicPerceptionsShaleGasUK_Mar2013.pdf.

O'Reilly, J.P., 1884. *A Catalogue of Earthquakes Having Occurred in Great Britain and Ireland During Historical Time*. Royal College of Science, Dublin.

Ottemöller, L. and Sargeant, S., 2013. A local magnitude scale ML for the United Kingdom. *Bulletin of the Seismological Society of America* 103: 2884–2893.

Ottemöller, L., Nielsen, H.H., Atakan, K. *et al*., 2005. The 7 May 2001 induced seismic event in the Ekofisk oil field, North Sea. *Journal of Geophysical Research*,110: B10301.

Parker, R.H., 1989. *Hot Dry Rock Geothermal Energy: Final Report of the Camborne School of Mines Project*. Pergamon Press plc, Oxford.

Pavlis, G., 1986. Appraising earthquake hypocenter locations errors: a complete practical approach for single event locations. *Bulletin of the Seismological Society of America* 76: 1699–1717.

Peterson, J., 1993. *Observations and Modelling of Background Seismic Noise*. Open-file report 93–322, US Geological Survey, Albuquerque, NM.

Pharaoh, T.C., Morris, J.H., Long, C.B. *et al*., 1996. *Tectonic Map of Britain, Ireland and Adjacent Areas*, sheet 1, scale 1:1,500,000. British Geological Survey, Keyworth.

Phillips, W.E.A., Stillman, C.J. and Murphy, T., 1976. A Caledonian plate tectonic model. *Journal of the Geological Society of London* 132: 579–605.

Pollard, D.D. and Segall, P., 1987. Theoretical displacements and stresses near fractures in rock: with applications to faults, joints, dikes, and solution surfaces. In Atkinson, B. K. (ed.), *Fracture Mechanics of Rock*. Academic Press, London.

Qian, Y., D'Humieres, D., Lallemand, P., 1992. Lattice BGK models for the Navier–Stokes equation. *Europhysics Letters* 17: 79–484.

Redmayne, D.W., 1988. Mining-induced seismicity in UK coalfields identified on the BGS National Seismograph Network. In *Engineering Geology of Underground Movements*. Geological Society Engineering Geology Special Publication No. 5, pp. 405–413.

Redmayne, D.W., Richards, J.A. and Wild, P.W., 1998. Mining-induced earthquakes monitored during pit closure in the Midlothian Coalfield, *Quarterly Journal of Engineering Geology* 31: 21–36.

Rhoades, D.A., 1996. Estimation of the Gutenberg-Richter relation allowing for individual earthquake magnitude uncertainties. *Tectonophysics* 258: 71–83.

Rhoades, D.A. and Dowrick, D.J., 2000. Effects of magnitude uncertainties on seismic hazard estimates. *Proceedings of the 12th World Conference on Earthquake Engineering*, Wellington, NZ, Paper 1179.

Richardson, M., 1975. *Seismicity of Ireland*. Electricity Supply Board, Dublin.

Richter, C.F., 1935. An instrumental earthquake magnitude scale. *Bulletin of the Seismological Society of America* 25: 1–32.

Roeloffs, E., 1996. Poroelastic techniques in the study of earthquake-related hydrologic phenomena. *Advances in Geophysics* 37: 135–195.

Roper, W., 1889. *A List of the More Remarkable Earthquakes in Great Britain and Ireland*. Thomas Bell, Lancaster.

Royal Society and Royal Academy of Engineering, 2012. *Shale Gas Extraction in the UK: A Review of Hydraulic Fracturing*. DES2597. Royal Society and Royal Academy of Engineering, London.

Rutledge, J.T. and Phillips, W.S., 2003. Hydraulic stimulation of natural fractures as revealed by induced microearthquakes, Carthage Cotton Valley Gas Field, East Texas. *Geophysics* 68: 441–452.

Rutledge, J.T., Phillips, W.S. and Mayerhofer, M.J., 2004. Faulting induced by forced fluid injection and fluid flow forced by faulting: an interpretation of hydraulic-fracture microseismicity, Carthage Cotton Valley Gas Field, Texas. *Bulletin of the Seismological Society of America* 94: 1817–1830.

Rydelek, P.A. and Sacks, I.S., 1989. Testing the completeness of earthquake catalogues and the hypothesis of self-similarity. *Nature* 337: 251–253.

Sargeant, S. and Ottemöller, L., 2009. *Lg* wave attenuation in Britain. *Geophysical Journal International* 179: 1593–1606.

Scholtz, C.H., 2002. *The Mechanics of Earthquakes and Faulting*, 2nd edition. Cambridge University Press, Cambridge.

Shapiro, S.A., Patzig, R. and Rothert, E., 2003. Triggering or seismicity by pore pressure perturbations: permeability related signatures of the phenomenon. *Pure Applied Geophysics* 122: 947–965.

Shapiro, S.A., Dinske, C. and Kummerow, J., 2007. Probability of a given-magnitude earthquake induced by a fluid injection. *Geophysical Research Letters* 34, L22: 314.

Shapiro, S.A., Dinske, C., Langenbruch, C. *et al*., 2012. Seismogenic index and magnitude probability of earthquakes induced during reservoir fluid stimulations. *Leading Edge* 29: 304–309.

Shearer, P.M. and Orcutt, J.A., 1987. Surface and near-surface effects on seismic-waves: theory and borehole seismometer results. *Bulletin of the Seismological Society of America* 77: 1168–1196.

Shememt, J.E., Eide, E.A., Hitzman, M.W. *et al*., 2012. The potential for induced seismicity in energy technologies. *Leading Edge* 31: 1438–1444.

Stauffer, D. and Aharony, A., 1994. *Introduction to Percolation Theory*. Taylor and Francis, London.

Stein, R.S., Barka, A.A. and Dieterich, J.H., 1997. Progressive failure on the North Anatolian fault since 1939 by earthquake stress triggering. *Geophysical Journal International* 128: 594–604.

Stork, A.L., Verdon, J.P. and Kendall, J.-M., 2014. The robustness of seismic moment and magnitudes estimated using spectral analysis. *Geophysical Prospecting* 62: 1365–2478.

Suckale, J., 2010. Moderate-to-large seismicity induced by hydrocarbon production. *Leading Edge* 29: 310–314.

Tinti, S., and Mulargia, F., 1985. Effects of magnitude uncertainties on estimating the parameters in the Gutenberg-Richter frequency-magnitude law. *Bulletin of the Seismological Society of America* 75: 1681–1697.

Toda, S. and Stein, R.S., 2003. Toggling of seismicity by the 1997 Kagoshima earthquake couplet: a demonstration of time-dependent stress transfer. *Journal of Geophysical Research* 108: 2567.

Toda, S., Stein, R.S., Beroza, G.C. *et al*., 2012. Aftershocks halted by static stress shadows. *Nature Geoscience* 5: 410–413.

Townend, J. and Zoback, M.D., 2000. How faulting keeps the crust strong. *Geology* 28: 399–402.

Trnkoczy, A., Bormann, P., Hanka, W. et al., 2009a. Chapter 7: site selection, preparation and installation of seismic stations. In Bormann, P. (ed.), *New Manual of Seismological Observatory Practice (NMSOP-2)*. IASPEI, GFZ German Research Centre for Geosciences, Potsdam. Available online: http://gfzpublic.gfz-potsdam.de/pubman/item/escidoc:43206/component/escidoc:352734/Chapter_7.pdf (accessed May 2016).

Trnkoczy, A., Havskov, J. and Ottemöller, L., 2009b. Chapter 8: seismic networks. In Bormann, P. (ed.), *New Manual of Seismological Observatory Practice (NMSOP-2)*. IASPEI, GFZ German Research Centre for Geosciences, Potsdam. Available online: http://gfzpublic.gfz-potsdam.de/pubman/item/escidoc:43210:8/component/escidoc:352736/Chapter_8.pdf (accessed May 2016).

Utsu, T., 1961. A statistical study of the occurrence of aftershocks. *Geophysical Magazine* 30: 521–605.

Van Eijs, R.M.H.E., Mulders, F.M.M., Nepveu, M., *et al*., 2006. Correlation between hydrocarbon reservoir properties and induced seismicity in the Netherlands. *Environmental Geology* 84: 99–111.

Veneziano, D. and Van Dyck, J., 1985. Analysis of earthquake catalogs for incompleteness and recurrence rates. Seismic parameter estimation methods. In EPRI/SOG (ed.), *Seismic Hazard Methodology for Nuclear Facilities in the Eastern United States (Draft 85–1)*. EPRI Research Project 2: A-6. Electric Power Research Institute, Palo Alto, CA.

Viegas, G., Baig, A., Coulter W. *et al*., 2012. Effective monitoring of reservoir-induced seismicity utilizing integrated surface and downhole seismic networks. *First Break* 30: 77–81.

Wald, D.J. and Heaton, T.H., 1994. Spatial and temporal distribution of slip for the 1992 Landers, California, earthquake. *Bulletin of the Seismological Society of America* 84: 668–691.

Wald, D., Quitoriano, V., Heaton, T. *et al*., 1999. TriNet ShakeMaps: rapid generation of peak ground motion and intensity maps for earthquakes in southern California. *Earthquake Spectra* 15: 537–555.

Walker, A.B., 1987. *Background and Induced Seismicity Monitoring for the HDR Geothermal Programme in Cornwall*. BGS Global Seismology Report 323. British Geological Survey, London.

Warpinski, N., Du, J. and Zimmer, U., 2012. Measurement of Hydraulic-Fracture Induced Seismicity in Gas Shales, *SPE* 151597. *Society of Petroleum Engineers* 27(3).

Ware, J., 1662. *Rerum Hibernicarum Henric Octavo Regnante, Annales*. Crook, Dublin.

Weichert, D.H., 1980. Estimation of the earthquake recurrence parameters for unequal observation periods for different magnitudes. *Bulletin of the Seismological Society of America* 70: 1337–1346.

Wells, D.L. and Coppersmith, K.J., 1994. New empirical relationships among magnitude, rupture length, rupture width, rupture area, and surface displacement. *Bulletin of the Seismological Society of America* 84: 974–1002.

Westbrook, G.K., Kusznir, N.J., Browitt, C.W.A. *et al*., 1980. Seismicity induced by coal mining in Stoke-on-Trent (UK). *Engineering Geology* 16: 225–241.

Whitmarsh, L., Nash, N., Lloyd, A. *et al*., 2014. *UK Public Perceptions of Shale Gas, Carbon Capture & Storage and Other Energy Sources & Technologies: Summary Findings of a Deliberative Interview Study and Experimental Survey.* Understanding Risk Research Group Working Paper 14-02, Cardiff University, Cardiff.

Woodcock, N.H. and Strachan, R.A., 2000. *Geological History of Britain and Ireland*. John Wiley and Sons, Chichester.

Zoback, M.D., 2012. Managing the seismic risk posed by wastewater disposal. *Earth Magazine* 57: 38–43.

Abbreviations

BGS	British Geological Survey
CB	Clare Basin
CORINE	Coordination of information on the environment
CRS	Coulomb Rate State
DEM	Digital Elevation Model
DETI	Department of Enterprise, Trade and Investment
DIAS	Dublin Institute of Advanced Studies
EMS	European Macroseismic Scale
EPA	Environmental Protection Agency
ESA	European Space Agency
GIS	Geographic Information System
GNSS	Global Navigation Satellite System
GPS	Global Positioning System
HDR	Hot Dry Rock
InSAR	Interferometric Synthetic Aperture Radar
IPTA	Interferometric Point Target Analysis
ISBAS	Intermittent Small Baseline Subset
JRP	Joint Research Programme
NCB	Northwest Carboniferous Basin
PS	Persistent Scatterer
PSI	Persistent Scatterer Interferometry
SAR	Synthetic Aperture Radar
SBAS	Small Baseline Subset
SNR	Signal-to-noise Ratio

Final Report 2: Baseline Characterisation of Seismicity

Authors: Brian Baptie, Colm Jordan, Ilaria Mosca, Francesca Cigna, Sean Burke, John McCloskey, Mairéad Nic Bhloscaidh, Chris Bean and Martin Möllhoff

Roinn Cumarsáide, Gníomhaithe ar son na hAeráide & Comhshaoil
Department of Communications, Climate Action & Environment

NIEA Northern Ireland Environment Agency
www.daera-ni.gov.uk

Unconventional gas exploration and extraction (UGEE) involves hydraulic fracturing ("fracking") of low permeability rock to permit the extraction of natural gas on a commercial scale from unconventional sources, such as shale gas deposits, coal seams and tight sandstone.

The UGEE Joint Research Programme (JRP) (**www.ugeeresearch.ie**) is composed of five interlinked projects and involves field studies (baseline monitoring of water and seismicity), as well as an extensive desk-based literature review of UGEE practices and regulations worldwide. The UGEE JRP was designed to provide the scientific basis that will assist regulators - in both Northern Ireland and Ireland - to make informed decisions about whether or not it is environmentally safe to permit UGEE projects/operations involving fracking. As well as research in Ireland, the UGEE URP looks at and collates evidence from other countries.

The JRP is funded by the Department of Communications, Climate Action and Environment, DCCAE (formerly the Department of Communications, Energy and Natural Resources (DCENR) and the Environment Division of the Department of Environment, Community and Local Government (DECLG)) and the Northern Ireland Environment Agency (NIEA). The research programme was managed by a steering committee comprising the EPA, representatives from DCCAE, the Geological Survey of Ireland, Commission for Energy Regulation, An Bord Pleanála, NIEA, the Geological Survey of Northern Ireland and the Health Service Executive.

List of Outputs:

- Final Report 1: Baseline Characterisation of Groundwater, Surface Water and Aquatic Ecosystems
- Summary Report 1: Baseline Characterisation of Groundwater, Surface Water and Aquatic Ecosystems
- Final Report 2: Baseline Characterisation of Seismicity
- Summary Report 2: Baseline Characterisation of Seismicity
- Final Report 3: Baseline Characterisation of Air Quality
- Summary Report 3: Baseline Characterisation of Air Quality
- Final Report 4: Impacts & Mitigation Measures
- Summary Report 4: Impacts & Mitigation Measures
- Final Report 5: Regulatory Framework for Environmental Protection
- Summary Report 5: Regulatory Framework for Environmental Protection
- UGEE Joint Research Programme Integrated Synthesis Report

EPA Research: McCumiskey House, Richiew, Clonskeagh, Dublin 14.

Phone: 01 268 0100
Twitter: @EPAResearchNews
Email: research@epa.ie

www.ugeeresearch.ie